

Ronaldo Gonçalves dos Santos

Fundamentals of Surface Thermodynamics

Phase Behavior and Its Related
Properties

 Springer

Fundamentals of Surface Thermodynamics

Ronaldo Gonçalves dos Santos

Fundamentals of Surface Thermodynamics

Phase Behavior and Its Related Properties

 Springer

Ronaldo Gonçalves dos Santos
Department of Chemical Engineering
University Center FEI
São Bernardo do Campo, São Paulo, Brazil

ISBN 978-3-031-52465-3 ISBN 978-3-031-52466-0 (eBook)
<https://doi.org/10.1007/978-3-031-52466-0>

© The Editor(s) (if applicable) and The Author(s), under exclusive license to Springer Nature Switzerland AG 2024

This work is subject to copyright. All rights are solely and exclusively licensed by the Publisher, whether the whole or part of the material is concerned, specifically the rights of translation, reprinting, reuse of illustrations, recitation, broadcasting, reproduction on microfilms or in any other physical way, and transmission or information storage and retrieval, electronic adaptation, computer software, or by similar or dissimilar methodology now known or hereafter developed.

The use of general descriptive names, registered names, trademarks, service marks, etc. in this publication does not imply, even in the absence of a specific statement, that such names are exempt from the relevant protective laws and regulations and therefore free for general use.

The publisher, the authors, and the editors are safe to assume that the advice and information in this book are believed to be true and accurate at the date of publication. Neither the publisher nor the authors or the editors give a warranty, expressed or implied, with respect to the material contained herein or for any errors or omissions that may have been made. The publisher remains neutral with regard to jurisdictional claims in published maps and institutional affiliations.

This Springer imprint is published by the registered company Springer Nature Switzerland AG
The registered company address is: Gewerbestrasse 11, 6330 Cham, Switzerland

Paper in this product is recyclable.

*To Ciro and Nilda (in memoriam)—from
heaven, they guide me through rainy days.*

*To Maria José—always on my side, she is the
brightest light of the universe.*

To all my family, for your love.

Preface

Interfacial phenomena are involved in a series of industrial processes and daily operations. These phenomena are related to the formation of emulsions and foams, adsorption on solid and fluid interfaces, wettability alteration, and others that strongly impact the quality and cost of products and processes. Understanding the interfacial phenomena encompasses inexorably the description of surface thermodynamics and the assessment of thermodynamic properties. The book *Fundamentals of Surface Thermodynamics* focuses on the basics of thermodynamics of interface from a point of view of chemical engineering thermodynamics and surface chemistry, together with the representation of the real-life phenomena related to giving significance to the abstract properties that are daily handled by scientists and engineers. The book is devoted to graduate and undergraduate courses in chemistry and engineering schools. The book content is also dedicated to industry professionals working with oil and gas, fluid transportation, nanotechnology, and other multiphase complex system operations, where the effectiveness is affected by interfacial phenomena. In this way, this content can be helpful for learning activities in science and engineering courses concerning chemistry, biochemistry, mechanics, materials, and environment. The book fundamentals can be extended to a wide range of applications.

The *Fundamentals of Surface Thermodynamics* results from a long-term analysis of the thermodynamics of homogeneous phases and interface sciences, to sum up and correlate their extensive content that is distributed in a multidisciplinary area. The book's scope requires an initial understanding of chemistry, physics, and chemical thermodynamics; however, an earnest effort was made to simplify and provide details on theoretical and descriptive lines. The central aspects of the surface thermodynamic theory are presented from step-by-step deduction to carefully carry the reader over the deep abstract means and elaborate mathematical approaches. The book's chapters were arranged to allow the reader to go from an overview of surface science, going across the fundamentals in the microscopic description of the phenomena and then achieving thermodynamic application to surfaces.

The *Fundamentals of Surface Thermodynamics* brings a single description of colloidal science, from conventional surfactant applications to responsive systems and nanomaterials applied to life science. Therefore, the illustrations are displayed on a generalized structure: values of properties are avoided on illustrations, graphics, and diagrams to give only a qualitative behavior. Data from experimental studies are recommended as references to the quantitative behaviors, which are often changeable according to the system's nature.

Finally, the book *Fundamentals of Surface Thermodynamics* travels across the fascinating world where small-dimension entities breathe. It intends to motivate students and professionals to analyze the interface thermodynamics in-depth, thereby contributing to support teaching activities and enabling industrial solutions.

São Bernardo do Campo, Brazil
September 2023

Ronaldo Gonçalves dos Santos

Acknowledgments

This journey involved the contribution and support of a significant number of people. I would like to express my heartfelt gratitude to all those who have been a part of this endeavor. First and foremost, I want to extend my deepest appreciation to my family for their unwavering encouragement during the long hours of writing and research. I am indebted to those who dedicated their time to discussing specific topics and providing guidance. Namely, I am grateful to Dr. Watson Loh (University of Campinas) and Dr. G. Ali Mansoori (University of Illinois at Chicago), who provided invaluable insights. I am incredibly grateful to Débora Umbelino for her lovely support with figures and text editing. I thank the resolute team at Springer Nature, especially Mr. Anthony Doyle and Mr. Padma Subbaiyan, for their professionalism and awareness. I also want to acknowledge the numerous researchers, scholars, and experts whose works have been a source of inspiration.

Thank you all for being a part of this remarkable journey.

September 2023

Ronaldo Gonçalves dos Santos

Contents

1	An Overview on the Surface Science	1
1.1	The Domain of the Surface Science	1
1.2	Description of the Interfacial Region	3
1.3	The Nature of Colloidal Systems	5
1.4	Aspects of the Colloidal Stability	7
	References	9
2	Colloidal and Self-Assembly Systems	11
2.1	Surface Active Agents	12
2.2	Interfacial Adsorption of Surface-Active Agents	15
2.3	Surfactant Solubilization and Critical Concentration	17
2.4	Surfactant Self-Assemble Structures	20
2.5	Mechanism of Micellization	21
2.6	Micelle Structure and Shape	25
2.7	Singular Optical Properties of Colloidal Dispersions	28
2.8	Solubilization in Micellar Solution	30
	References	32
3	Forces Acting in Colloidal Systems	33
3.1	Nature of Interparticle Forces	34
3.1.1	Van Der Waals Interactions	35
3.1.2	Electrostatic Forces (Electrical Double Layer Interactions)	39
3.1.3	Steric Interactions	49
3.1.4	Hydrophobic Interactions	51
3.1.5	Brownian Forces	52
3.1.6	Hydration Interactions	54
	References	55
4	Phase Equilibria of Colloidal Systems	57
4.1	Liquid Phase Equilibria	58
4.2	Colloidal Phase Equilibria	60

4.3	Rheology of Colloidal Surfactant	64
4.4	Microemulsion and Macroemulsion	64
4.4.1	Macroemulsions	65
4.4.2	Microemulsion	68
4.5	Solubilization	70
	References	72
5	Surface Tension and Its Derivative Properties	73
5.1	The Basic of Interfacial Thermodynamics	74
5.2	Gibbs Adsorption Equation	78
5.3	Dynamic Interfacial Adsorption	83
5.4	Curved Surfaces and Capillarity	85
	References	87
6	Phase Behavior of Interfacial Films	89
6.1	Two-Dimensional Monolayers	90
6.2	Physical State of the Interface Monolayers	92
6.3	Phase Behavior of Interfacial Films	96
6.4	Polymer Monolayers	102
6.5	Cohesive Surface Pressure	103
6.6	Phase Transition of Interfacial Films	105
6.7	Mixed Monolayers	107
6.8	Charged Monolayers	111
6.9	Surface Potential	112
	References	113
7	Rheology of Surface Films	115
7.1	Basic Fundamentals of Rheology	116
7.2	Viscoelastic Behavior	119
7.3	Interfacial Layer Rheology	129
7.3.1	Dilatational Interfacial Rheology	130
7.3.2	Interfacial Shear Rheology	134
7.4	Dimensions of Interfacial Elasticity Moduli	137
7.5	Isothermal Surface Compressibility	138
	References	139
8	Liquid-Liquid Interfaces	141
8.1	The Nature of Fluid Interfaces	141
8.2	Thin Liquid Film	142
8.3	Surface Curvature	147
8.4	The Disjoining Pressure	150
8.4.1	Stability of Liquid Thin	152
8.5	Emulsion Stability	156
	References	159

9	Solid–Liquid Interfaces	161
9.1	The Solid–liquid Interface	162
9.2	Wetting Behavior on Solid Surface	163
9.3	Wettability of Solid Surface	167
9.4	Relationship Between Adsorption and Wettability	169
9.5	Surfactant as Dispersion Agents	171
	References	174
10	Recent Developments and Applications	175
10.1	Nanotechnology	176
10.2	Energy Science and Technology	176
10.3	Life Science and Technology	177
10.4	Environmental Science and Technology	178
10.5	Final Remarks	179

Chapter 1

An Overview on the Surface Science



Surface science is a multidisciplinary field that lies at the intersection of physics, chemistry, materials science, and engineering, delving into the intriguing world of interfaces. It focuses on understanding the properties, behaviors, and interactions of matter at the surface, where the bulk properties of materials often undergo significant changes. The fundamentals of surface science are applied in various technological advancements, from developing novel materials and catalysts to designing cutting-edge electronic devices and biomedical applications. The scope of surface science is broad since it deals with phenomena occurring in the interfaces between different states of matter. Interface phenomena act as the meeting points where fundamental physical and chemical phenomena occur, drawing an exciting science field. The region between two different phases has a crucial protagonist in determining the behavior and performance of materials, as they often dictate the reactivity, equilibrium, and transport properties. Interfacial phenomena are involved in a series of industrial processes and daily operations. These phenomena are related to the formation of emulsions and foams, adsorption on solid and fluid interfaces, wettability alteration, and other manifestations that strongly impact the quality and cost of products and processes. The understanding of the interfacial phenomena encompasses the description and the assessment of surface thermodynamic properties.

1.1 The Domain of the Surface Science

In surface science, describing the surface's microscopic structure and macroscopic manifestation is the fundamental drive. The interface possesses unique atomic and molecular arrangements that can differ significantly from their bulk counterparts. Advanced experimental techniques, such as scanning probe microscopy and surface-sensitive spectroscopies, allow the visualization and analysis of surface structures with remarkable accuracy, providing valuable descriptions of surface reactivity,

adsorption, and the growth of thin films and nanostructures. In addition, surface chemical reactions can exhibit distinct mechanisms and kinetics compared to bulk reactions, and they are a particular topic of surface chemistry. Surface reactions often involve the adsorption–desorption process and diffusion of chemical species, leading to the formation of new chemical bonds or surface modifications (for an overview on interfacial phenomena see Davies and Rideal 1963).

Surface chemistry is related to the recent development of advanced technologies that encompasses, for instance, the design of efficient catalysts for green-chemical reactions, optimization of the performance of energy storage devices, and development strategies for surface functionalization and surface modification techniques. Surface characterization techniques, such as X-ray photoelectron spectroscopy (XPS) and Auger electron spectroscopy (AES), enable the identification and quantification of the surface elemental composition, chemical composition, and oxidation states. Surface analysis techniques also facilitate understanding surface contamination, surface cleanliness, and the effects of environmental factors on surface properties, which are critical considerations for industries such as semiconductor manufacturing and aerospace materials.

Molecular dynamic simulations and density functional theory calculations provide valuable tools for exploring and predicting surface properties and behaviors at the atomic and molecular levels. Computational modeling and simulation bridge the gap between experimental observations and theoretical understanding, enabling the unraveling of complex surface phenomena, evaluation of the empirical models, and design of materials with advanced properties.

An intriguing aspect of surface science is the description of surface forces and interactions. van der Waals forces, electrostatic interactions, and capillary forces, among non-conventional others, engage in adhesion phenomena and self-assembly of nanoscale structures (see Chap. 2), and they have a special participation in determining the stability and behavior of colloidal systems (see Chap. 3). The surface forces are not only significant at the macroscopic scale but also they become increasingly relevant at the nanoscale, where the area-to-volume ratio becomes adequately high (see Chap. 4). By understanding and manipulating these forces, it is possible to develop new materials with tailored surface properties, design advanced coatings with improved durability, and engineer surfaces with controlled wettability and anti-fouling properties.

The interfacial phenomena deal with the dynamic interplay between distinct phases, exhibited at solid, liquid, and gas states. The interface must be described as the two-dimensional region that acts as the meeting point between two or more phases, where vital physical and chemical interactions occur. One of the most common manifestations of interfacial phenomena is the formation of interfacial films (see Chaps. 6 and 7) in systems containing emulsions and foams (see Chap. 8). Emulsions are colloidal suspensions of one immiscible liquid within another, such as oil droplets dispersed in water. Conversely, foam consists of a dispersion of gas bubbles in a liquid or solid medium. Both emulsions and foams find applications in various industries, ranging from food and cosmetics to petroleum and pharmaceuticals. Understanding the mechanisms behind their formation and stability allows for optimizing product

formulations and enhancing shelf life. Interfacial phenomena also include the well-known process of molecular adsorption on solid and fluid interfaces (for details see Harkins 1952). The interfacial adsorption is governed by surface energy, molecular interactions, and the properties of the adsorbate and adsorbent (see Chap. 5). Similarly, the phenomena of liquid spreading on solid surfaces, termed wettability, is on the surface science focus (see Chap. 9). Surface wettability participates in processes such as inkjet printing, coating, and enhanced oil recovery (for details see de Gennes et al. 2004).

The intricate behavior of interfacial phenomena is subject of investigation of surface thermodynamics. Surface thermodynamics designate interfaces' energetics and equilibrium state, bringing a similar approach to the bulk solution thermodynamics. The surface thermodynamic principles provide the fundamental understanding of interfacial behavior (see Chap. 5). Experimental techniques such as surface tension measurements, contact angle analysis, and interfacial rheology allow the quantitative characterization of interface properties. The experimental assessment assists in predicting and optimizing the behavior of complex systems involving interfaces, leading to the improved product formulations, process design, and overall efficiency.

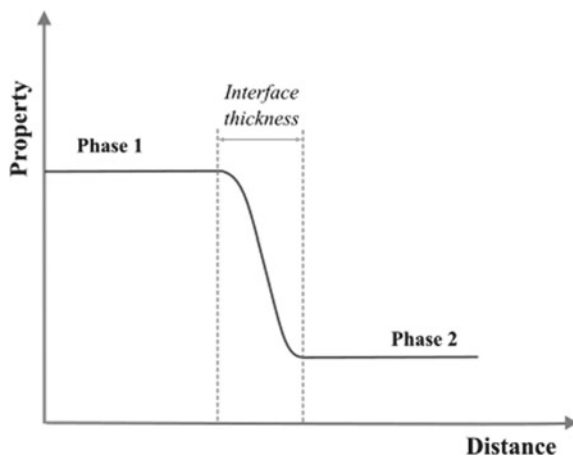
The occurrence of the interfacial phenomena is ubiquitous in various industrial processes and daily operations. From the formation of emulsions and foams to adsorption on solid and fluid interfaces and wettability alteration, these phenomena profoundly impact the quality and cost of products and processes. By comprehending the principles of surface thermodynamics and assessing thermodynamic properties, the interfacial phenomena can be manipulated to optimize industrial processes, improve product performance, and drive innovation across diverse industries.

1.2 Description of the Interfacial Region

The term *interface* presupposes the existence of a phase boundary. It represents the region between two distinct phases in which occurs the variation of the properties from one phase to another. Figure 1.1 displays, on a broad view, the variation of a specific property (as density, solute concentration, and Gibbs energy) through the interface region dividing two separate phases (as liquid–gas, liquid–liquid, solid–liquid, and solid–gas two-phase systems). The interface must be represented by a two-dimensional region with finite thickness (for details see Adamson and Gast 1997).

The interfacial region is characterized by some unique features and phenomena that are distinct from the bulk properties of the individual materials (for details on the characterization and structure of interface see Starov 2010). At the atomic and molecular scale, the interfacial region often exhibits structural, electronic, and chemical properties that differ from both the bulk phases. The more critical aspect of the interfacial region is its increased surface area compared to the bulk materials.

Fig. 1.1 Representation of the interfacial region between two separate phases and the property change across the interface



The interfacial region can undergo various processes, including adsorption, desorption, diffusion, and reactions. Interfacial adsorption is the reversible process by which molecules or atoms from the surrounding environment accumulate on the surface of a material. When a material is exposed to a gas or liquid, the molecules or atoms can interact with the surface through weak attractive forces, such as van der Waals or electrostatic interactions (for details see Holmberg et al. 2002 and Adamson and Gast 1997). This leads to the adsorption of the species onto the surface. The adsorbed species must form a surface layer, depending on the system conditions and the nature of the surface. Desorption is the reverse process of adsorption. It involves the release of molecules or atoms from the surface back into the surrounding environment. Desorption can occur due to changes in temperature, pressure, or exposure to other species that can compete for binding sites on the surface. Interfacial diffusion refers to the movement of species within the interface region. Diffusion can be influenced by temperature, surface structure, and the presence of other species. Additionally, reactions can occur between molecules or atoms in the interfacial region, leading to the formation of new compounds or the modification of existing ones. The close proximity of distinct species in the interfacial region enhances the likelihood of chemical reactions compared to the bulk phases. Surface reactions can involve adsorbed species, leading to the formation of new chemical bonds, surface restructuring, or changes in the surface properties.

Surfaces have been characterized by advanced techniques with high resolution, including scanning probe microscopy (SPM), X-ray photoelectron spectroscopy (XPS), and surface-sensitive spectroscopies.

Scanning Probe Microscopy (SPM) encompasses several powerful techniques that enable the imaging and manipulation of surfaces at the atomic and molecular scale. SPM techniques allow for the visualization of surface features, such as atomic arrangements, surface roughness, and surface defects. The most common types of SPM comprise atomic force microscopy (AFM) and scanning tunneling microscopy (STM). AFM uses a sharp probe to scan the surface, measuring the forces between

the probe and the surface to create a topographic image with nanoscale resolution. On the other hand, STM utilizes a sharp tip and a voltage bias to image the surface by measuring the tunneling current between the tip and the surface.

X-ray Photoelectron Spectroscopy (XPS) is a widely used surface analysis technique that provides information about the chemical composition of the interfacial region. It involves irradiating the surface with X-rays, which causes the emission of photoelectrons from the surface. By measuring the kinetic energies of these emitted electrons, XPS can determine the elemental composition and chemical states of the elements present in the top few nanometers of the surface. XPS is particularly valuable for identifying surface contaminants, analyzing thin films, and probing surface chemistry.

Surface-Sensitive Spectroscopies techniques are employed to probe the electronic and vibrational properties of the interfacial region. These techniques include infrared spectroscopy (IR), Raman spectroscopy, and angle-resolved photoemission spectroscopy (ARPES). IR spectroscopy measures the absorption and reflection of infrared light by the surface, providing information about molecular vibrations and functional groups present in the interfacial region. Raman spectroscopy measures the inelastic scattering of laser light, providing information about molecular vibrations and crystal lattice properties. Raman spectroscopy can help identify specific molecules or phases in the interfacial region. ARPES is a technique that measures the energy and momentum of photoelectrons emitted from a surface. By analyzing the emitted electrons, ARPES can provide information about the electronic band structure and Fermi surface of the material, revealing valuable insights into the electronic properties of the interfacial region.

1.3 The Nature of Colloidal Systems

Colloids (or colloidal dispersions) are defined as mixtures consisting of two or more substances, where one substance is dispersed in another as tiny particles. The dispersed particles are substantially larger than individual molecules but small enough to remain them suspended and dispersed throughout the surrounding medium. The dispersed particles constitute a discontinuous phase, which can be solid, liquid, or gas, whereas the dispersing medium is typically named continuous phase. The particles in colloidal dispersion, labeled as colloidal particles, present at least one characteristic linear dimension ranging approximately from 10^{-9} m (1 nm) to 10^{-6} m (1 μ m) (see Rosen 1989).

Colloidal dispersions exhibit unique properties and behaviors due mainly to their specific dispersed particle size and the interaction between the dispersed phase and the continuous medium. These properties can differ significantly from those of the individual components in their bulk. For example, colloidal systems can display unusual optical properties, such as the Tyndall effect, where light is scattered by the colloidal particles, making the solution appear cloudy or milky (see Chap. 2). Colloids can also exhibit distinctive rheological properties, affecting their flow behavior and

mechanical characteristics. Colloidal particles tend to aggregate or settle. However, the stability of colloidal systems can be enhanced by employing methods to prevent particle agglomeration and maintain the dispersed state of the colloid for extended periods (for details see Everett 1989 and Tadros 2018).

Colloids can also be categorized based on the relative affinity between the dispersed particles and the continuous phase. On this classification, colloids are defined as lyophilic (solvent-attracting) and lyophobic (solvent-repelling) colloids. For systems containing an aqueous phase as continuous media, the colloids are often termed hydrophilic (water-attracting) and hydrophobic (water-repelling). Particles in lyophilic colloids exhibit strong interactions with the dispersing medium, resulting in good stability and uniform dispersion. Lyophobic colloids, on the other hand, have weak interactions with the dispersing medium, leading to poor stability and agglomeration of particles (see Tadros 2018).

Two-phase colloidal systems have been broadly classified concerning the nature of the dispersed and continuous phase into five main categories:

- (i) **Sols:** Sols are colloidal dispersions in which the dispersed phase is composed of solid particles suspended in a liquid or solid medium. The liquid sols are generally composed of dispersed particles finely divided with size small enough to keep them suspended due to Brownian motion. Examples of sols include paint pigments, ink, and certain types of nanoparticles.
- (ii) **Gels:** These are colloidal systems with a dispersed phase consisting of a three-dimensional network of interconnected particles or molecules, often referred to as a gel matrix, dispersed in a liquid medium. The gel matrix imparts a rheological solid-like behavior to the colloidal system, giving it a semi-solid or jelly-like consistency. Gels can be formed from various materials, including polymers, proteins, and even certain types of food products like jelly or custard.
- (iii) **Emulsions:** Emulsions are colloidal systems in which two immiscible liquids, such as oil and water, are dispersed in each other. Emulsions typically consist of one liquid phase dispersed as tiny droplets within the other liquid phase, stabilized by the presence of an emulsifying agent or surfactant. Examples of emulsions include milk, mayonnaise, and various cosmetic creams and lotions.
- (iv) **Aerosols:** The colloidal systems in which solid or liquid particles are dispersed in a gas medium are termed aerosols. Aerosols can occur naturally, such as in the form of fog or mist, or they can be artificially generated, as in the case of spray paint or inhalable drug formulations. The behavior and stability of aerosols depend strongly on the particle size and composition.
- (v) **Foam:** Foams are described as colloidal dispersions consisting of gas bubbles dispersed in a liquid or solid medium. The bubbles in a foam are typically stabilized by surface-active agents, which reduce the surface tension and prevent the coalescence or collapse of the bubbles. Foams can be found in daily life as whipped cream, and lathered soap, for instance. In industrial applications, foams are utilized for insulation, firefighting, cosmetics, food processing, and many other purposes.

1.4 Aspects of the Colloidal Stability

Controlling the stability of colloids is a critical aspect of their practical use. Colloid stability refers to the ability of colloidal particles to remain dispersed or suspended in a medium without undergoing aggregation or settling over time. The stability of colloidal systems can be influenced by several factors, including particle size, charge, and surface chemistry. Several factors contribute to the stability of colloidal systems, and these can be broadly categorized into two main types: kinetic stabilization and thermodynamic stabilization. It is essential to highlight that colloid stability is influenced by a delicate balance of multiple factors and mechanisms, such as stabilizing agents, nature of the particles, composition of the dispersing medium, and external conditions such as temperature and pH (for details see Porter 1993 and Adamson and Gast 1997).

Kinetic stabilization occurs when particle aggregation or sedimentation rate is hindered or slowed down. The stabilization by kinetic ways can be achieved through mechanisms such as:

- (i) **Steric Stabilization:** Steric stabilization involves using polymers or surfactants that adsorb onto the surface of colloidal particles, creating a protective layer or *steric barrier* that prevents close contact and aggregation. The repulsive forces generated by the polymer chains or surfactant molecules effectively keep the particles separated, maintaining the stability of the colloid.
- (ii) **Electrostatic Stabilization:** Electrostatic stabilization relies on the presence of an electrostatic double layer around the particles. When charged particles are dispersed in a medium, ions from the medium can accumulate around the particles, creating a diffuse layer of counterions with an opposite charge. This produces electrostatic repulsion between particles of like charges, preventing their aggregation. The thickness and charge of the double layer can be manipulated by adjusting the pH ionic strength or adding specific electrolytes to control colloidal stability.
- (iii) **Brownian Motion:** The random thermal motion of particles, described as the well-known Brownian motion, plays a crucial role in stabilizing colloidal systems. The constant collisions and diffusion of particles due to Brownian motion disrupt the aggregation and settling process, maintaining the colloid's stability.

On the other hand, thermodynamic stabilization relies on minimizing the free energy of the system by ensuring that the dispersed state is more energetically favorable than the aggregated or settled state. This can be achieved mainly through solvation and dispersion forces that arise due to the solvent molecules being attracted to the surface of colloidal particles. These solvation forces can stabilize the particles by creating a barrier against aggregation. Dispersion forces, such as van der Waals forces, also contribute to colloid stability by providing attractive forces between particles that counteract aggregation. In addition, modifying the surface properties

of colloidal particles through functionalization or coating can enhance thermodynamic stability. This can involve introducing hydrophilic or hydrophobic groups to control the interactions between particles or utilizing specific surface coatings that repel other particles (for details see Stokes and Evans 1997).

Characterizing and assessing the stability of colloids can be achieved through various experimental techniques and theoretical models, including dynamic light scattering, zeta potential, sedimentation tests, and rheological analysis. Dynamic light scattering (DLS) is a common technique used to measure colloidal particles' size distribution and stability by analyzing the intensity fluctuations of scattered light caused by Brownian motion. This method provides information about the particle size and the presence of any changes or aggregation over time. Zeta potential measurements assess the surface charge of colloidal particles and can provide insights into the stability of the system (see Chap. 3). The zeta potential represents the electrostatic potential at the shear plane, which is the boundary between the particle surface and the surrounding medium. A higher absolute value of zeta potential indicates greater repulsive forces between particles, leading to increased stability. Sedimentation tests involve monitoring the rate at which colloidal particles settle under the influence of gravity or centrifugation. Faster settling rates indicate lower stability, while stable colloids show minimal or no sedimentation over time. Rheological analysis is also useful for studying the flow and mechanical properties of colloidal systems as well as changes in dispersed particle size (see Chap. 7).

In addition to experimental techniques, theoretical models and simulations are employed to gain a deeper understanding of colloid stability. These models consider factors such as interparticle forces, Brownian motion, and thermodynamic properties to predict the stability of colloidal systems. These models provide insights into the underlying mechanisms governing stability by incorporating parameters such as particle size, surface charge, and interactions between particles. The DLVO (Derjaguin-Landau-Verwey-Overbeek) theory is a widely applied model for understanding the stability of colloidal systems based on the interparticle forces. It considers the combined effects of van der Waals forces and electrostatic forces between colloidal particles.

The DLVO theory predicts stability by comparing the attractive van der Waals and repulsive electrostatic forces. The total potential energy function that describes the interactions between colloidal particles is a classical method to describe the colloidal stability since it incorporates parameters, such as van der Waals forces, electrostatic forces, steric repulsion, and solvent-mediated interactions. Monte Carlo Simulations are computational methods used to model and simulate the behavior of colloidal systems. These simulations involve randomly sampling configurations of colloidal particles based on the interactions and forces between them. By calculating the system's total energy and allowing the particles to move and interact, Monte Carlo simulations can provide insights into the stability, phase behavior, and self-assembly of colloidal systems. Molecular dynamics (MD) simulations replicate the behavior of individual particles in a colloidal system over time, using classical mechanics and considering interatomic forces to model the motion and interactions

of particles. MD simulations can provide information about colloidal systems' diffusion, aggregation, and structural properties. Brownian dynamics simulations focus on modeling the motion and behavior of colloidal particles under the influence of Brownian movement. It incorporates stochastic forces to simulate the random thermal motion and interactions of particles, predicting the aggregation, diffusion, and transport properties of colloids.

References

- Adamson AW, Gast AP. Physical chemistry of surfaces. John Wiley & Sons, Inc.; 1997.
- Davies JT, Rideal EK. Interfacial Phenomena. Academic Press; 1963.
- de Gennes P, Brochard-Wyart F, Quere D. Capillarity and wetting phenomena: drops, bubbles, pearls, waves. Springer Science Business Media New York; 2004.
- Everett DH. Basic principles of colloid science. The Royal Society of Chemistry; 1989.
- Harkins WD. The physical chemistry of surface films. New York: Reinhold; 1952.
- Holmberg K, Jönsson B, Kronberg B, Lindman B. Surfactants and polymers in aqueous solution. 2nd ed. Wiley; 2002.
- Porter MR. Handbook of surfactants. New York: Springer Science + Business Media; 1993.
- Rosen M. Surfactants and interfacial phenomena. New York: Wiley; 1989.
- Starov VM. Nanoscience: colloidal and interfacial aspects. CRC Press; 2010.
- Stokes RJ, Evans DF. Fundamentals of interfacial engineering. Wiley-VCH; 1997.
- Tadros, TF. Formulation science and technology: basic theory of interfacial phenomena and colloid stability. De Gruyter; 2018.

Chapter 2

Colloidal and Self-Assembly Systems



Colloidal dispersions are systems containing dispersed particles with sizes typically between 1 and 1000 nm evenly distributed throughout the continuous phase, which can be a liquid, solid, or gas. They are generally complex mixtures that exhibit a wide range of physical and chemical properties, making them useful in a variety of scientific and technological applications, such as drug delivery, food processing, and nanotechnology. Some physical and chemical properties, including Brownian motion, surface area, and surface charge govern the behavior of colloidal solutions. Brownian motion refers to the random movement of particles in a fluid, caused by collisions with solvent molecules. This movement keeps the particles suspended and prevents them from settling out. The surface area of the particles in a colloidal solution is huge compared to their volume, which makes them highly reactive and capable of adsorbing other molecules or ions onto their surfaces. This property can be used in many applications, such as in water treatment, where colloidal particles can adsorb contaminants from the water. Most colloidal particles have a net charge on their surfaces, which can be positive or negative, depending on the nature of the particles and the surrounding medium. This charge can influence the stability of the colloidal solution by affecting the way in which the particles interact with each other and with the solvent molecules. Micelles are colloidal particles formed by the association of surfactant compounds driven by energy minimization. Surfactants display the ability to adsorb on the interface, altering the interfacial energy and self-associating into ordered structures with well-defined colloidal dimensions. The Hydrophobic-hydrophilic dualistic affinity of surface-active agents by the solvents demands a response to minimize the unfavorable interactions. Hydrophobic and hydrophilic interactions are opposite effects influencing the kinetics and dynamics of many processes in chemistry, biochemistry, and physics.

2.1 Surface Active Agents

Amphiphilic molecules are compounds containing both hydrophilic and hydrophobic portions linked by covalent bonds on their molecular chemical structure, exposing chemical affinity to both aqueous and oily phases, named amphipathy or amphiphilicity. Figure 2.1 illustrates the typical chemical structure of amphiphilic compounds. The lyophilic-lyophobic dual nature of amphiphilic molecules in a given solvent produces a thermodynamic incongruity that guides the system to a unique ordering and outlines its principal properties, such as it occurs in dyes, drugs, bile salts, surfactants, and other macromolecules (for details on behavior of amphiphiles in solution see Porter 1993; Tadros 2018). It must be highlighted that both hydrophilic and hydrophobic portions of the amphiphilic molecules must be much more complex than the simplified illustration in Fig. 2.1 since they are usually composed of intricate chemical functionalities.

A fundamental aspect of amphiphilic molecules elapses from the affinity between their dualistic moieties and the solvent, leading to singular properties related to the surface activity and self-organization in solution. Surfactants (an acronym for surface active agents) are representative amphiphilic compounds with distinctive hydrophilic and hydrophobic groups that concede a pronounced surface activity to the species. Surfactants display the ability to adsorb on the interface, altering the interfacial energy, and self-associate into ordered structures with well-defined colloidal dimensions. The interfacial energy, given by energy unit per unit area, represents the minimum amount of work required to create a unit area—it is the main property measured from interfacial tension determination.

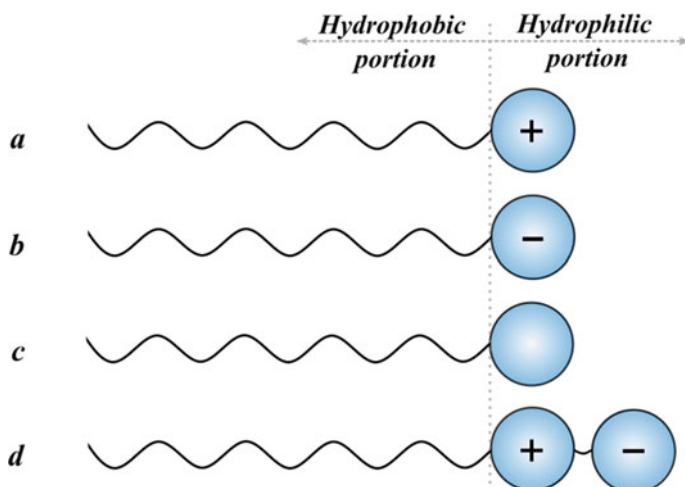


Fig. 2.1 Simplified illustration of the typical chemical structures of amphiphilic compounds. **a** Cationic surfactant. **b** Anionic surfactant. **c** Nonionic surfactant. **d** Zwitterionic surfactant

The primary characteristics of conventional surface-active agents result from the attempt to maintain the lyophobic group immersed in a particular solvent as an imposition from the lyophilic group that completes the molecule. In these systems, the hydrophobic portion expresses a solid tendency to escape from contact with the solvent, triggering the surface adsorption phenomenon. A gradual addition of amphiphilic molecules into the solvent leads to their successive accumulation of molecules on the interface, carrying out the system to an equilibrium state where the complete covering of the surface area is achieved—titled *surface saturation*. Further amphiphile adding would leave aggregation as the only possible choice for the lyophobic portion to avoid contact with the polar medium, conducting to the formation of self-assembly structures (for details see Holmberg et al. 2002).

It is evident by means of this discussion that amphiphile aggregation is driven by the low solubility of the hydrophobic moiety (in polar solvent) and the hydrophilic moiety (in non-polar solvent). The low solubility of weakly interacting hydrophobic groups in polar solvents results from the high cohesive energy between solvent molecules, and it consequently arises from the hydrophobic interactions. For a given hydrophobic moiety, the higher the solvent cohesive energy, the higher the aggregation driving force. Table 2.1 displays data of the Hildebrand Solubility Parameter as an expression of the cohesive energy of several solvents. This phenomenon is related to the solubility of non-polar species (such as hydrocarbons) in a high-cohesion solvent (such as water) (for details see Davies and Rideal 1963; Adamson and Gast 1997).

Surfactants are usually categorized according to the chemical characteristics of their hydrophilic group as nonionic, anionic, cationic, and zwitterionic (see Fig. 2.1). Nonionic surfactants are non-electrolytes and non-charged compounds, containing nondissociative hydrophilic groups. This aspect makes them tolerant to the addition of inorganic salts in aqueous solutions. Nonionics can adsorb on both hydrophilic and hydrophobic surfaces without generally a significant alteration in the surface charge. They are well-known emulsifier agents used in a wide range of applications because of their intense detergency activity, including cosmetics, herbicides, and pharmaceuticals.

A class of ionic surfactants, which carry out electrical charges on their structure, comprises anionic, cationic, and zwitterionic surfactants. Anionic surfactants are electrolyte compounds that dissociate, leaving a cation from the hydrophilic portion when dissolved in an aqueous solution. The surface-active agents are the associated anion. They are characterized by strong adsorption on surfaces, attributing to the surface a negative charge. Anionic surfactants commonly have strong detergency and foamy power. Cationic surfactants are also electrolytes that dissociate, producing surface-active agents as a positively charged structure in aqueous solutions. Since cationic surfactants are prone to adsorb on negatively charged surfaces through electrostatic attraction, orienting their hydrophobic moiety into the solution results in a hydrophilic surface with sometimes a neutral charge. Since live organisms have negative surfaces, including proteins and nucleic acids of bacteria, cationic surfactants are commonly used in the formulation of fabric softeners and germicides. Zwitterionic surfactants are surface-active compounds able to accommodate both positive and

Table 2.1 Hildebrand solubility parameters for some common substances

Substance	δ (MPa ^{1/2})
n-Pentane	14.4
n-Hexane	14.9
n-Heptane	15.3
Diethyl ether	15.4
n-Dodecane	16.0
Cyclohexane	16.8
Carbon tetrachloride	18.0
Ethyl acetate	18.2
Toluene	18.3
Benzene	18.7
Chloroform	18.7
Methyl ethyl ketone	19.3
Acetone	19.7
Methylene chloride	20.2
Pyridine	21.7
n-Propyl alcohol	24.9
n-Butyl alcohol	28.7
Methyl alcohol	29.7
Ethylene glycol	34.9
Water	48.0

negative charges on their structures at the same time. Their ionic nature can change according to the pH of the solution, allowing neutral, positive, and negative charges on the molecule. This aspect enables the zwitterionic surfactants to adsorb in turn on positively charged and negatively charged surfaces, keeping still a surface net charge. Zwitterionic surfactants are generally used as cosurfactants in cleaning and foamy product formulation.

The hydrophobic portions have a minor effect on the surfactant nature. These groups are generally C₈-C₂₀ hydrocarbons derived from either fossil or renewable sources, containing a broad type of organic structures, including straight and branched alkyl chains, alkylbenzene and alkyl naphthalene derivatives, perfluoroalkyl groups, and sugar- and lignocellulose-derived groups. On the other hand, the characteristics of the hydrophilic groups strongly impact the surface-active application. For instance, branched and unsaturated chains promote lower surfactant insolubility in polar solvents than the corresponding straight and saturated chains, whereas straight and saturate chains tend to gather in a closer surface packing and solution self-assembly.

Front of a wide range of types of surface-active agents, the selection of the proper agent for a specific application must consider (i) the nature of the interfacial phenomena involved in the application (it means, cleaning, wetting, emulsification, aggregation, and so on), and (ii) structural and physical-chemistry properties of the surfactant (it means their nature, solubility, chemical affinity, biodegradability, and so on). Since surfactants account for a significant fraction of the cost in almost of formulations, economics must be carefully well thought out. Finally, scientific screening of previous experiences and usage can avoid time-consuming trials and deflect unsuccessful scenarios. Surfactant performance can be evaluated employing two main parameters: *efficiency* and *effectiveness* (for details see Rosen 1989). The surfactant *efficiency* is defined by the ratio between the surfactant surface concentration ($C_{\text{interface}}$) and surfactant bulk concentration (C_{bulk}) at the equilibrium and it is related to the Gibbs energy change (ΔG) that occurs during the displacement of the surfactant from the solution bulk to the interface, which is given by Eq. 2.1. The surfactant *effectiveness* represents the surfactant's effective action to achieve a given limiting phenomenon, such as surface saturation and surface tension reduction. Thus, *effectiveness* is used to compare the performance of different surfactants on the same phenomena.

$$\frac{C_{\text{interface}}}{C_{\text{bulk}}} = \exp\left(-\frac{\Delta G}{RT}\right) \quad (2.1)$$

2.2 Interfacial Adsorption of Surface-Active Agents

The adsorption of amphiphiles on interfaces is governed by physical interactions—termed physisorption—, consisting of the fundamental dispersion forces and electrostatic interactions, in contrast to the chemical adsorption. The adsorption of surface-active agents from an aqueous solution bulk into liquid–gas (L-G), liquid–liquid (L-L), and solid–liquid (S-L) interfaces is driven by the low solubility of hydrophobic groups in high cohesive-energy solvents (see data in Table 2.1) that arises from the hydrophobic interactions. The strong cohesive energy of water (about 146 mJ m^{-2}) overcomes the adhesion work between hydrophobic chains and water (about 50 mJ m^{-2} for alkyl chains), moving the water molecules away from the vicinity of the hydrophobic chains where the potential energy of water molecule is high due to the molecular ordering. To overcome the entropy reduction, the hydrophobic moiety goes to adsorb on the interface where it can withdraw from the water interactions, restoring a dynamic equilibrium state. Due to the high cohesive energy of the water, the total energy of the system increases, carrying it to an unstable state.

Then, the scape of amphiphilic molecules from the solution bulk to avoid the interactions between the hydrophobic moieties with water (or other polar solvents)

constitutes a thermodynamic process similar to phase separation, leading to a lower energy state. The amphiphile adsorption on interfaces is typically accompanied by a significant entropy increase caused by the breaking of interactions between the hydrophobic moiety and water molecules, releasing the water molecules back to the solution bulk. The result is a large and negative Gibbs energy, indicating obviously a favorable process, even with a minor enthalpic contribution. Equation 2.2 gives the adsorption Gibbs energy.

$$\Delta G_{ad} = \Delta H_{ad} - T \Delta S_{ad} \quad (2.2)$$

The increases in the hydrophobic character of the amphiphilic molecules leads to a reduction of their solubility in polar solvents and, consequently, to more pronounced surface activity. For a homologous series of a given hydrophobic chain, a general behavior states that there will be a maximum length chain to balance the hydrophobic character of the molecule and its solubility in water. This behavior is named *Fergusson effect*. The solubility X_i of hydrocarbon compounds depends on their relative activity (a_i) in solution and the heat of solution, which can be expressed by Eq. 2.3. The argument of the exponential on the right side of Eq. 2.3 represents the heat of solution, where V_i is the hydrocarbon molal volume, φ_s is the solvent volume fraction, and δ_i and δ_s represent the solubility parameters of the hydrocarbon and the solvent, respectively. Since the difference between the solute and the solvent solubility parameters is kept about constant for a hydrocarbon homologue series, the heat of solution is approximately proportional to the hydrocarbon chain length, and consequently the logarithm of the solubility of hydrocarbon compounds displays a linear decay with the chain length growth. The heat of solution of surfactant solutions is enabled to be accurately measured by advanced calorimetric methods.

$$X_i = a_i \cdot \exp \left[- \frac{V_i \cdot \varphi_s^2 \cdot (\delta_i - \delta_s)^2}{RT} \right] \quad (2.3)$$

It is important to recall the total heat of solution for ionic solids is composed of two main terms: (i) The lattice enthalpy, energy applied to separate ions in the crystalline structure into individual gaseous ions, and (ii) the hydration enthalpy, energy change due to the surrounding of individual gaseous ions by water molecules (see details on solubilization of chemical species in Shinoda 1991).

The affinity of the hydrophilic groups with water molecules acts contrarily to the amphiphile insolubility, attempting to keep the amphiphile molecule in the solution bulk. The hydration of the hydrophilic group avoids the total expelling of the amphiphile molecule from the solution and therefore its phase separation. The hydrophilic group hydration is similar to the hydration of atomic ions, where water molecules are clustered in the vicinity of the charged particle by mainly ion–dipole interactions.

Experimental adsorption data are of foremost importance to determining the concentration and orientation of amphiphilic molecules at the interface and determining the energy changes involved in interfacial processes in which species adsorb on surfaces. The concentration of amphiphiles at the interface is a measure of the molecule amount covering the surface area (and the extension of the covered area by a given number of molecules), whereas the molecular surface orientation is defined by the surface hydrophilicity and intermolecular interactions occurring between the species and the surface as well as between the species themselves.

The relationship between surface activity and species accumulation at the interface is given by the Gibbs adsorption equation (see Chap. 5), which provides an indirect way to determine the amount of interfacially adsorbed material per unit area from experimental measurements of interfacial tension. The adsorption of molecules at the interface results in the formation of films or oriented molecular layers, whose thickness depends on the quantity and orientation of the molecules. Interfacial films formed by a single layer of molecules (termed *monomolecular films* or *molecular monolayers*), especially those with high surface concentrations, are often disposed of in a straightforward arrangement. The accurate study of monolayer properties can provide scientific evidence about size, shape, and orientation of the adsorbed molecules (see details in Chap. 5).

2.3 Surfactant Solubilization and Critical Concentration

The dualistic affinity of surface-active agents by the solvents demands a response to minimize the rise of the system energy produced by unfavorable interactions. The escape of the surfactant molecules from the solution bulk, followed by their adsorption on the interfaces, is the (natural) primary mechanism leading to the energy reduction. The increase of the surfactant concentration in solution promotes a progressive accumulation of surfactant molecules in the interface up to the surface saturation, where it is recognized the complete covering of the surface area.

At higher surfactant concentrations, the hindrance of the surfactant to adsorb on the surface enables an alternative mechanism to reduce the Gibbs energy of the system: *aggregation*. By means of the aggregation mechanisms, surfactant molecules arrange themselves in thermodynamically stable molecular structures in which the unfavorable interactions are evaded, producing an overall reduction of the system Gibbs energy. Figure 2.2 illustrates the general routes naturally adopted for the decrease in the Gibbs energy of systems containing surfactants in solution. It demonstrates the surfactant solvation as monomers, its adsorption on the surface, and then the surfactant aggregation. At specific conditions, crystallization can take place.

The aggregation produces abrupt changes in the physical–chemical properties of the surfactant solution, including interfacial tension, conductivity, density, and detergency. The concentration at which the surfactant aggregation produces micelles is termed *Critical Micelle Concentration* or *Critical Micellization Concentration* (CMC). CMC denotes a notable change in the solution bulk due to the alteration

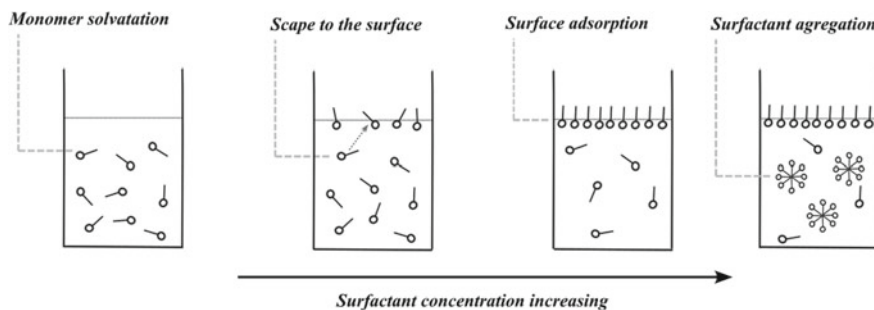


Fig. 2.2 General behavior of the surfactant in solution: Equilibrium to minimize the unfavorable interaction between surfactant molecule and solvent

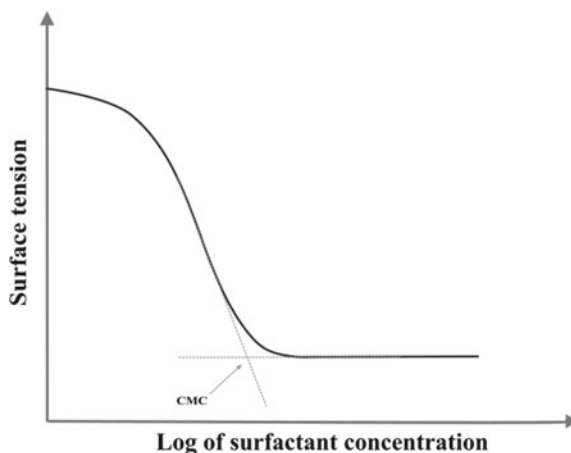
of the nature of the solubilized species. Changes in surface tension (associated with the adsorption), in electrical conductivity (associated with the variation in the mass per charge unit), and turbidity (associated with the presence of species with greater size) are common evidence of the aggregation of surfactants at well-defined concentrations. Surface tension is the primary method to determine the critical micelle concentration employing experimental measurements (see Chap. 5). Curves of surface tension (γ) against surfactant concentration (C) display a markable break, corresponding to the CMC.

Figure 2.3 displays a typical surface tension—concentration plot for conventional surfactant solutions, given by γ versus $\log C$. For concentration below the CMC, the surface tension decreases about linearly with the increase in the surfactant concentration. Above the CMC, the surface tension remains effectively unchangeable, denoting a maximum value of surface concentration, which is equivalent to the surface saturation found in the CMC. However, the surface saturation concentration can be considerably lower than the CMC, especially for ionic surfactants, due to the counterion concentration close to the interface. Even after reaching the surface saturation concentration, surface tension can decline because of the increase of the surfactant activity in the solution.

The process of aggregate formation resembles the crystallization process of conventional solutes where single chemical species are associated to form a solid crystal or a crystalline hydrate (see details on crystallization in Mersmann 2001). During the aggregation, monomers are consumed to produce aggregates. At concentrations higher than CMC, monomers and aggregates can co-exist, but aggregates will be the predominant state. In this way, the overall surfactant solubility depends on both the surfactant monomer solubility and their ability to arrange as micellar aggregates.

Surfactant solubility is strongly dependent on the surfactant nature and the temperature, displaying a singular behavior on the solubility—temperature curve. Ionic surfactants exhibit an abrupt growth of solubility at a specific critical temperature, defined as *Krafft temperature* (T_k). The *Krafft temperature* is the temperature at

Fig. 2.3 Typical plot of surface tension against the logarithm of the surfactant concentration in the bulk solution



which the surfactant solubility is equal to its CMC. Figure 2.4 shows the solubility—temperature curve for an ionic surfactant. Below the *Krafft temperature*, the surfactant solubility is relatively low, and it is governed by the crystal lattice energy and the heat of hydration. Above of the *Krafft temperature*, the solubility of the surfactant monomer is substantially high to enable the aggregation process.

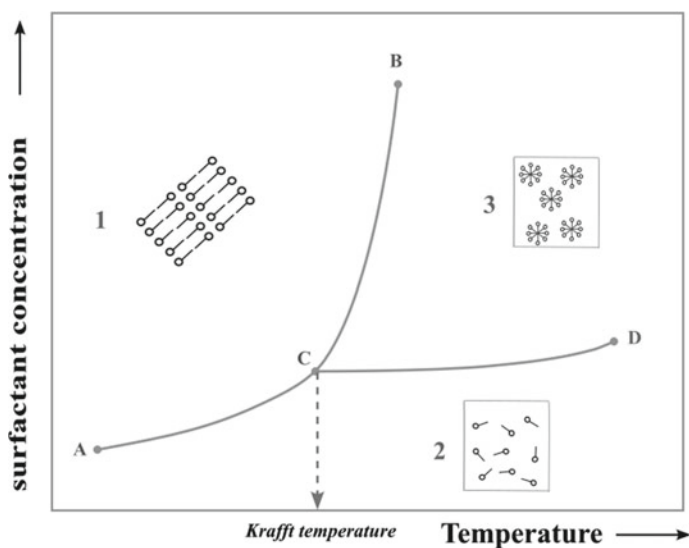


Fig. 2.4 Phase diagram of the surfactant behavior in dilute solution. Segment AB represents the solubility—temperature curve. Segment CD represents the CMC—temperature curve

Figure 2.4 shows the *Krafft point* on the surfactant concentration—temperature diagram as the intersection point between the solubility-temperature and the CMC-temperature curves. In Region 1, the surfactant is found as a solid hydrated crystal. In Region 2, surfactant constitutes a molecular solution as solvated monomers. In Region 3, the surfactant is found as micelles in equilibrium with molecularly dispersed monomers.

The mechanism of solubilization of ionic and nonionic surfactants is quite dissimilar. In contrast with ionic surfactants, the solubility of nonionic surfactants decreases with the temperature increase, indicating a lower critical solution temperature. The temperature increasing produces a steep growth of the micelle size of nonionic surfactants and a reduction of the intermicellar repulsion, carrying the system to a reversible two-phase state composed of a dilute solution of surfactant and a surfactant-rich micellar solution. The system is then revealed as a visibly turbid suspension. The temperature at which the phase separation occurs is termed *Cloudy point*.

2.4 Surfactant Self-Assemble Structures

Self-assembly is an auto-organizing process wherein amphiphilic macromolecules are spontaneously associated through physical interactions into ordered units of species, building complex structures from single components, whose the size and shape are prone to change in response to the alteration of the composition, temperature, and pressure. One well-known example of molecular self-assembly is the formation of lipid bilayers, which are essential components of cell membranes. Lipid molecules, such as phospholipids, self-assemble into bilayer structures due to their hydrophobic (water-repelling) tails and hydrophilic (water-attracting) heads. The hydrophobic tails interact with each other, forming a hydrophobic inside, while the hydrophilic heads interact with the surrounding water, creating a hydrophilic outside. Another example of molecular self-assembly is the formation of protein structures, such as the folding of individual protein molecules into their characteristic three-dimensional shapes. The stability of these structures is influenced by various intermolecular forces, including electrostatic interactions, hydrogen bonding, hydrophobic interactions, and van der Waals forces. Then, the chemical characteristics of the hydrophilic and hydrophobic groups and their interactions with the solvent will exert a crucial influence on molecular associative arrangement.

The molecule gathering through the aggregation process will conduct to an associative structure with lower energy. For the aggregation to promote an effective detachment of the contact between hydrophobic moiety and water, gathering a substantial number of surfactant molecules is necessary. The aggregate form and size depend strongly on the chemical structure of the surfactant molecule, its concentration in solution, and temperature. Typical aggregate structures include micelles, liquid crystals, and lamellae. Micelles are molecular aggregates with specific form parameters, displaying usually spherical, cylindrical, and planar shapes. Figure 2.5 depicts a simplified illustration of the micelle and other associative structures.

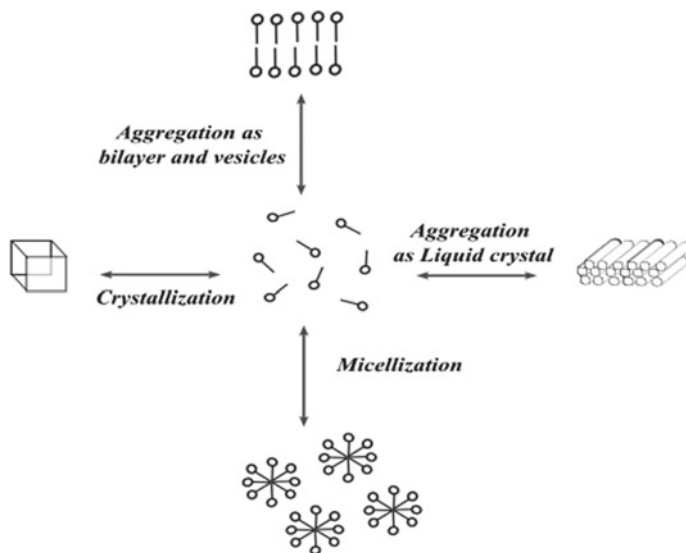


Fig. 2.5 Aggregation routes carrying the surfactant in solution to the associative structures with reducing surface energy

At high concentrations, the periodic long-range ordering of micelles may result in liquid crystal structures. Micelles have well-defined forms and sizes. If the resulting aggregate has not the micelle characteristics, the aggregation concentration is termed *Critical Aggregation Concentration (CAC)*.

Although the aggregation leads to a minimization of unfavorable interactions between hydrophobic groups and solvent molecules, therefore, reducing the Gibbs energy, the molecule regular ordering produces a loss of freedom, and many times repulsive forces between the groups narrowed internally in the aggregate. The occurrence of aggregation phenomena depends on the balance of factors affecting the thermodynamic equilibrium.

2.5 Mechanism of Micellization

Micelles behave as a substance in liquidlike state, and they represent the simplest self-assembly structures. The aggregative process to form micelles can be characterized by well-defined and experimentally proved aspects: (i) the surfactant solubility, given by the critical micelle concentration, (ii) the micelle size, given by the aggregation number, and (iii) the micelle shape, given by the packing parameter. Surfactant solubility is related to the interactions taken between surfactant molecules and solvent, as previously discussed.

The micellization is somewhat similar to the solid particle aggregation, however, micellar aggregates reach an equilibrium particle size, instead of flocculating and grow into macroscopic dimensions. The classical theory of micelle formation involves two main concepts: (i) the mass action law, which considers surfactant monomers and micellar aggregates as species in chemical equilibrium—termed the *closed-association model*—, and (ii) the phase separation, which considers surfactant monomer solution and micellar aggregates as two distinct phases—termed *pseudophase model*. The micellization concepts are both based on classical thermodynamics (for details see Hunter 2001).

The closed-association model considers micellization as the assembling of a number of surfactant monomers (N) producing one aggregate (S_N) by means of the relation given in Eq. 2.4.



The corresponding equilibrium constant for micellization can be written according to Eq. 2.5. The brackets indicate the concentrations of the species in the solution. In this case, species activity has been replaced by species concentrations, considering the activity coefficients for the species equals unity since the process must occur at low concentration.

$$K_N = \frac{[S_N]}{[S]^N} \quad (2.5)$$

The molar (standard) Gibbs energy for the formation of micelle is expressed by Eq. 2.6.

$$\Delta G(N) = -RT \cdot \ln K_N \quad (2.6)$$

Replacing Eq. 2.5 into Eq. 2.6, the standard Gibbs energy of micelle formation per mole of surfactant monomer will be written as Eq. 2.7. The closed-association model describes the initial and final stages of the micellization process, going from the individual surfactant molecules to surfactant aggregate structures.

$$\Delta G_{mic} = -\frac{RT}{N} \cdot \ln[S_N] + RT \cdot \ln[S] \quad (2.7)$$

The *pseudophase* model considers the micellization as a phase *pseudoseparation* process leading to a two-phase system constituted by a solution, where the individual surfactant is solvated, and a micellar pseudophase, where the surfactant is self-associated. From this point of view, the standard energy of micelle formation (ΔG_{mic}) can be designated by the difference between the standard chemical potential of the surfactant in the micelle ($\mu_{micelle}$, final thermodynamic state) and the standard chemical potential of the surfactant in the dilute solution ($\mu_{solution}$, initial thermodynamic state), as illustrated in Eq. 2.8.

$$\Delta G_{mic} = \mu_{micelle} - \mu_{solution} \quad (2.8)$$

For dilute solutions, such as those found below the critical micelle concentration, the difference in the chemical potential will be a function of the solute concentration. At the start of the micellization process, the surfactant concentration equals CMC. Then, the standard energy of micelle formation can be obtained from Eq. 2.9.

$$\Delta G_{mic} = RT \cdot \ln CMC \quad (2.9)$$

Since Eq. 2.9 is related to the CMC, it is circumscribed to the starting conditions for surfactant self-assembly, failing to describe the aspects such as the size and shape of the aggregates achieved at the end of the assembling process. Anyway, Eq. 2.9 is a valuable tool to obtain a reasonable estimative of the standard energy of micelle formation from the CMC data, which can be accurately assessed by single experimental methods.

For ionic surfactants, the standard energy of micelle formation must consider the equilibrium between the ionized monomer, the counterions, and the micelles. In these systems, counterions occupy the area close to the charged headgroups, reducing the electrostatic repulsion among the ionized micelles. Charged surfactant aggregates are characterized by counterion binding, and their standard energy of micelle formation can be expressed by Eq. 2.10. The parameter β is the degree of dissociation of the micelle.

$$\Delta G_{mic} = (2 - \beta) \cdot RT \cdot \ln CMC \quad (2.10)$$

The theory of molecular self-assembly can be described mathematically using a thermodynamic approach. The Gibbs energy provides a rigorous way to determine the stability state of self-assembled structures based on the interaction heat and entropy.

The energy minimization occurring in the aggregation process will point out the system spontaneity to reach the final thermodynamic state. However, the single variation of enthalpy and entropy is not enough to describe the formation of complex aggregative structures in solution. At low concentrations, the Gibbs energy of surfactant self-assembly involves three key features:

- (i) hydrophobicity, acting favorably to carry out the hydrocarbon chains into the aggregate inner region due to the positive change in the Gibbs energy caused by surfactant nonpolar moiety and water,
- (ii) surface forces, acting dualistically on the surfactant association. Keeping the surfactant headgroups together to minimize interactions between hydrocarbon and water is favorable to the micellization; keeping the surfactant headgroups distant themselves by means of electrostatic repulsion, hydration, and steric hindrance is unfavorable to the micellization, and
- (iii) packing factor, a geometrical restriction to the aggregate shape.

The features related to the energy interactions involved in the Gibbs energy change of surfactant self-assembly lead to a simplified decomposition of the standard energy

of micelle formation into three main terms as

$$\Delta G_{mic} = \Delta G_{hydrophobic} + \Delta G_{packing} + \Delta G_{headgroup} \quad (2.11)$$

The $\Delta G_{hydrophobic}$ is the hydrophobic Gibbs energy contribution. The $\Delta G_{hydrophobic}$ represents the Gibbs energy change for the full transference of the hydrocarbon chain from the solvent into the micelle. It can be assessed from the transferring energy for hydrocarbon chains from the water into an oily phase. The $\Delta G_{hydrophobic}$ can be figured out by the Eq. 2.12.

$$\Delta G_{hydrophobic} = A - B \cdot n_c \quad (2.12)$$

A and B are constant parameters related to the chemical structure of apolar compounds. n_c stands for the total number of carbon atoms of the hydrocarbon compound.

The hydrophobic Gibbs energy contribution considers the apolar chains have been completely excluded from contact with the water. However, even after the migration to the micelle structure, the apolar chain is still exposed to considerable contact with the solvent, producing a positive Gibbs energy change (labeled ΔG_{hcsol}) that must be added to the hydrophobic energy contribution. This energy change is proportional to the aggregate external area, similarly to the surface Gibbs energy, and it can be expressed as a function of the aggregate surface area (A_{mic}) and the number of molecules in the aggregate (N), such as it can be seen in Eq. 2.13. In Eq. 2.13, the parameter b is a coefficient related to the surface tension of the system containing the aggregate.

$$\Delta G_{hcsol} = b \cdot \frac{A_{mic}}{N} \quad (2.13)$$

The conformational effects raised from the change of the monomer solution into the micellar aggregate result in a loss of the chain conformational freedom produced by micelle-solvent interaction and constraining between neighborhood chains. The overall effect is a positive Gibbs energy contribution due to the molecular packing ($\Delta G_{packing}$), which can be simply described by Eq. 2.14. The parameter a is a constant and the parameter b represents a coefficient related to the surface tension of the system containing the aggregate. Noticeably, the Gibbs energy contribution attributed to the molecular packing is strongly dependent on the molecular structure of the surfactant.

$$\Delta G_{packing} = a - b \cdot \frac{A_{mic}}{N} \quad (2.14)$$

The interactions involving the headgroup of the surfactant molecules give raise to a strong energy contribution ($\Delta G_{headgroup}$) that affects significantly the micellization Gibbs energy. Whereas the hydration of the hydrophilic group opposes micellization, the lateral interaction between the headgroups constituting the micelle surface

depends on the headgroup nature, and its surface charge, size, polarity, and so on (for details on the description of the headgroup interaction in the micellization process see Evans and Wennerstrom 1999).

2.6 Micelle Structure and Shape

The self-assembly of amphiphiles into well-defined structures, such as micelles and bilayers, is governed by forces that arise primarily from two fundamental interactions occurring at the hydrocarbon-water interface. Hydrophobic attraction, which induces the amphiphilic molecules to associate, occurs between the hydrophobic (water-repelling) regions of the amphiphiles, driving them to cluster together in order to minimize their contact with the surrounding water molecules. Hydrophilic, ionic, or steric repulsion of the headgroups, which arises from the hydrophilic (water-attracting) or charged regions of the amphiphiles, acts as a counterforce to the hydrophobic attraction, preventing complete aggregation of the hydrophobic regions and ensuring that the headgroups remain in contact with water. In nonpolar media, the structure of micelles exhibits a reversed arrangement compared to polar media. In this case, the interior region of the micelles is composed of hydrophilic heads, while the outer region encloses the hydrophobic groups.

The two opposing interactions—hydrophobic attraction and hydrophilic/repulsive forces—constitute the primary driving forces in the interfacial region of self-assembled amphiphiles (for details on forces in self-assembly systems see Israelachvili 2011). They compete with each other, resulting in an intricate energy balance. The hydrophobic attraction tends to decrease the interfacial area per molecule exposed to the aqueous phase, while the hydrophilic/repulsive forces tend to increase it. The interplay between these opposing forces gives rise to the self-assembly of amphiphiles into well-defined structures, enabling the formation of micelles, bilayers, and three-dimensional networks.

The interfacial energy contribution of total attractive interactions driving the amphiphile self-assembly can be simplified as the product $\gamma \cdot a$, where the constant γ is the strength of the attractive forces, typically ranging between 20 and 50 mJ m^{-2} . a represents the molecular surface area. The repulsive contributions involved in the amphiphiles self-assembly are highly complex and challenging to be explicitly express. Nevertheless, their combined influence can be accounted for by considering the overall repulsive energy as inversely related to the surface area occupied per headgroup, which simplifies the analysis of self-assembly phenomena. Figure 2.6 illustrates the energy balance occurring in molecular self-assembling.

The total interfacial energy resulting from the repulsive and attractive forces in a given hydrophilic-hydrophobic interface can be represented by Eq. 2.15, where μ is the total interaction energy, γ is the interfacial energy, a is the molecular surface area, and k is a constant parameter.

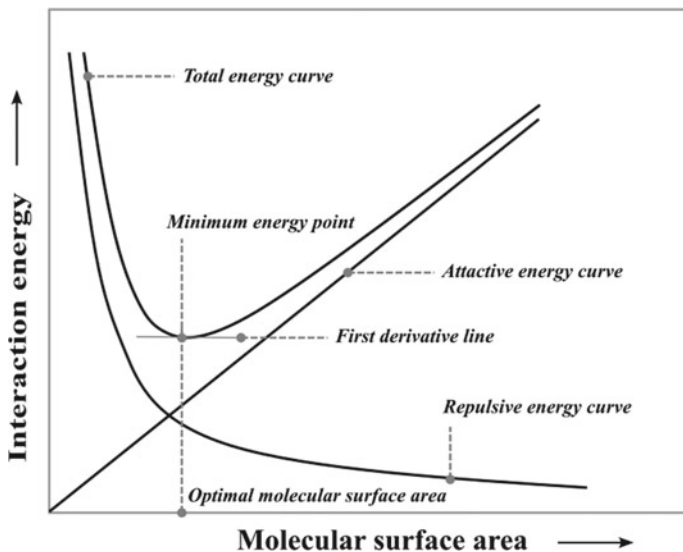


Fig. 2.6 Balance between attractive and repulsive forces leading to the surfactant aggregation

$$\mu = \gamma \cdot a + \frac{k}{a} \quad (2.15)$$

The minimum interaction energy is mathematically defined when the first derivative of the interaction energy against the area equals to zero, which results in Eq. 2.16.

$$a_o = \left(\frac{k}{\gamma} \right)^{\frac{1}{2}} \quad (2.16)$$

Substituting the unknown constant k from Eq. 2.16 into the Eq. 2.15 results in the description of the total interaction energy as a function of the surface area per molecule using two measurable parameters, γ , and a_o , such as represented in Eq. 2.17.

$$\mu = 2 \cdot \gamma \cdot a_o + \frac{\gamma}{a} \cdot (a - a_o)^2 \quad (2.17)$$

The parameter a_o is defined as the optimal surface area per molecule headgroup to achieve the self-assembly minimum energy. Consequently, the minimum interaction energy will be given by Eq. 2.18.

$$\mu_{min} = 2 \cdot \gamma \cdot a_o \quad (2.18)$$

The micelle shape is governed by the optimal surface area of the hydrophobic headgroups (a_o) and the packing of the hydrophobic groups of the surfactant

molecule. The hydrophobic group packing is related to their volume (v_H) and length in the micellar core. In aqueous media, the hydrophobic moieties are confined in the inner region of the micelle. Therefore, the hydrophobic chain defines the micelle internal radius, which can reach the length of the full extended chain. The critical chain length (l_c) stands for the upper limit of the effective length that the chains can reach. The l_c is a semiempirical parameter that represents to some extent the approximate cutoff distance. It writes down the length at which hydrocarbon chains can no longer be considered fluid. Although the precise l_c value is not well-defined, it is expected to be comparable to, albeit slightly shorter than, the fully extended molecular length of the chains (l_{max}).

The critical chain length (l_c) and the volume occupied by the hydrophobic group (v_H) can be figure out from the Eq. 2.19 (given in nm) and Eq. 2.20 (given in 10^{-3} nm³), respectively.

$$l_c \approx 0.154 + 0.165 \cdot n \quad (2.19)$$





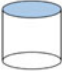

$$v_H \approx 27.4 + 26.9 \cdot n \quad (2.20)$$

For a certain optimal surface area (a_o), hydrocarbon chain volume (v_H), and critical length (l_c) for a specific surfactant molecule, it is possible to determine the most suitable structures in which the molecules can arrange themselves within imposed geometric constraints. The achievable aggregate structures are conveniently analyzed by a dimensionless parameter termed as the *critical packing parameter* (or *packing factor*). The packing parameter is defined as the ratio $v_H/(a_o \cdot l_c)$, and it supplies the micelle shape achieved within the prescribed geometric limitations. Table 2.2 displays the corresponding structures of the micelle according to the packing parameter.

The micelle geometric configuration is closely related to the quantity of gathered surfactant molecules. The micellar aggregation number refers to the average number of surfactant molecules that come together and assemble to form a single micelle. The micellar aggregation number is primarily related to the size of the micelle rather than its specific shape; however, it provides a useful indication of the size and capacity of the micelle to solubilize or encapsulate other molecules within its internal structure. In the context of surfactant micelles, the aggregation number is an essential characteristic that provides insights into the micellar structure.

Experimental techniques such as light scattering, small-angle neutron scattering (SANS), cryo-electron microscopy, or nuclear magnetic resonance (NMR) spectroscopy can be employed to assess the micellar aggregation number.

Table 2.2 Packing parameter and the corresponding structures to the minimum interaction energy

Packing parameter $\left[\frac{v_H}{a_o^2 l_c} \right]$	Surfactant structure	Micelle shape
0–1/3		Spherical
1/3–1/2		Ellipsoidal and worm-like structures
~ 1/2		Cylindrical and rod-like structures
1/2–1		Lamellar and interconnected structures
~ 1		Vesicles and planar bilayers
> 1		Inverted structures

2.7 Singular Optical Properties of Colloidal Dispersions

Colloidal dispersions show unique physical and chemical properties. The main colloid properties come from the dimension of the dispersed particles that are intermediate in size between molecules and visible particles. The colloidal particle dimensions range typically from 1 to 1000 nm in diameter, which can be evenly distributed throughout a continuous liquid, solid, or gas phase. The large surface area of colloidal particles makes them highly reactive and capable of adsorbing other molecules or ions onto their surfaces. The surface charge of the particles can also affect the behavior of the colloidal solution, since like-charged particles will repel each other, and unlike-charged particles will attract each other. This can influence the stability of the solution and the intensity of particle–particle and particle-solvent interactions.

The size of colloidal particles is figured out mostly by the chemical composition of the particles, the method of preparation, and the conditions under which they are formed. Size distribution refers to the range of sizes of colloidal particles within a sample. In general, colloidal size distribution can be described by a statistical distribution such as a Gaussian or log-normal distribution. Smaller particles have a higher surface area-to-volume ratio, which can lead to increased reactivity and greater stability in some cases. In addition, particles with a narrow size distribution

may exhibit more uniform properties and behaviors compared to those with a broad size distribution.

Colloidal optical properties refer to the way that light interacts with particles that are suspended in a liquid medium. Optical properties have significant colloidal applications in fields such as materials science, biophysics, and chemistry. When light passes through a colloidal suspension, it can be scattered or absorbed by the particles, which can affect the color, opacity, and other optical properties of the liquid. Light scattering is an important optical property in colloidal solutions. It is based on the principles of optics, and it is related to the size and concentration of the particles in the solution. By measuring the intensity and distribution of scattered light, valuable information about the size, shape, and refractive index of particles in colloidal solutions are obtained.

One of the key optical properties of colloidal suspensions is related to the well-known phenomenon termed the Tyndall effect, which refers to the scattering of light by suspended particles. This effect makes the suspension appear partially cloudy or opaque. The amount and angle of scattering depend on the size and concentration of the particles, as well as the wavelength of the incident light. Tyndall effect occurs because the particles in the solution are large enough to scatter light waves but small enough to remain suspended in the solution. The intensity of the scattered light is proportional to the number and size of the particles in the solution, which makes the Tyndall effect a valuable way for characterizing colloidal solutions.

Colloidal suspensions can also show singular optical properties due to their size and shape. For example, nanoparticles can exhibit a phenomenon known as plasmon resonance, where they absorb and scatter light at specific frequencies, leading to exclusive colors and optical effects. Likewise, certain types of liquid crystals can show optical properties such as birefringence, where light passing through the material is split into two polarized components with different refractive indices.

On this, light scattering is a powerful technique used to study the properties of colloidal solutions. When light passes through a colloidal solution, the particles in the solution scatter the light, causing it to deviate from its original path. The laws that govern light scattering in colloidal solutions are based on the principles of optics and are related to the size and concentration of the particles in the solution. The light scattering phenomena in colloidal solutions are governed mainly by Rayleigh scattering and the Mie scattering laws.

The Rayleigh scattering law describes the scattering of light by small particles that are much smaller than the wavelength of the incident light. The Rayleigh scattering law applies to colloidal solutions in which the particle size is less than approximately one-tenth of the wavelength of the incident light. The intensity of the scattered light is proportional to the concentration of the particles in the solution and inversely proportional to the fourth power of the wavelength of the incident light. The Rayleigh scattering law is expressed mathematically as Eq. 2.21 for spherical particles.

$$I = \frac{8 \cdot \pi^4 \cdot a^6}{r^2 \cdot \lambda^4} \cdot \left(\frac{n^2 - 1}{n^2 + 2} \right)^2 \cdot (1 + \cos^2 \theta) \quad (2.21)$$

In Eq. 2.21, I is the intensity of the scattered light from a single particle, n is the ratio between the refractive index of the particles and the medium in which the particles are suspended, a is the radius of the particles, λ is the wavelength of the incident unpolarized light, θ is the scattering angle, and r is the distance from the particle.

Equation 2.21 shows that the intensity of the scattered light is proportional to the square of the refractive index difference between the particles and the surrounding medium, and inversely proportional to the fourth power of the wavelength of the incident light—this is why the blue light is more scattered than the red light. For particle that the refractive index is equal to the medium refractive index, n equals to 1 and the light is scattered. Since the scattered light intensity growth with the sixth power of the particle radius, larger particles dominate the light scattered. This is mainly important in polydisperse systems.

The Rayleigh scattering law is an essential tool for studying the properties of colloidal solutions, and it is widely used in fields such as materials science, biophysics, and chemistry. By measuring the intensity and distribution of scattered light, researchers can gain valuable information about the size, concentration, and refractive index of particles in colloidal solutions. However, the Rayleigh scattering theory is restricted to the dilute disperse systems with particle size much smaller than the wavelength of light. Also, the Rayleigh scattering law takes no account the particle shape.

The Mie scattering law describes the scattering of light by particles that are larger than the wavelength of the incident light. Mie law applies to colloidal solutions in which the particle size is comparable to or larger than the wavelength of the incident light. The intensity of the scattered light is proportional to the concentration of the particles in the solution and depends on the size, shape, and refractive index of the particles.

2.8 Solubilization in Micellar Solution

The micellar solubilization is related to the enhanced solubility of a given compound, facilitated by the presence of surfactant micelles or inverted micelles within a solution. A notorious instance of solubilization involves the transference of oil molecules into the nonpolar core of surfactant and polymer micelles (Fig. 2.7). In this phenomenon, the oil (often characterized by negligible solubility in the aqueous medium) undergoes a conversion into a water-soluble solute by sequestration within the confines of micellar structures. The pertinence of solubilization transcends theoretical boundaries, finding substantial practicality in everyday phenomena, including industrial washing process, personal care formulations, and household cleaning agents (See Stokes and Evans 1997). However, solubilization depends on the ability of micelles formed by surfactant and polymeric compounds to

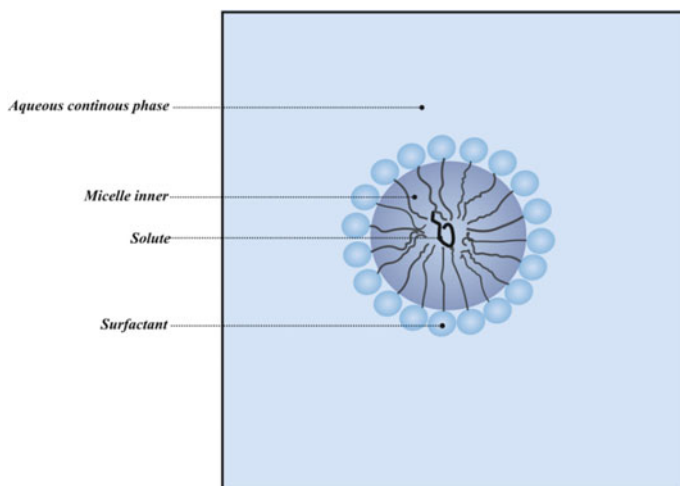


Fig. 2.7 Solubilization of nonpolar material in a swollen surfactant micelle

incorporate oil molecules. The introduction of additives, as copolymers and cosurfactants, which are able to form mixed micelles alongside conventional surface-active agents, serves as a means to regulate and enhance micelle-mediated solubilization.

Two principal kinetic mechanisms of solubilization have been established.

Bulk-reaction solubilization is a mechanism concerning oils with a relatively high solubility in pure water, such as aromatic hydrocarbons. It involves the molecular dissolution and diffusion of oil into the aqueous phase, followed by the oil molecule catching by micelles, which is characterized kinetically by a mass transfer coefficient. Initially, oil molecules dissolve from the oil droplet surface. Subsequently, the dispersed oil molecules infiltrate via molecular diffusion into the water continuous phase, where they are able to interact with the micelles.

Surface-reaction solubilization mechanism involves predominately the molecular interfacial uptake of oils exhibiting high insolubility in water. Therefore, the process encompasses the adsorption of micelles at the oil–water interface, followed by the oil uptake, and finally the desorption of swollen micelles, with constant rate across the sequential process. In systems involving solid solutes, surfactant molecules are prone to arrive at the interface in a monomeric state and swollen micellar aggregates are built at the phase boundary, eventually undergoing desorption. It is possible to identify the formation of an interfacial liquid-crystalline phase produced by the infiltration of surfactant solutions into the oil phase. Also, hemimicelles can be formed even at surfactant concentrations below the critical micelle concentration. Solubilization can also incorporate the partial fusion of micelles with the oil–water interface, leading to a phase separation step, especially for solubilization by microemulsion.

Multicomponent systems show higher solubilization rates for nonionic than that for ionic surfactants, indeed due to electrostatic repulsion between similarly charged micelles and the surfactant adsorption monolayer at the oil–water interface. In

contrast, copolymers efficiently solubilize hydrophobic compounds, even without low molecular-weight surfactants, and can act as effective solubilization promoters.

The incorporation of hydrophobic additives into the inner region of the supramolecular assembly has been extensively employed to augment the pore dimensions of mesoporous materials. It is imperative that a swelling agent with appreciable volatility, like aromatics and alkyl hydrocarbons. The inclusion of cosurfactants is typically imperative to uphold a substantial inner micellar volume, attributable to their influence on film curvature. Furthermore, one must consider the micellar configuration, as certain micellar structures show intense time-dependent behavior, necessitating the presence of supplementary additives to keep the stability.

References

- Adamson AW, Gast AP. Physical chemistry of surfaces. John Wiley & Sons, Inc.; 1997.
- Davies JT, Rideal EK. Interfacial phenomena. New York and London: Academic Press; 1963.
- Evans DF, Wennerström H. The colloidal domain—where physics, chemistry, biology, and technology meet. Wiley; 1999.
- Holmberg K, Jönsson B, Kronberg B, Lindman B. Surfactants and polymers in aqueous solution. 2nd ed. Wiley; 2002.
- Hunter RJ. Foundations of colloid science. Oxford Academic Press; 2001.
- Israelachvili JN. Intermolecular and surface forces. Academic Press; 2011.
- Mersmann, A. Fundamentals of crystallization. In: Mersmann A, editor. Crystallization technology handbook. New York: Marcel Dekker; 2001.
- Porter MR. Handbook of surfactants. New York: Springer Science e Business Media; 1993.
- Rosen M. Surfactants and interfacial phenomena. New York: Wiley; 1989.
- Shinoda K. Principles of solution and solubility. University Microfilms; 1991.
- Stokes RJ, Evans DF. Fundamentals of interfacial engineering. Wiley-VCH; 1997.
- Tadros TF. Formulation science and technology: basic theory of interfacial phenomena and colloid stability. De Gruyter; 2018.

Chapter 3

Forces Acting in Colloidal Systems



The particle–particle, particle–surface and surface–surface interactions are involved in daily and industrial applications. They play a crucial role in several types of processes, such as colloidal particle aggregation, dispersion, and fluidity. In colloidal systems, the behavior of disperse particles is influenced by a series of different forces acting on the whole system. These forces can act in a complex way to control the stability and the phase behavior of colloidal particles. The colloid stability is governed by the resulting energy from the balance between attractive and repulsive forces, which involves both kinetic and thermodynamic aspects. Attractive interactions commonly come from dispersion forces, while repulsive interactions are consequences of electric double-layer forces. DLVO is the leading theory to describe the stability of colloidal systems. The interaction between the colloidal particles can also be divided into static and dynamic components, respectively related to the particle–particle static forces and the motion of particles due to the solvent movement. The macroscopic response to the attractive–repulsive balance forces is manifested in gas condensation and liquid compressibility, for instance. The instability of dispersions can lead to flocculation because of the attractive forces acting to hold the particles together. If strong enough repulsive forces act to keep the dispersed particles away from each other, the dispersion can achieve an appropriate stable state, avoiding particle flocculation. Solvation and steric interactions are usual repulsive forces that can prevent coalescence. Besides, the balance of attractive and repulsive forces in colloidal systems can also be regulated by adding components that alter the particle–particle and solvent–particle interactions, such as surface agents and electrolytes, leading to the desired conditions for dispersion.

3.1 Nature of Interparticle Forces

The interparticular forces have intimal relationship with the matter arrangement: macroscopic bodies exploited into molecules, molecules into nuclei and electrons, and finally nuclei into protons and neutrons. On a point of view from physicists, the forces responsible to keeping the macroscopic bodies interacting between them and the elemental parts of the matter clustered are grouped into four main types: (i) gravitation forces, (ii) electromagnetism forces, (iii) the strong forces, and (iv) the weak forces (see Fig. 3.1). Gravitation forces are weak, long-range, and attractive forces that appears between two macroscopic bodies, according to their quantity of matter, whose the strength varies with the inverse of the square of distance separating them. Electromagnetism forces are long range forces that act between charged bodies (matter carrying an electrical charge), depending on the charge nature (positive or negative) and intensity and, similarly to the gravitation forces, on the square inverse of the distance between them. Strong forces are very strong, short-range, (almost always) positive forces, which are responsible to holding together the subatomic particle in the atom nuclei. Weak forces are very weak, short-range forces, occurring in subatomic particle decomposition, such as a radioactive decay and neutron fragmentation into electrons and protons (for an overview of forces acting on interfacial phenomena see Davies and Rideal 1963; Israelachvili 2011).

Whereas strong and weak forces act between elementary particles at very short distances (typically less than 10^{-5} nm), electromagnetic and gravitational forces act over a very large range of distances and a wide type of species (from elementary particles to planets, for instances). Consequently, electromagnetic, and gravitational are the main forces to control macroscopic phenomena show in everyday life, such as molecular self-assembly and capillary rising. Especially, intermolecular interactions are set up from electromagnetic forces.

The nature and strength of interparticle forces depend on a large number of factors, including the size and shape of the molecules, their polarity, media pH and salinity, and the temperature and pressure of the system. Intermolecular forces play a key role in figuring out the phase (solid, liquid, or gas) and physical properties of a substance, such as its boiling and melting points, viscosity, and surface tension. In a general statement, the interparticle interactions occurring in a colloidal

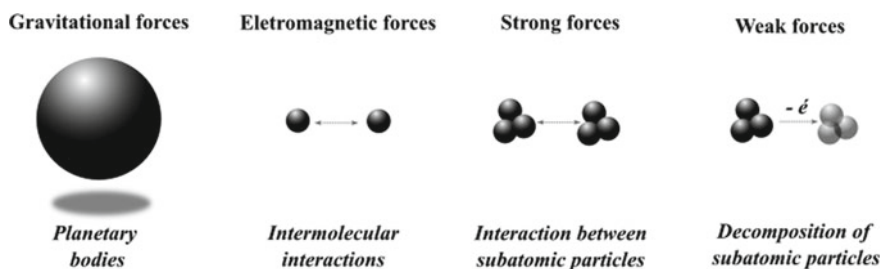


Fig. 3.1 Four main forces acting in the microscopic and macroscopic phenomena

solution can be categorized as (i) van der Waals interactions, (ii) electrostatic interactions, (iii) steric interactions, (iv) hydrophobic forces, (v) Brownian forces, and (vi) hydration forces. These forces can be gathered in three main groups, according to the nature of the phenomena governing them: (i) Purely electrostatic forces, that arise from the interaction between charged species; (ii) Purely entropic forces, that arise from the molecular motion, (iii) Quantum mechanical forces, that arise from chemical bonding and steric forces (for details on nature and strength of interparticle forces see Lyklema 2000; van Oss 2006; Birdi 2009).

3.1.1 *Van Der Waals Interactions*

The van der Waals (*vdW*) interactions are long-range forces that arise from fluctuations in the electron cloud surrounding the particles. van der Waals interactions are essentially electrostatic forces, and they play a crucial role in determining the stability of colloids since they need to be balanced with other forces to keep the particles dispersed. The van der Waals forces refers to a mean dipole–dipole interaction composed of three key force components:

1. The randomly oriented permanent dipole–dipole forces, known as orientation forces (Keesom interactions),
2. The randomly oriented permanent dipole-induced dipole forces, known as induction forces (Debye interactions), and
3. The fluctuation dipole–dipole interactions, known as dispersion forces (London interactions).

Keesom and Debye forces are based on the classic electrostatic fundamentals. In these interactions between molecules presenting a permanent electric moment (dipole moment), the interaction potential is a function of their relative orientations, which depend strongly on the temperature. Keesom interactions (orientation forces) are Boltzmann-averaged interactions between two permanent dipoles, which is often resulting from covalent bond polarization. Orientation forces promote a strong dipole alignment due to the molecule interaction with the electric field. The strength of the Keesom interaction between the dispersed particles can be altered by the particle shape effects on the dipolar potential. A neutral species can be polarized by the action of a polarizing field of a permanent dipole moment occurring in a neighboring molecule, similarly to the induced dipole caused by an ion. Induction forces take places between induced dipole and permanent dipole. Debye interactions occurring between polar and non-polar molecules, where the polar specie (with a permanent dipole) induces an asymmetrical charge distribution on non-polar species (without no permanent dipole) structure. The induced charge distribution is linearly proportional to the electric field on the dipole moment—the proportionality constant is defined as molecule *polarizability*, which define the capacity of internal charges to be shift. Polar species are also prone to the electric field induction effects, then Keesom forces account partially Debye forces.

Hydrogen bonding is often considered a particular type of dipole–dipole interaction that occurs between molecules that hold bonds between hydrogen and highly electronegative atoms (such as nitrogen, oxygen, or fluorine).

Dispersion forces are quantum mechanics interactions resulting from the natural fluctuation of the electron cloud in a particle, generating a corresponding fluctuation in the neighboring particle. London interactions are universal long-range forces, acting in all atom and molecule interactions, even neutral species. They are the predominate interactions in condensate systems, playing key role in a wide range of daily and industrial phenomena, such as adhesion, wettability, thin films, adsorption and flocculation. However, dispersion forces are influenced by the presence of neighborhood species, then they are naturally not pairwise additive, especially in interaction between large particles and surfaces.

Equation 3.1 gives the total potential energy for binary vdW interactions between the species i and j at a distance r . The α_{ij} is a constant that depends on interaction properties (such as media character, dipole moment, and molecule polarizability). The potential energy $u(r)$ allows to obtain the total potential energy of the system by integration on the all the pairs of molecules, considering the potential energy at infinite distance is zero (for details on molecular polarization mechanisms, see Israelachvili 2011).

$$u(r) = -\frac{\alpha_{ij}}{r^6} \quad (3.1)$$

The force components that compose the total van der Waals potential are also all proportional to the inverse of the intermolecular radius, as displayed in Eq. 3.2 (Keesom interactions), Eq. 3.3 (Debye interactions), and Eq. 3.4 (London interactions).

$$u(r) = -\frac{\mu_i^4}{kT \cdot r^6} \quad (3.2)$$

$$u(r) = -\frac{\alpha_i \cdot \mu_i^2}{r^6} \quad (3.3)$$

$$u(r) = -\frac{3}{4} \cdot \frac{\alpha_i^2 \cdot h\nu}{r^6} \quad (3.4)$$

μ_i is the dipole moment, k is the Boltzmann's constant (1381×10^{-23} J K⁻¹), α_i is the molecule polarizability, h is the Plank's constant (6626×10^{-34} J s), ν is the frequency of fluctuation, and T is the absolute temperature. The polarizability describes the response of the electron cloud in molecules and atoms to an external field. Typical values of static average electric dipole polarizability are presented in Table 3.1 (for details see Haynes 2015). Due their electrostatic basis, both Keesom (Eq. 3.2) and Debye (Eq. 3.3) forces are affected by the dielectric permittivity (or dielectric constant), such as it is seen for Coulomb forces. These forces are weaker in non-vacuo media.

Table 3.1 Static average electric dipole polarizability of some species (adapted from Haynes, 2014–2015)

Species	Static average electric dipole polarizability (10^{-30} m^3)	Species	Static average electric dipole polarizability (10^{-30} m^3)
<i>Atoms</i>			
H	0.667	He	0.205
C	1.67	O	0.802
F	0.557	Cl	2.18
Fe	8.4	Cu	6.2
<i>Molecules</i>			
CH ₄	2.59	Propane	6.29
Butane	8.20	1-Butene	7.97
Hexane	11.9	Benzene	10.0
Ethanol	5.41	water	
Thiophene	9.67	Pyridine	9.5

Assuming nonretarded and additive interactions, the pairwise summation of the dispersion forces (London interactions) between two macroscopic species can be evaluated by means of the Hamaker's approach (1937). Hamaker states that the London interactions occurring at short distances between two molecules of a species i in *vacuo* are governed by the molecule polarizability (α_i), Plank's constant (h) and fluctuation frequency (ν), which can be written as a function of the number of atoms per volume (q_i) and the well-known London's constant (β_{ii}) in Eq. 3.5.

$$A_{ii} = \pi^2 \cdot q_i^2 \cdot \beta_{ii} \quad (3.5)$$

A_{ii} is the Hamaker's constant for the interaction two species i . The London constant is given by $\beta_{ii} = (3/4) \cdot \alpha_i \cdot h\nu$, then A_{ii} is always positive. For dispersion energies between two distinct species i and j interacting in *vacuo*, the Berthelot combining rule provides the Hamaker constant (A_{ij}) and London constant (β_{ij}) from Eq. 3.6 and Eq. 3.7, respectively.

$$A_{ij} = \sqrt{A_{ii} \cdot A_{jj}} \quad (3.6)$$

$$\beta_{ij} = \sqrt{\beta_{ii} \cdot \beta_{jj}} \quad (3.7)$$

For dispersion energies between two particles of the species i interacting in a given media k , different of *vacuo*, the Hamaker constant will be given by the Eq. 3.8.

$$A_{ii}^k = A_{ii} + A_{kk} - 2A_{ik} = \left(\sqrt{A_{ii}} - \sqrt{A_{kk}} \right)^2 \quad (3.8)$$

For dispersion energies between two distinct species i and j interacting in a media κ , different of *vacuo*, the Hamaker constant will be given by the Eq. 3.9.

$$A_{ij}^{\kappa} = A_{ij} + A_{\kappa\kappa} - A_{i\kappa} - A_{i\kappa} = \left(\sqrt{A_{ii}} - \sqrt{A_{\kappa\kappa}}\right) \cdot \left(\sqrt{A_{jj}} - \sqrt{A_{\kappa\kappa}}\right) \quad (3.9)$$

The right side of Eq. 3.8 confirms the Hamaker constant A_{ii}^{κ} is always positive for two identical species interacting in a non-vacuo media, and consequently the London potential energy will be attractive. However, the Eq. 3.9 demonstrates that the Hamaker constant A_{ij}^{κ} for two distinct species interacting in a non-vacuo media can be negative, resulting in repulsive London potential energy. Besides, negative London potential energy found at short interparticle distances (typically lower than 100Å) can become positive at greater distances.

Particularly in condensate media, the pairwise additivity is scarcely hold. Retardation is a distance-dependent phenomenon characterized by the fast decaying of the dispersion interaction energy between two species. The Hamaker constant for systems containing condensed phase can be obtained from an alternative approach, known Lifshitz macroscopic theory (1956). Lifshitz theory is based on (total) macroscopic properties originate from interactions between species, instead the (individual) single interactions, avoiding the restrictions inserted in the pairwise summation of the dispersion forces. In Lifshitz theory, the individual species are considered as a continuous phase exhibiting phase properties (such as dielectric permittivity and refractive index) uniformly. The microscopic atomic structures of the interacting species are ignored, and the inter-species forces are derived from bulk properties.

The electromagnetic propagation frequency (ν) governs the nature of interactions occurring in the media. Then, the Hamaker constant (A_H) can be categorized into two main terms, according to the electromagnetic propagation frequency, as given in Eq. 3.10. $A_{ii}^{\kappa(\nu=0)}$ represents the Hamaker constant at frequency zero, which is related to the electrostatic contribution to the van der Waals forces, gathering the orientation and induction interactions. $A_{ii}^{\kappa(\nu>0)}$ denotes the Hamaker constant at frequency higher than zero, which accounts for the dispersion interactions.

$$A_H = A_{ii}^{\kappa(\nu=0)} + A_{ii}^{\kappa(\nu>0)} \quad (3.10)$$

The Hamaker constant for a system containing two phases i interacting in a given non-vacuo media κ obtained from Lifshitz theory is expressed by the Eq. 3.11.

$$A_H = A_{ii}^{\kappa} = \frac{3}{4} \cdot kT \cdot \left(\frac{\varepsilon_i - \varepsilon_{\kappa}}{\varepsilon_i + \varepsilon_{\kappa}}\right)^2 + \frac{3}{16\sqrt{2}} \cdot h\nu \cdot \frac{(n_i^2 - n_{\kappa}^2)^2}{(n_i^2 + n_{\kappa}^2)^{\frac{3}{2}}} \quad (3.11)$$

In Eq. 3.11, ε_i and ε_{κ} are the dielectric constants for i and κ phases, respectively. n_i and n_{κ} are the visible-light refractive index for the i and κ phases. h is the Planck constant, and ν is the main electronic absorption frequency for the media. The Hamaker constant derived from Lifshitz theory enable the determination of the van der Waals energy potential, described in Eqs. 3.2–3.4, from a more reliable route.

3.1.2 *Electrostatic Forces (Electrical Double Layer Interactions)*

The interaction potential between two individual charged species, such as atoms and ions, is determined by the Coulomb force, such as described in Eq. 3.12.

$$u(r) = \frac{1}{4} \cdot \frac{z_1 \cdot z_2 \cdot e^2}{\pi \cdot \epsilon_0 \cdot \epsilon \cdot r} \quad (3.12)$$

z_1 and z_2 stands for the ionic valency of the species 1 and 2, respectively. The ϵ and ϵ_0 represents the dielectric constant of the media and the vacuo, respectively. r is the distance between the species and e is the elementary electron charge, equivaling 1.602×10^{-19} C. The Coulomb interactions are long-range, electrostatic-originated and the strongest physical forces occurring between molecules. These forces can be both positive and negative, according to the sign for the ionic charges of the particles.

Coulomb forces are inverse-square force law; however, they are attenuated according to the media dielectric constant, becoming weaker in high dielectric media as the water. In an electrolyte solution, a charged species moving in the solvent acquires in its neighborhood a higher density of the opposite charged that the single model of pair interaction. The complexity of the interactions between charged species in electrolyte solutions usually produces a decaying of the electric field, becoming the Coulomb forces shorter range than an inverse square force law. The interactions between charged species in electrolyte solutions are crucial to state the stability of colloidal systems. The interaction between charged particles can lead to the formation of ion pairs, and these ion pairs can cause the colloidal particles to be aggregate or flocculate.

Equation 3.8 states that van der Waals force between particles of the same species in a given media will be attractive. Attractive forces must be balanced by opposite (repulsive) forces acting to keep the species separated in a way to prevent the particle agglomeration and define a disperse equilibrium stable state. Electrostatic interactions can arise from the charged particles in condensed media (especially, high dielectric constant liquids) as repulsive force to oppose with the attractive intermolecular interactions, avoiding the prompt particle association that can lead to the particle growth and phase separation.

Electric charging can occur in solid–liquid and liquid–liquid interfaces. The electric charging mechanisms, labeled *charge regulation*, to produce a charged surface stand up from three main physical–chemical phenomena:

1. Dissociation of specific surface groups, producing a charged surface with the opposite charge;
2. Adsorption of charged species from bulk solution onto neutral surface, providing to the surface the same species charge; and
3. Charge exchange between two dissimilar surfaces at short distances through protons or electrons transference.

The *charge regulation* leads to an electric structure where the charge distribution is divided in a layer of ions bounded to the surface—termed *co-ions*—and a layer holds opposite charge free-ions—termed *counterions*. The contact of most species (for example, macromolecules, aggregates, droplets, and solid particles) with high dielectric constant liquids leads to the spontaneous ionization of their functional surface groups. In this way, charge regulation corresponds the dynamic equilibrium between co-ions and their corresponding counterions. The interfacial region where the interactions between co-ions and counterions resultant of the charge regulation take place in an electrolyte solution is denominated *electrical double layer*. The electrical double layer designates the distribution of charged species nearby a charged interface (such as the interface between a solid and a polar liquid), playing a crucial role in processes of colloid stabilization, corrosion, electrodeposition, and electrocatalysis.

The electrical double layer is composed of two charged well-defined layers: (i) the inner steady layer containing charged species attached to the surface—labelled *Stern layer*—, and (ii) the outer diffuse layer having mobile ions distributed according to the electrical forces and thermal motion—labelled *Gouy* (or *Gouy-Chapman*) layer. A simplified arrangement of charges constituting an electrical double layer is displayed in Fig. 3.2. Inside the Stern layer, the charge and energy potential distribution depends on the short-range interactions, and the geometry and size of the charged species. A more realistic model includes solvated ions in the Stern layer, making it wider.

The limiting region holding the steady surface-attached species is defined by the *shear plane*. In the diffuse region, although attracted to the charged interface, species can diffuse away due to the thermal movement, setting up a charge equilibrium described by the Boltzmann distribution. In addition, the counterion distribution and therefore the thickness of the diffuse layer depends on the potential between the dispersed electrical charges, which described by the Poisson equation. The diffuse layer extends from shear plane up to the Gouy plane, which separate the diffuse layer from the solution bulk, and it is the maxima distance from the charged surface where the ions are effectively prone to the actions of the surface charge.

The electrical potential of the electrical double layer is determined by the balance between the attractive forces between the charged interface and the ions, and the repulsive forces between the ions themselves. This balance of forces determines the potential energy of an ion at a given local field. The specific position of an ion inside at a local field is given by a probability function described by the Poisson-Boltzmann equation, which is a partial differential equation that relates the potential distribution to the solution ionic concentration. For an ionic solution, the Poisson-Boltzmann equation can be written as Eq. 3.13, which must observe the following statements: (i) the ions are simple charge structures; (ii) the ionic adsorption energy has purely electrostatic nature; (iii) the solvent is a structureless continuum media.

$$\frac{d^2\psi}{dx^2} = -\frac{z \cdot e \cdot \rho_0}{\varepsilon \cdot \varepsilon_0} \exp\left(-\frac{z \cdot e \cdot \psi}{kT}\right) \quad (3.13)$$

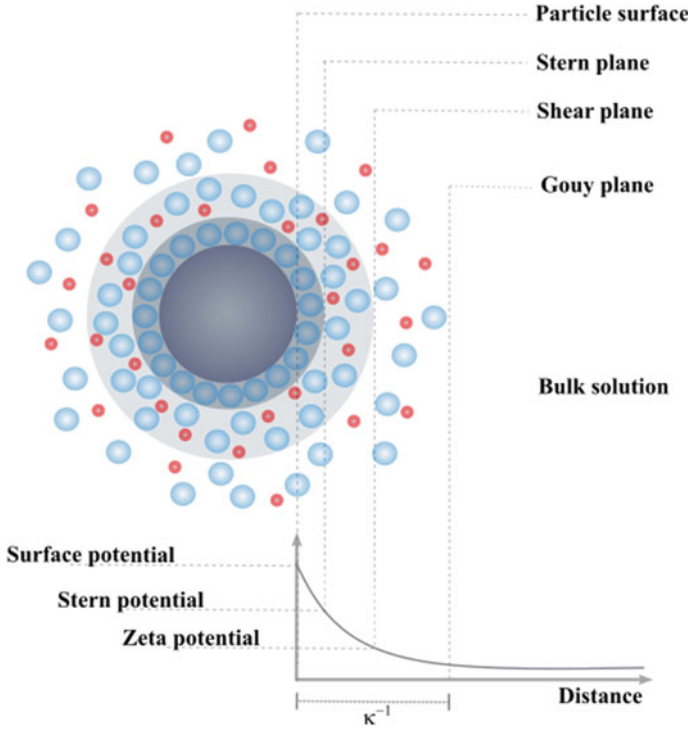


Fig. 3.2 Schematic illustration of charge distribution in electric double layer and its corresponding energy potential

Equation 3.13 allows to obtain the electrical potential ψ at a distance x from the charged surface. ϵ and ϵ_0 are the medium and vacuum permittivity, e is the elementary charge, k is the Boltzmann constant, and T is the absolute temperature. The charge density ρ for a Boltzmann distribution of ions at a given distance from the surface is given by the Nernst equation, according to the Eq. 3.14.

$$\rho = \rho_0 \cdot \exp\left(-\frac{z \cdot e \cdot \psi}{kT}\right) \tag{3.14}$$

Here ρ_0 is the ion density at the surface.

The electrical potential of the electrical double layer can also be described by the Debye-Hückel theory (for details on the theoretic models describing the electric potential see Evans and Wennerstrom 1999). The Debye-Hückel theory assumes separate contributions from long range coulombic forces (especially ion-ion and solvent-ion interactions) and van der Waals forces especially London. The Debye-Hückel model stands for a simplified electrolyte solution composed by a spheric single ion inserted in a continuous media with constant permittivity whose the charge distribution is given by the Poisson-Boltzmann equation. On infinite dilution concentrations, and

consequently at slight electrical potential, the Debye-Hückel model results in exact description of the electrolyte solution. For low values of term inside the exponential argument in a way that resulting in *z.e.* $\psi \ll kT$, a solution of Eq. 3.13 can be obtained as

$$\psi(x) = \psi_\delta \cdot \exp(-\kappa \cdot x) \quad (3.15)$$

ψ_δ is the potential measured at the Stern layer. $1/\kappa$ is a characteristic dimension of the diffuse electrical double layer, termed *Debye length*, given by Eq. 3.15. The Debye length is the distance from the charged surface at which the potential ψ becomes ψ_δ/e and it represents the effective thickness of the diffuse double layer.

$$\kappa = \left[\sum_i \frac{\rho_{\infty i} \cdot (e \cdot z_i)^2}{\varepsilon \varepsilon_0 \cdot kT} \right]^{\frac{1}{2}} \quad (3.16)$$

$\rho_{\infty i}$ is the ionic density of i ions in the solution bulk, where the potential is zero. Regardless the significant restrictions, the Debye-Hückel model presents a consolidate basis for other electrolyte models. It allows to obtain the extension of the effective action of the electrical potential from a charged surface as a function of the ion concentration and valence, as well as the media permittivity and temperature. Equation 3.15 states strictly at low ion concentration the Debye length will be shorter and consequently the diffuse parts of the double electrical layer will be thicker and less dense. However, an effective electrical shield can be structured even at low concentration since highly charged ions display high ionic strength. Once that electrostatic interactions take place mainly across the diffuse layer, the Debye length has an important influence on colloid stability.

Figure 3.2 displays the distribution of the electrical potential around a charged particle as a function of the distance from the surface. At the surface, the electrical potential assumes the maximum value and it is labelled surface potential ψ_o . At a Stern plane with thickness δ , the electrical potential is termed Stern potential ψ_δ . Finally, at the shear plane, the electrical potential is defined as zeta potential ζ . Experimental measurements are not available to directly determine the surface potential by means the Eq. 3.14. However, zeta potential can be assessed by a set of adequate experimental techniques. Zeta potential is typically assessed from ultimate models describing the electrokinetic phenomena, as electroosmosis and electrophoresis, and then it is commonly termed *electrokinetic potential*.

Since the direct measurement of both surface potential and Stern potential are challenging to be settled, zeta potential is often the only experimental parameter used to describe the electrical double layer. In fact, zeta potential is not directly measurable, nevertheless, it can be assessable employing theoretical models using experimental data from electrokinetic mobility. The electrokinetic measurement techniques are based on the induced movement of species in an electric field, which includes (i) Electrophoresis (the most usual method to zeta potential determination); (ii) Electroosmosis; (iii) streaming potential; and (iv) sedimentation potential.

Electroacoustic techniques, in which the difference of density between species and continuum medium induces a dipole moment, are also applied effectively to the zeta potential determination. The zeta potential values are almost slightly higher than the Stern potential values.

The zeta potential value is straightly related to the stability of colloidal dispersions since ζ -potential designates the electrostatic repulsion between charged particles in an ionic dispersion. Stable ionic dispersions are generally obtained at high values of zeta potential, even negative or positive. Table 3.2 displays representative values of ζ -potential and the corresponding stability foreseen to the electrolyte systems. High values of zeta potential must guarantee a suitable resistance to the aggregation in colloidal systems. On another hand, low ζ -potential can consent attractive forces to surpass the interparticular repulsion, leading to agglomeration and subsequent flocculate. Zeta potential equals zero denotes the species go to a fast interaction that tends to lead to the phase separation (for details on the relation between the ζ -potential and colloidal dispersion stability see Rosen 1989; Trados 2018).

The point at which the zeta potential equals to zero can be referred as *isoelectric point*, which corresponds to the *point of zero charge*. The accurate determination of the *point of zero charge* dependence on the pH and ionic concentration on the zeta potential. The *point of zero charge* is defined by the *isoelectric point* found at the same pH regardless the electrolyte concentration (see Fig. 3.3).

The properties of the electrical double layer are influenced by solution properties (such as the ionic concentration, the ionic size, and the charge of the ions), as well as the properties of the charged interface, such as the surface potential and the surface charge density. The double layer structure plays a fundamental role in many daily phenomena. For example, a double layer covering the fat droplets dispersed in milk assure the stability, preventing their agglomeration. Electrical double layers show up in a wide number of heterogeneous fluid-based systems, including cosmetic, petroleum, food, blood, paint, ink, and slurry. The electrical double layer has numerous applications in various scientific fields. In electrochemistry, the electrical double layer is important for describing the behavior of electrodes in processes, as corrosion, electrodeposition, and electrocatalysis. In colloid science, it contributes to the stability and behavior of colloidal suspensions, and emulsions. In environmental science, it is key aspect to the remediation of natural systems, as

Table 3.2 Estimative of the stability behavior of colloidal systems, according to values of the zeta potential

Zeta potential (mV)	Colloidal behavior
$-15 < \zeta < +15$	Instability with quick flocculation
$-30 < \zeta < -15$ and $+15 < \zeta < +30$	Incipient instability
$-40 < \zeta < -30$ and $+30 < \zeta < +40$	Moderate stability
$-60 < \zeta < -40$ and $+40 < \zeta < +60$	Good stability
$\zeta < -60$ and $\zeta > +60$	Excellent stability

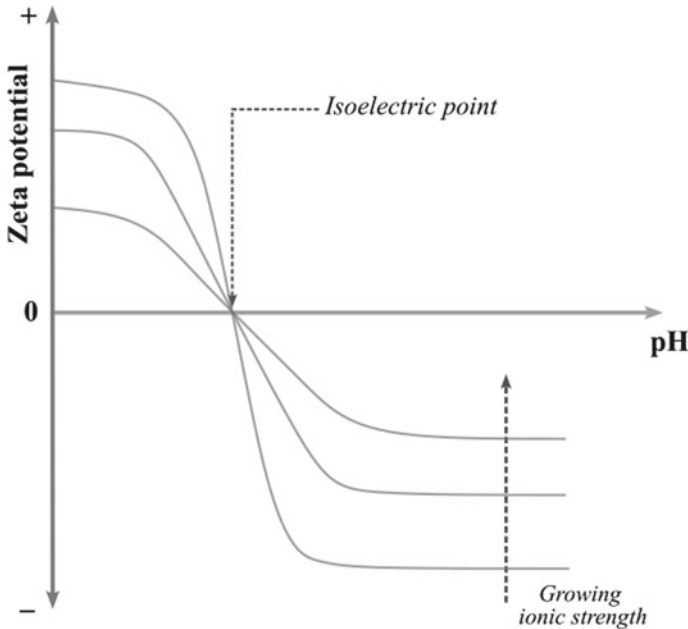


Fig. 3.3 Illustration of the zeta potential against pH for dispersed particles in solution at different ionic strength

groundwater and soils. Therefore, it is crucial to assess the potential across the electrical double layer to estimate the interaction between charged particles in an aqueous media.

Total potential energy of interaction

The interactions between particles in solution act over a short-range distance between them. They are consequences of matter's subatomic arrangement. These forces are significantly weaker than the intramolecular forces that keep the atoms and ions attached.

Intermolecular forces have an electromagnetic origin, and they encompass: (i) electrostatic interactions, constituted by coulombic and induction forces; (ii) electrodynamic interactions, represented by dispersion forces; (iii) donor–acceptor interactions, where hydrogen bonds are included, and (iv) repulsive interactions caused by the electron cloud overlapping. The interaction potential describes the potential energy of interaction between two particles based on their distance of separation. The potential equation accounts for the difference between attractive forces (dipole–dipole, dipole-induced dipole, and fluctuation dipole–dipole interactions) and repulsive forces, as it can be seen in Fig. 3.4.

Figure 3.4 displays a primary minimum at noticeably short distances, which is a typical behavior of systems containing small species and thick electrical double layer. This aggregative behavior is termed *coagulation*, and it is usually noted when

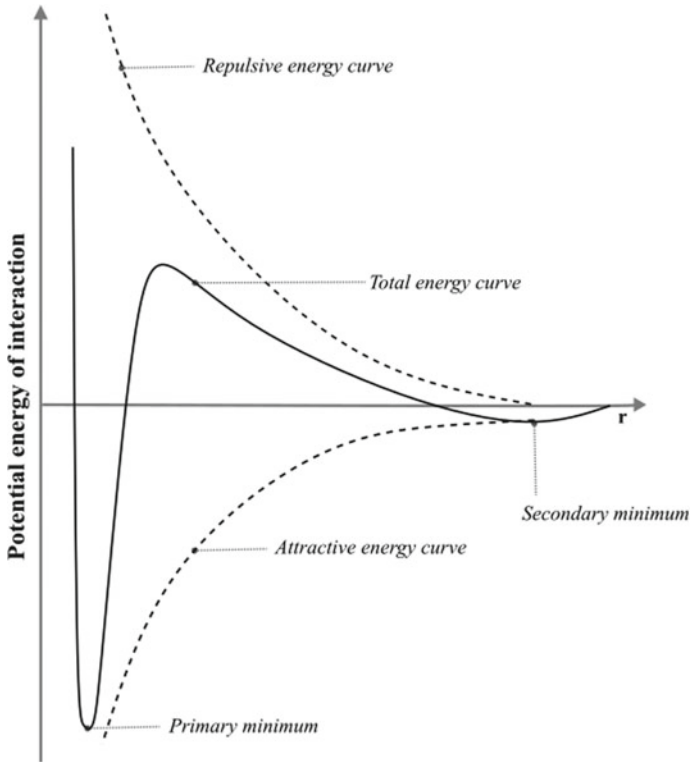


Fig. 3.4 Potential energy of interaction between two particles

small ratio of particle size to double layer thickness ($ka \ll 1$). Some systems display a secondary minimum on the curve of the total potential energy at a relatively large interaction distance, corresponding to an aggregative process labelled flocculation. In secondary minimum, the species interacts on low potential energy, becoming the flocculation easily reversible by slight agitation.

The potential energy is defined as the work done to separate two simple spheric species from a specific distance r to an infinite distance of separation, as described in Eq. 3.16. F is the resulting force between the species, and r is the distance between the interacting species. $\psi(r)$ is the potential energy as a function of r . The negative signal is conventionally due to the expenditure of work during force application. In addition, attractive forces are settled as negative and repulsive forces are settled as positive, by arbitrary convention.

$$F = -\frac{d\psi(r)}{dr} \tag{3.17}$$

Equation 3.17 assumes the force F on only one space coordinate. A more general form of Eq. 3.16 should consider F acting on other coordinates, such as

described in Eq. 3.18, which are found in interactions between asymmetrical and more complicated structures. r , θ and z are space coordinates.

$$F = -\frac{d\psi(r, \theta, z)}{dr} \quad (3.18)$$

The total potential energy must take in account both repulsive and attractive forces. Equation 3.19 gives the total potential energy of two nonpolar species interacting at a distance r , known as Mie potential.

$$\psi(r) = \frac{A}{r^n} + \frac{B}{r^m} \quad (3.19)$$

The terms in the right of Eq. 3.19 are the repulsive and attractive potential energies, respectively. A , B , n , and m are positive constants. The m parameter comes from the theory of dispersion forces (London interactions) as $m = 6$. The n parameter has been calculated as $n = 12$. A more appropriate form can be derived from the Mie potential to designate the balance between attractive and repulsive forces acting in a pair of symmetrical nonpolar species that states the equilibrium interaction. A widespread representation of the potential energy function is given by the Lennard-Jones potential, illustrated in Eq. 3.20. The Lennard-Jones model comprises a repulsive term and an attractive term (representing the London dispersion forces).

$$\psi(r) = 4\epsilon \cdot \left[\left(\frac{\sigma}{r} \right)^{12} - \left(\frac{\sigma}{r} \right)^6 \right] \quad (3.20)$$

Equation 3.1 represents the Lennard-Jones potential of interaction between two particles. $\psi(r)$ is the intermolecular potential energy between the two particles. ϵ represents the potential energy achieved at a minimum equilibrium distance, therefore ϵ is located at the well depth in the total potential curve (see Fig. 3.4) and it is a measure of how strongly the two particles attract each other. σ is the distance at which the intermolecular potential between the two particles is zero, referred to as the *van der Waals radius*, which is denoted as one-half of the internuclear distance between nonbonding particles. r is the distance of separation between both particles (from the center of one particle to the center of the other particle).

The Lennard-Jones potential is related to the interaction between the nuclei of two species. Figure 3.4 shows, at an infinite distance between the species, the interaction probability function reaches a minimum and the binding potential energy is considered zero. As the separation distance between species becomes smaller, the probability of interaction increases. The species progressively approach each other until a given separation region, where the binding potential becomes negative. The interaction distance between the species is limited to a certain distance of separation at which the potential energy achieves a minimum value, which specifies the equilibrium state. If the species are forced beyond the equilibrium distance, repulsion begins to prevail on the attraction forces due to the overlapping of electronic orbitals. Despite

the repulsive force between the two species, the binding potential energy increases rapidly becoming increasingly positive and energetically unfavorable as the separation distance decreases. On the other hand, the potential energy is negative at long distances between species, tending to zero as the separation distance goes forward to infinity. This writes down that at long range distances, species experience to some extent stabilizing force. Finally, the separation between the two particles reaches the value of the equilibrium radius, the system reaches a maximum stability, constituting the state of equilibrium. Although the Lennard–Jones model is not the most accurate representation of the surface potential energy, it is widespread used due its computational fittingness.

DLVO theory

The well-established DLVO theory often describes interparticle forces to outline the stability of dispersions. The DLVO theory is named as an acronym for Derjaguin, Landau, Verwey, and Overbeek, who independently contribute to theory conceptual formulation. In DLVO theory, interactions between particles can be categorized into attractive van der Waals forces and repulsive electrical forces (electric double-layer forces).

DLVO theory is a model extensively used in colloid science to predict the stability of colloidal suspensions. It is based on the interplay of two opposing forces: van der Waals attraction and electrostatic repulsion. The van der Waals attraction between particles is inversely proportional to their surface distance square. The electrostatic repulsion between particles is due to the repulsion of their electrical charges. The DLVO theory predicts that the stability of a colloidal suspension is defined by the balance of these two forces. If the repulsive electrostatic forces are greater than the attractive van der Waals forces, the particles will remain dispersed, and the system will be stable. If the attractive van der Waals forces become dominant, the particles will aggregate, and the suspension will become unstable. The DLVO theory has been used to explain a wide range of phenomena related to colloidal suspensions, including flocculation, sedimentation, and aggregation. It has also been used to develop strategies for controlling the stability of colloidal suspensions, such as by adding surfactants or adjusting the pH of the medium. DLVO theory has been confirmed by many experiments and has been successfully applied in various fields, including pharmaceuticals, cosmetics, food science, and environmental science (for details see Israelachivili 2011; Lyklema 1995).

The attraction potential energy can be written as in Eq. 3.3. ψ_A represents the attractive forces in the vacuum of similar spheres of radius whose center distance is R . A represents the Hamaker constant (or van der Waals constant) and H represents the closest distance between the particle surfaces (given by $H = R - 2a$).

$$\psi_A = -\frac{A \cdot a}{12H} \quad (3.21)$$

The potential energy of attraction is always negative since it equals zero at an infinite distance and decreases as the particles approach. However, if the interparticle

interaction occurs in a liquid dispersion medium, A must be replaced with an effective Hamaker constant (A_{eff}).

The repulsive potential energy between two spherical particles at a distance H between them, as described earlier, is given by the Derjaguin approximation (Eq. 3.22). In Eq. 3.22, the repulsion potential energy assumes always positive values. It equals to zero at an infinity distance and it increases according to the particles are kept closer.

$$\psi_R = \frac{\epsilon_r a \psi_0^2}{R} \cdot e^{-\kappa H} \quad (3.22)$$

a is the particle radius, ψ_0 is the surface potential, ϵ is the dielectric constant of the dispersing medium, and k is the reciprocal of the effectiveness thickness of the electrical double layer.

One of the main limitations of the DLVO theory is that it assumes a constant potential and charge distribution around the particles, which may be especially inadequate to the heterogeneous surfaces. Furthermore, the DLVO theory is limited to the dilute suspensions, where the particles are well separated, and the effects of particle–particle interactions dominate over particle-solvent interactions. In concentrated suspensions, the interactions between the particles become more complex, and other factors such as particle size distribution, interparticle forces, and hydrodynamic effects may need required. In some cases, the presence of specific ions in the solution can modify the strength of the repulsive and attractive forces between the particles, leading to unexpected changes of the disperse behavior.

In general, the stability of a dispersed system is given by the rate of change in the number of particles n during the initial stages of aggregation. The Smoluchowski equation can be used to assess the diffusion-controlled coalescence rate of spherical particles dispersed in a medium as a result of collisions in the absence of any energy barrier to coalescence. The Smoluchowski equation is a partial differential equation used to describe the time evolution of a probability density function for the positions of a large number of small particles undergoing Brownian motion, written as Eq. 3.23.

$$\frac{\partial \rho}{\partial t} = \frac{1}{k} \cdot D \cdot \nabla^2(k \cdot \rho) \quad (3.23)$$

where ρ is the probability density function, t is time, D is the diffusion coefficient, k is the drag coefficient, and ∇^2 is the Laplace operator. However, the equation can be better represented in a simplified form, as shown by Eq. 3.24

$$-\frac{dn}{dt} = 4\pi D \cdot r \cdot n^2 \quad (3.24)$$

The Smoluchowski equation can be used to describe a variety of phenomena, including the motion of colloidal particles, the diffusion of small molecules in a

liquid, and the dynamics of polymers. It is a valuable tool in statistical physics and has numerous applications in materials science, chemistry, and biophysics.

3.1.3 Steric Interactions

Steric interactions are forces that arise due to the presence of a surface layer between species. This layer can be created by the adsorption of macromolecules such as surfactants or polymers (including naturally-occurring and biological polymers) on the particle surface, for instance, and act as a protective barrier. Though, steric forces are especially important for liquid–liquid (as in emulsions) and liquid–solid (as in solid dispersion) interfaces when the covered surfaces approach themselves, since the adsorbed layer can prevent the particle aggregation. Molecules and particles attached to the surface can generate a thermally diffuse interface with species thermally mobile. In order the distance between the species-attached surfaces is reduced, three main forces can emerge:

1. Steric repulsion, a repulsive osmotic pressure between the surfaces aroused from the entropy decreasing associated to the dangling species compression;
2. Interchain attraction, an attractive interaction between the chain (or chain segments) of the confining molecules, occurring especially in poor solvent;
3. Bridging attraction, an attractive interaction where the species interacts with two particle surfaces, creating a bridge between them.

Steric forces are non-DLVO interactions, derived from a series of mechanisms that acts in particle surface covered by large molecules. The macromolecule interfacial conformation depends primarily on the molecule chemical structure, surface concentration, and solvency of the media. The interactions between chain segments can be sufficiently attractive to eliminate the entire mobility of the molecule chain, especially in poor solvents where molecule–molecule interactions overcame molecule–solvent interactions. In this case, the macromolecule tends to collapse into a close-packed structure. Figure 3.5a shows the typical arrangement of collapsed (folded) macromolecule structure, which occurs often in polymer as proteins, for instance.

The molecule solvency can be increasingly improved by temperature changes that privilege the molecule–solvent interactions up to a critical solubility state is reached. The critical solubility state for polymers is characterized by fully free rotation of the molecule chain, without interference of the interactions between chain segments. Then, the polymer structure assumes a random arrangement defined by a characteristic dimension termed radius of gyration (R_G), as can be seen in Fig. 3.5b. The radius of gyration is the defined as the distance between the two extremities of the polymer chain in the critical solubility and it is given by Eq. 3.25. At critical solubility conditions, the solvent is labelled theta solvent. In solubility higher than the critical solubility, the solvent is considered good, and the polymer chain

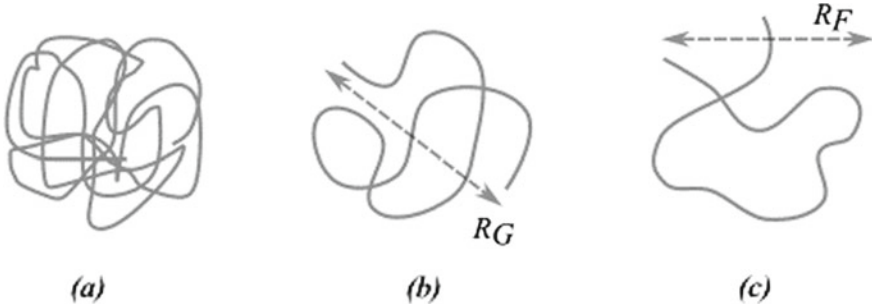


Fig. 3.5 Polymer arrangement according to the solvent quality

assumes an expanded coil arrangement (see Fig. 3.5c), characterized by the Flory radius (R_F), given by $R_F = \alpha \cdot R_G$. The parameter α is the intramolecular expansion factor distinguishing of the molecule.

$$R_G = \frac{l \cdot \sqrt{\frac{M}{M_0}}}{\sqrt{6}} \quad (3.25)$$

The repulsive steric interaction between two identical surfaces containing terminally anchored macromolecule chain in a theta solvent (described as a solvent in which the polymer coil behaves like an ideal chain) can be figured out as a function of the distance (h) by means of Eq. 3.26 (if $h < L_0$) and Eq. 3.27 (if $h > L_0$) (see details in Dolan and Edwards 1974).

$$f(h) = \Gamma \cdot kT \cdot \left[\frac{\pi^2}{3} \cdot \frac{L_0^2}{h^2} - \ln \left(\frac{8\pi}{3} \cdot \frac{L_0^2}{h^2} \right) \right] \quad \text{for } h < \sqrt{3} \cdot L_0 \quad (3.26)$$

$$f(h) = 4\Gamma \cdot kT \cdot \exp \left(\frac{-3h^2}{2L_0^2} \right) \quad \text{for } h > \sqrt{3} \cdot L_0 \quad (3.27)$$

Γ represents the surface concentration and k is the Boltzmann constant. Both Eqs. 3.26 and 3.27 give the energy per unit area to a molecule attached at a low coverage surface (see Fig. 3.6a), assuming no overlap and no interaction between neighborhood chains on the same surface. L_0 represents the end-to-end length of chain, as displayed in Fig. 3.6a. In short distances ($h < 3^{1/2} \cdot L_0$) the steric energy is resulting from osmotic pressure between the chains and from elastic energy decreasing due to the mutual compression of the chains (given respectively by the first and the second term in the right side of the Eq. 3.26).

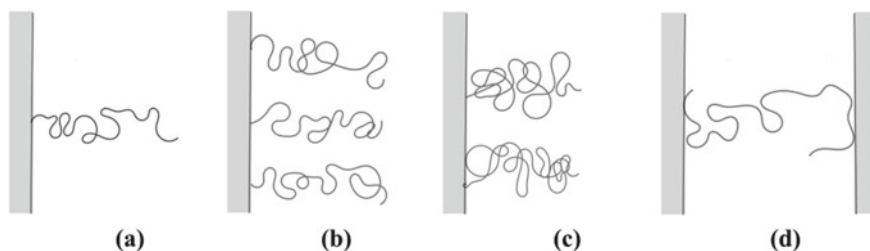


Fig. 3.6 Polymer arrangement according to its interaction with surfaces. **a** Terminally anchored chain at low coverage surface; **b** anchored chains on high coverage surface (brush); **c** molecule coins adsorbed on surface; and **d** adsorbed chains bridging between two surfaces

3.1.4 Hydrophobic Interactions

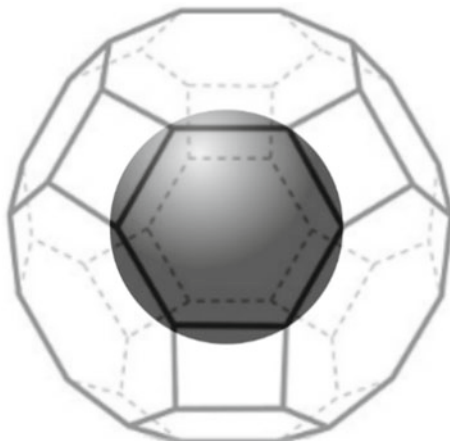
Hydrophobic interactions are forces that result from the interaction between non-polar species (particles or molecules) and the polar solvent (strictly, water). The hydrophobic interactions are consequent from the termed hydrophobic effect that arises from the cohesive free energy of the hydrogen bonds of the water molecules surrounding the species. Non-polar species solubilization changes the liquid water structure, which is arranged by strong attractive hydrogen bonds, creating a higher degree of molecular ordering around the species. The molecular ordering leads to a decreasing of the system entropy (ΔS) rather than enthalpy changes (ΔH), resulting in an unfavorable change in Gibbs energy (ΔG), as shown by Eq. 3.28. The pronounced entropic nature of the hydrophobic interaction explains the unusual attraction between non-polar species in water, known as hydrophobic attraction (data from Gibbs energy for hydrocarbon interactions can be find in Prausnitz et al. 1998). Similar effect is manifest in other polar liquids having high cohesive energy, even so their cohesion be much weaker than that of water. In this case, the phenomenon is named by a general terminology: *solvophobic effect*.

$$\Delta G = \Delta H - T \Delta S \quad (3.28)$$

The entropic nature of the hydrophobic effect is related to the arrangement of water molecules.

A particular effect takes place when the contact with a non-polar lead to the breaking of the hydrogen bonds between water molecules, leading the system to a high energy, unstable state. This state induces the water molecules to the intense arrangement, looking for reducing the energy level, through the establishment of new hydrogen bonds in greater number and stronger. Because the peculiar association of the water molecules, the resulting structure is termed *iceberg*. The *iceberg* structure is formed around the nonpolar species, in a way that the nonpolar species are confined into the water associative structure. Water molecules in *iceberg* structures have high ordering than the water molecules in the bulk that results in unfavorable Gibbs energy. However, these structures present substantial stability at specific

Fig. 3.7 Illustration of clathrate cages formed by water molecules around small dissolved nonpolar (hydrophobic) solute molecules



temperature and pressure conditions. Particularly at low temperature and high pressure, polyhedral (tetrahedral and dodecahedral, for instances) structures can be found retaining nonpolar species in associative assemblies similar to the solid-like lattices, trapping high concentrations of organic components such as methane and carbon dioxide (see Fig. 3.7).

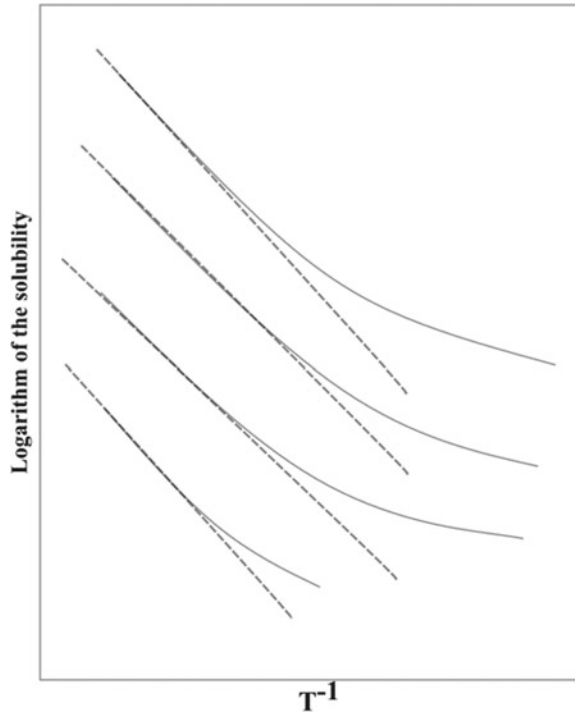
The formation of iceberg structures keeps the nonpolar species in a high distance between them, which results in weaker hydrophobic interaction and consequently increase in the solubility of nonpolar species in polar solvents. The solubility of compounds can be described by the regular solution theory, which states the solubility must be greater at higher temperatures, following a linear behavior on the plot of logarithm of the solubility (S) against the reciprocal of the temperature ($1/T$), such as illustrated in Fig. 3.8. At elevated temperature, the regular solution theory describes adequately the solubility of hydrocarbons in water, since at high energy the species experience vigorous molecular motion that tend to favor the entropic term in Eq. 3.28. However, it is evident the deviation between the expected behavior from the regular solution theory and solubility experimental data at low temperature. The point where the experimental solubility curve is unlinked to the linear decaying given by the regular solution theory is ascribed to the *iceberg* formation, and the corresponding temperature is termed *iceberg formation temperature*.

In aqueous systems containing amphiphiles, the hydrophobic forces allow the particles to aggregate, leading to the formation of micelles or other self-assembly structures.

3.1.5 *Brownian Forces*

Brownian forces are random forces that arise due to the thermal motion of molecules in a continuous dispersing fluid. The Brownian motion results from collisions

Fig. 3.8 Illustration of plots of logarithm of the solubility (S) against the reciprocal of the temperature. Solid lines represent behavior from experimental data. Broken lines show the hypothetical solubility following the regular solution theory. The slope of lines gives the enthalpy of the solution as a regular solution



between the particles and the dispersing media molecules, leading the dispersed particles to experience an arbitrary and erratic movement that affects the rate of particle–particle interactions. The collisions between particles and molecules of fluid acts to prevent the aggregation of particles and to keep the stability of the colloidal suspension, supporting the particles to prevent the settling out of the solution.

In colloidal Brownian motion, the particles are typically much larger than the molecules in the surrounding fluid, which means that they experience a large number of collisions from all directions. These collisions cause the particles to move in a zigzag pattern, with no apparent direction and foreseeability. The laws that govern colloidal Brownian motion are based on the principles of statistical mechanics. They are related to the properties of the particles and the fluid in which they are suspended.

The two main rules that govern colloidal Brownian motion are intrinsically related to particle motion randomness and thermal behavior. Particle randomness results in an unpredictable motion of colloidal particles. The direction and speed of each particle are influenced by the complex interactions between the particle and the fluid molecules. The Brownian interactions are strongly influenced by the temperature of the medium in which they are suspended. As the temperature increases, the fluid molecules move faster and collide more frequently with the particles, causing them to move more rapidly and in a more aleatory manner. The relationship between the temperature and the speed of the particles is described by the *Einstein–Smoluchowski* equation.

The *Einstein–Smoluchowski equation*, also known as the *Stokes–Einstein equation*, is the fundamental equation for the description of the Brownian motion since it relates the diffusion coefficient of a particle to its size, the temperature of the fluid, and the viscosity of the dispersing fluid. The *Einstein–Smoluchowski equation* is given by Eq. 3.29.

$$D = \frac{kT}{6\pi\eta r} \quad (3.29)$$

In Eq. 3.29, D is the diffusion coefficient of the particle, which describes how rapidly the particle moves through the fluid. k is the Boltzmann constant, which relates temperature to energy. T is the absolute temperature. η is the fluid viscosity, and r is the particle radius. Equation 3.29 states that the diffusion coefficient of a particle is directly proportional to the temperature of the fluid and the particle radius, and inversely proportional to the fluid viscosity. This means particle Brownian motion is more thoughtful at higher temperatures, lower fluid viscosities, and smaller particles.

3.1.6 Hydration Interactions

The forces acting between surfaces separated by a thin layer composed of a polar solvent are labelled as solvation forces—often referred as structural forces. Solvation forces are monotonical repulsive forces, working in particles at distances commonly about 1–3 nm. If the solvent is water, these forces are referred to as hydration forces, which were initially proposed to explain the surprising stability of uncharged colloidal particles in solution. Solvation forces are non-DLVO forces that perform between hydrophilic surfaces on an exponential decay as a function of the distance between the surfaces, according to the Eq. 3.30.

$$F = F_o \cdot \exp\left(-\frac{D}{\lambda}\right) \quad (3.30)$$

F is the hydration force. F_o is a constant given by the force amplitude associated to the surface hydration (typically 3–30 mJ m⁻²). D is the surfaces spacing, and λ is the decay length (typically 0.6–1.1 nm).

Hydration forces are short-range forces that bestow stability to the systems having macromolecules, membranes, soap films, nanoparticles and others dispersion systems. The firstly identified by the abnormal phenomena occurring on surfaces of clay particles in water, termed swelling. These forces have origin in the dehydration energy to remove the water around two hydrophilic surfaces. The molecular ordering of liquid molecules around a single surface has been proved to be altered by the approaching of another similar surface. At short distances (< 1.5 nm) between surfaces, the liquid density profiles and the respective interaction pair-potentials are

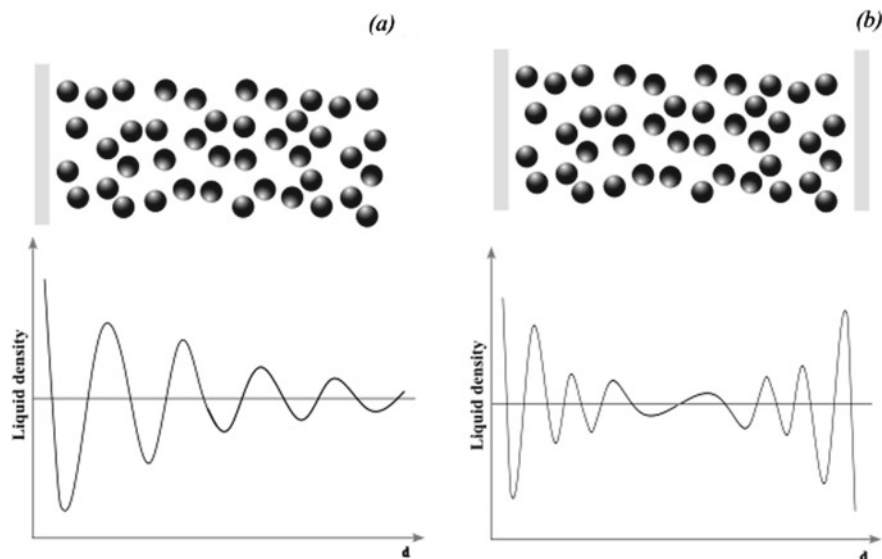


Fig. 3.9 The hydration forces between two solid surfaces. **a** Liquid density profile at a single solid–liquid interface. **b** Liquid density profile between two hard walls

expected to oscillate under a few molecular sizes range with a frequency almost corresponding to the molecular dimeter.

The hydration forces between two solid surfaces differ from those acting between amphiphiles in water solution, which form soap films and membranes. These forces have a similar nature to the steric (thermal fluctuation) forces that arise in polymer-covered surfaces, such as displayed in Fig. 3.9.

References

- Birdi KS. Handbook of surface and colloid chemistry. CRC Press, 2009.
- Davies JT, Rideal EK. Interfacial phenomena. New York and London: Academic Press; 1963.
- Dolan AK, Edwards SF. Theory of the stabilization of colloids by adsorbed polymer. Proc Roy Soc Lond Ser A. 1974;337(1611):509–16.
- Evans DF, Wennerström H. The colloidal domain—where physics, chemistry, biology, and technology meet. Wiley; 1999.
- Hamaker HC. The London—van der Waals attraction between spherical particles. Physica. 1937;4(10):1058–72.
- Haynes WM. Handbook of chemistry and physics. CRC Press; 2014–2015.
- Israelachvili JN. Intermolecular and surface forces. Academic Press; 2011.
- Lifshitz EM. The theory of molecular attractive forces between solids. Sov Phys JETP. 1956;2:73–83.
- Lyklema J. Fundamentals of interface and colloid science. Vol. II. Academic Press; 1995.
- Lyklema J. Fundamentals of interface and colloid science. Vol. III. Academic Press; 2000.

- Prausnitz JM, Lichtenthaler RN, Azevedo EG. Molecular thermodynamics of fluid-phase equilibria. Pearson; 1998.
- Rosen M. Surfactants and interfacial phenomena. New York: Wiley; 1989.
- Tadros TF. Formulation science and technology: basic theory of interfacial phenomena and colloid stability. De Gruyter; 2018.
- Van Oss CJ. Interfacial forces in aqueous media. CRC Press; 2006.

Chapter 4

Phase Equilibria of Colloidal Systems



Phase equilibria describe the various states of a colloidal system, including the solid, liquid, and gas phases, and the transitions between these phases. The colloidal phase behavior is affected by the dispersed species properties (as concentration, form and volume, molecular structure, and chemical nature), properties of the solvent (as solubility parameter, and chemical nature), temperature, and the interparticle interactions. However, the physical and chemical phenomena involved in phase equilibria that control the behavior of colloidal systems need to be properly described to allow applications in fields such as materials science, drug delivery, and environmental remediation. The complex phase behavior of colloidal systems, involving self-assembly and solubilizations, and versatile applications make the description of these systems intriguing. Especially, microemulsions, thermodynamically stable and optically transparent dispersions of oil, water, and surfactant molecules, require a separate treatment. Their spontaneous formation arises from the delicate balance between interfacial tension, solubilization, and the packing parameters of the surfactant molecules. The well-known Winsor system is used to describe the behavior and phase transitions that occur in liquid–liquid systems consisting of oil, water, and surfactant molecules. These systems are characterized by the presence of multiple phases and show unique phase behavior depending on the concentration of the surfactant. The phase transitions described in Winsor system can be induced by varying surfactant concentration, temperature, and the nature of the oil and surfactant. The phase behavior of Winsor systems is governed by the balance of interfacial forces, such as interfacial tension, solubilization, micellization, and the interactions between oil, water, and surfactant molecules. The type of surfactant, temperature, and the presence of co-surfactants can influence the phase transitions.

4.1 Liquid Phase Equilibria

Phase equilibrium in colloidal dispersions refers to the stable coexistence of distinct phases within the system, involving colloidal particles and the surrounding medium. These phases can include the dispersed phase (colloidal particles) and the continuous phase (liquid or gas medium). The equilibrium state is achieved when the interparticle and interfacial forces balance each other, resulting in a stable distribution and arrangement of particles in the dispersion. The description of phase diagrams enables to link the manifestation of specific interactions between the particle or molecular species with the occurrence of macroscopic phenomena (for details on nature and strength of specific interactions see Lyklema 2000, van Oss 2006, and Birdi 2009).

The phase equilibrium is defined by the total energy of the system, which is related to the chemical potential of the species in multicomponent systems. The Gibbs energy changes achieved during the process will define the phase behavior at constant temperature and pressure. Resembling regular solutions, the entropy and enthalpy that compose the Gibbs energy of mixing define if the mixture will be constituted by a homogeneous system, resulting in a fully miscibility, or if it will be composed by separate phases. The colloidal phase equilibrium can be described using the thermodynamic approaching similar to the liquid–liquid equilibrium of regular solution. The Fig. 4.1 illustrates the possible scenarios involved in multicomponent mixing. The mixing of pure components can result in (i) formation of a homogeneous single-phase mixture, (ii) formation of the distinctive phases, holding different compositions, (iii) unmixed system, containing the pure components. In the later, even so visually immiscible components, it is expected to be found tiny amounts mixed by some extension.

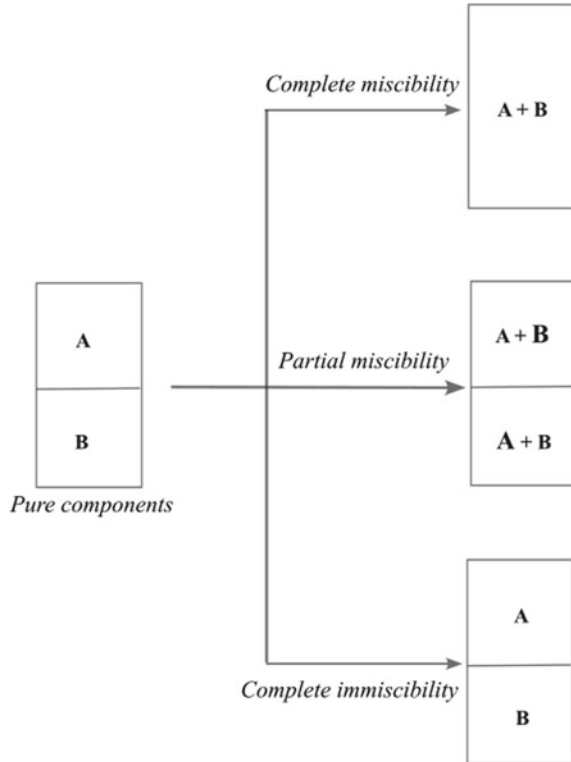
The change of the Gibbs energy during the mixing (ΔG_{mix}) is the key property to determine the phase distribution in the end of the process. The necessary and required condition to liquid system to achieve the miscibility in the entire composition range at constant temperature and pressure is given by Eq. 4.1 and Eq. 4.2 (for details of the phase equilibrium criteria, see Tester and Modell 1996). This means that the mixing process must lead to a reduction in the Gibbs energy of the system and the second order derivative of the Gibbs energy change must produce a minimum point over the fully range of composition.

$$\Delta G_{\text{mix}} < 0 \quad (4.1)$$

$$\left(\frac{\partial^2 \Delta G_{\text{mix}}}{\partial x^2} \right)_{T,P} > 0 \quad (4.2)$$

The Eqs. 4.1 and 4.2 must be simultaneously satisfied to assure the complete miscibility at a given temperature and pressure. Consequently, an unstable homogeneous system can satisfy the Eq. 4.1, even so a reduction of the Gibbs energy is observed, leading to a two-phase system at given composition. Nevertheless, usually

Fig. 4.1 Mixing process leads to different phase distribution for multicomponent systems



temperature changes promote miscibility gaps in liquid mixtures, which are pointed out as the upper and lower critical solution temperatures.

Figure 4.2 shows the three main mixture phase behavior presented in Fig. 4.1, illustrated by ΔG_{mix} —composition curves.

In Fig. 4.2, the curve *i* stands for a complete miscibility for the system. The curve *ii* exhibits a region where a local maximum is found. In this region, the Eq. 4.2 is not satisfied and then the system will be composed of two phases in equilibrium in the corresponding composition interval. The curve *iii* represents a typical immiscible system, which the mixing of the individual components leads to an increase in Gibbs energy for the entire composition range.

The phase equilibrium between liquid phases can be strongly disturbed by temperature changes. Even slight variation in the system temperature is able to displace the equilibrium state to a new configuration. Figure 4.3 presents a temperature-composition phase diagram describing the liquid–liquid equilibrium of single substance. The equilibrium curve, termed binodal curve, delineates the single phase and two-phase regions, and it is characterized by an upper critical solution that defines the maximum temperature in which the two phases can coexist. The dashed line, inside the two-phase region, is the spinodal curve, represented by the state where the second order derivative of the Gibbs energy change equals to zero. In this way,

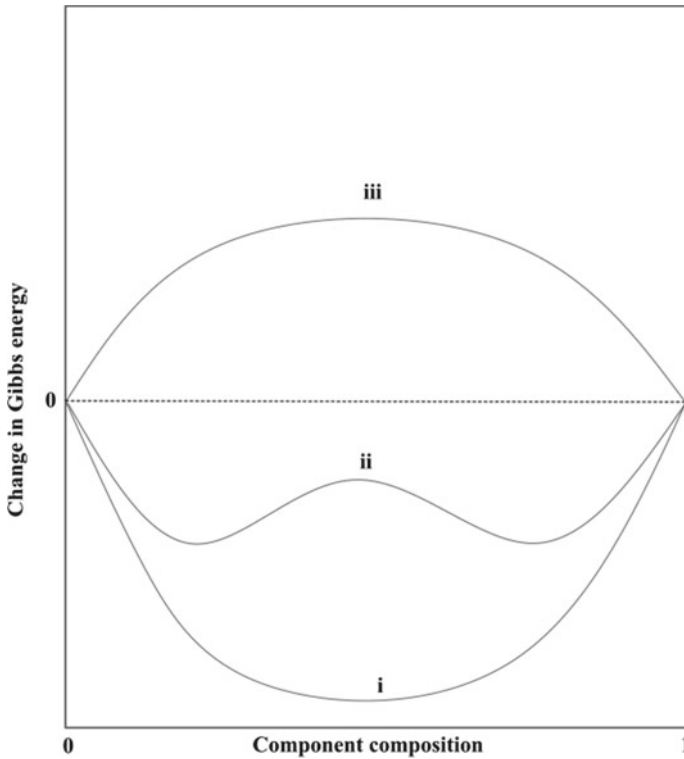


Fig. 4.2 Changes in Gibbs energy during the mixing of individual components. (i) miscible system, displayed as homogeneous phase, (ii) partially miscible system, displaying two-phase system, and (iii) immiscible system

the spinodal curve separates the phase instability region from the metastable region. Any temperature-composition condition within the unstable region will result in a spontaneous phase separation.

4.2 Colloidal Phase Equilibria

When a sufficient number of micelles are present in a solution, they begin to arrange themselves into different geometric patterns based on their shape, known as *liquid crystals*. Liquid crystals possess an ordered molecular arrangement similar to solid crystals but retain the mobility characteristic of liquids. The organized arrangement of molecules in liquid crystals leads to an increase in the viscosity of the solution phase, often to a significant extent. Specifically, spherical micelles pack together to form cubic liquid crystals, cylindrical micelles arrange themselves into hexagonal liquid crystals, and lamellar micelles create lamellar liquid crystals. Hexagonal

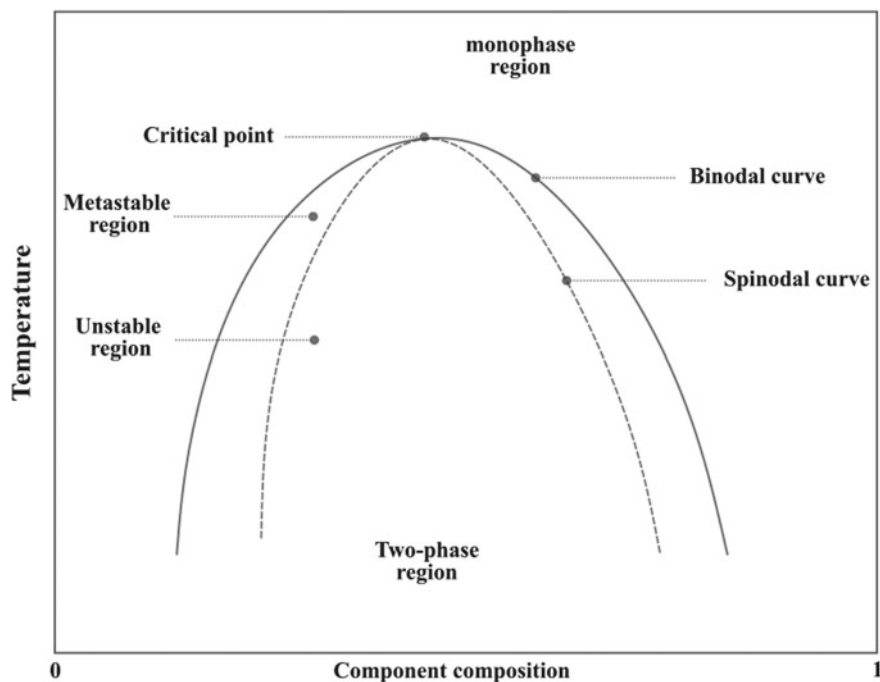


Fig. 4.3 Temperature composition diagram of a mixture at constant pressure

phases are more likely to form when surfactant molecules have a bulky head group, while lamellar phases are favored by surfactants with two alkyl groups. Both normal cylindrical micelles in aqueous media and reverse cylindrical micelles in nonpolar media are supposed to give rise to hexagonal liquid crystals (see further discussion in Shaw 1992 and Tadros 2018).

The transition from spherical to cylindrical to lamellar micellar structures occurs with an increase in surfactant concentration. Consequently, hexagonal phases are typically encountered at lower surfactant concentrations compared to lamellar phases. As surfactant concentration rises, some cylindrical micelles can become branched and interconnected, leading to the formation of a bicontinuous liquid crystalline phase where individual micelles are not discernible. Hexagonal and lamellar phases are anisotropic and can be visualized under a polarizing microscope. Hexagonal liquid crystals manifest as fan-shaped structures or display various irregular shapes, whereas lamellar liquid crystals show structural patterns (for details see Porter 1993 and Evans and Wennerstrom 1999).

Hexagonal phases, found in certain colloidal systems, display higher viscosity compared to lamellar phases, being that later are still more viscous than ordinary solutions. This variation in viscosity arises from the unique molecular arrangements and interactions within each phase. In a hexagonal phase, the colloidal particles or micelles are arranged in a hexagonal lattice structure. This arrangement leads to a

more packed and ordered configuration of the particles, resulting in stronger interparticle interactions. These stronger interactions require more energy to disrupt the structure and flow, leading to higher viscosity. The tightly packed hexagonal arrangement restricts the movement of particles, making it more difficult for them to slide past each other, thus increasing the overall resistance to flow. On the other hand, lamellar phases are characterized by a layered structure, with alternating layers of colloidal particles or micelles and the surrounding medium. This layered arrangement introduces additional friction and resistance to the flow of the system, resulting in higher viscosity compared to ordinary solutions. The alignment of particles in the lamellar structure restricts their mobility and makes it more challenging for them to move past one another. In contrast, ordinary solutions typically consist of randomly distributed molecules or particles in a solvent. The lack of organized structure and weaker intermolecular interactions in these solutions result in lower viscosity compared to the more ordered hexagonal and lamellar phases.

At high concentration of surfactants, spherical micelles tend to aggregate or cluster together. This aggregation leads to the formation of cubic liquid crystals, which are characterized by a three-dimensional arrangement of the micelles. The resulting cubic phases can display gel-like behavior, displaying extremely high viscosity. Cubic phases can also arise from bicontinuous structures. Bicontinuous structures are formed when the surfactant molecules arrange themselves in a way that creates two interpenetrating continuous regions. These structures have a complex network of interconnected channels and surfaces. Then, under certain conditions, these bicontinuous structures can transform into cubic phases, where the continuous regions form a cubic lattice-like arrangement. Both normal (where the hydrophilic heads are on the outside) and reverse (where the hydrophobic tails are on the outside) micelles and bicontinuous structures can give rise to cubic phases. The formation of cubic phases from various micellar and bicontinuous structures highlights the versatility and adaptability of surfactant systems. These cubic phases have unique properties and can exhibit high viscosity, resembling gels.

The cubic phases, similar to spherical micelles, are isotropic structures, which implies they cannot be directly seen using a polarizing microscope. However, their presence can be detected by employing dyes that are soluble in water or oil, as these dyes interact distinctively with the separate phases of the systems.

Typically, aqueous surfactant system displays multiple distinct phases, including micellar solutions, liquid crystals, and gels. The phase region and the phase transition are usually illustrated as temperature—surfactant concentration phase diagram. Figure 4.4 presents a generic phase diagram (without denoting the system) that point out the influence of temperature and surfactant concentration on the different solution phases observed in an aqueous surfactant system. This phase diagram demonstrates the representative sequential order of liquid crystal phases that occur as the surfactant concentration increases starting from monomer surfactant solvated going into micellar solutions, progressing to hexagonal phases, followed by bicontinuous cubic phases, and finally reaching lamellar phases. This ordering of liquid crystal phases is commonly found in various surfactant systems.

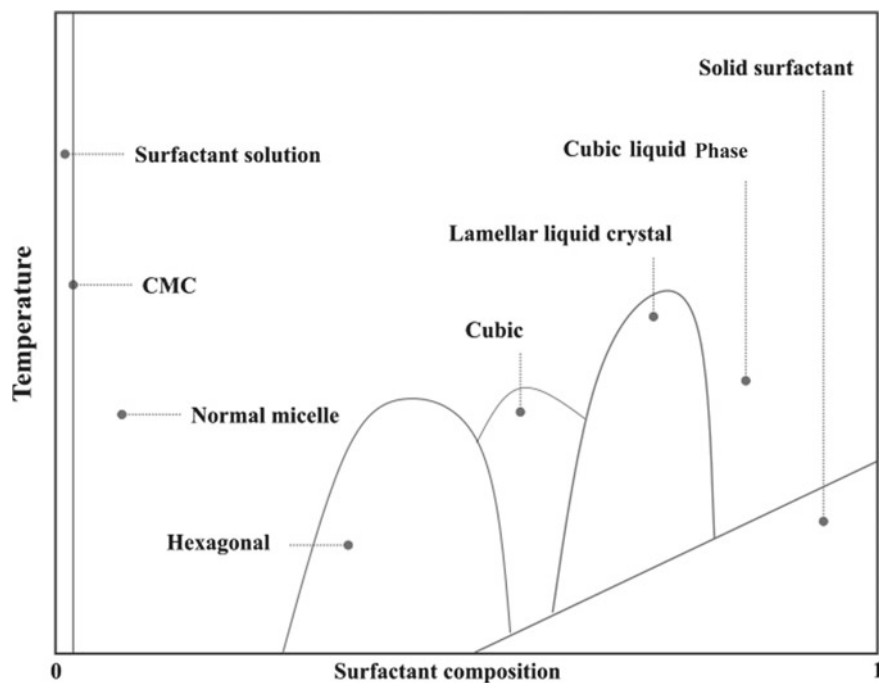


Fig. 4.4 Temperature-composition phase diagram

The effect of temperature on the phase behavior in Fig. 4.4 is typical for surfactants whose solubility increases with temperature. As the temperature rises, all the liquid crystal phases undergo a transition and transform into micellar solutions. This temperature-driven transition leads to the dissolution of the ordered structures representative of liquid crystal phases, and the system becomes homogeneous in the form of micelles. However, it is important to note that at high surfactant concentrations and low temperatures, there is a possibility of solid surfactant precipitating out of the solution. This occurs when the surfactant concentration exceeds its solubility limit at the given temperature, leading to the formation of solid particles within the system.

The phase boundaries in a phase denotes the sensitivity of the phase transition to the temperature. Ionic surfactants tend to present boundary lines almost vertical, indicating a typical inattentiveness to the temperature changes.

Hydrotropes are organic additives that can be employed to reduce the tendency of surfactant systems to form crystalline structures. These nonsurfactant organic compounds have been utilized for many years due to their ability to enhance the solubility and decrease the viscosity of organic substances in water. Although hydrotropes possess a structure similar to surfactants, featuring both a hydrophilic and a hydrophobic group in their molecules, they differ in the nature of their hydrophobic component. Typically, hydrotropes have a relatively short, cyclic, or branched hydrophobic group.

Various hydrotropes can be used in surfactant systems to achieve the desired effects. Some common examples include p-cymenesulfonates, 2-hydroxy-1-naphthalenesulfonate, and sodium 2-ethylhexyl sulfate. These compounds effectively enhance the solubility of organic substances in water by reducing their tendency to form crystalline structures. Incorporating hydrotropes into surfactant formulations, the solubility of organic compounds can be improved, leading to enhanced performance in various applications such as cleaning products, detergents, and industrial processes.

4.3 Rheology of Colloidal Surfactant

The rheological properties of surfactant solutions are primarily concerned with their flow behavior, which is closely associated with solution viscosity. At low concentrations, surfactant solutions form uniform spherical micelles and show often Newtonian fluid behavior. In this case, the applied shearing stress is directly proportional to the rate of shear, resulting in a linear relationship between stress and strain. However, as the surfactant concentration increases, the shape of the aggregate change from uniform spherical micelles to more asymmetrical structures such as large micelles, cylinders, or bilayers. This change in aggregate shape leads to a non-Newtonian behavior in the solutions, where the relationship between stress and strain becomes nonlinear. The viscosity of the solutions also increases significantly with higher surfactant concentrations.

The non-Newtonian behavior observed in surfactant solutions at higher concentrations is a result of the complex interactions and arrangements of the surfactant molecules within the aggregates. These structural changes introduce additional resistance to flow, causing the viscosity of the solution to rise sharply. The flow behavior of these solutions may display shear-thinning (decreasing viscosity with increasing shear rate) or shear-thickening (increasing viscosity with increasing shear rate) tendencies, depending on the specific surfactant system and concentration.

4.4 Microemulsion and Macroemulsion

Systems constituted by water, oil and surfactant are especially important to the industrial application. These systems can be drawn on a wide variety of phase distribution and a numerous range of properties.

Emulsification is a process that plays a crucial role in various industries due to its ability to create stable emulsions from two liquid phases that are ordinarily immiscible. The practical applications of emulsification are extensive, ranging from the production of paints, polishes, and pesticides to the formulation of metal cutting oils, margarine, ice cream, cosmetics, metal cleaners, nanoparticles, and textile processing oils.

An emulsion is a mixture of two immiscible liquids in which one liquid is dispersed as small droplets within another one, which represents the continuous phase. Emulsion has the ability to keep unchanged its structure and properties for a desired period, which can vary from few minutes to several years depending on the intended application. It is important to note that the formation of emulsions requires the presence of an emulsifying agent. Two immiscible pure liquids alone cannot form a stable emulsion. The emulsifying agent, typically a surface-active agent or surfactant, acts as a stabilizer by reducing the interfacial tension between the two immiscible liquids. Although surfactants are commonly used as emulsifying agents, other substances such as finely divided solids can also fulfill this role. In fact, the most effective emulsifying agents often consist of mixtures of two or more substances, as their combined properties can enhance emulsion stability and functionality.

Emulsions are classified into three main types based on the size of the dispersed particles:

- (i) **Macroemulsions:** These are the most well-known type of emulsions and are characterized by their opaque appearance. The particles in macroemulsions are larger than $0.4\ \mu\text{m}$ ($400\ \text{nm}$) in size, making them easily visible under an optical microscope. These macroemulsions often exhibit distinct phases and are commonly encountered in conventional products;
- (ii) **Microemulsions:** Unlike macroemulsions, microemulsions are transparent dispersions. The particles in microemulsions are much smaller, typically less than $0.1\ \mu\text{m}$ ($100\ \text{nm}$) in size. Microemulsions have a unique structure with a high degree of mixing at the molecular level, resulting in enhanced stability and transparency.
- (iii) **Nanoemulsions (miniemulsions):** Nanoemulsions have particle sizes that fall between those of macroemulsions and microemulsions, ranging from $0.1\text{--}0.4\ \mu\text{m}$ ($100\text{--}400\ \text{nm}$). They show a distinctive blue-white appearance. Due to their unique properties attributed to their nanoscale structure, nanoemulsions are gaining increasing attention in various applications, particularly in pharmaceuticals and cosmetic formulations.

4.4.1 Macroemulsions

Macroemulsions can be classified into two main types: oil-in-water (O/W) and water-in-oil (W/O) emulsions. In O/W emulsions, an immiscible oil phase is dispersed as droplets within an aqueous phase, with the oil being the discontinuous phase and water the continuous phase. On the other hand, W/O emulsions involve the dispersion of water or an aqueous solution as droplets within an immiscible oil phase, where water becomes the discontinuous phase and oil the continuous phase. The type of emulsion formed depends on the nature of the emulsifying agent, the preparation process, and the proportions of oil and water used.

The stability of O/W and W/O emulsions is typically governed by the Bancroft rule. According to this rule, an emulsion is more stable when the emulsifying agent

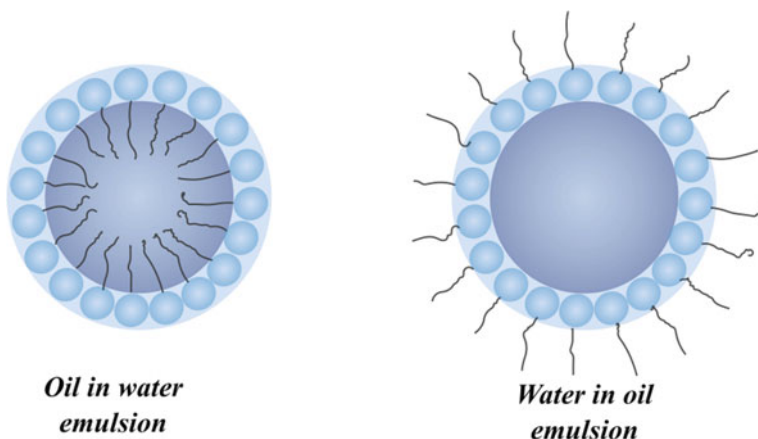


Fig. 4.5 Illustration of arrangement of oil, water and surfactant on oil and water droplets of emulsions

is more soluble in the continuous phase compared to the discontinuous phase. O/W emulsions are formed when the emulsifying agent is more soluble in water, while W/O emulsions are produced when the emulsifying agent is more soluble in the oil phase. The configuration of dispersed droplets in oil in water and water in oil emulsions is displayed in Fig. 4.5.

O/W and W/O emulsions are not in thermodynamic equilibrium with each other. However, the emulsion type can be inverted by changing the conditions, resulting in the conversion of an O/W emulsion into a W/O emulsion or vice versa. This process is known as the inversion of the emulsion. Experimental methods can be employed to distinguish between these two types of emulsions, including dilution, electrical conductivity, and refractive index measurements. O/W emulsions can be easily diluted with more of the outer phase (water), while W/O emulsions are not easily diluted with the inner phase (oil). O/W emulsions show electrical conductivities similar to that of the water phase, while W/O emulsions do not conduct significant electrical current. Microscopic examination of emulsion droplets can also aid in determining their nature based on differences in refractive indices. Droplets with higher refractive indices than the continuous phase appear brighter when focused upward, while droplets with lower refractive indices appear darker.

When macroemulsions are formed, one of the immiscible liquids is dispersed as particles within the second liquid. However, the interfacial tension between these immiscible liquids is always greater than zero, resulting in a significant increase in the interfacial energy. Consequently, the formed emulsion is thermodynamically unstable compared to the separate bulk phases. Strictly, pure immiscible liquids cannot form stable emulsions. The emulsifying agent plays a crucial role in stabilizing this inherently unstable system for a certain duration, allowing it to serve its intended purpose. The emulsifying agent achieves stabilization by adsorbing at the interface between the two liquids, forming an oriented interfacial film (see Chap. 5).

The interfacial molecular adsorption has two primary roles. Firstly, it reduces the interfacial tension between the liquids, thereby decreasing the thermodynamic instability caused by the increased interfacial area. The reduction in interfacial tension minimizes the amount of mechanical work required to disperse the inner liquid into particles. Secondly, it creates mechanical, steric, and/or electrical barriers around the dispersed liquid particles, hindering their coalescence. Steric and electrical barriers prevent close contact between particles, while the mechanical barrier enhances their resistance to coalescence upon collision.

The rate of coalescence of droplets in a macroemulsion serves as a quantitative measure of its stability. The rate of coalescence can be assessed by counting the number of droplets per unit volume of the emulsion over time. The coalescence rate will be affected by:

- (i) Physical–chemical properties of the interfacial film: The characteristics of the emulsifying agent’s film at the interface play a crucial role in determining the stability of the emulsion. The film’s thickness, composition, and ability to withstand mechanical forces and disruption affect the coalescence rate;
- (ii) Electrical and steric barriers on the droplets: Emulsifying agents can create electrical or steric barriers around the dispersed droplets. Electrical barriers arise from charged particles or surfactants adsorbed at the droplet interface, preventing close approach and coalescence. Steric barriers occur when large molecules or polymers adsorb at the interface, creating a physical hindrance to droplet coalescence;
- (iii) Viscosity of the continuous phase: The viscosity of the continuous media affects the mobility of the dispersed droplets. High viscosity impedes droplet movement and reduces the chances of coalescence;
- (iv) Droplet size distribution: The size distribution of the dispersed droplets is a key factor in stability. Emulsions with a narrow size distribution tend to be more stable since smaller droplets have a higher surface area and are more prone to coalescence.
- (v) Phase volume ratio: The ratio of the dispersed phase to the continuous phase can influence stability. Optimal phase volume ratios can enhance stability by providing a balance between droplet dispersion and interfacial coverage;
- (vi) Temperature: Particle mobility and interactions between droplets and the continuous phase are affected by the temperature. Temperature changes can alter the coalescence rate and overall stability of the emulsion.

In a scientific context, gelation refers to the transformation of a liquid colloidal system into a gel, which shows solid-like behavior. This process involves the formation of physical or chemical crosslinks between the particles or droplets present in the system. These crosslinks can be spontaneous, occurring due to particle interactions, or they can be induced by adding a crosslinking agent. The formation of a gel network imparts structural integrity to the system, resulting in the solid-like properties typically seen in gels. The characteristics of the gel, such as its flexibility or brittleness, depend on the strength and type of crosslinks formed between the particles or droplets.

Flocculation, on the other hand, describes the aggregation or clumping together of particles or droplets in a colloidal system, leading to the formation of larger structures that are visible to the naked eye. Flocculation can be triggered by changes in the concentration or pH of the system. It can also occur when the stabilizing agents or surfactants present in the system are no longer effective in preventing particle interactions. The aggregation of particles in flocculation is reversible, meaning that the larger structures formed can often be easily dispersed back into the system. Coagulation is similar to flocculation but occurs on a larger scale and typically involves irreversible aggregation of particles or droplets. Coagulation can be induced by high temperatures, changes in pH and ionic strength, or the presence of coagulating agents, including metal ions. When coagulation takes place, the particles or droplets lose their individual identities and form irreversible aggregates, leading to the formation of larger clumps or solids.

Sedimentation refers to the settling of particles or droplets in a colloidal system to the bottom of the container under the influence of gravity. This process occurs over time as a result of the density difference between the particles or droplets and the surrounding medium. Sedimentation can lead to the separation of components in a colloidal system, with the denser particles or droplets settling at the bottom while the lighter components remain in the upper layer.

4.4.2 *Microemulsion*

Microemulsions are stable and transparent dispersions composed of two immiscible liquids, with particle sizes ranging from 10 to 100 nm. Unlike macroemulsions, which require vigorous agitation for their formation, microemulsions can be obtained by gentle mixing of the ingredients. Microemulsions can be categorized as water-external (O/W), oil-external (W/O), or bicontinuous, meaning both phases are continuous throughout the system (for details on microemulsions see Evans and Wennerstrom 1999 and Lyklema 1995).

There are two ways to conceptualize a microemulsion: (i) as a solution in one liquid where micelles are swollen by a solubilized second liquid, (ii) as a dispersion of tiny droplets of one liquid in a second liquid. In either case, the interfacial tension between the microemulsion and the two liquids it contains must be close to zero. In the first case, the system exists as a single phase with no interface against either liquid as long as the micelles can solubilize more of the second liquid. In the second case, the interfacial area is so large that an extremely low interfacial tension is needed to form the microemulsion with minimal energy. The interfacial region must also be highly flexible to accommodate the curvature necessary to surround very small particles or to facilitate the transition between oil-continuous and water-continuous structures typically observed in microemulsions.

The clear, fluid middle phase found in a three-phase system, situated between a nonpolar phase (O) and an aqueous phase (W), is commonly reported as a microemulsion. Increasing the surfactant concentration in the middle phase causes the merging

of both oil and water phases into a single microemulsion phase. The formation of microemulsions can be guided by the Winsor R ratio, which measures the capacity for water solubilization relative to oil. Altering the surfactant structure, temperature, cosurfactant addition, or electrolyte incorporation can modify the solubilization capacity of the system for water, oil, or both.

Winsor ratio is the most spread method to categorize the phase behavior of microemulsion systems, outlining equilibrium stages depicted in Fig. 4.6. The Winsor system is a framework for understanding the behavior of surfactant systems and their ability to form different types of microemulsions. Winsor categorized microemulsions into four types: Type I, Type II, Type III, and Type IV. Initially, in the absence of any surfactants, the oil and water phases are immiscible and separate.

Type I microemulsion (O/W) is formed when a surfactant system is added to the mixture. In this type, the surfactant-rich water phase is in equilibrium with the oil phase, and the surfactants exist as monomers at low concentrations. The surfactant molecules reduce the interfacial tension between the oil and water, facilitating the formation of small oil droplets dispersed in the continuous water phase.

Type II microemulsion (W/O) occurs when the surfactant-rich oil phase combines with the surfactant-poor aqueous phase. Here, the surfactants are primarily present in the oil phase, leading to the formation of small water droplets dispersed in the continuous oil phase.

If the surfactant system has the ability to form a stable microemulsion, a third phase known as Type III microemulsion appears at the interface between the oil and water phases. In this case, both the water and oil phases are deficient in surfactant content. Type III microemulsions are characterized by the coexistence of small oil droplets and water droplets, with surfactants forming an interfacial layer around them. The interfacial tension between the oil and water phases is significantly reduced in this type of microemulsion.

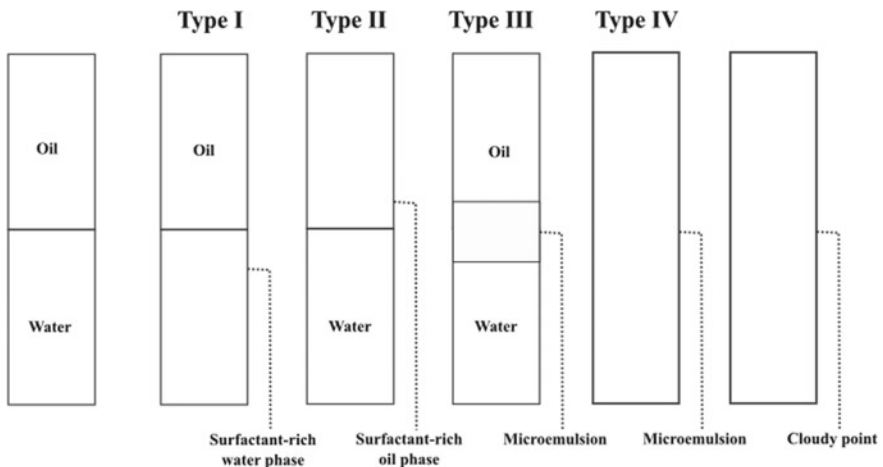


Fig. 4.6 Winsor classification of systems containing microemulsions

Type IV microemulsion is an extension of Type III microemulsion at higher surfactant concentrations. As more surfactant is added, the middle phase expands and becomes a single-phase microemulsion. In this type, the entire system forms a homogeneous mixture with no visible distinction between the oil and water phases. Beyond the Type IV microemulsion, further addition of the surfactant system leads to phase separation, known as the *cloud point* (see Chap. 2). This occurs when the surfactant concentration exceeds the maximum capacity of the system to form a stable microemulsion, resulting in the separation of the oil and water phases.

4.5 Solubilization

Solubilization is a crucial phenomenon that occurs when surfactant molecules form micelles in a solvent and incorporate insoluble substances into their structures, resulting in their dissolution. It refers to the spontaneous dissolution of a substance, whether it is a solid, liquid, or gas, through reversible interactions with surfactant micelles in a solvent. Solubilization occurs when substances that are normally insoluble or poorly soluble in the solvent come into contact with the surfactant micelles. The hydrophobic regions of the micelles have an affinity for the insoluble substance, allowing it to be incorporated into the micellar structure. This process is driven by reversible interactions, such as van der Waals forces, hydrophobic interactions, and hydrogen bonding.

The result of solubilization is the formation of a thermodynamically stable isotropic solution. In this solution, the solubilized material is dispersed throughout the solvent in a molecularly dispersed form, rather than as separate particles. This leads to a reduction in the thermodynamic activity of the solubilized material, meaning its concentration is effectively reduced and its interactions with other substances in the solution are altered. Solubilization has significant practical implications in various fields. It enables the incorporation of water-insoluble ingredients into aqueous formulations, eliminating the need for organic solvents or co-solvents. Also, solubilization helps in the removal of oily soils by dissolving them into the surfactant micelles. In addition, it also plays a role in micellar catalysis, emulsion polymerization, and enhanced oil recovery processes (See Stokes and Evans 1997).

Even in non-aqueous media, solubilization is of paramount importance in dry cleaning processes. For example, the solubilization of materials in biological systems giving insights into the mechanisms of interaction between drugs, pharmaceutical substances, and lipid bilayers and membranes.

The solubilization behavior of surfactants in relation to temperature is a complex phenomenon. When considering ionic surfactants, an increase in temperature generally enhances the solubilization of both polar and nonpolar solubilizates. This effect can be attributed to the greater thermal agitation present at higher temperatures, which provides increased space within the micelle for the solubilizates to interact with the surfactant molecules. For nonionic surfactants, the solubility behavior in response to temperature changes depends on the characteristics of the solubilizate.

Nonpolar solubilizates, such as aliphatic hydrocarbons and alkyl halides, are solubilized within the inner core of the micelle. As the temperature rises, their solubility tends to increase, and this trend becomes more pronounced as the critical point is approached. In contrast, the solubility behavior of polar solubilizates, which are solubilized within the surround layer of the micelle, displays a different pattern. Initially, as the temperature increases, the solubilization of polar solubilizates shows a slight to moderate increase. This initial increase can be attributed to the enhanced thermal agitation of the surfactant molecules within the micelles, which promotes solubilization. However, as the temperature continues to rise, the solubilization of polar solute decreases. This decrease in solubilization is caused by increased dehydration and tighter coiling of chains, which leads to reduced available space within the palisade layer of the micelle. This effect is particularly significant for short-chain polar compounds that are solubilized near the surface of the micelle.

Figure 4.7 shows the solubilization curve of nonpolar compounds in aqueous solution of nonionic surfactant as a function of the temperature and hydrophobic chain length of the surfactant. The amount of nonpolar compound is limited to the size, structure and aggregation number of the surfactant aggregate.

When molecules are incorporated into a micelle, it can have a significant impact on the micelle's nature and shape. Specifically, when nonpolar material is introduced into the micelle's inner core, the packing parameter increases. This increase in the structure parameter leads to heightened asymmetry of the micelle when it is in an aqueous medium. As the asymmetry increases, a normal micelle can undergo a transformation and become a lamellar micelle. Furthermore, as more nonpolar material is added, the lamellar micelle can further change its shape and become an inverted

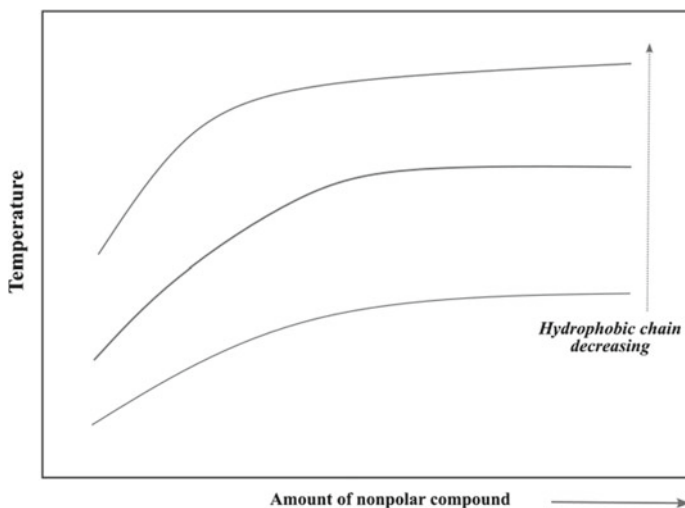


Fig. 4.7 Solubilization curve of nonpolar compounds in aqueous solution of nonionic surfactant as a function of the temperature and alkyl-chain length

lamellar micelle. In a nonpolar medium, continued incorporation of nonpolar material can ultimately result in the formation of a spherical inverted micelle. Conversely, the reverse process is also possible. In an aqueous medium, an inverted micelle that exists in a nonpolar medium can transform back into a normal micelle with the addition of increasing amounts of water.

In addition to these micellar structures, the presence of liquid crystalline phases is dependent on parameters including the specific structure of the surfactant, the characteristics of the nonpolar solubilize, and the ratios of surfactant to water and nonpolar material in the system. The inclusion of medium-chain alcohols, which are solubilized near the micelle's surround layer, has a notable effect on the micelle's behavior. This inclusion increases the molecular area, a parameter associated with the micelle's size. As the value of molecular area increases, there is a greater tendency for the formation of spherical micelles (see Table 2.2). On the other hand, an increase in the ionic strength of the aqueous solution or the concentration of an ionic surfactant in the aqueous phase has a contrasting effect. It reduces the value of the molecular area and promotes the formation of cylindrical or lamellar micelles instead of spherical ones.

References

- Birdi KS. Handbook of surface and colloid chemistry. CRC Press; 2009.
- Evans DF, Wennerström H. The colloidal domain—where physics, chemistry, biology, and technology meet. Wiley; 1999.
- Lyklema J. Fundamentals of interface and colloid science. Vol. II. Academic Press; 1995.
- Lyklema J. Fundamentals of interface and colloid science. Vol. III. Academic Press; 2000.
- Porter MR. Handbook of surfactants. New York: Springer Science e Business Media; 1993.
- Shaw DJ. Introduction to colloid and surface chemistry. Elsevier; 1992.
- Stokes RJ, Evans DF. Fundamentals of interfacial engineering. Wiley-VCH; 1997.
- Tadros TF. Formulation science and technology: basic theory of interfacial phenomena and colloid stability. De Gruyter; 2018.
- Tester JW, Modell M. Thermodynamics and its applications. Prentice Hall; 1996.
- Van Oss CJ. Interfacial forces in aqueous media. CRC Press; 2006.

Chapter 5

Surface Tension and Its Derivative Properties



Interfacial science reports the phenomena came from interactions at the region between two different phases, such as a solid and a liquid or a gas and a liquid. These phenomena have been the subject of extensive study in surface thermodynamics due to their incidence in many natural and industrial systems. Surface tension is the key thermodynamic property in interfacial phenomena. The surface tension is a measure of the energy required to increase the interface surface area, and it is often used as a standpoint to describe the interface behavior, equilibrium, and properties. Surface tension is directly related to the concept of surface free energy—a measure of the total energy of the interface—and it represents a physical property that arises due to the cohesive forces between the molecules at the surface. The molecules in the inner of a liquid experience attractive forces from neighboring molecules in all directions. However, the molecules at the surface do not have the same neighboring molecules on all sides, resulting in an imbalance of forces. This imbalance leads to the surface acting like a stretched elastic membrane, which gives rise to surface tension. To describe the interfacial phenomena, a combination of experimental techniques, theoretical models, and computational simulations is employed. Experimental methods include surface characterization techniques, such as spectroscopy, microscopy, and surface-sensitive probes. Theoretical models and simulations help explain and predict interfacial behavior by considering molecular interactions, thermodynamics, and transport phenomena at interfaces. Surface thermodynamics is based on the principles of classical thermodynamics, consolidating itself as a critical field of investigation due to the very broad range of applications.

5.1 The Basic of Interfacial Thermodynamics

The internal energy (U) for a closed system can be derived from the coupling of the First and Second thermodynamics laws. Whereas the heat (Q) and work (W) are *way functions*, the resulting coupled equation is constituted only of *state functions*, as described in an extensive form by Eq. 5.1, designated *Thermodynamic Fundamental Equation*.

$$d(n \cdot U) = T \cdot d(n \cdot S) - P \cdot d(n \cdot V) \quad (5.1)$$

In Eq. 5.1, T , S , P , and V represent respectively temperature, molar entropy, pressure, and molar volume. n is the number of moles of the system. Equation 5.1 is applied to single, monophasic systems, where external forces such as electrical, tensile, and others are not acting. In this view, the extensive form of the internal energy can be written as a two-variable function $U = U(S, V)$. Equation 5.1 provides the essential and satisfactory information to describe any stable equilibrium state of a simple closed system. However, S is not a fully accessible variable. Conversion of non-measurable variables into measure variables is feasible through transforming derivate methods, Jacobian transformation, and Legendre transformation (see details in Tester and Modell, 1996).

By Euler integration, the Gibbs energy (G) can be related to the internal energy (U) in closed systems by Eq. 5.2.

$$G = U + P \cdot V - T \cdot S \quad (5.2)$$

The differentiation of the Eq. 5.2, using the chain rule expansion, along with Eq. 5.1 produces the total differential of the extensive Gibbs energy ($n \cdot G$) represented as a two-variable function $G = G(P, T)$, given by Eq. 5.3.

$$d(n \cdot G) = -(n \cdot S) \cdot dT + (n \cdot V) \cdot dP \quad (5.3)$$

Equation 5.3 can be expressed in terms of its partial derivatives, such as illustrated in Eq. 5.4.

$$d(n \cdot G) = \left[\frac{\partial(n \cdot G)}{\partial T} \right]_{P,n} \cdot dT + \left[\frac{\partial(n \cdot G)}{\partial P} \right]_{T,n} \cdot dP \quad (5.4)$$

If now the system boundaries allow the mass exchange (constituting an open system), the total differential of the Gibbs energy must include the mass as a variable that can affect the system properties. In this case, Gibbs energy must be written as a three-variable function $G = G(T, P, n)$. For a system containing N components, Gibbs energy becomes a $N + 2$ variables function $G = G(T, P, n_1, n_2, n_3, \dots, n_N)$, which is described by the Eq. 5.5.

$$d(n \cdot G) = \left[\frac{\partial(n \cdot G)}{\partial T} \right]_{P,n} \cdot dT + \left[\frac{\partial(n \cdot G)}{\partial P} \right]_{T,n} \cdot dP + \sum_{i=1}^N \left[\frac{\partial(n \cdot G)}{\partial n_i} \right]_{T,P,n_j} \cdot dn_i \quad (5.5)$$

n_i is the total number of moles of the i -component in the system. The j -subscript represents all other substances in a way that n_j is kept constant while n_i changes. The subscript in the partial derivatives shows the variables which are kept constant. Mathematically, j -components are all of components whose the number of moles does not change, whereas i -component is added or removed from the system. Equation 5.5 represents the total differential of the extensive Gibbs energy for a system in what the temperature, pressure and mass can change. Equation 5.5 can be applied to any simple, open systems, where it is not incident on the Gibbs energy effects as surface deformation work, electric charge transport, magnetic polarization, elastic deformation, among others. Table 5.1 displays the further thermodynamic functions derived from the thermodynamic fundamental equation for simple systems.

Particularly for an interfacial system on which a substance is allowed to be adsorbed or desorbed on the interface, the Gibbs energy must take in account the changes in interface area caused by the unbalanced forces between the two phases. Then, the contribution from the interfacial area changes on the Gibbs energy must be an additional term in the total differentiate of system Gibbs energy, such as displayed in Eq. 5.6.

$$d(n \cdot G) = \left[\frac{\partial(n \cdot G)}{\partial T} \right]_{P,n} \cdot dT + \left[\frac{\partial(n \cdot G)}{\partial P} \right]_{T,n} \cdot dP + \sum_{i=1}^N \left[\frac{\partial(n \cdot G)}{\partial n_i} \right]_{T,P,n_j} \cdot dn_i + \left[\frac{\partial(n \cdot G)}{\partial (nA)} \right]_{T,P,n} \cdot dA \quad (5.6)$$

Table 5.1 Thermodynamic equations for simple systems

Thermodynamic property	Canonical coordinates	Total differential
Gibbs energy (G)	T, P, n_i ($i = 1, \dots, N$)	$d(n \cdot G) = -(n \cdot S) \cdot dT + (n \cdot V) \cdot dP + \sum_{i=1}^N \mu_i \cdot dn_i$
Helmholtz energy (A)	T, V, n_i ($i = 1, \dots, N$)	$d(n \cdot A) = -(n \cdot S) \cdot dT + P \cdot d(n \cdot V) + \sum_{i=1}^N \mu_i \cdot dn_i$
Intern energy (U)	S, V, n_i ($i = 1, \dots, N$)	$d(n \cdot U) = T \cdot d(n \cdot S) - P \cdot d(n \cdot V) + \sum_{i=1}^N \mu_i \cdot dn_i$
Enthalpy (H)	S, P, n_i ($i = 1, \dots, N$)	$d(n \cdot H) = T \cdot d(n \cdot S) + (n \cdot V) \cdot dP + \sum_{i=1}^N \mu_i \cdot dn_i$

Equation 5.6 describes the variation of the Gibbs energy in a system whose the heat, work and mass can be moved in or moved out and the area is allowed to change caused by interfacial phenomena. Since that postulate $N + 2$ independent variables to specify the system equilibrium state is still hold, the thermodynamic laws were not violated. The two first terms on the right side of the Eq. 5.6 are defined by comparison between Eqs. 5.3 and 5.4. From this, it is possible to write the partial derivate of the total Gibbs energy with regard to the temperature as the opposite of the entropy ($-n \cdot S$) and the partial derivate of the total Gibbs energy concerning the pressure as the volume ($n \cdot V$), both given as extensive properties. The third term on the Eq. 5.6 shows the partial differentiate of the total Gibbs energy in relation to the total number of moles of the i -component, keeping constant the temperature, pressure, interfacial area, and the total number of moles of all other components (j -components). This partial differentiate defines the *chemical potential* of the i -component, designate as μ_i . The *i -component chemical potential* is an important thermodynamic property to indicate the thermodynamic equilibrium state, and it shows the response on the Gibbs energy of the system from a perturbation on *i -component* mole number. Legendre transformation enables to obtain μ_i concerning the internal energy, changing the restrain from T, P and n_j to S, V and n_j .

Lastly, the fourth term on Eq. 5.6 displays the G partial differentiate in relation to the area, dictating the contribution of a perturbation in the area amount on the Gibbs total energy of the entire system, which defines another especially important thermodynamic entity: the *interfacial tension* (γ_i). The interfacial tension (IFT) represents the amount of energy required to extend an interface by one unity of area employing an isothermal, isobaric and reversible process. The IFT can be defined by the ratio between the utilized energy amount (E) and the total area (A) that was created on the interface (Eq. 5.7). Correspondingly, the interfacial tension can be given by the ratio between the resulting force acting to displace an interface (F) and the respective distance displaced (L) (Eq. 5.8), which has been applied to the IFT experimental determination in commercial apparatus (see further discussion in Shaw 1992).

$$\gamma = \frac{E}{A} \quad (5.7)$$

$$\gamma = \frac{F}{L} \quad (5.8)$$

Inserting the properties defined by the partial differentiates into Eq. 5.6 results in Eq. 5.9.

$$d(n \cdot G) = -(n \cdot S) \cdot dT + (n \cdot V) \cdot dP + \sum_{i=1}^N \mu_i \cdot dn_i + \gamma \cdot d(n \cdot A) \quad (5.9)$$

Equation 5.9 is a fundamental relationship of the Gibbs energy applied to opened and single-phase systems with significant contribution from the tensive forces. Then, it can be labelled as a *generator* function that allows obtain similar relationships to other primary thermodynamic properties of the system, i.e. enthalpy (H), entropy (S), Helmholtz energy (A), using conveniently the methods for transforming derivatives.

Each term in the right side of the Eq. 5.9 encompasses a potential of energy and work acting in the system. According to the forces acting in the system, other potentials formed by thermodynamic conjugate variables should be added to Eq. 5.9. Some common types of energy and work interactions are presented in Table 5.2.

Whereas the integration of the total differentiate of Gibbs energy represented by the Eq. 5.9 outlines the system equilibrium state, the primary thermodynamic properties are obtained from the first differentiate of the Gibbs energy function. The Gibbs energy second-order derivatives (corresponding to the first-order derivatives of the primary thermodynamic properties) indicate the partial molar properties (in relation to the number of moles) and associated response functions (in relation to the temperature and pressure), such as it can be seen in Table 5.1. Partial molar properties (\bar{M}_i) express the response from the total extensive property ($n \cdot M$) to a perturbation in the molar quantity of the i -component. The representative equations to the isobaric heat capacity (C_p), isothermal compressibility (κ_T), and isobaric thermal expansivity (α_p) are also response functions. These relationships are comprehensively presented in Table 5.3.

Table 5.2 Typical energy and work potentials acting in non-simple systems (adapted from Tester and Modell 1996)

Phenomenon	Interaction potential
Expansion-compression work	$-P \cdot dV$
Reversible heat	$T \cdot dS$
Mass flow energy	$\mu_i \cdot dn_i$
Surface deformation energy	$\gamma \cdot dA$
Electrical charge transport	$\varepsilon \cdot dq^a$
Generalized work	$F \cdot dx$

^a ε is the medium permittivity and q is the electric charge

Table 5.3 Response functions derivate from Gibbs energy equation (adapted from Koga 2007)

Response Function	First order derivative	Second order derivative
C_p	$T \cdot \left(\frac{\partial S}{\partial T}\right)_P$	$-T \cdot \left(\frac{\partial^2 G}{\partial T^2}\right)_P$
κ_T	$\frac{-1}{V} \cdot \left(\frac{\partial V}{\partial P}\right)_T$	$\frac{-1}{V} \cdot \left(\frac{\partial^2 G}{\partial P^2}\right)_T$
α_p	$\frac{1}{V} \cdot \left(\frac{\partial V}{\partial T}\right)_P$	$\frac{1}{V} \cdot \left[\frac{\partial}{\partial T} \left(\frac{\partial G}{\partial P}\right)_T\right]_P$

5.2 Gibbs Adsorption Equation

At constant temperature and pressure, the fundamental relationship of the Gibbs energy given by Eq. 5.9 is reduced to Eq. 5.10. On this form, the Eq. 5.10 is adequate to describe the mass variation on systems where surface tension has substantial effects on the total energy of the system, as adsorption and desorption interfacial processes.

$$d(n \cdot G) = \sum_{i=1}^N \mu_i \cdot dn_i + \gamma \cdot d(n \cdot A) \quad (5.10)$$

A thorough analysis of the Gibbs energy variation for a system in which heat, work, and mass are exchangeable, and the system's interfacial area is permitted to undergo changes shows the partial derivatives in the first and the second terms in Eq. 5.6 are taken on constant total number of moles (n). Then n can be moved out from the derivative, resulting in Eq. 5.11.

$$\begin{aligned} d(n \cdot G) = n \cdot \left[\frac{\partial(G)}{\partial T} \right]_P \cdot dT + n \cdot \left[\frac{\partial(G)}{\partial P} \right]_T \cdot dP \\ + \sum_{i=1}^N \left[\frac{\partial(n \cdot G)}{\partial n_i} \right]_{T,P,n_j} \cdot dn_i + \left[\frac{\partial(n \cdot G)}{\partial(nA)} \right]_{T,P,n} \cdot dA \end{aligned} \quad (5.11)$$

The left side of Eq. 5.11 is the differentiate of the product $n \cdot G$, which can take it as Eq. 5.12. Also, in the third term in Eq. 5.11, n_i can be written as the product of the i -component molar fraction (x_i) by the total number of moles of the system (n). So, $d(n_i) = d(x_i \cdot n)$, which is derivative as displayed in Eq. 5.13. Lastly, n can be removed from the partial derivative in the last term in Eq. 5.11, and the derivative of the extensive area can be expressed as $d(n \cdot A) = n \cdot d(A) + A \cdot dn$.

$$d(n \cdot G) = n \cdot dG + G \cdot dn \quad (5.12)$$

$$d(n \cdot x_i) = n \cdot dx_i + x_i \cdot dn \quad (5.13)$$

Substituting Eqs. 5.12 and 5.13 in Eq. 5.11 and rearranging it results in Eq. 5.14.

$$\begin{aligned} n \cdot \left\{ dG - \left[\frac{\partial(G)}{\partial P} \right]_T \cdot dP - \left[\frac{\partial(G)}{\partial T} \right]_P \cdot dT - \sum_{i=1}^N \left[\frac{\partial(G)}{\partial x_i} \right]_{T,P,x_j} \right. \\ \left. \cdot dx_i - \left[\frac{\partial(G)}{\partial(A)} \right]_{T,P,n} \cdot dA \right\} \\ + \left\{ G - \sum_{i=1}^N x_i \cdot \left[\frac{\partial(nG)}{\partial n_i} \right]_{T,P,n_j} - \left[\frac{\partial(nG)}{\partial(nA)} \right]_{T,P,n} \cdot A \right\} \cdot dn \end{aligned} \quad (5.14)$$

Considering a reliable opened system, n and dn are hinder to be null. Then, the trivial solution of the Eq. 5.14 is given simultaneously by Eqs. 5.15 and 5.16, where Gibbs partial derivates are replaced by the corresponding thermodynamic properties. These equations stand for the total Gibbs energy of the system and its total differentiate.

$$dG = -S \cdot dT + V \cdot dP + \sum_{i=1}^N \mu_i \cdot dx_i + \gamma \cdot dA \quad (5.15)$$

$$G = \sum_{i=1}^N x_i \cdot \mu_i + \gamma \cdot A \quad (5.16)$$

Equation 5.15 is merely the intensive form of the Eq. 5.9. The Eq. 5.16 is the functional equation of the Gibbs energy for open systems submitted to tensive forces at constant temperature and pressure. The differentiation of the Eq. 5.16 results in an alternative arrangement of the total differential of the Gibbs energy of the system, as it can be seen in Eq. 5.17.

$$dG = \sum_{i=1}^N \mu_i \cdot dx_i + \sum_{i=1}^N x_i \cdot d\mu_i + \gamma \cdot dA + A \cdot d\gamma \quad (5.17)$$

If dG given by the Eq. 5.17 replaces dG in Eq. 5.15, a more convenient and useful equation is resultant, expressed in the form of Eq. 5.18.

$$S \cdot dT - V \cdot dP + \sum_{i=1}^N x_i \cdot d\mu_i + A \cdot d\gamma = 0 \quad (5.18)$$

Equation 5.18 is the *Gibbs Adsorption Equation*, a fundamental relationship between surface tension and adsorption process variables at given temperature and pressure (for details see Adamson and Gast 1997). *Gibbs adsorption equation* provides a quantitative evaluation of the adsorption extension of a substance on a surface from surface tension data. For adsorption processes occurring at constant temperature and pressure, the Eq. 5.18 is summarized to Eq. 5.19.

$$\sum_{i=1}^N x_i \cdot d\mu_i + A \cdot d\gamma = 0 \quad (5.19)$$

Rearranging and applying to a two-dimension system, Eq. 5.20 is obtained.

$$d\gamma = - \sum_{i=1}^N \left[\frac{n_i^\sigma}{(n \cdot A)} \right] \cdot d\mu_i \quad (5.20)$$

n_i^σ is defined as surface excess amount of i -component. It is the amount of i -component present in an ideal (two-dimensional) plane surface. The plane surface is a mathematical plane that constitutes the interface between two phases. Then, n_i^σ is given by the difference between the total quantity of i -component in the entire system and the sum the quantities of i -component in each one of the system phases, according to Eq. 5.21.

$$n_i^\sigma = n_i - (n_i^\alpha + n_i^\beta) \quad (5.21)$$

n_i is the total number of moles of the i -component in the whole system, containing the phase α and phase β . n_i^α and n_i^β are the numbers of moles of the i -component in the phase α and phase β , respectively. Figure 5.1 illustrates the region accumulating the surface excess amount of i -component in a system holding α and β phases. It is important highlight that a plane two-dimensional surface must be consider an unrealistic system, since that a surface having a substance with finite dimensions it will exhibit itself as a three-dimensional system. The hypothetical plane surface is termed *Gibbs dividing surface* and it must be located in the real three-dimensional regional, according described in Fig. 5.1.

Similarly, surface excess concentration of the i -component (Γ_i) is defined by mean of the Eq. 5.22 (For details on surface excess concentration see Davies and Rideal 1963 and Birdi 2009).

$$\Gamma_i = \frac{n_i^\sigma}{A^\sigma} \quad (5.22)$$

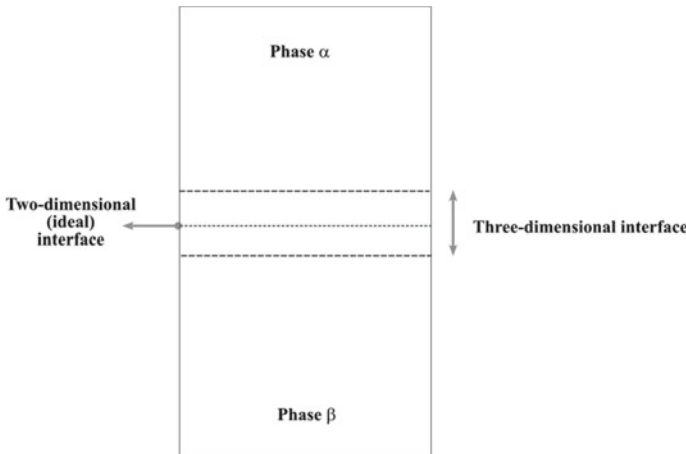


Fig. 5.1 Schematic illustration of the Gibbs dividing surface, displaying an ideal two-dimensional line and a three-dimensional region

In Eq. 5.22, A^σ represents the extensive surface area, which is given by $A^\sigma = n \cdot A$. Substituting A^σ in Eq. 5.20, the Eq. 5.23 is obtained.

$$d\gamma = - \sum_{i=1}^N \Gamma_i \cdot d\mu_i \quad (5.23)$$

Γ_i represents the surface excess concentration of each solute (i -component) relative to the solvent. For a binary solution, having one single solvent and one single solute, Γ_{solvent} can be set to zero (because the convenient position of the two-dimension plane surface) and then the *Gibbs Adsorption Equation* will be designated as Eq. 5.24.

$$d\gamma = -\Gamma_1 \cdot d\mu_1 \quad (5.24)$$

The Eq. 5.24 is the general arrangement of the Gibbs adsorption equation. Since Eq. 5.24 is derived from rigorous thermodynamic arguments, it can be applied broadly on a considerable number of systems, including solid–gas, solid–liquid and liquid–liquid systems. The total differential of the chemical potential ($d\mu_1$) can be expressed as in Eq. 5.25, where R is the ideal gas constant, T is the absolute temperature, and x_1 is the molar fraction and δ_1 is the activity coefficient of the i -component.

$$d\mu_1 = R \cdot T \cdot d\ln(x_1 \cdot \delta_1) \quad (5.25)$$

Since the product $x_1 \cdot \delta_1$ gives the chemical activity of the component 1, denoted as $a_1 = x_1 \cdot \delta_1$, substituting $d\mu_1$ in Eqs. 5.24 and 5.25 the surface excess concentration is given as Eq. 5.26.

$$\Gamma_i = - \frac{1}{R \cdot T} \cdot \left(\frac{d\gamma}{d\ln a_i} \right). \quad (5.26)$$

By arrangement,

$$\Gamma_i = - \frac{a_i}{R \cdot T} \cdot \left(\frac{d\gamma}{da_i} \right). \quad (5.27)$$

For ideal and very dilute solutions, Eq. 5.27 becomes itself Eq. 5.28, which gives the surface excess concentration of the i -component as a function of its solution bulk concentration. For very non-ideal systems, the activity coefficient must be accurately determined using Gibbs energy models, such as UNIQUAC and NRTL (see details on Excess Gibbs energy models to obtain the activity coefficient in Prausnitz et al. 1998).

$$\Gamma_i = - \frac{C_1}{R \cdot T} \cdot \left(\frac{d\gamma}{dC_1} \right). \quad (5.28)$$

Only a limited number of successful experimental tests for demonstration of the validation of the *Gibbs adsorption equation* has been available because the direct measurement of the adsorbed material amount is mostly difficult, especially to fluid–fluid interfaces. Although, successful experimental validations by means of the direct measurement of species concentration in the interface were reported (for details see Ross and Morrison, 1988). However, there is no reason to distrust the validation and application of Eq. 5.25 and its derived equations. The Eq. 5.25 is the phenomenological description of the interfacial adsorption of components on surfaces since it has been obtained rigorously from the fundamental laws of thermodynamics. It applies itself in the adsorption of any species on fluid–fluid and solid–fluid interfaces.

The Gibbs adsorption equation enables the determination of the amount of component adsorb on the surface (Γ , given in amount of component per area) from a plot of the γ (the surface tension at the air/water interface or interfacial tension at the liquid/liquid interface) against the logarithm of the species concentration.

Experimental data for surface tension of aqueous solution of amoxicillin in presence of poly-ethylene glycol are displayed in Fig. 5.2. The results show a nearly linear decrease of γ with $\log C$ at concentrations below the critical micelle concentration.

For fluid–fluid interfaces, interfacial tension can be directly measured, but the surface excess concentration must be calculated from interfacial data since Γ may not be accurately measurable. For another hand, in fluid–solid interfaces Γ can be entirely measurable. Since the solid surface tension can be obtained from adsorption data, Gibbs equation can be properly verified.

The Eq. 5.28 can be applied in the data form Fig. 5.2 to assess the surface excess concentration. The resulting surface excess concentration is presented in Table 5.4.

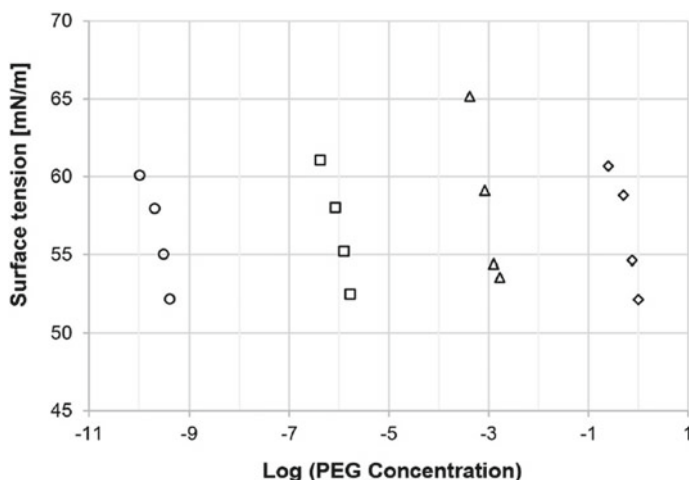


Fig. 5.2 Surface tension of amoxicillin solution versus PEG concentration logarithm at 20 °C. PEG concentration given in mol/L. \diamond PEG 400; Δ PEG 600; \square PEG 1000; \circ PEG 4000 (from Vieira et al., 2018)

Table 5.4 Surface excess concentration of amoxicillin aqueous solution containing polyethylene glycol at pH 6.5 and 20 °C (from Vieira et al. 2018)

PEG molecular weight (g mol^{-1})	Surface excess concentration (mol m^{-2})
400	0.0054
600	0.0082
1000	0.0057
4000	0.0052

5.3 Dynamic Interfacial Adsorption

The Gibbs adsorption equation is useful to describe the adsorption process of surface-active substances from liquid solutions and gaseous mixtures on interfaces in each equilibrium state. However, to reaching the surface adsorption equilibrium the species must move from the bulk to the interface between the phases. The displacement of the molecules from the bulk to the interface depends on a series of factors, which includes molecule size, molecule-solvent interactions, bulk viscosity, species concentration and other parameters affecting the molecule mobility.

The surface tension is contingent upon the surface concentration, as designate by Gibbs adsorption equation, and the surface concentration changes up to reach the equilibrium concentration then surface tension will be nominated a time-dependence function. This is especially true for low concentration surfactant solutions encompassing large and asymmetrical species, where the time to achieve the equilibrium surface tension must take from milliseconds to several minutes. A typical surface tension curve for conventional surfactant solution is shown in Fig. 5.3. The surface tension decreases progressively on the time up to achieve the equilibrium tension (γ_{eq}). Surface tension—time curves for some amphiphiles with weak surfactant character display a continuous decreasing and scarcely exhibit an equilibrium surface tension at a finite time.

Surface tension of dilute solution decreases with the time as far as the surface is occupied by surfactant molecules. The equilibrium surface tension is reached when the total surface area is filled by molecules. Clearly, it must be taken in solute concentration lower than the critical micellar concentration. The surface tension of pure liquids is time-independent under long-term measurement time. However, the presence of impurities in mono-component liquids can become time-dependent their surface tension. The factors affecting the time-dependence of the surface tension can be gathered in three main phenomena: (1) diffusion rate of the species to the surface, (2) kinetic barrier to specie adsorption, and (3) re-orientation and re-arrangement of the species on the surface.

For dilute solution, the adsorption equilibrium time is distinctively attributed to species diffusion. A simple model to describe the diffusion-controlled adsorption of species from the solution toward the surface is given by Fick's second law (Eq. 5.29), where the i -species concentration C_i is a function of the time (t) and distance (x).

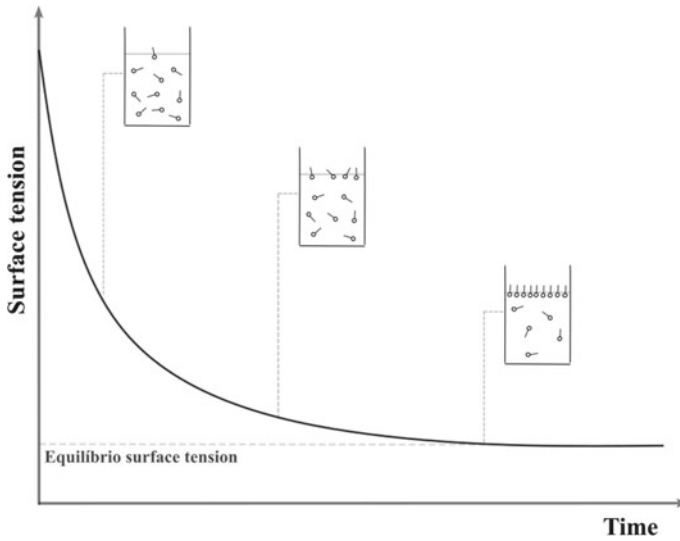


Fig. 5.3 Decreasing of the surface tension of surfactant dilute solution with the time due to the progressively adsorption

$$\frac{\partial C}{\partial t} = D \cdot \frac{\partial^2 C}{\partial x^2} \quad (5.29)$$

In Eq. 5.29, t is the time, C is the species concentration in solution, D is the species diffusion coefficient, and x is the distance between molecule and surface. The C parameter is related to the surface excess concentration (Γ) by Gibbs adsorption equation. The diffusion-controlled adsorption model mostly fails to fit adsorption data of systems having ionic surfactants, concentrated surface-active species (substantially above their critical micellar concentration) and some amphiphiles like alcohols, which exhibit adsorption process slower than predicted by the diffusion-controlled model. Equation 5.29 is applied to the systems comprising nonionic species, whose the bulk concentration (C) depends on the position (x) and time (t). Consequently, the surface tension (γ) and surface concentration (Γ) vary along the time. At the surface, $x = 0$ and the solution concentration (C) equals itself to the surface concentration (Γ). Solving Eq. 5.29 on the latest boundary conditions, it is possible to find the surface concentration as a time function $\Gamma(t)$ for the mentioned species, as represented in Eqs. 5.30 (for short times) and 5.31 (for long times).

$$\Gamma(t) = \Gamma_0 + 2\sqrt{\frac{D \cdot t}{\pi}} \cdot [C_t - C_0] \quad (5.30)$$

In Eq. 5.30, Γ_0 and C_0 are respectively the surface concentration and the bulk concentration at initial time ($t = 0$), C_t is the concentration at time t , and D is the species diffusion coefficient.

$$\Gamma(t) = \Gamma_0 + 2\sqrt{\frac{D \cdot t}{\pi}} \cdot [C_\infty - C_0] \quad (5.31)$$

The energy involved in the change of the molecule from the solution bulk to the interface can be calculated utilizing the variation of the chemical potential of the component from state 1 (solute in the solution bulk, denoted as μ_b) to state 2 (solute at interface, denoted as μ_s), such as described in Eq. 5.32.

$$\mu_s - \mu_b = RT \cdot \ln\left(\frac{x_b}{x_s}\right) \quad (5.32)$$

In Eq. 5.32, μ represents the chemical potential and x represents the correspondent concentration. The right side of the Eq. 5.32 gives the difference of the partial molar Gibbs energy between the solute in the solution bulk and on the surface. For non-ideal solutions, the ideal behavior deviation must be computed by addition of the activity coefficient (δ). In this case, x_i will be replaced by $x_i \cdot \delta_i$. If the system is disturbed, the equilibrium should be restored to keep the consistency of the Eq. 5.32. For instances, if the surface area is reduced, the molecule must be desorbed from the surface into the solution bulk, dropping the surface concentration and then establishing a new equilibrium state where the chemical potentials of the component in the bulk and in the surface become again equals.

5.4 Curved Surfaces and Capillarity

Curved surfaces participate in so many interfacial phenomena, especially in systems containing surfactants, emulsions, foams, and disperse deformed droplets and bubbles, as well as wetting and capillarity. Capillarity refers to the tendency of a liquid to rise in a narrow tube or a porous material due to the intermolecular forces between the liquid and the solid surface. Capillarity phenomenon is resulting from the balance between adhesive forces (between the liquid and the material surface) and cohesive forces (between the liquid molecules). The capillary liquid rising occurs when adhesive forces are greater than the cohesive forces, which is particularly important in small tubes or porous materials where the surface area to volume ratio is high and the intermolecular forces are dominant, such as it occurs in the movement of groundwater in soil and the absorption of water by natural plants. In these cases, the porous material acts as the tube, and the capillary action helps to move the water.

The attractive and repulsive forces acting between fluid bodies in a surface are responsible for the existence of interfacial tension. Subsequently, it has been stated that on a curved surface a net force proportional to the surface's mean curvature must act on a superficial constituent to force it towards the center of curvature of the surface. A similar result is obviously found for a spherical surface. The surface deformation is related to changes in the surface area, which requires a substantial amount of energy.

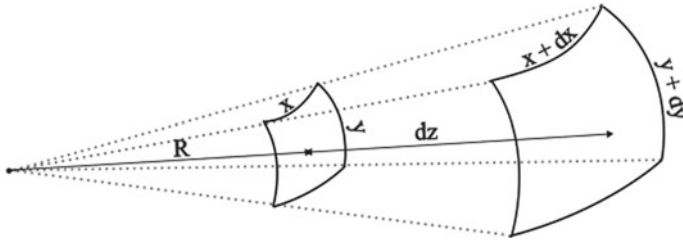


Fig. 5.4 Two-dimensional curved surface with curvature radii R_1 and R_2 on the geometric plans x and y , respectively

Consider a two-dimensional curved surface with curvature radii R_1 and R_2 on the geometric plans x and y , respectively, which define an area element A_1 , such as shown in Fig. 5.4. If the surface area is expanded from A_1 to A_2 by a differential increasing in diameter size of dz , then the new surface A_2 will have dimension $x + dx$ and $y + dy$. The differential change in area will be $dA = (x + dx) \cdot (y + dy) - x \cdot y$, resulting in $dA = x \cdot dy + y \cdot dx$ (neglecting $dx \cdot dy$ term given by the product $dx \cdot dy$). The differential work (δW) required to extent the surface area by dA from A_1 to A_2 is given by Eq. 5.33.

$$\delta W = \gamma \cdot dA \quad (5.33)$$

If the area extension is associated to an expansion work, the required work is represented as the product of the force ($\Delta P \cdot x \cdot y$) acting on the area A_1 by displacement (dz). ΔP is assigned as the *Capillary pressure*, since it is the resulting from the pressures acting on the internal and external phases. Besides, using the trigonometric triangle similarity for R_1 per x and $(R_1 + dz)$ per $(x + dx)$ even as R_2 per y and $(R_2 + dz)$ per $(y + dy)$ lead to $dx = x \cdot dz \cdot R_1^{-1}$ and $dy = y \cdot dz \cdot R_2^{-1}$. Replacing dx and dy into dA , and then inserting δW and dA in Eq. 5.32, results in the *Young–Laplace equation* (see Eq. 5.34).

The Young–Laplace equation describes the relationship between the pressure difference across a fluid interface and the curvature of the interface.

$$\Delta P = \gamma \cdot \left(\frac{1}{R_1} + \frac{1}{R_2} \right) \quad (5.34)$$

In Eq. 5.34, ΔP is the pressure difference across the interface, γ is the surface tension of the liquid, and R_1 and R_2 are the principal radii of curvature of the interface. The Young–Laplace equation states that the pressure difference across a curved liquid interface is directly proportional to the surface tension of the liquid and the magnitude of the curvature of the interface. The Eq. 5.34 is used to understand phenomena such as capillary action, formation of droplets and bubbles, and the behavior of fluids in small-scale structures such as microfluidic devices.

For a spherical surface, R_1 and R_2 are equal, resulting in Eq. 5.35.

$$\Delta P = \frac{2 \cdot \gamma}{R} \quad (5.35)$$

R is the constant curvature radius of the spherical surface.

The Eq. 5.34 has been written on the generalized form displayed in Eq. 5.36 to describe curved surfaces different than the spherical curvature.

$$\Delta P = \gamma \cdot H \quad (5.36)$$

ΔP is the pressure difference across an interface that separates adjacent bulk phases and H represents the surface curvature. Wide-ranging expressions for the surface curvature (H) can be found in the literature on different geometry. The surface is typically a zero-thickness region, exhibiting a surface density according to the presence of components in the surface. Planar surfaces are two-dimensional regions analogous to a volumetric region in three-dimensional systems. Surface areas are defined as the single geometric extensive property for planar surface. In this context, the Eq. 5.36 is used to describe the shape of liquid interfaces and the behavior of fluids in confined spaces, such as capillary tubes and porous media. It is also used to model various physical processes, including the formation of droplets, bubbles, and wetting phenomena. Besides, Young–Laplace equation provides a necessary condition for mechanical equilibrium of a fluid interface.

References

- Adamson AW, Gast AP. Physical chemistry of surfaces. John Wiley & Sons, Inc.; 1997.
- Birdi KS. Handbook of surface and colloid chemistry. CRC Press; 2009.
- Davies JT, Rideal EK. Interfacial phenomena. New York and London: Academic Press; 1963.
- Koga Y. Solution thermodynamics and its application to aqueous solutions. Elsevier; 2007.
- Prausnitz JM, Lichtenthaler RN, Azevedo EG. Molecular thermodynamics of fluid-phase equilibria. Pearson; 1998.
- Ross S, Morrison ID. Colloidal systems and interfaces. New York: Wiley; 1988.
- Shaw DJ. Introduction to colloid and surface chemistry. Elsevier; 1992.
- Tester JW, Modell M. Thermodynamics and its applications. Prentice Hall, 1996.
- Vieira LB, Casimiro MW, Santos RG. Surface tension of aqueous amoxicillin+PEG systems. Colloid Interf Sci Commun. 2018;24:93–7.

Chapter 6

Phase Behavior of Interfacial Films



Molecular films consist of thin layers of organic or inorganic material, typically with a thickness of less than 100 nm, which are deposited onto a substrate. The formation of film monolayers relies on the unique properties of amphiphilic molecules. In an aqueous environment, these molecules can self-assemble at the air–water interface due to the hydrophobic effect. The hydrophilic regions of the molecules interact with the water molecules, while the hydrophobic regions are oriented away from the water, creating a stable film at the interface. The study of molecular films has attracted significant attention due to their potential applications in a variety of fields, including electronics, optics, and biomedicine. Intermolecular interactions between the film molecules and the substrate determine the stability and structure of the film, playing a crucial role in its thermodynamic and hydrodynamic properties. The strength of the interaction is defined by a variety of factors, including the chemical nature of the film and substrate, the orientation of the film molecules, and the presence of defects or impurities. In order to describe interface phenomena, a variety of mathematical equations have been developed, such as the van der Waals equation and the Langmuir–Blodgett equation. The chemical composition and properties of both the film molecules and the substrate play a significant role in achieving the intermolecular interactions. Compatibility between the film and substrate, such as similar functional groups or complementary charges, can lead to stronger interactions and better film stability. The arrangement and orientation of the film molecules at the substrate interface can impact the intermolecular interactions. Ordered packing or self-assembly of the molecules can result in favorable interactions and enhance the stability of the film. The stability, phase behavior, and phase transitions of molecular films are determined by intermolecular interactions. The energy associated with these interactions influences the film’s thermodynamic properties, such as its melting point, glass transition temperature, and crystallization behavior.

6.1 Two-Dimensional Monolayers

Amphiphilic molecules can adsorb on the surfaces, leading to the lowering of the interface tension, according to the Gibbs adsorption equation (see Chap. 5). The continuous adsorption of molecules on the interface conducts to a building of a close-packed molecular layer. The adsorbed layer can be represented as a two-dimensional film arranged by the lateral interactions between the surface molecules, which has been ascribed as *monomolecular film* or *surface monolayer*. Monolayers are two-dimensional self-associate systems typically formed by a thin layer of amphiphiles (especially conventional surfactants) in fluid–fluid interfaces. The regular organization of the molecules in the monolayers come from the adhesive intermolecular forces and it results in important physical–chemical properties that enable them to be directed to scientific applications, including medical, pharmaceutical, optical, among others.

An exciting scientific scenario is pictured by monolayer formed by insoluble amphiphiles, termed conventionally *insoluble monolayers* or *insoluble monomolecular films*, since the molecules are not present in the solution bulk, instead they are exclusively located in the interface. Insoluble monolayers are built by deposition of small amount of amphiphile solution (usually a volatile organic solvent) on an immiscible liquid (typically water) followed by the solvent evaporation, in a way to leading the amphiphilic layer adsorbed onto the surface. This layer-building procedure allows the direct quantitative determination of the material amount on the interface and consequently the surface concentration, without having to apply the Gibbs adsorption equation. The amphiphiles arrangement as a surface monomolecular layer is often utilized to elucidate the properties (size, shape, orientation, physical state, fluid dynamics, and interaction nature) of the individual molecules as well as of their aggregation state. Therefore, many analytical techniques have been applied to characterize surface films—such as Nuclear Magnetic Resonance (NMR), Fourier Transform Infrared (FTIR), Ion Cyclotron Resonance (ICR), Scanning Electron Microscopy (SEM), Atomic Force Microscopy (AFM), X-ray Diffraction (RD), rheometry, and others.

The surface tension (γ_i) definition from Eq. 5.6 (explicit in Eq. 6.1) imposes the interfacial area of a pure fluid to be contracted under normal tensile forces, because the presence of distinct intermolecular forces in the interface produces an increase of the Gibbs energy.

$$\gamma_i = \left[\frac{\partial(n \cdot G)}{\partial(nA)} \right]_{T,P,n} \quad (6.1)$$

The spreading of amphiphile molecules on the surface to produce the insoluble monolayer results in a lowering of the surface tension of the immiscible liquid phase. Then, the packing of molecules on interface tends to expand the interface area and the surface enlargement faces the resistance from the original surface tension forces of the fluid, limiting the film spreading area by means of an opposite force. The film

spreading resistance is defined as *surface pressure*, denoted as π . The surface pressure represents the force exerted per length to restrict the film expansion to a state where the Gibbs energy increase assures a stable interface. It denotes the expansion pressure acting against the normal contracting tension that leads to the surface area reduction. Then, the surface pressure (π) is given by the difference between the surface tension of the amphiphile-free interface (γ_o) and the surface tension of interface containing the amphiphile insoluble film (γ), as displayed in Eq. 6.2 (for details on the surface pressure of amphiphile monolayers see Evans and Wennerstrom 1999).

$$\pi = \gamma_o - \gamma \quad (6.2)$$

The surface amphiphilic molecules interact themselves through two-dimensional translational bonds that origin the film surface pressure. It can be illustrated as an analogy to the pressure noted in three-dimensional systems that has origin in the collision of molecules against the vessel wall, as seen in confined gas. Then, surface pressure can be used to evaluate qualitatively the nature and intensity of the intermolecular forces acting in surface films and consequently to define the physical state of the film and its thermodynamic and transport properties. In this way, surface pressure can be assessed using force measurement apparatus.

The Langmuir trough (also termed *Langmuir-Adam surface balance* or simply *Langmuir balance*) is the most widespread device to characterize surface films in both liquid-liquid and gas-liquid interfaces. Langmuir balance consists of a trough holding two superhydrophobic float-moveable barriers that can compress the surface (see Fig. 6.1). Earlier Langmuir troughs used a torsion wire on a surface float to the direct measurement of the surface force. In modern Langmuir troughs a microbalance is installed on the surface to record the film response faces the pressuring using a substrate, such as Wilhelmy plate (for details on Langmuir trough see Shaw 1992; Evans and Wennerstrom 1999).

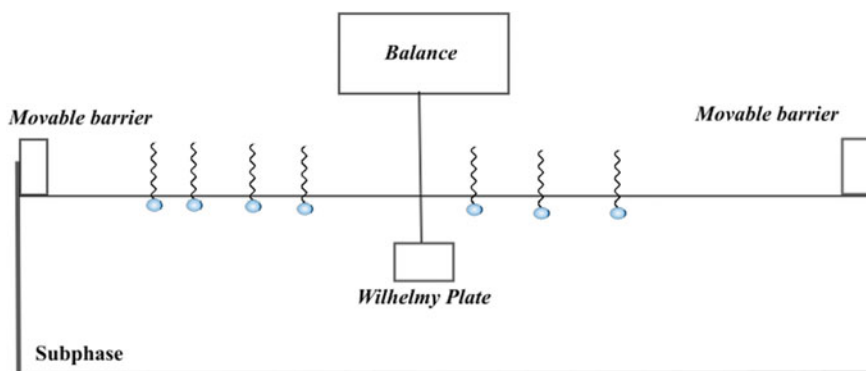


Fig. 6.1 Langmuir trough illustration

The Langmuir trough operation comprises firstly to spreading an amphiphilic solution on a very pure surface, generally termed *subphase*—high purity water is usually a convenient option—to assuring the absence of impurities. Secondly, time must be spent to allow the fully solvent evaporation—volatile solvents as dichloromethane and petroleum ether are required in the amphiphilic solution preparation (30–45 min tend to be enough), then producing a uniform insoluble monolayer. Finally, the barriers are moved forward to make the surface molecules closer and closer, changing the surface area. The barrier position is accurately recorded to designate the corresponding surface area.

Surface pressure is measured as a result of the horizontal forces that the film exerts on the microbalance probe in contact with the surface. Up-to-date Langmuir troughs are computer-controlled instruments with accurate force and displacement determination and that allows the couple the analytical devices to obtain simultaneously surface pressure and other film properties, including surface potential, morphology, and rheology. Langmuir troughs are able to operate on compression-expansion mode (describing the film hysteresis and recovery) and oscillating mode (describing the film rheology).

6.2 Physical State of the Interface Monolayers

Surface pressure measurements are commonly carried out at temperature constant, and the results are represented by curves describing the surface pressure as a function of area, denoted as *surface pressure—surface area* (π - A) *isotherms* or π - A *curves*. π is the monolayer expanding pressure acting against the area reduction that results in surface tension lowering. Figure 6.2 shows a descriptive π - A isotherm illustrating the wide-ranging phase behavior of surface monolayers.

It is over useful the analogy with three-dimensional bulk systems (see details in Tester and Modell 1996). The behavior of the π - A curves is definitely similar to the P - V curves shown in Fig. 6.3. However, it is important to highlight that first-order phase transition in isotherms for three-dimensional systems occurring on a horizontal linear curve, whereas monolayer isotherms display typically a non-horizontal curve. The shape of π - A curves is determined by amphiphile-amphiphile interactions and amphiphile-subphase interactions, whereas P - V curve shape is given by interactions between the components in the solution.

For a three-dimensional system, such a gas confined in a cylinder, the isothermal phase transition can be carried out by continuous reduction of the cylinder volume. In this case, the gas molecules are compiled to keep closer in a way that the interaction energy between them is increased up to reach the saturation point where the phase transition starts itself. For pure substances the phase transition going from gas to liquid occurs at constant temperature and pressure (Fig. 6.3a), For another hand, for simple mixtures the isothermal reduction of volume inside the two-phase region promotes a growing in the system total pressure (Fig. 6.3b), which means the temperature and pressure are not keep simultaneously constant during the phase transition.

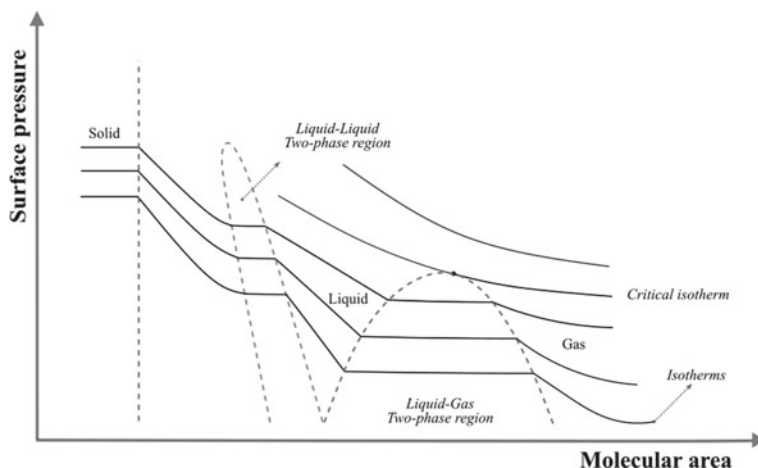


Fig. 6.2 Illustrative description of surface pressure—area isotherm, demonstrating the phase transition and monolayer physical state

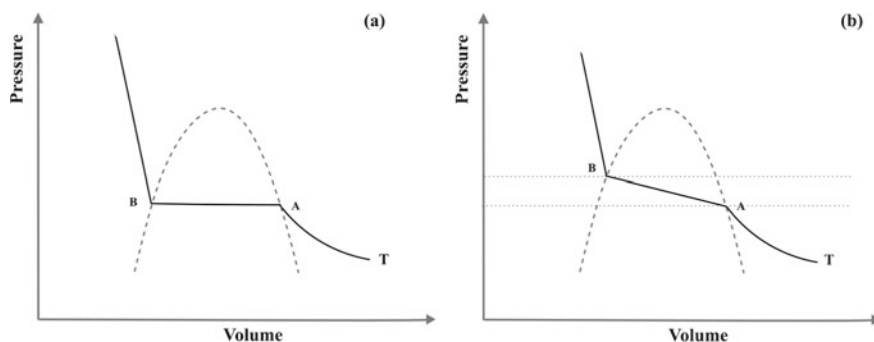


Fig. 6.3 Three-dimensional gas-liquid transition: **a** pure substance; **b** mixtures

Above the critical temperature isotherm, π -A is supposed to display a monotonic curve, especially for large macromolecules.

Analogous to three-dimensional systems, two-dimensional monolayers are prone to experience phase changes under isothermal continuous compression. The monolayer physical state has been classified regarding their intermolecular distances. The intermolecular distance is directly related to the lateral (adhesion or cohesion) forces occurring among the several species in the film and it has been elucidated via optical, microscopic and diffraction advanced methods. Here it is imperative to highlight that monolayers may be constituted of molecular aggregates instead individual molecules. Especially in complex colloidal systems, associative structures can be formed if the critical aggregative concentration is achieved (CAC). The CAC is occasionally so

low that, at the spread concentration to produce the monolayer, the aggregation phenomena have effect on the subphase.

Resembling the physical state of three-dimensional systems, surface monolayers can display phase behavior corresponding to gaseous, liquid, and solid phase. Nevertheless, the monolayer physical states are more roughly categorized taking in account the molecular packing inside the film, defining particularly the three main physical states: gaseous, liquid-expanded and condensed. However, surface pressure—area curves are not enough to the definite identification and characterization of the phases of surface films and the phase boundaries. Instead, advanced techniques must be applied to elucidate the microscopic structures of the monolayers.

Gaseous surface (G) films are formed at low pressures (larges areas) and represent low density films. In these films, the area available for each molecule is enough large in relation to the total surface area to allow the individual and independent movement of the molecules. This requirement corresponds to components having small molecular relative area (area occupied by one molecule) and very weak lateral cohesive and adhesive forces.

Liquid-expanded (LC) films are two-dimensional isotropic phases similar to highly compressible liquids. Liquid-expanded monolayers are very fluid and coherent phases with intermolecular distance widely larger than the typical distance between the molecules in a homogeneous liquid solution, hindering a direct correspondence to three-dimensional liquid phases. LC films are supposed to partially lie down on the surface in a way that the head polar groups are permitted to move more freely than the non-polar hydrocarbons chains because the attractive interactions.

Condensed surface films are characterized by the molecular close packing and the steeply orientation about the surface plan. The condensed film category encompasses a series of types of the densest film phases: solid phase (S) and the liquid-condensed phase (LC). Condensed phases are especially constituted at higher pressures (small areas) and lower temperatures (high interactions), and they are almost similar to mesophases having short-range translational order (S) and long-range correlational order (LC). Condensed films may be present even at low surface pressure due to the occurrence of attractive interactions that keep associated the surface molecules, in many cases, as small clusters.

Adhesive and cohesive intermolecular forces strongly affect the film packing, since they are dependent on the nature, geometry, and orientation of the surface molecules. The presence of bulky head, ionizable groups, branched and unsaturated chains, aromatic nuclei are structural aspects noticeably affecting the molecular packing in the film, as well as subphase properties like pH, salinity and temperature. An illustrative phase diagram is shown in Fig. 6.4.

The distribution of components in equilibrium state between two phases α and β in a mixture is given by the equality of the chemical potential of the i -component in all the phases, thermodynamically described by Eq. 6.3 (for details see Adamson and Gast 1997). The application of the Eq. 6.3 depends on the statement of the convenient system restrictions.

$$\mu_i^\alpha = \mu_i^\beta \quad (6.3)$$

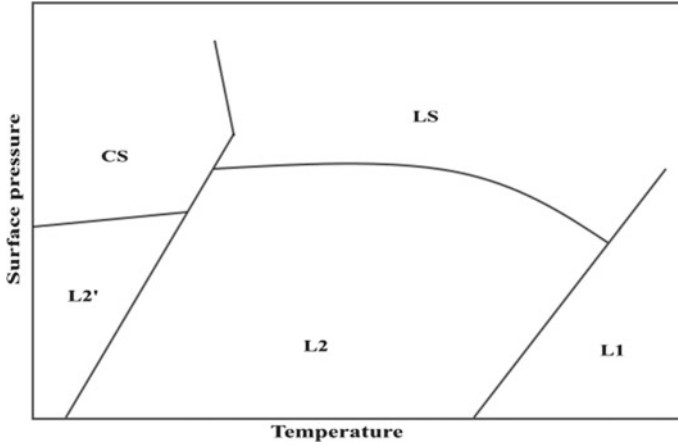


Fig. 6.4 Generalized π - T phase diagram

The chemical potential μ_i pointed out in Eq. 6.3 has been previously defined as the partial molar Gibbs energy (see Chap. 5). It means μ_i is written as a partial derivative of Gibbs energy with respect to the material amount of the i -component (Eq. 6.4). However, μ_i can be written as a relationship of other thermodynamic fundamental properties under the proper restrictions. The chemical potential written as partial derivative of intern energy U (using entropy and volume restrictions), enthalpy H (using entropy and pressure restrictions) and Helmholtz energy A (using temperature and volume restrictions) are shown in Eqs. 6.5–6.7. In fact, the restriction variables are chosen according to the experimental conditions, which must be settled to allow the suitable set of physically measurable quantities (see details on chemical potential in Prausnitz et al. 1998).

$$\mu_i = \left[\frac{\partial(n \cdot G)}{\partial(n_i)} \right]_{T, P, n_j} \quad (6.4)$$

$$\mu_i = \left[\frac{\partial(n \cdot U)}{\partial(n_i)} \right]_{S, V, n_j} \quad (6.5)$$

$$\mu_i = \left[\frac{\partial(n \cdot H)}{\partial(n_i)} \right]_{S, P, n_j} \quad (6.6)$$

$$\mu_i = \left[\frac{\partial(n \cdot A)}{\partial(n_i)} \right]_{T, V, n_j} \quad (6.7)$$

6.3 Phase Behavior of Interfacial Films

Figure 6.5 shows an illustrative schematic description of the π -A phase diagram, unfolding the monolayer phase existing.

At low pressure, the amphiphiles are spread on a high surface area. If the amphiphilic amount is very small, the surface concentration will be low enough to be considered dilute. In this situation, the molecule size is generally much minor than the total surface area, making the amphiphilic-amphiphilic interactions negligible. This gaseous film state behaves as an ideal gaseous film, resembling the ideal gas state for three-dimensional systems. In a monolayer on ideal gaseous state, the changes of the surface tension (γ) with the amphiphilic concentration follows a linear relationship, written according to Eq. 6.8 (for an overview on interfacial phenomena see Davies and Rideal 1963).

$$\gamma = \gamma_o - b \cdot C \quad (6.8)$$

where γ_o is the surface tension of the pure subphase, C is the amphiphilic concentration, and b is a constant that defines the angular coefficient. Figure 6.6 shows the linear adjust for the surface tension as a function of the surfactant concentration with slope equal to $-b$ and linear adjust coefficient equals to the surface tension of the pure liquid corresponding to the subphase, given by Eq. 6.8. It can be seen the linear relationship is valid only to low surfactant concentrations. At high concentration, deviation from linearity is clear.

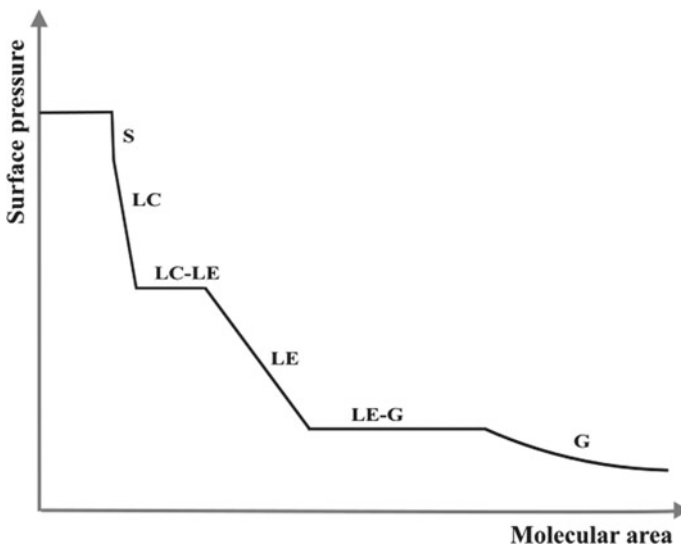


Fig. 6.5 Schematic description of the π -A phase diagram for interfacial monolayers

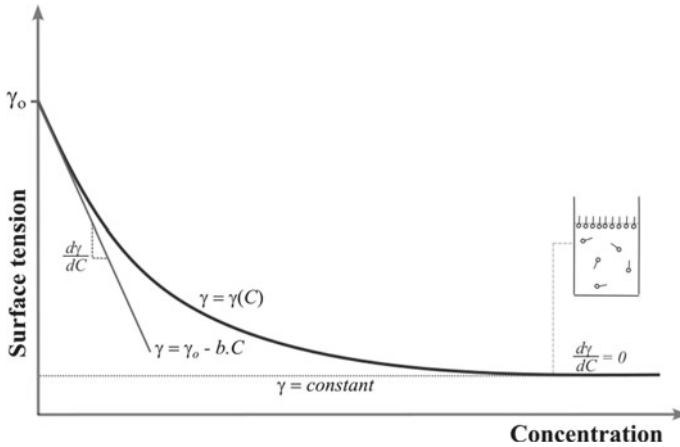


Fig. 6.6 Surface tension as a function of the surfactant solution concentration

By comparison between Eqs. 6.2 and 6.8, it possible to sustain a linear increasing of the surface pressure with the concentration rise, such as given in Eq. 6.9.

$$\pi = b \cdot C \tag{6.9}$$

Therefore, the differentiate of the Eq. 6.2 with regard the concentration results in a constant, showed as $-b$ in Eq. 6.10.

$$\frac{d\gamma}{dC} = -b \tag{6.10}$$

Substituting the Eqs. 6.9 and 6.10 into the Gibbs adsorption equation, as written in Eq. 5.28, the surface pressure can be computer from the excess surface concentration, given in Eq. 6.11.

$$\pi = \Gamma \cdot RT \tag{6.11}$$

Applying the surface excess concentration, the resulting Eq. 6.12 is the simplest model to describe the state of a surface film when the surface pressure tends to zero (or total surface area tends to infinite).

$$\pi \cdot A = RT \tag{6.12}$$

In Eq. 6.12, π is the surface pressure, A represents the surface molar area (area per mole), R is the universal gas constant and T is the absolute temperature. The Eq. 6.12 is entirely comparable to the ideal gas law, and it must be written concerning Boltzmann constant k (instead R) if A is given as molecular area (area per molecule). This mathematical model assumes the attractive and repulsive interaction between

the film molecules are negligible and the only energy contribution comes from the surface entropy, such as happen with ideal gas molecules confined in a volume. Deviation from the surface ideal gaseous model is evaluated through the curves of the compressibility factor Z (Eq. 6.13) against the surface pressure π .

$$Z = \frac{\pi \cdot A}{RT} \quad (6.13)$$

Figure 6.7 shows Z versus π plot for a series of *n*-alkyl carboxylic acids with linear chains ranging from 4 to 12 carbons at constant temperature. There is an evident deviation from the ideal behavior, demarcated as $Z = 1$. Negative deviation ($Z < 1$) occurs in low pressure, becoming more pronounced to the higher alkyl chain length.

Equation 6.12 corresponds to a two-dimensional equation of state applied to ideal gaseous films. The ideal model considers strictly the surface pressure has origin in the particle kinetic movement, with kinetic energy kT , being a linear limiting law that must be obeyed when surface pressure tends to zero. Figure 6.8 shows the validate of the surface ideal gaseous model for an organic acid, given as plot of π versus $1/A$.

The linear relationship between the surface tension and the surface concentration, illustrated in Eq. 6.8 for dilute solutions, is the definitive description the ideal gaseous surface behavior. Ideal conditions are easily found in solutions having low interfacial activity amphiphiles, where the bulk concentration is substantially greater than the surface concentration. However, once the solute exhibits an intense surface active,

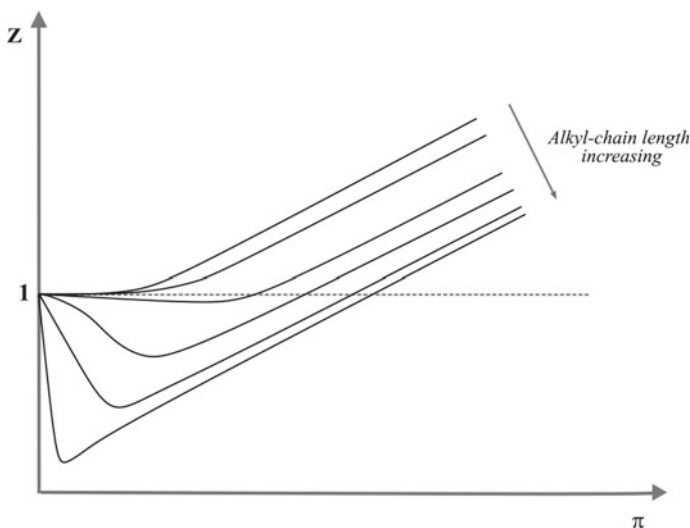


Fig. 6.7 Compressibility factor for *n*-alkyl carboxylic acid as a function of the length of the *n*-alkyl chains

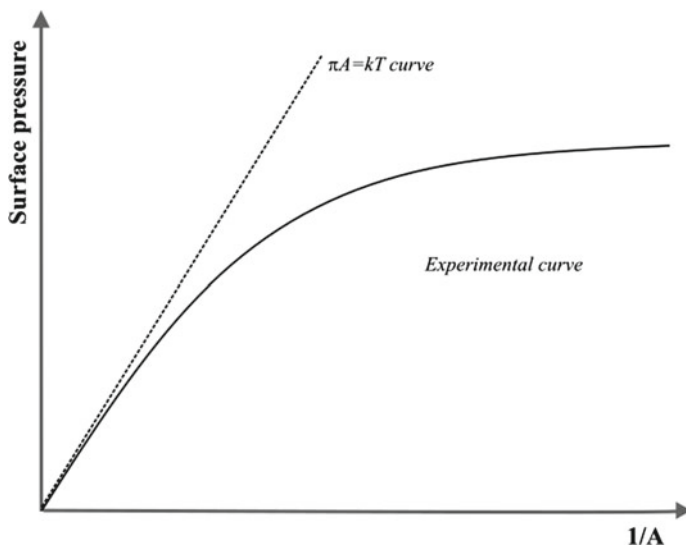


Fig. 6.8 Plot of π versus $1/A$

such as conventional surfactants, the surface film scarcely manifest ideal behavior due to the hard conditions to be experimentally achieved. As a result, many systems containing surface-active agents display substantial deviation from the ideal gaseous surface behavior. The mathematical models describing the non-ideal behavior of the surface films must consider, first of all, the finite size of amphiphilic molecules. Considering the molecules have a finite area, this area must be taken in account on the changes of the total surface area. The equation of state derivate from the molecular area correction of the ideal gas model can be represented as in Eq. 6.14.

$$\pi \cdot (A - A_0) = RT \quad (6.14)$$

Equation 6.14 is the well-known *Langmuir equation* (or still termed *one-parameter Volmer simplified equation*) since it applies only the covolume correction to the ideal gas model. A_0 is defined as the *limiting area*, and it is the area occupied by one mole of substance on the surface (area excluded by an adsorbed molecule at the interface). If Eq. 6.14 is written in terms of kT , A_0 is given as the area per molecule. In gaseous state film, A_0 can be illustrated as the total projected area of the adsorbed molecules on the surface, as seen in Fig. 6.9. Then, long chain amphiphiles have generally large values of A_0 . On the other hand, A_0 depends on the interactions between the amphiphilic and the interface subphase, which can produce a series of different surface conformations. Nevertheless, Eq. 6.14 represents adequately the surface behavior of electrically neutral films where the intermolecular interactions are negligible, at air–water and oil–water interfaces.

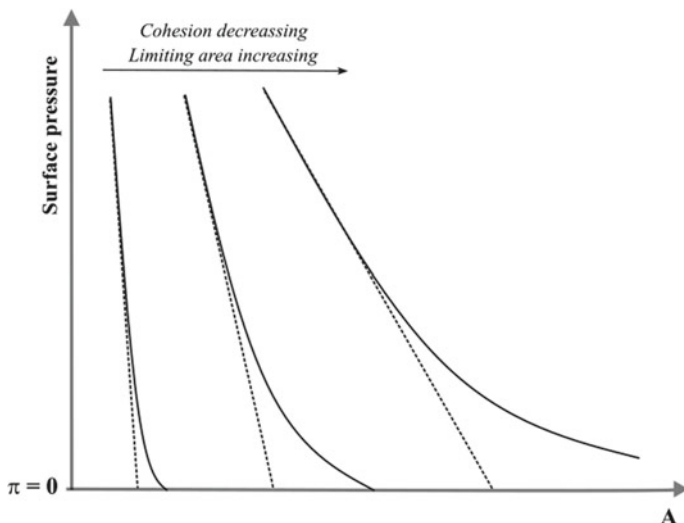


Fig. 6.9 Total area of the adsorbed molecules on the surface from π -A isotherm

Because the assumption of negligible interactions between the molecules in ideal gaseous state films, Eq. 6.14 fails often to describe gaseous surface films under high pressure. On these conditions, both pressure and volume must be corrected, such as shown in Eq. 6.15. The Eq. 6.15 is almost termed the *two-parameter Volmer equation*. It is mostly useful to surface films containing amphiphiles with linear hydrocarbon chains under low to moderate pressure.

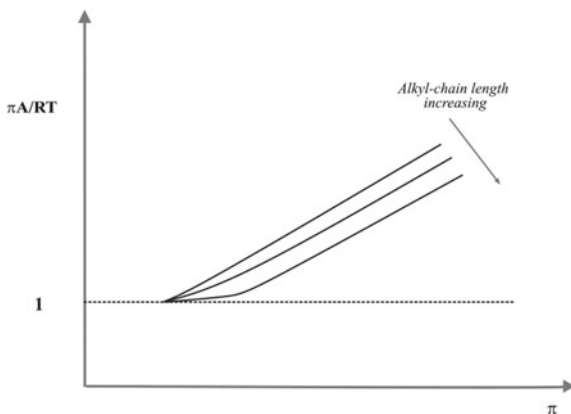
$$(\pi - \pi_o) \cdot (A - A_o) = RT \quad (6.15)$$

Equation 6.15 may also be written in the form shown in Eq. 6.16, known as corrected Langmuir Equation.

$$\pi \cdot (A - A_o) = \alpha \cdot RT \quad (6.16)$$

The parameter α is a correction for the cohesive forces. Equation 6.16 can be rearranged to give $\pi \cdot A$ as a function of π (it means the product of the surface pressure by the surface area as a function of the surface pressure), according to the Eq. 6.17). On this form, the equation of state is particularly valuable to verify the effect of molecular size and lateral interaction on the films. The curve $\pi \cdot A$ versus π allows to identify the fitting adjusting of the model to the experimental data. Figure 6.10 shows the Eq. 6.17 has good adjust to the experimental data obtained from alkyl alcohol films in the air–water interface. In this case, molecules were supposed to be oriented perpendicularly to the surface plan, giving a limiting area (or projected area) of about 22 square angstroms.

Fig. 6.10 Adjust for $\pi A - \pi$ plot of a homologue series of alkyl alcohols



$$\pi \cdot A \cdot \frac{1}{RT} = \frac{A_o}{RT} \cdot \pi + \alpha \quad (6.17)$$

A convenient way to describe the non-ideal behavior of surface monolayers is the modification of three-dimensional equation of state (3D EOS) to interfacial systems. Equation 6.18 is the correspondent two-dimensional van der Waals equation. It applies corrections in area and pressure to overcome the ideal gas model limitations.

$$\left(\pi + \frac{a}{A^2} \right) \cdot (A - A_o) = RT \quad (6.18)$$

The term a/A^2 corresponds to the cohesive pressure, attributed to the van der Waals forces acting between the hydrocarbon chains of the amphiphile. a is the two-dimensional equivalent parameter to the van der Waals attraction constant applied to the gaseous surface film. A_o denotes the excluded area. At oil–water interfaces hydrocarbon chains are surrounded by the organic solvent and then they are somehow impeded to interact laterally one with other, becoming the cohesive pressure equal to zero. So, the two-dimensional van der Waals equation of state for films in the oil–water interfaces can be written as Eq. 6.19. Equation 6.19 corresponds to the linear form of the Eq. 6.14, where the area is a function of inverse pressure. In this form, the plot of A versus $1/\pi$ is a linear relation which intercept (linear adjust coefficient) giving the limiting area of the adsorbed molecule.

$$A = \frac{RT}{\pi} + A_o \quad (6.19)$$

6.4 Polymer Monolayers

Very long-chain materials are prone to adsorb on surfaces similarly to the conventional surfactants. Polymers are materials able to be spread at surfaces and built resistant interfacial films by means of intense cohesive interactions. Natural and synthetic polymer films are complex systems that have been studied on a wide range of application. Enzymes, proteins, phospholipids, and cholesterol are biological macromolecules well-known by their surface activity. Polymer monolayers, including especially biological polymers, are used to produce biomedical sensors and devices, optical and electronic films. They have been also studied to characterize structure and properties of biological membranes. The polymeric macromolecules may assume the linear, rod, spheric in solution. The surface arrangement of these macromolecules depends on the intramolecular forces. Strong cohesive interactions produce rigid and coiled molecules, making them to lie like a non-flexible two-dimensional disc on the surface plan. Weak intramolecular forces tend to produce highly flexible and random chains, as indicated in Fig. 6.11. The broken lines in Fig. 6.11 shows the effect of intrachain interactions on the chain mobility and flexibility (w).

The interfacial behavior of polymeric macromolecules can be represented by π - A isotherms, considering the surface film by way of the Flory–Huggins model for polymer solutions. A generalized equation for polymer films on fluid surfaces was proposed by Singer (see details in Singer 1948), as displayed in Eq. 6.20 (in terms of $k \cdot T$).

$$\pi = \frac{x \cdot kT}{A_o} \cdot \left[\ln\left(\frac{A}{A - A_o}\right) + \frac{x - 1}{x} \cdot \frac{z}{2} \cdot \ln\left(1 - \frac{2A_o}{z \cdot A}\right) \right] \quad (6.20)$$

A_o is the molecular area, x is the polymerization degree and z is the coordination number in the two-dimensional quasi-lattice. For completely rigid molecule, $z = 2$. Whereas, for completely flexible film, $z = 4$. The polymer chain flexibility (w) is defined as the number of available sites for additional neighboring molecular units, represented in Eq. 6.21 in terms of the inter-chain cohesive forces (ω), which has origin in the attractive forces of van der Waals. If cohesive force is zero, w depends on the steric factors and then w is denoted as w_o . Equation 6.21 provides the effect

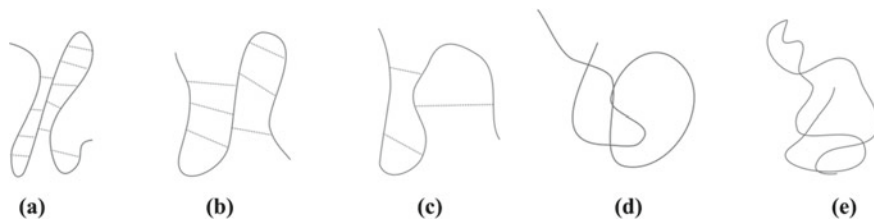


Fig. 6.11 Polymer chain arrangement: **a** completely rigid ($w_a = 0$), **b** slight flexibility ($w_b > w_a$), **c** moderate flexibility ($w_c > w_b$), and **d** high flexibility ($w_d > w_c$)

of the temperature on the molecular flexibility; however, attention must be taken to assure the molecule solubility is not significantly changed with the temperature and affect the surface pressure, masking the flexibility value.

$$w = w_o \cdot \exp\left(-\frac{\omega}{kT}\right) \quad (6.21)$$

The coordination number is then given as a function of the interchain cohesive interactions by Eq. 6.22.

$$z = 2 + w_o \cdot \exp\left(-\frac{\omega}{kT}\right) \quad (6.22)$$

For rigid and coiled molecules with $x = 1$, Eq. 6.20 is reduced to Eq. 6.23, which is known as equation of state of *Frumkin and Volmer*. Equation 6.23 assumes that the molecule is fixed at the specific points on the surface through the monomer interaction with the subphase. Frumkin and Volmer equation of state differs of the two-parameter Volmer equation since the latter considers the molecules completely mobile on the surface. In fact, the mobility of molecules on the surfaces impacts the surface behavior, especially for single-chain hydrocarbon macromolecules at small areas (typically lower than 100 Angstrom).

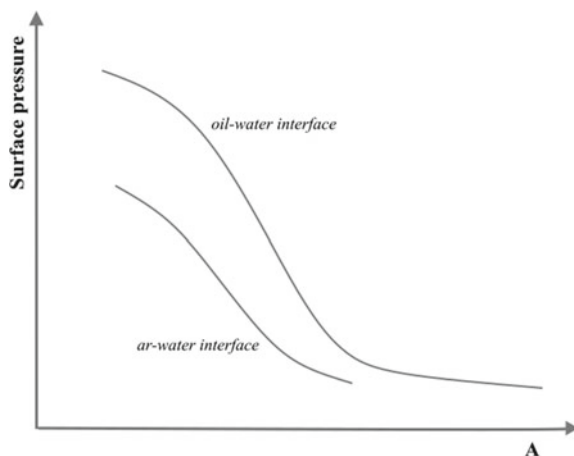
$$\pi \cdot A_o = kT \cdot \ln \frac{A}{A - A_o} \quad (6.23)$$

Typical π -A curves for polymer films on air–water and oil–water interfaces is shown in Fig. 6.12. Surface behavior depends on the molecular weight, intramolecular forces, and intermolecular forces. Intramolecular interactions govern the shape of the polymer molecule in the surface film, according to Fig. 6.11. Strong cohesive forces produce coiling and rigid structures, resulting in surface pressure substantially lower that produced by highly flexible random chains. At low pressure, polymer films often behave as ideal gaseous films, mainly in oil–water interfaces. If the molecule concentration is sufficiently low to negligence the intermolecular forces, the polymer molecular weight can be obtained by mean of the molar area (area per mole of the molecule) using the plot of $\pi \cdot A$ against π .

6.5 Cohesive Surface Pressure

Cohesive surface pressure is the pressure that acts in two adjacent particles that are held together by cohesive forces, such as the intermolecular forces between atoms or molecules. The cohesive forces can include van der Waals forces, hydrogen bonding, electrostatic interactions, and other intermolecular forces that hold the material together. The strength of these forces depends on the nature of the materials and

Fig. 6.12 Typical π -A curve for polymer films at air–water and oil–water interfaces



their chemical and physical properties, such as their molecular structure, surface energy, and temperature.

The attractive cohesive pressure (π_o) acting in interfacial monolayers has been denoted in Eq. 6.18 as the ratio between the two-dimensional van der Waals parameter and the area. However, cohesive surface pressure can be determined experimentally by measuring the surface pressure of the same molecule at the air–water interface (π_{aw}) and the oil–water interface (π_{ow}) for a given area. Since cohesive interactions between non-polar chains is zero at oil–water interfaces, one can write π_o as Eq. 6.24.

$$\pi_o = \pi_{ow} - \pi_{aw} \quad (6.24)$$

Then, knowing that $\pi_o = a/A^2$, a (the two-dimensional equivalent parameter to the van der Waals attraction constant applied to the gaseous surface film) can be directly calculated. A derivative property from cohesive pressure is the film thickness (τ), which can be obtained from Eq. 6.25.

$$\tau = \frac{a_{vw}}{a + kT \cdot A} \quad (6.25)$$

In Eq. 6.25 a_{vw} is the three-dimensional van der Waals attraction constant, a is the two-dimensional equivalent parameter to the van der Waals attraction constant, k is the Boltzmann constant, T is the absolute temperature, and A is the surface area. The film thickness can provide information on the surface molecular conformation. Table 6.1 presents the two-dimensional equivalent parameter to the van der Waals attraction constant and the film thickness calculated through Eq. 6.25 for organic acid compounds in air–water interface. Experimental data has shown that the τ for monobasic acids obtained from Eq. 6.25 are similar to the length of the alkyl chain completely stretched and oriented vertically at the air–water interface.

Table 6.1 van der Waals constant of the monolayers at A/W interfaces (Adapted from Chattoraj 1979)

Molecule	a_s (ergs cm^{-2} molecule $^{-2}$)	τ (angstrom)
Butyric acid	0.80	7.8
Valeric acid	1.29	9.9
Caproic acid	1.69	12.5
Caprylic acid	2.92	15.7

The van der Waals constant of a monolayer is a measure of the strength of the van der Waals interactions between the molecules within the monolayer. The van der Waals interactions are weak, attractive forces that occur between molecules due to fluctuations in their electron distributions. If the molecules within the monolayer are highly polar, such as in the case of fatty acid monolayers, then the van der Waals constant may be relatively low due to the presence of strong dipole–dipole interactions. In contrast, if the molecules within the monolayer are nonpolar, such as in the case of alkanes, then the van der Waals constant may be relatively high due to the dominance of London dispersion forces.

6.6 Phase Transition of Interfacial Films

Under continuous compression, surface films can show phase transition as illustrated in Fig. 6.13. Well-defined phase transitions have been widely reported to a very large number of substances. The physical state of the monolayer under specific surface pressure and corresponding surface area is governed by the interfacial interactions between non-polar chains, non-polar chains—subphase, polar group—subphase, and polar groups. The type and intensity of interfacial interactions define both the molecular packing and the molecular conformation.

Figure 6.13 shows a typical π -A diagram, displaying solid (S), liquid (L), and gas (G) homogeneous phases, and (pseudo) two-phase regions, besides the phase transition isotherms. At low pressure, the lateral interactions due to van der Waals forces in amphiphile molecules are deemed insignificant and then the molecules are kept distant each other. The gaseous monolayer behavior is described by Eq. 6.13, where Z determines if there is any deviation from the ideal gas model. If the gaseous film experiences a two-dimensional isothermal compression process, the molecules are pushed continuously to closer until to achieve the saturation point (look like the three-dimensional dew point).

In the saturation point the system will start up the first phase transition, initiating a region where intermediary behavior between gas and liquid is verified, resembling three-dimensional vapor–liquid transition. If the monolayer behaves itself as a single component system the vapor–liquid transition will be hold at constant temperature and pressure, indicated by a horizontal line, whereas the surface area is reduced. The two-phase region shows a maximum point that represents the critical point, where the pressure is given by the critical temperature (T_c). Some compression processes

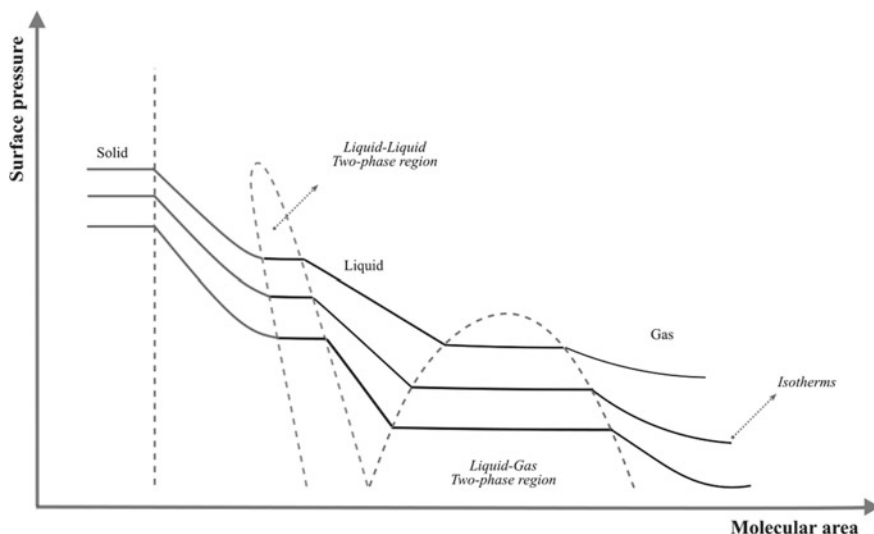


Fig. 6.13 Full description of phase transition of monolayers

are carried out at temperature higher than T_c , and the monolayer isotherm does not intercept the saturation point. In this case, the film goes across a supercritical region that can lead directly to the condensed phase state. The energy amount involved in the vapor–liquid transition can be analysis by mean of surface pressure as a function of temperature data, using the two-dimensional *Clapeyron equation* (Eq. 6.26).

$$\Delta H = T \cdot \Delta A \cdot \frac{d\pi}{dT} \quad (6.26)$$

ΔH is the latent heat of vaporization of the expanded-liquid film and ΔA is the area change during the vaporization process. Further compression on the monolayer leads the system from gas to entirely liquid at an extreme of the two-phase region (look like the three-dimensional bubble point). From this point, the monolayer performs quite as a liquid film. Liquid monolayers can display a vast variety of configurations (categorized as coherent films), according to the intermolecular forces acting. The liquid films are defined by their isotherm compressibility. Commonly a gaseous film compression originates a liquid-expanded phase, which is a highly compressible film because the long spacing between the surface molecules. Further isothermal compression of the liquid-expanded film results in an aslope increasing of the surface pressure, while the molecules approaching themselves up to the molecular spacing is sufficient reduced to result in a new phase transition. Then a liquid-condensed phase appears, and the monolayer coexists as a two-liquid phase system. Liquid-condensed films are very slightly compressible. If the liquid mixture behaves as an ideal liquid (pure liquid phase), the phase transition from liquid-expanded to liquid-compressed occurs at constant temperature and pressure under area reduction.

Table 6.2 Typical values of isothermal surface compressibility

Monolayer	K_T (dyne cm^{-1})
Protein	1–20
Liquid expanded	12.5–50
Liquid condensed	100–250
Solid	1000–2000

The two-liquid phase region exhibits a maximum point equivalent to high critical temperature seen in three-dimensional liquid–liquid systems. At very reduced area, the condensed monolayer behaves as a solid with long-range translational order, corresponding very often to a crystalline solid. Solid monolayer can present rigid or elastic response to the compression, revealing some compressible character. In solid state, surface molecules are subjected to the very strong van der Waals forces, causing sudden increasing the surface pressure with exceedingly small area changes. However, if enough high-surface pressure is achieved, the solid film can collapse into complex structures, as three-dimensional multilayers arranged in the interface like stacks, stripes, and others.

The monolayer physical state can be identified utilizing the slope of the surface pressure isotherm. The slope of the π -A isotherms represents the ration between the variation of the surface pressure and the variation of the surface area. Since this slope is related to the molecular packing and compressible character, each monolayer states denote a characteristic surface compressibility. By analogy to the three-dimension systems, isothermal surface compressibility (K_T) is defined as Eq. 6.27. By Eq. 6.27, K_T can be calculated from data of surface area and surface pressure trough Langmuir balance experiment. A convenient mathematical model that describes the π -A relationship is useful to calculate the surface compressibility at area values across the isotherm. The phase state and phase transition are given by substantial change in K_T value.

$$K_T = - \left[\frac{d(\ln A)}{d\pi} \right]_T \quad (6.27)$$

Typical values of isothermal surface compressibility are presented in Table 6.2.

6.7 Mixed Monolayers

Important systems holding more than one amphiphilic have been rigorous subject of investigation because their industrial application, notably polymeric and biological interfacial systems. These systems can result in monolayers formed by different amphiphiles, known as mixed films. Considerable attention has been directed to mixed insoluble monolayers formed by two amphiphiles existing at air–water interface as a liquid phase film. The amphiphilic mixture can behave as ideal or non-ideal

solution, besides immiscible solution. The molecular surface area of each amphiphilic in the mixture is usually different from the corresponding of the pure amphiphilic area. Exception is noticed for amphiphiles with size, volume, and intermolecular interactions nature and intensity remarkably similar. The actual area of the components in the mixture is given by the partial molar area, defined by Eq. 6.28, rendering to the definition of partial molar properties.

$$\bar{A}_i = \left[\frac{\partial(n \cdot A)}{\partial n_i} \right]_{T,P,n_j} \quad (6.28)$$

For a binary ideal film, the mixture molar area (A^{id}) is given by Eq. 6.29.

$$A^{id} = x_1 \cdot A_1 + x_2 \cdot A_2 \quad (6.29)$$

where A^{id} is the mixture ideal area, and A_1 and A_2 are the molar area of the pure components 1 and 2, respectively, evaluated at given surface pressure. x_1 and x_2 are respectively the molar fractions of components 1 and 2 in the mixture. The mixture excess area (A^E) is defined by Eq. 6.30 as the difference between the mixture area evaluated on actual conditions (A) and the ideal mixture area (A^{id}). A^E denotes the deviation of the system description of ideal model.

$$A^E = A - A^{id} \quad (6.30)$$

Analogously, as shown in Eq. 6.31, the excess Gibbs energy of the mixing process (G_{mix}^E) is given as the difference between the Gibbs energy to produce the mixture evaluated on actual conditions (ΔG_{mix}) and that evaluated on ideal conditions (ΔG_{mix}^{id}).

$$G_{mix}^E = \Delta G_{mix} - \Delta G_{mix}^{id} \quad (6.31)$$

The (actual) Gibbs energy involved in the mixing process (ΔG_{mix}) is defined as the difference between the Gibbs energy (G) of the mixture and the Gibbs energy of the pure components (G_1 and G_2) before the mixing, as illustrated in Eq. 6.32.

$$\Delta G_{mix} = G - (x_1 \cdot G_1 + x_2 \cdot G_2) \quad (6.32)$$

From Eq. 6.4 and knowing that the chemical potential equivaless to the partial molar Gibbs energy, it is feasible to write the Eq. 6.33.

$$dG_i = -A_i \cdot d\gamma \quad (6.33)$$

Differentiating the Eq. 6.2 and replacing $d\gamma$ into Eq. 6.33, the Gibbs energy for the mixture (G) and pure components (G_1 and G_2) at surface pressure π are given by Eq. 6.34 in an integration interval going from a very low pressure π^* to the surface

pressure π in which the mixture is being evaluated.

$$G_i = \int_{\pi^*}^{\pi} A_i \cdot d\pi \tag{6.34}$$

Applying Eq. 6.34 for binary mixture formed from pure components put together at π^* followed by compression of the mixture up to π , the (actual) Gibbs energy involved in the mixing process is obtained by Eq. 6.35.

$$\Delta G_{mix}^c = \int_{\pi}^{\pi} (A - x_1 \cdot A_1 - x_2 \cdot A_2) \cdot d\pi \tag{6.35}$$

Equation 6.35 gives the Gibbs energy resulting the compression of two-component monolayers from a negligible (close to zero) pressure up to a substantial pressure π . However, the Gibbs energy resulting from the spreading of the pure components must be computed to Eq. 6.35 to give the total Gibbs energy related to the mixing process, such described in Fig. 6.14. ΔG_{mix}^s represents the Gibbs energy to spread the pure components and produce a binary monolayer at a pressure π^* low enough to allow the monolayer to be consider ideal. The formation of the ideal monolayer is represented by the process going from state 1 to state 2, and the related Gibbs energy is given by ΔG_{mix}^{id} . Then $\Delta G_{mix} = \Delta G_{mix}^c + \Delta G_{mix}^s$, where $\Delta G_{mix}^s = \Delta G_{mix}^{id}$, resulting in Eq. 6.36.

$$\Delta G_{mix} = \Delta G_{mix}^c - \Delta G_{mix}^{id} \tag{6.36}$$

The Gibbs energy involved in surface ideal mixing process depends only on the mixture composition, resembling the Gibbs energy involved in three-dimensional ideal mixtures, and it can be expressed as Eq. 6.37.

$$\Delta G_{mix}^{id} = RT \cdot (x_1 \cdot A_1 - x_2 \cdot A_2) \tag{6.37}$$

<i>State 1</i>	<i>State 2</i>	<i>State 3</i>
Component 1	Component 1	Component 1 - Component 2 mixture
+	+	
Component 2	Component 2	
Pure individual components before mixing	Spread on subphase up to the surface pressure π^*	Mixed monolayer formed by compression of the spread film from π^* up to π
ΔG_{mix}^s		ΔG_{mix}^c

Fig. 6.14 Illustration of the mixing process to produce a binary film from pure components

R is the ideal gas constant. T is the absolute temperature. x_1 and x_2 represent the molar fraction of the components 1 and 2 respectively in the mixture.

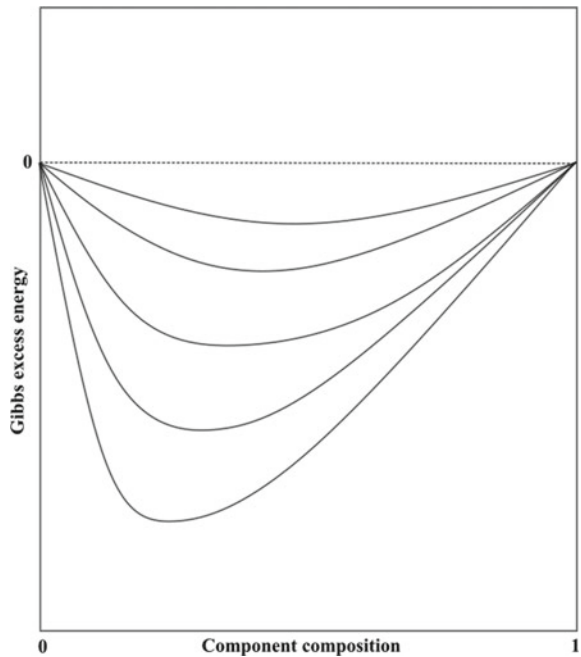
Replacing Eqs. 6.35 and 6.36 into Eq. 6.31 results in Eq. 6.38.

$$G_{mix}^E = \int_{\pi}^{\pi} (A - x_1 \cdot A_1 - x_2 \cdot A_2) \cdot d\pi \quad (6.38)$$

Equation 6.38 is particularly useful to determine the Gibbs excess energy for binary condensed mixed films. Usually, excess energy data are presented as a function of the mixture composition. Figure 6.15 displays a typical Gibbs excess energy—composition of binary mixtures for interfacial film at different surface pressures. The excess energy due to the mixture process of surface-active agents becomes more pronouncedly negative when the pressure is increased.

Mixed films are especially important when the addition of amphiphilic can improve the required properties of a pure component film. Partially soluble amphiphiles can be included in an insoluble one-component monolayer, constituting the *penetration phenomena*. The additional component is supposed to modify the film properties, such as surface elasticity and electrical potential. For instances, coagulation can be avoided in dispersion droplets surrounded by a conventional surfactant layer by addition of alcohols that reduce the repulsion forces acting in the film, making more stable emulsions.

Fig. 6.15 Gibbs excess energy for binary monolayers



6.8 Charged Monolayers

Charged Langmuir monolayers are two-dimensional molecular assembly formed at the air–water and oil–water interface, typically composed of amphiphilic molecules with a charged headgroup and a hydrophobic tail. The Langmuir monolayer can be charged by introducing charged headgroups into the amphiphilic molecules. This can be achieved by introducing either cationic or anionic groups, depending on the desired charge of the monolayer (see Chap. 2). The presence of charged headgroups results in electrostatic interactions between the molecules, which can lead to the formation of ordered structures and surface domains. Charged monolayers has been used as model systems for studying interfacial phenomena in protein–ligand interactions and lipid-protein interactions. They can also be used as templates for the synthesis of functional materials, such as nanoparticles and polymers. Additionally, charged Langmuir films have potential applications in areas such as biosensing, drug delivery, and energy storage.

Amphiphilic molecules can be ionizable in contact with an aqueous subphase, attaining electric charges to the surface monolayer. Molecules and particles can also acquire electric charge by dissociation of the ionogenic groups and preferential ion adsorption. At these interfaces, there is a distribution of charged species, which can include ions, ionized molecules, and charged colloidal particles. The concentration and valence of the ions in the electrolyte solution can affect the degree of charge screening at the interface, which can affect the electrostatic potential and thus the surface pressure. The interaction of the charged species with the surrounding medium results in an electrostatic potential at the interface, which must affect the surface pressure. The surface charge density can affect the distribution of charged species at the interface, while the surface area can affect the degree of interaction between the charged species and the surrounding medium.

The presence of electric charges on surface alters the interfacial force balance. In electrically charged interfaces, the total surface pressure is determined by a combination of the properties of the charged species at the interface, the presence of electrolytes in the surrounding medium, and the properties of the interface itself. The total surface pressure for electrically charged interfaces must include the kinetic forces (π_k), the van der Waals forces (π_c) arisen from alkyl chain interactions, and electrostatic forces (π_e) resulting of the interaction between charged surface molecules, such as it is expressed by Eq. 6.39.

$$\pi = \pi_k + \pi_c + \pi_e \quad (6.39)$$

π_e denotes the pressure caused by the repulsion between adsorbed ions and work of charging the interfacial double layer. At low surface pressure, the presence of electrolyte on the kinetic pressure can be represented by Eq. 6.40.

$$\pi_k = p \cdot \frac{kT}{A - A_o} \quad (6.40)$$

p is an adjustable parameter of the equation of state described by Eq. 6.40. For ionized monolayer (type R-I, where an alkyl chain R is bonded to an ionized distinct group I), π has been found to equal to 1 in presence of a neutral salt, whereas in absence of neutral salt p equals to 2. p values can be obtained from π -A curves, using Eq. 6.40.

6.9 Surface Potential

The surface potential is a measure of the electrical potential difference between the surface and the bulk of a material (ΔV). It is an important property of interfacial films, as it directly affects the behavior of the material at the interface between two different phases. The surface potential Ψ of an interfacial film can be described by the Eq. 6.41.

$$\Psi = \Psi_s - \Psi_b \quad (6.41)$$

In Eq. 6.41, Ψ_s is the potential at the surface and Ψ_b is the potential in the bulk. Usually, Ψ is denoted as ΔV .

The surface potential of an interfacial film is affected by several factors, including the dielectric constant of the material, the charge density on the surface, and the presence of adsorbed ions or other surface charges. The surface potential can also be influenced by the presence of external electric fields and can play a role in determining the stability of the interface and the wetting behavior of the material.

There are several techniques for measuring the surface potential of interfacial films, including Kelvin probe microscopy and electrostatic force microscopy. These techniques allow for precise determination of the surface potential and can provide valuable information for understanding the behavior of materials at the nanoscale. Surface potential is a critical property of interfacial films that can impact the stability, wetting behavior, and electrical properties of materials at the interface. A thorough understanding of surface potential is crucial for the development of new materials and technologies.

The surface potential of interfacial films refers to the electrical potential difference between the solid surface and the surrounding electrolyte solution, and it is an important property that affects the stability and behavior of interfacial films. This potential can be described by the Gouy-Chapman model, which is based on the assumption that the interfacial film is composed of an electric double layer composed of anions and cations adsorbed at the surface.

The surface potential can be described mathematically by the following equation:

$$\Psi = \Psi_o + \frac{RT}{F} \cdot \ln\left(\frac{C_o}{C_b}\right) \quad (6.42)$$

where Ψ is the surface potential, Ψ_o is the surface potential in the absence of any adsorbed ions, R is the ideal gas constant, T is the temperature, F is Faraday's

constant, C_0 is the bulk electrolyte concentration, and C_b is the concentration of ions at the surface of the interfacial film.

The first term Ψ_0 is a constant that depends on the nature of the surface and the electrolyte solution. Whereas, the second term, $(RT/F) \ln(C_0/C_b)$, represents the contribution of the electric double layer to the surface potential. The value of the surface potential is determined by the balance between the electrostatic repulsion of the adsorbed ions and the attractive forces between the surface and the ions.

It is important to highlight that the surface potential can vary depending on the pH, ionic strength, and temperature of the electrolyte solution. The surface potential measurement can be useful to characterize many processes involving phenomena as electrochemical reactions, stability of colloids and suspensions, and the formation of self-assembled monolayers.

References

- Adamson AW, Gast AP. Physical chemistry of surfaces. John Wiley & Sons, Inc.; 1997.
- Chattoraj DK. The Gibbs adsorption equation and the concept of the Gibbs surface excess. *J Indian Chem Soc.* 1979;LVI:1065–70
- Davies JT, Rideal EK. Interfacial phenomena. New York and London: Academic Press; 1963.
- Evans DF, Wennerström H. The colloidal domain—where physics, chemistry, biology, and technology meet. Wiley; 1999.
- Prausnitz JM, Lichtenthaler RN, Azevedo EG. Molecular thermodynamics of fluid-phase equilibria. Pearson; 1998.
- Shaw DJ. Introduction to colloid and surface chemistry. Elsevier; 1992.
- Singer SJ. Note on an equation of state for linear macromolecules in monolayers. *J Chem Phys.* 1948;16:872–6.
- Tester JW, Modell M. Thermodynamics and its applications. Prentice Hall; 1996.

Chapter 7

Rheology of Surface Films



Interfacial rheology concerns to the description of the mechanical behavior exhibited by interfaces and the resulting impact of surface properties on the dynamics of complex systems. It deals with the measurement and analysis to providing insights on the response of interfaces to external forces and deformations. Specifically, it focuses on the interface mechanical behavior to understand and quantify their viscoelastic properties, including surface tension, shear elasticity, and interfacial viscosity. Especially, rheology of fluid interfaces has a strongly impact on the properties of systems, exposing daily phenomena. In the food and beverage sector, interfacial rheology ensures the stability of systems such as salad dressings and mayonnaise, while also optimizing foam properties in products like whipped creams and ice creams. In pharmaceuticals, it is useful to design drug delivery systems like liposomes, enhancing drug release efficiency. In oil and gas field, it is crucial to enhanced oil recovery methods. Additionally, interface rheology has a key feat in stability and consistency of disperse systems, foaming processes in chemical industry, nanoparticle behavior in materials science, wastewater treatment, cleaning product properties in the surfactant industry, emulsion polymerization in petrochemical sector, and biological interfaces as cell membranes and lipid bilayers, which have applications in drug delivery and diagnostics. The fundamental of interfacial rheology bear a close analogy to three-dimensional rheology, even descriptive models. A pronounced endeavor has been dedicated to improving the rheological delimitation of interfacial films. Dilatational rheology has provided useful information to elucidate compositional effects in mixed interfacial layers, whereas shear rheology has allowed the evaluation of interface structures. On dilatational strains, the bubble and oscillating droplet tensiometry are the most commonly used methods, while oscillating probe and biconus rheometers are more used for shear strains. Interface rheology modelling is an essential tool for understanding the behavior of fluids and soft materials near interfaces.

7.1 Basic Fundamentals of Rheology

Rheology is the field of science that describes the flow and deformation of matter, particularly liquids, soft solids, and complex fluids. Rheology studies explore how materials respond to applied forces or stresses and how the material shape and flow change over time. The response of rheological description of matter encompasses properties, such as viscosity, elasticity, shear, and strain. The rheological properties of materials represent macroscopic responses, although they are closely related to their microscopic characteristics. In this sense, the fundamental concepts of rheology and its conservation equations are strictly valid to materials assumed to be continuous (a reference to the materials that have a continuous or uninterrupted structure without distinct boundaries or phases in a scale substantially higher than molecular dimension).

Rheological science is concerned with two fundamental concepts: *stress* and *strain*. Stress refers to the force applied to a material per unit area. Stress (σ) represents the intensity of the internal forces within a material that counteract deformation, given in units of force per unit area. Therefore, stress is labelled as a measure of the strength of the material internal forces. When a material is subjected to an external force, such as stretching, compressing, or shearing, it experiences internal resistance in response to this force. This internal resistance inhibits the material from deforming or changing shape. In essence, stress represents the material capability to withstand the applied force without undergoing significant deformation. Mathematically, stress (σ) is defined as the ratio of the force (F) applied to a material to the cross-sectional area (A) over which the force is applied, as it is expressed by Eq. 7.1.

$$\sigma = \frac{F}{A} \quad (7.1)$$

The nature of the stress can come in different forms according to the direction of the applied force. Normal stress denotes the force (F) per unit area acting perpendicular (at right angles) to the material surface that results in either compression (positive normal stress) or tension (negative normal stress), depending on whether the material is being pushed together or pulled apart. On another hand, shear stress represents the force (F) per unit area acting parallel to the material surface, tending to cause deformation by sliding or shearing the material layers. The origin of the shear stress is a tangential or shearing force.

Strain refers to the resulting deformation or change in shape of a material when subjected to an applied stress. Thereby, strain defines the extension of the material dimension length or shape changes in response to external forces or stresses, representing a ratio of lengths or sizes and therefore a dimensionless quantity (as given in Eq. 7.2). The nature of the strain depends on the direction of the stress. Normal strain (ϵ) measures the change in length or size (stretching or compression) of a material along the direction of the applied stress, which relates the change in length with the original length. Whereas shear strain (γ) denotes the change in shape between two originally perpendicular lines in the material, defining the material response to

applied shear stress by measuring the extent of deformation. When the material elongates or expands in response to stress (as it occurs if material is stretched or under tension), strain is considered positive. When the material contracts or compresses in response to stress, strain is regarded as negative.

$$\gamma = \frac{\delta x}{\delta y} \quad (7.2)$$

In a physical sense, the strain is intrinsically linked to the alteration of a material shape. According to the nature of the strain, the material can present two main types of deformation: deformation by elongation and deformation by shear. Elongational deformation, also termed as extensional deformation, refers to the deformation of a material in which it experiences an increase in length or elongation in one direction while contracting or reducing in thickness in the perpendicular directions. Elongational deformation is associated to normal strain and it results in a uniaxial or one-dimensional deformation characterized by changes in the material stretching or elongation along the axis of applied force, being often accompanied by a decrease in cross-sectional area perpendicular to the direction of stretching, as displayed in Fig. 7.1a. Shear deformation, associated to shear strain, results in a two-dimensional deformation where the material experiences a change in shape without significant changes in its length. The shear deformation of the material occurs by sliding or shearing of adjacent layers parallel to each other, as it can be seen in Fig. 7.1b.

A straightforward representative of shear deformation can be illustrated when a fluid is placed between two parallel surfaces with a gap distance h between them, in a way that the lower surface remains stationary, while the upper surface is steadily moved at a constant velocity v by means of the acting of a force F , such as displayed in

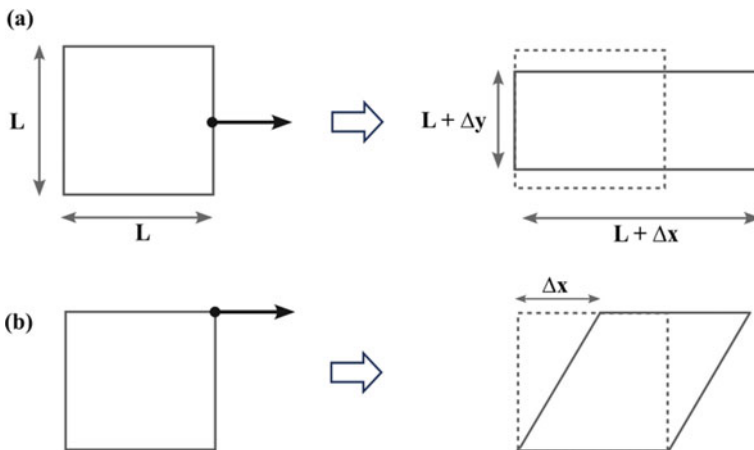


Fig. 7.1 Material deformation caused by a stress: **a** Elongational strain and **b** Shear strain. Dashed lines show the original material shape and length

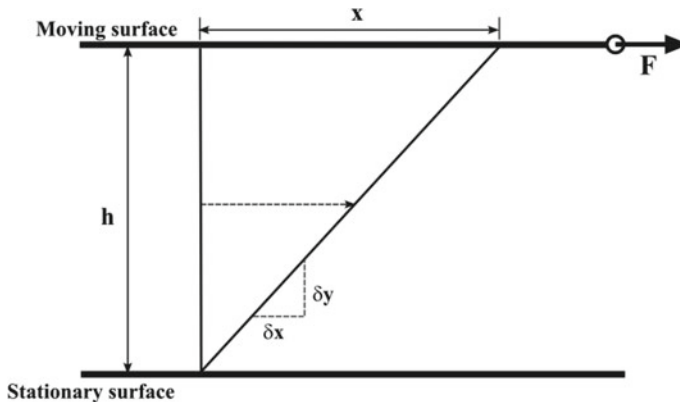


Fig. 7.2 Shear strain producing fluid flow

Fig. 7.2. Considering there is no slippage in the contact between the fluid and surface, shear strain will be described as the phenomenon where layers of a fluid slide over one another, with each layer moving faster than the one immediately below it. The uppermost layer of fluid achieves the highest velocity, while the lowermost layer remains stationary.

The occurrence of shear strain requires the application of a shear force on the fluid. This external force is quantified as a shear stress (σ), produced by the force (F) acting per unit area (A). In response to applied force, the upper layer displaces a certain distance x , while the lower layer remains motionless. Subsequently, a displacement gradient across the fluid can be expressed by the Eq. 7.2, which corresponds to the shear strain (γ). In Eq. 7.2, dx is the displacement of the moving surface in the direction of the applied force F , whereas dy represents the height of the fluid element under stress, as shown in Fig. 7.2. If the distance between the surfaces h is tiny, the shear strain must be kept constant during the fluid deformation. In this case, the shear strain will be given by Eq. 7.3.

$$\gamma = \frac{x}{h} \quad (7.3)$$

In the case of a solid that behaves as a single, unyielding block of material, the strain remains constant when subjected to an applied stress, resulting in the absence of any flow. On the contrary, for a fluid where the individual components can move relative to each other, the shear strain progressively increases as long as the applied stress persists. The variation of shear strain with the time produces a velocity gradient defined as the strain rate (or more commonly shear rate), represented by Eq. 7.4.

$$\dot{\gamma} = \frac{d\gamma}{dt} \quad (7.4)$$

When a fluid experiences the application of shear stress, *momentum* is effectively transferred during the fluid flow. The shear stress corresponds to the flow of momentum or the rate of momentum exchange with the upper layer of the fluid. Momentum is transferred among the fluid layers through collisions and interactions with other constituents of the fluid, resulting in a decrease in fluid velocity and kinetic energy. The ratio between shear stress to shear rate is defined as shear viscosity or dynamic viscosity (η), as illustrated in Eq. 7.5. The shear viscosity corresponds quantitatively to the internal friction inside the fluid, and it is associated with the damping or dissipation of kinetic energy within the system.

$$\eta = \frac{\sigma}{\dot{\gamma}} \quad (7.5)$$

At a microscopic level, viscosity is a result of the interactions between the molecules or particles in a fluid. The species in a fluid are attracted to each other by cohesive forces, which tend to keep them together, and they are also in constant motion due to their thermal energy (kinetic energy). When a force is applied to make the fluid flow, the molecules resist this motion, manifesting the shear viscosity. Viscosity is the main property describing the fluid resistance to flow. It is a fundamental fluid dynamic parameter to label how liquids and gases behave under various conditions.

Fluids in which the relationship between shear stress and shear rate is linear are termed *Newtonian* fluids, resulting in a constant viscosity regardless of changes in shear rate or shear stress. Common examples of Newtonian fluids include water, simple hydrocarbons, and very dilute colloidal dispersions. On the other hand, non-Newtonian fluids are those in which viscosity varies depending on the applied shear rate or shear stress. It must be highlighted the dependence of the viscosity on both pressure and temperature. Typically, viscosity tends to increase with higher pressure and decrease with higher temperature. Temperature, in particular, plays a more critical role in viscosity changes. For instance, high-viscosity fluids like asphalt or bitumen are significantly more temperature-dependent than low-viscosity fluids such as water. In addition, some materials exhibit time-dependent rheological behavior, meaning their properties change over time when subjected to a constant force or deformation. The viscosity time-dependent property, termed as *thixotropy* (decreasing viscosity over time) or *rheopexy* (increasing viscosity over time), is important in applications like paints and gels. The rheological modelling of the fluids points out the internal arrangement (for details on viscosity measurement and modelling see Barnes 2000).

7.2 Viscoelastic Behavior

A material which experiences a deformation and return to its original shape and size when the applied forces are removed, is defined as an elastic material. When an elastic solid is subjected to external forces, it deforms reversibly by stretching or

compressing. Under strain, a perfectly elastic material stores internally all the energy used during the deformation, releasing completely the stored energy when the strain is removed—this behavior characterizes the *ideal elastic behavior*. The ideal elastic deformation of the material is linearly proportional to the applied forces within the elastic limit, defining an ideal elastic solid, often simply referred to as *ideal solid*. The behavior of ideal elastic solids is quantitatively described by *Hooke's Law*, which states that the force (stress) applied to the material is directly proportional to the deformation (strain) it undergoes. In a simple shear deformation, the Hooke's Law is described in Eq. 7.6.

$$\sigma = G \cdot \gamma \quad (7.6)$$

In Eq. 7.6, σ is the shear stress (given in force per unit area), and γ is the shear strain (dimensionless). G is the constant of proportionality, defined as the modulus of elasticity (also known as elastic modulus or Young's modulus). The modulus of elasticity is given in unit of stress. The modulus of elasticity is a quantity attributed to solid materials, which is related to their physicochemical nature, especially the magnitude of intermolecular or interatomic interactions. The extent of the modulus of elasticity defines the resistance of the material against deformation. In turns, G represents a quantification of stiffness or the ability to resist deformation, similar to the manner like viscosity (η) measures resistance to flow (see Eq. 7.5). If the tension is applied to an anisotropic three-dimensional material, the deformation will occur along with the three dimensions, and it must be represented mathematically as a tensor. For non-isotropic materials with a predominant unidirectional symmetry, the elastic properties are described in terms of modulus of elasticity (Young's modulus). The Young modulus is a measure of the interface elasticity and can be influenced by factors such as the composition and temperature of the fluids involved, the presence of surfactants or other additives, and the presence of other interfaces or boundaries.

In the case of a purely elastic material (ideal solid), there is no time-dependent behavior. Consequently, when stress is applied, an instantaneous strain occurs, controversially when the stress is relieved, the strain promptly dissipates. Although, if the applied stress exceeds the material characteristic *yield point*, full recovery becomes unattainable, leading to the onset of creep deformation. In more straight-forward terms, the solid will exhibit flow-like behavior. A spring has been used as a representative of an ideal elastic material (see Fig. 7.3a).

In contrast to elastic solid, viscous materials are substances that exhibit significant resistance to flow and deformation when subjected to an applied force or shear stress, being characterized by the viscosity. A viscous material can be accurately modeled using the Newton's law of viscosity. When stress is exerted on a viscous material, the material promptly initiates deformation and continues to deform at a constant strain rate until the applied stress is removed. The energy needed for the material deformation or displacement is dissipated inside the fluid, usually as heat, and the resulting deformation is permanent. An ideal viscous liquid is that which the deformation is entirely preserved. A dashpot is a representative of the ideal viscous behavior (see Fig. 7.3b). Newton law of viscosity, also known as Newton's law of

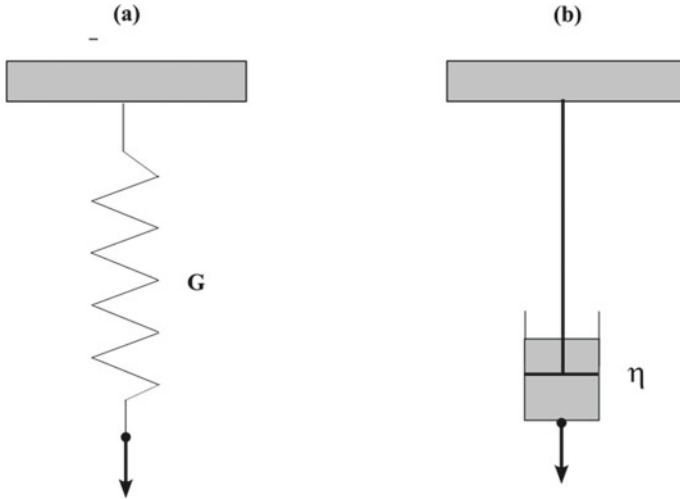


Fig. 7.3 Mechanical analogues of ideal material deformation: **a** representation of the Hookean spring (purely elastic behavior), and **b** representation of Newtonian dashpot (purely viscous behavior)

fluid friction, states that the viscous force is directly proportional to the velocity gradient, which the relative coefficient is the dynamic viscosity of the fluid, given by Eq. 7.5.

The work used in the deforming process of a perfectly elastic material is fully recovered when the material restores its original undistorted state. In turn, all the work used to maintain the flow is irreversibly dissipated as heat. Elasticity is related to the recoverable energy in deformation, while viscosity is related to the energy converted into heat.

Some materials can exhibit either a perfectly elastic behavior (solid-like) or a purely viscous behavior (liquid-like). Nevertheless, an extensive range of materials presents at least in some extension both elastic and viscous behavior. Viscoelasticity is defined as the property exhibited by certain materials that combine both elastic (the ability to return entirely to their original shape after deformation) and viscous (the ability to flow like a fluid under deformation) behaviors. These materials, known as *viscoelastic materials*, demonstrate a time-dependent response to applied stress or deformation, similarly to electrical circuits, for instances. The viscoelasticity constitutive equations comprise the three main conservation laws: Continuity equation, law of conservation of energy, and law of conservation of momentum. Viscoelasticity is commonly observed in a wide range of substances, including polymers, biological tissues, and some geological materials (for details on viscoelastic models see Barnes 2000).

The viscoelastic behavior of materials can be effectively described combining a purely elastic model (described by Hookean spring) and a purely viscous model (described Newtonian dashpot), which is illustrated in Fig. 7.4. Under a constant

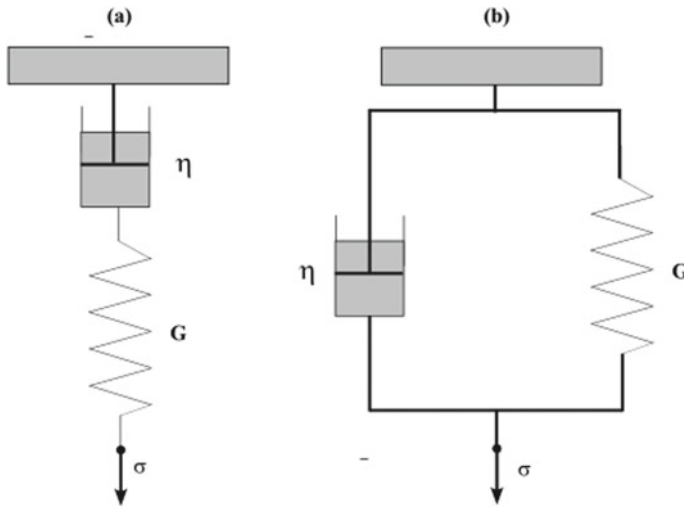


Fig. 7.4 Two-element mechanical analogues: **a** Maxwell model (element disposed in series), and Kelvin-Voigt (element disposed in parallel)

stress or strain, the rheological behavior of a viscoelastic material agrees initially to Hooke Law, demonstrating an elastic response. However, distinct to purely elastic, viscoelastic materials deform continuously over time due to their inherent viscous nature. This implies that if a stress is applied and held, the material will progressively deform, awarding a gradual and time-dependent response. Despite the time-dependent deformation, viscoelasticity materials are able to recovery its original configuration once the applied stress or strain is removed. This distinctive feature is an outcome of the material elastic component. However, the rate at which the original state is recovered can vary notably according to the material characteristics.

The simplest representation of a viscoelastic liquid involves arranging a spring and dashpot in series, which is commonly referred to as the *Maxwell model* (see Fig. 7.4a). In the Maxwell model, a linear viscoelastic model, the material behaves as a viscoelastic solid at short timescales. When a sudden stress is applied, the spring responds immediately, causing an initial deformation, and the response is predominantly elastic and governed by the modulus of elasticity (G). However, as time progresses, the dashpot gradually dissipates the energy, and the material eventually behaves like a viscous fluid at long timescales, making predominant the viscous behavior governed by the dynamic viscosity (η).

Conversely, a viscoelastic solid can be analogously depicted using the *Kelvin-Voigt model*, another linear viscoelastic model, employing the spring and dashpot connected in parallel (see Fig. 7.4b). The Kelvin-Voigt model describes the material behaves as a viscoelastic fluid at short timescales, since the presence of the dashpot retards the response of the spring. When a sudden stress is applied, the spring and dashpot respond in parallel. At longer timescales, the material behaves as a viscoelastic solid due to the influence of the spring.

Besides, the mechanical models built from spring and dashpot elements, linear viscoelasticity can be specified in terms of integral equations, states by the *Boltzmann Superposition Principle* (also termed Integral Representation of the Viscoelasticity) (For details on viscoelasticity constitutive equations see Miller and Fainerman 2004).

On a time-domain, the ratio of shear viscosity to modulus of elasticity is commonly denoted by Eq. 7.7, relating the time it takes for a material to return to equilibrium or its initial state after being subjected to a perturbation or disturbance. In the Maxwell model, τ is referred to as the stress *relaxation time*, and it signifies the time it takes for stress to relax in the material. In the Kelvin-Voigt model, τ represents the time needed for a spring to return to its equilibrium length under a constant stress and is termed the *retardation time*.

$$\tau = \frac{\eta}{G} \quad (7.7)$$

On the time of response, a widely adopted parameter involves the comparison of a characteristic time of deformation to a natural time inherent to the fluid, resembling relaxation or characteristic time. The ratio between the characteristic times of the material and the process is known as the *Deborah number* (De), a dimensionless parameter which has been represented by Eq. 7.8. It is apparent that, particularly in processes where fluid element deformation occurs very slowly, it is plausible for the release of elastic forces to be governed by the inherent forces of relaxation. In operations conducted quickly, viscous flow is limited, and deformation is succeeded by recovery upon the removal of stress.

$$De = \frac{\text{Characteristic time of fluid}}{\text{Characteristic time of the process}} \quad (7.8)$$

The characteristic time of a fluid, often represented as the relaxation time, denotes the duration necessary for a specified amount of deformation to occur when subjected to an abruptly applied reference load. In contrast, the characteristic time of the process, termed material time, signifies the time required to reach a given reference strain, with faster loading rates achieving the reference strain more rapidly. Alternatively, the relaxation time reflects the time essential for the stress induced by a suddenly applied reference strain to diminish by a specific reference magnitude. This parameter encompasses both the elasticity and viscosity of the material. At lower Deborah numbers, the material exhibits more fluid-like behavior, characterized by Newtonian viscous flow. In contrast, at higher Deborah numbers, the material's behavior shifts into the non-Newtonian realm, increasingly governed by elasticity and displaying solid-like characteristics.

The Maxwell and Kelvin-Voigt models are simplifications of the complex viscoelastic behavior found in real materials but provide valuable insights into material responses under different loading conditions, including consideration on time response. Equation 7.9 represents conveniently the constitutive equation for the Maxwell model.

$$\eta \cdot \dot{\gamma} = \tau \cdot \frac{d\sigma}{dt} + \sigma \quad (7.9)$$

The Kelvin-Voigt model can be represented by Eq. 7.10.

$$G \cdot \gamma = \sigma - \eta \cdot \dot{\gamma} \quad (7.10)$$

A linear stress–strain relationship occurs at small deformations, and it defines the well-known *Linear Viscoelasticity Region*. At large deformation, the stress is larger than is estimated by Hooke law. Inside the Linear Viscoelasticity Region, the applied stresses are insufficient to induce structural breakdown (yielding) within the material structure. Consequently, the measurements conducted focus on capturing microstructural properties. However, when the applied stress exceeds the yield stress threshold, nonlinearities emerge, hindering to establish straightforward correlations between measurements and material microstructural properties. Whence, the viscoelastic properties are most usually measured through small amplitude oscillatory shearing, where the sample undergoes oscillation around its equilibrium position (the rest state) in a continuous cyclic mode.

The assessment of material rheological properties through oscillatory testing entails repetitive movement, typically in a back-and-forth routine, with a specified stress or strain amplitude and frequency. The outcome from the cyclic motion can be graphically depicted as a sinusoidal wave, with the stress or strain amplitude depicted on the y-axis and time on the x-axis, such as it is displayed in Fig. 7.5. The oscillatory motion bears a close connection to circular motion, where a complete cycle of oscillation can be likened to a 360° (or 2π radians) revolution. The amplitude of oscillation corresponds to the maximum applied stress or strain, while the frequency (or angular frequency) signifies the number of oscillations occurring per second.

To produce an oscillatory behavior, a sinusoidal stress s input is applied to the material. The material response is given as a corresponding sinusoidal strain γ

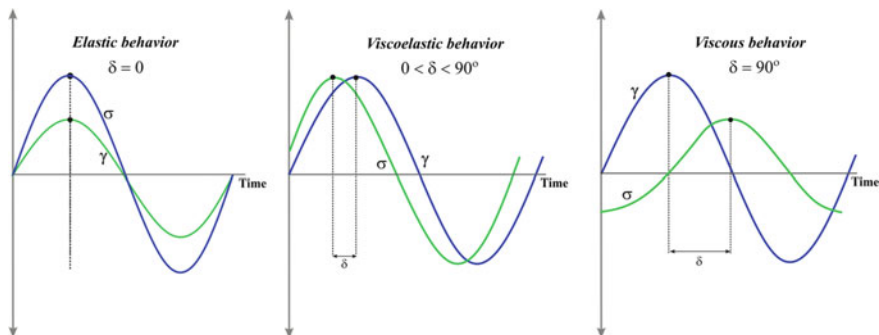


Fig. 7.5 Relationship between stress (σ) and strain (γ) for viscoelastic materials under oscillatory regime

composed by a solid-like elastic contribution (in phase with the input) and a liquid-like viscous contribution (out of phase with the input). The sinusoidal stress input and the sinusoidal strain output are presented in Eqs. 7.11 and 7.12, respectively. The input can alternatively be given as strain γ , producing a stress σ output.

The *phase angle* (δ) provides insights into dualistic contribution between the viscous and elastic characteristics. For a purely elastic material, $\delta = 0$, while for a purely viscous material, $\delta = 90^\circ$. Viscoelastic materials exhibit a δ value ranging between 0 and 90° . A $\delta = 45^\circ$ denotes the pivotal threshold between solid-like and liquid-like behavior, indicating a potential gelation point that marks the initiation of network formation (or its dissolution).

$$\sigma = \sigma_o \cdot \sin(\omega t) \quad (7.11)$$

$$\dot{\gamma} = \gamma_o \cdot \sin(\omega t + \delta) \quad (7.12)$$

In Eqs. 7.11 and 7.12 ω is the angular frequency, d is the phase angle, and t is the elapsed time.

Similar to simple shear deformation given by Eq. 7.6, where the stress is proportional to the strain, the oscillatory flow of linear viscoelastic materials can be described by a generalized Hooke law using a constant complex modulus (represented as G^*). The complex modulus is defined by the proportionality constant in the linear relationship between the applied stress and the maximum responsive strain, as shown in Eq. 7.13. The complex modulus can be decomposed in an elastic component and a viscous component. The component of complex modulus attributed to elasticity is labelled to as the storage modulus (G'), indicating the energy stored within the material. Equally, the component associated with viscosity is labelled as the loss modulus (G''), indicating the dissipation of energy.

$$\sigma = G^* \cdot \gamma \quad (7.13)$$

The storage modulus (G') is given by

$$G' = G^* \cdot \cos \delta \quad (7.14)$$

The loss modulus (G'') is given by

$$G'' = G^* \cdot \sin \delta \quad (7.15)$$

Hence, the phase angle can be represented by

$$\tan \delta = \frac{G''}{G'} \quad (7.16)$$

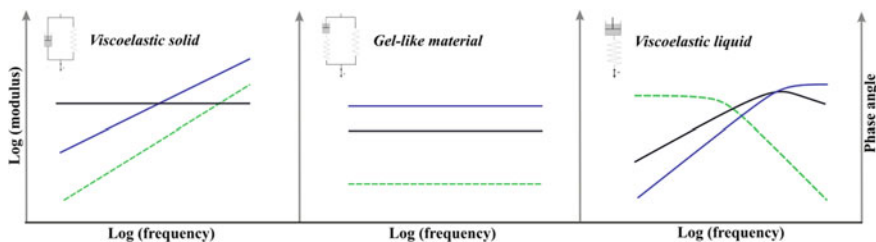


Fig. 7.6 Typical responses for different materials under frequency variation. Black solid line—storage modulus G' . Blue solid line—loss modulus G'' . Dashed line—phase angle δ

The parameters G' and G'' have both pressure units. The angular frequency (ω) is given by $2\pi f$, where f is the frequency in hertz (Hz). If an ideal spring is subjected to the oscillation across wide-range frequencies, the spring storage modulus (G') remains constant and equal to the spring modulus (G), while the loss modulus (G'') remains at zero. Conversely, if a perfect dashpot is oscillated, the loss modulus (G'') is determined by product between the viscosity (η) and the angular frequency (ω), while the storage modulus (G') consistently equals zero.

The evaluation of angular frequency sweep represents an in-depth examination of the structural properties of the material under rheological investigation. Angular frequency sweep test is performed across a spectrum of oscillation frequencies while keeping the strain or stress values constant within the Linear Viscoelastic Region. The material response under frequency sweeps provides valuable insights into distinguishing between viscoelastic materials, such as illustrated in Fig. 7.6. It is feasible to monitor changes in the two constituents of the complex modulus: the elastic modulus (G') and the viscous modulus (G''), contrasting their relative magnitude. Low-frequency measurements shed light on the material behavior over extended time intervals, revealing its response on a longer time scale, while high-frequency data capture the material behavior on shorter time scales.

A viscoelastic material can be characterized by a generalized description of the viscosity. It can also establish a complex viscosity denoted as η^* that represents the comprehensive resistance to flow, contingent on angular frequency (ω). As it is shown in Eq. 7.17, the complex viscosity is defined by the ratio between the complex modulus and the angular frequency, which gives the maximum strain rate amplitude.

$$\eta^* = \frac{G^*}{\omega} \quad (7.17)$$

As it can be seen in Eq. 7.18, the complex viscosity (η^*) can be represented as a complex number that includes both a real part (η') and an imaginary part (η''). The real part of the complex viscosity (η') represents the viscous behavior of the material, quantifying the material resists deformation and dissipates energy. The

imaginary part of the complex viscosity (η'') represents the elastic behavior of the material, characterizing the ability of the material to return to its original shape after deformation.

$$\eta^* = \eta' + i \cdot \eta'' \quad (7.18)$$

The dynamic viscosity is related to the loss modulus according to Eq. 7.19.

$$\eta' = \frac{G''}{\omega} \quad (7.19)$$

Similar to complex viscosity, the complex modulus can be written as a complex number that includes both a real part (G') and an imaginary part (G''), according to Eq. 7.20. G' and G'' represent the storage modulus and the loss modulus, respectively, according to Eqs. 7.14 and 7.15.

$$G^* = G' + i \cdot G'' \quad (7.20)$$

The viscoelastic behavior of complex materials can be comprehensively understood as a combination of Kelvin-Voigt and Maxwell models, as illustratively depicted in Fig. 7.4. In Fig. 7.4 representation the Kelvin-Voigt model is able to characterize material behavior at extremely high frequencies, while the Maxwell model pertains to lower frequency responses. Figure 7.7 illustrates a descriptive viscoelastic spectrum that encompasses a wide range of frequencies, stating different regions conform to the frequency interval. It is significant to highlight, employing standard rheometric techniques, the typical observation of the spectrum may be restricted. The extent of the observed spectrum is contingent on the sensitivity of the rheometer and the relaxation time inherent to the material being evaluated. To bridge the gap between higher and lower frequencies, higher temperatures can be employed, leveraging the time–temperature superposition principle.

Figure 7.7 presents the characteristic mechanical spectrum of a typical viscoelastic material into particular frequency range. Under growing of the angular frequency, the initial section is known as the viscous or terminal region, because the material response is marked by the dominance of the storage modulus (G') and the prevalence of viscous or flow behavior. The viscous region is always present in the rheological behavior of all materials, including solid materials which demonstrate creep over extended periods. However, the uncovering of the behavior exhibited in the terminal region requires often extremely low frequency values, making it challenging for most oscillatory instruments to detect this zone of the rheological curve. At appropriately low frequencies, the loss modulus (G'') displays linear behavior concerning the frequency, while the storage modulus (G') follows a quadratic pattern. In the viscous region, the longest relaxation time (τ_{\max}) can be computed from G' divided by the product $G'' \cdot \omega$. The following region is known as the transition-to-flow region due to the domain exchange between the storage and loss moduli. An intersection point between the G' and G'' lines is clearly identified, characterizing a change in the

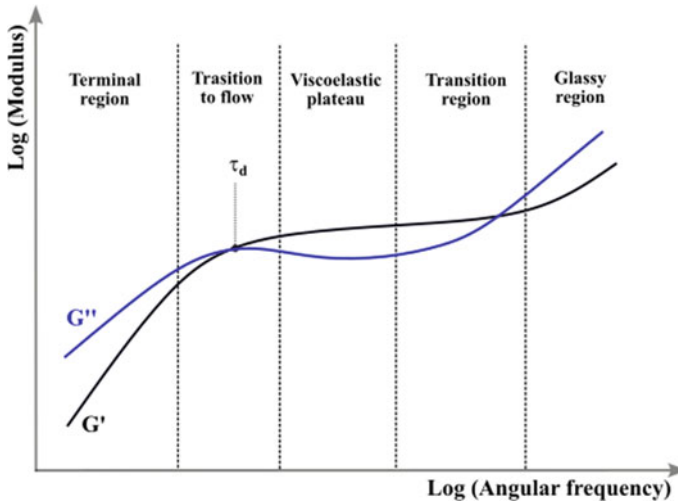


Fig. 7.7 Descriptive viscoelastic spectrum exhibiting the characteristic rheological behavior of a typical viscoelastic material under frequency sweep

material behavior, where the loss modulus G'' domain that characterizes the viscous or flow-related behavior is transferred to the elastic behavior, given by G' . The marked point, where the storage modulus equals to the loss modulus, is defined as a singularity frequency. For the Maxwell model, the crossover frequency is inversely related to the relaxation time (τ).

In the plateau region (also known *rubbery zone*), the elastic behavior is dominant, making the G' values higher the G'' values. While rubbery zone might appear many times as a nearly flat plateau, it typically is characterized by a slight increase in the storage modulus (G') with increasing frequency. Nevertheless, the G' increasing is often quite slight, and the loss modulus G'' is consistently lower than G' . The region referred to as the transition region indicates a higher transition crossover region (sometimes termed *leathery region*), which is characterized by a rise in the value of G'' due to high-frequency relaxation and dissipation mechanisms. G'' increases at a faster rate than G' , and a singular crossover frequency can once more be defined when G' equals G'' , leading to the determination of another characteristic time. Finally, at the highest frequency commonly applied in sweep test, the material exhibits a glassy region where the loss modulus G'' predominates and continues to increase at a faster rate than the storage modulus G' .

7.3 Interfacial Layer Rheology

Mechanical behavior of interfaces is characterized by deformation and flow in response to applied stresses. The primary types of deformations in an interfacial layer include dilatation (elongation) and shearing, keeping resemblance with bulk deformation as pictured in Fig. 7.1. Dilatation involves expansion and compression (deformation with constant shape but altering area), while shear implicates in deformation at constant area with changing shape. In the two-dimensional rheology, corresponding to three-dimensional bulk rheology, the deformation behavior can be described using springs and dashpots, as shown in Figs. 7.3 and 7.4. Shear rheology, applicable to interfacial layers containing amphiphiles and surfactants, provides primarily qualitative insights into the chemical structure of the interface. In contrast, interfacial dilatational rheology applied to the adsorbed layers is directly correlated with the dynamics of adsorption mechanisms and the thermodynamic state (for details see Davies 1961).

Unlike liquid bulk, which can be often assumed as incompressible, a comprehensive analysis of interfaces in rheology should consider not only the deformation due to flow but also the changes in surface area. The surface flow maintaining a constant surface area allows the accurate measurement of rheological properties like surface shear viscosity, dynamic shear moduli, and interfacial shear compliance. Moreover, in the case of many Langmuir films, where molecules are constrained to keep at the interface, the interfacial layers exhibit incompressibility in specific regions of the phase diagram, making it possible to disregard dilatational effects.

Surface rheology is comprehensively characterized by a set of four fundamental rheological parameters, encompassing the elasticity and viscosity pertinent to both compression and dilatation processes, as well as those associated with shear. In each of these instances, the dynamics of surface flow are intricately interlinked with the hydrodynamics inherent to the contiguous liquid bulk phase. The rheological behavior of interfaces can be described by mechanical analogue models, discussed early, where a spring represents an ideal elastic response governed by Hooke law, and a dashpot symbolizes an ideal viscous response, according to Newton law (see Fig. 7.3). Nonetheless, interfacial rheological parameters for one component systems (containing pure liquid subphases, for instance) are exceedingly low when contrasted with values observed in the presence of an absorbed or deposited interfacial films. Additionally, a noteworthy challenge arises from the arduous resolving of the desired measurements from the substrate and bulk material in many interfacial rheological techniques. Experimentally the interface dilatational rheology can be categorized as low, and high frequency tests. The interfacial shearing involves essentially continuous shear, creep and oscillation tests.

Surface-active agents are able to form Gibbs monolayers, when adsorbed from a bulk solution, and Langmuir films, when insoluble layers are created by amphiphiles spreading at the interface (for details see Rosen 1989). For both layers, the surface tension of the system containing the interfacial film is lower than the pure liquid surface, such as discussed in Chap. 6. The adsorbed film is characterized by the

surface pressure π , denoted in Eq. 6.2, which indicates the reduction in surface energy per unit area resulting from the spontaneous adsorption of the film. However, in practical applications, interfaces often undergo external mechanical perturbations, such as changes in shape or size. The interface's response to a change in size at constant shape is measured by dilatational elasticity and viscosity, while its response to shape deformation at constant size is described by shear elasticity and viscosity. The storage modulus (G') and loss modulus (G'') perform as essential phenomenological parameters directly acquired from rheological experiments. To comprehensively account for surface elasticity and viscosity, encompassing both shear and dilatational aspects, it becomes imperative to adopt a specific viscoelastic model, such as Kelvin–Voigt, and the Maxwell model.

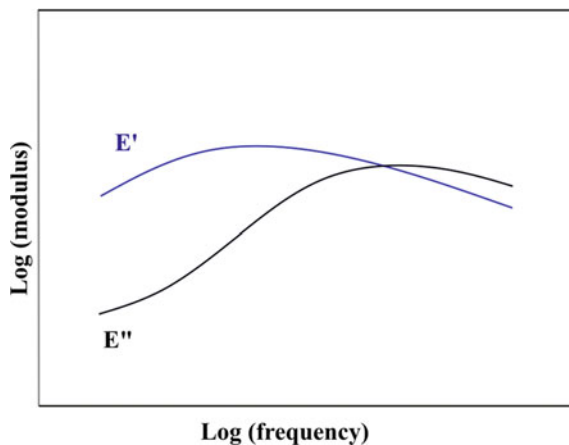
7.3.1 Dilatational Interfacial Rheology

Dilatational rheology refers to the behavior of a material under deformation that causes dimensional change, such as stretching or pulling. When a fluid interface is subjected to elongational deformation, it can exhibit a variety of behaviors depending on the properties of the fluids involved and the intensity and rate of the deformation. For example, the interface may become thinner and more elongated, or it may break up into droplets. The interface dilatational rheology is specified typically by the relationship between the stress applied to the fluid interface and the corresponding deformation, as given in Eq. 7.5.

For interfaces characterized by purely elastic behavior, the dynamic response of interfacial tension exhibits an immediate correlation with changes in interfacial area. In these specific cases, there is no discernible phase lag between the variations in interfacial tension and alterations in interfacial area. However, in a broader context encompassing diverse material systems, the relationship between interfacial tension and changes in interfacial area typically introduces a delay. This temporal lag arises from the intricate interplay of relaxation processes occurring within the interfacial layer itself and between the interface and the neighboring bulk phases. Consequently, the dynamic interfacial tension response exhibits a phase shift relative to the changes in interfacial area, reflecting the time required for these relaxation phenomena to manifest and equilibrate. The relaxation phenomenon underscores the complexity of interfacial dynamics, where multiple mechanisms influence the temporal coupling between interfacial tension and interfacial area changes, a subject of intense interest in the realm of interfacial science and its implications are extensively explored in scientific literature.

The dilatational stress experienced by a system undergoing a surface area expansion or contraction can be expressed as the summation of two distinct terms, producing expression similar to Eqs. 7.9 and 7.10. However, the fundamental parameter employed for delineating the dilatational rheological characteristics of adsorption layers is the interfacial dilatational viscoelasticity, widely known as the *interfacial viscoelastic modulus*. The interfacial viscoelastic modulus (E) is a key parameter

Fig. 7.8 Descriptive illustration of the dilatational elastic modulus (E') and dilatational viscous modulus (E'')



formally represented as a complex quantity, defined through the ratio of variations in interfacial tension to the changes in relative interfacial area. E is equivalent to the elasticity modulus G in Hooke model (Experimental data of the elasticity modulus is found in Kabbach and Santos 2018).

The interfacial viscoelastic modulus (E) displays frequency-dependent characteristics as a complex quantity. In complex representation, the real component of the interfacial viscoelastic modulus (E') corresponds to the dilatational elasticity ($E' = E_0$), while the imaginary component (E'') is intricately associated with the dilatational viscosity through the angular frequency ($E'' = \omega \cdot \eta$). Similar to Eq. 7.20, the viscoelastic modulus (E) can be written as Eq. 7.21.

$$E = E' + i \cdot E'' \quad (7.21)$$

The Fig. 7.8 presents a descriptive illustration of the dilatational elastic modulus (E') and dilatational viscous modulus (E''), including their crossing line.

The frequency-dependent behavior of the dilatational modulus (E) arises as a consequence of the intricate relaxation processes occurring inside the interfacial layer. As a result, dilatational rheology has been used as a valuable tool for probing the dynamic aspects of surfactant adsorption and the underlying mechanisms such as diffusion and other rearrangements within the adsorbed layer. The dilatational viscoelasticity is governed by a combination of the thermodynamic attributes of the adsorbed layer and its kinetic characteristics. Notably, while the interfacial tension dependency on surface area encapsulates the two-dimensional equation of state, a relationship particularly evident in the context of insoluble surfactants, the frequency dependence of the dilatational modulus (E) is intimately tied to the kinetics of re-equilibration processes within the interfacial layer. This intrinsic connection underscores the intricate interplay between thermodynamics and kinetics in the description of dilatational rheological behavior.

For interfacial harmonic perturbations covering small amplitudes of the angular frequency, the system demonstrates linear behavior, and the interfacial viscoelastic modulus (E) can be described as Eq. 7.22.

$$E = \frac{d\gamma}{d \ln A} \quad (7.22)$$

γ is the interfacial tension and A is the surface area covered by adsorbed or spread molecules. Considering the surface adsorption, the viscoelasticity modulus can be represented by Eq. 7.23. The viscoelasticity modulus E depends both on the thermodynamic and kinetic characteristics of the adsorbed layer.

$$E = -E_o \cdot \frac{d \ln \Gamma}{d \ln A} \quad (7.23)$$

The Eq. 7.23 is referred to as *Gibbs elasticity*, a function fundamentally equivalent to the surface equation of state. Γ represents the surface excess concentration, giving the surfactant adsorption. E_o is the viscoelasticity modulus at high frequency. E_o can be calculated by the Eq. 7.24, using a suitable adsorption model.

$$E_o = -\frac{d\gamma}{d \ln \Gamma} \quad (7.24)$$

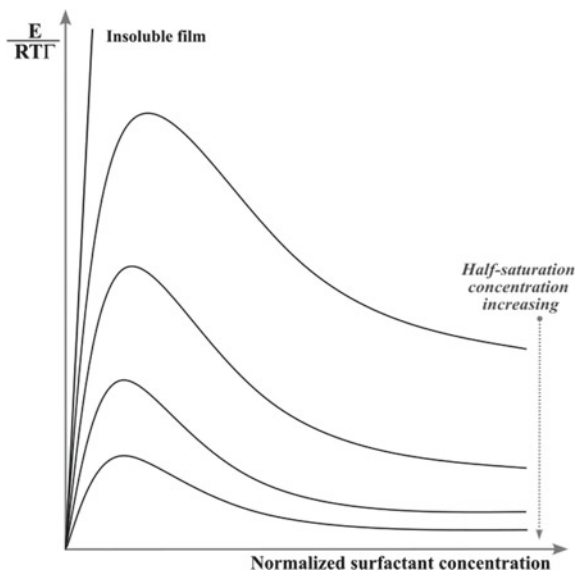
An inconsistency similar to that observed in high-frequency elasticity, is also evident in the analysis of experimental data pertaining to the molecular exchange parameter. The molecular exchange parameter is denoted as the *characteristic frequency of diffusional relaxation* (ωD), given by Eq. 7.25.

$$\omega D = D \cdot \left(\frac{d\Gamma}{dC} \right)^{-2} \quad (7.25)$$

where D is the surfactant diffusion coefficient and C represents the surfactant concentration. Notably, at elevated surfactant concentrations, the characteristic frequency of diffusional relaxation assessed by the *Langmuir (or Frumkin) model* significantly surpasses the corresponding experimental values by several orders of magnitude. The mentioned discrepancy underscores that prevailing theoretical models yield markedly underestimated values of $d\Gamma/dC$ under conditions of high surfactant concentrations.

The Gibbs elasticity demonstrates a consistent reliance on surfactant concentration, as represented in Fig. 7.9, while upholding a constant film thickness. Within the lower concentration spectrum, a discernible linear augmentation of elasticity becomes evident. This incremental trend reaches its high point at a specific concentration denoted as half-saturation concentration, indicating a state where the surface attains an approximate half-saturation level with surfactant molecules. Nevertheless, as concentrations exceed this pivotal juncture, a decrement in elasticity ensues. This diminishment can be ascribed to the escalating diffusion phenomenon, progressively

Fig. 7.9 Gibbs elasticity as a function of normalized surfactant concentration for different concentration saturations. Normalized surfactant concentration is the ratio between the surface concentration and the half of concentration to achieve the full concentration. Surface pressure and film thickness are kept constant



infusing the surface with surfactant molecules, thereby alleviating the initial gradient in interfacial tension.

Gibbs elasticity is a fundamental parameter in the study of surface and interfacial phenomena, particularly in the context of surfactant adsorption. It plays a pivotal role in elucidating the behavior of interfaces, especially how they respond to changes in surfactant concentration. Typically, at low surfactant concentrations, there is a linear increase in Gibbs elasticity. This linear regime signifies a proportional adsorption of surfactant molecules at the interface. As surfactant concentration increases, a singular point where the surface is approximately half-saturated with surfactant molecules. At this critical concentration, Gibbs elasticity reaches its maximum value. However, as surfactant concentrations continue to rise beyond this point, the Gibbs elasticity begins to decline. This decline is primarily attributed to the increasing diffusion of surfactant molecules from the bulk solution to the interface. The enhanced diffusion effectively replenishes the surface with surfactants, mitigating the initial gradient in interfacial tension.

An intriguing aspect of the Gibbs elasticity analysis is that the maximum observed in elasticity is not a result of molecular interactions occurring at the surface. Rather, it exclusively emanates from the mounting diffusion processes emerging at higher concentrations, which effectively level the playing field concerning surface tension gradients. In this particular context, it warrants mention that molecular interactions remain negligible, given that Langmuir adsorption operates within the framework of ideal surface behavior, restraining the involvement of such interactions. This observation underscores the importance of distinguishing between thermodynamic and kinetic factors in understanding interfacial behavior.

7.3.2 Interfacial Shear Rheology

In interfacial shear rheology measurements, the interfacial area remains constant throughout the process. Although the interfacial shear methodology is similar to the expansion interfacial rheology, but the shear modulus (G) and the elasticity modulus (E) are distinct parameters, providing unique interfacial rheological information. One pertinent challenge in interfacial shear rheology arises from relatively weak interfacial rheological properties, which can pose difficulties for measurement equipment. To achieve heightened sensitivity, a paramount objective is to maximize the discernible interfacial contribution while minimizing the influence of the bulk phase. In all cases, achieving accurate determinations of interfacial shear properties necessitates the separation of purely interfacial effects from those originating in the adjacent bulk liquid (for experimental data see Neves and Santos 2021). The required resolving is precisely quantified by the *Boussinesq number*, denoted as Bo , such as described in Eq. 7.26. Bo serves as a metric for assessing the relative significance of interfacial stress contributions compared to those originating within the underlying subphase.

$$Bo = \frac{\eta_s}{\eta \cdot L} \quad (7.26)$$

η_s is the viscosity of the interface, η is the viscosity of the bulk phase, and L corresponds to a length scale associated with the dimensions of the employed probe. For liquid–liquid interfaces, it is imperative to consider the viscosities of both phases, as shown in Eq. 7.27.

$$Bo = \frac{\eta_s}{(\eta_1 + \eta_2) \cdot L} \quad (7.27)$$

In Eq. 7.27, η_1 and η_2 represent the viscosities of the upper and lower phases, respectively. The Boussinesq number assumes paramount importance in guiding the selection of the most suitable probe for accurately determining interfacial shear properties. If Bo is much higher than 1, the predominant influence on the measuring probe is due to the drag experienced within the interface. Conversely, If Bo is markedly lower than 1, the measurements primarily reflect the properties of the surrounding medium. Thus, the Boussinesq number plays a pivotal role in the identification of the optimal probe for precise interfacial shear property assessment.

An extension to the analysis of viscoelastic interfaces incorporates the information that both the real and imaginary components of the viscoelastic surface moduli exhibit a dependence on the Boussinesq number. In this context, the Boussinesq number assumes a complex, frequency-dependent form, shown in Eq. 7.28.

$$Bo(\omega) = \frac{G''(\omega) - i \cdot G'(\omega)}{\omega \cdot \eta \cdot L} \quad (7.28)$$

Methods used for description of the interfacial shear rheology can be categorized as direct or indirect. Indirect methods, the determination of interfacial shear viscosities encompass velocity profile measurements through instruments like the channel surface viscometer, deep-channel surface viscometer, or the rotating knife-edge wall surface viscometer, demanding the assessment of fluid flow dynamics employing visible inert particles. Indirect methods primarily find application at gas/liquid interfaces, although certain adaptations of the deep-channel technique have been devised for investigations at liquid/liquid interfaces.

For insoluble spread monolayers, the assessment of interfacial shear viscosity (η) can be conducted in a manner analogous to the application of the *Hagen-Poiseuille law* for determining the bulk viscosity of liquids by means of *channel surface viscometry*. It approach relies on the quantification of the flow rate of a monolayer film through a confined channel or slit under the influence of an applied two-dimensional pressure difference ($\Delta\pi$). This method is not suitable for adsorbed films, primarily because it requires the presence of a surface pressure gradient to sustain the flow. The shear surface viscosity can be determined by Eq. 7.29.

$$\eta_s = \frac{\Delta\pi \cdot W^3}{12Q \cdot L} - \frac{W \cdot \eta}{\pi} \quad (7.29)$$

W and L denote respectively the width and length of the channel. Q represents the material flow directed towards the region of the trough where the surface pressure (π) is lower. η is the bulk viscosity.

Deep-channel surface viscometry relies on the application of viscous-traction forces to induce fluid flow, without the requirement of surface pressure gradients. The measurement apparatus comprises two concentric stationary vertical cylinders and a rotating flat-bottomed dish, creating a channel with a moving base. The base rotates at a constant angular velocity, inducing rotational motion in the fluid within the channel, resulting in shear forces exerted by the channel walls. This enhanced interaction with the interface enables the measurement of interfacial shear rheological properties. An inert particle placed within the fluid surface tracks the centerline surface motion within the channel. The axisymmetric geometry allows for the isolation of the interfacial shear viscosity as the sole interfacial property influencing the azimuthal component of the tangential stress balance. Deep-channel surface viscosimeters are overly sensitive equipment for both liquid/air and liquid/liquid interfaces under various conditions, including steady-state, relaxation, and oscillation regimes.

Rotating wall knife-edge surface viscometers assess the interfacial shear viscosity through the precise measurement of the displacement ratio between surface velocity and the angular velocity of a rotating outer ring. Analogous to the deep-channel surface viscometer, a particle is strategically positioned within the interface to accurately monitor the rotational speed of the fluid interface. The technique is exceptionally sensitive, yielding values interfacial shear viscosity in the range of 10^{-5} mN s m⁻¹.

In contrast to indirect methods, direct methods are employed to directly ascertain the torsional stress values experienced by the interface when subjected to contact with a probe. These techniques involve intricate geometries of various measurement probes and employ specialized techniques to detect the resulting motion or stress. Many of direct methods are applied in rotational modes, including steady rotation, transient regimes of deformation, or oscillating modes. Steady rotation can be implemented following the Couette principles, while transient deformations encompass relaxation and creep experiments. Oscillatory modes involve forced and damped oscillation experiments. Conventional apparatus utilized for the direct evaluation of interfacial shear properties typically involve a circular measuring probe suspended by a small torsion wire, which is carefully positioned at the interface.

The magnetic needle method stands out for its notably high Boussinesq number in relation to the other techniques. By the magnetic needle method, a thin needle positioned at the interface is subjected to controlled vibrations induced by a magnetic field. The precise movement of the needle is meticulously tracked through camera monitoring, facilitating the characterization of viscoelastic properties at the interface. This method is often synergistically employed with Langmuir troughs, permitting experiments to be conducted as functions of molecular or particle packing density, thereby offering valuable insights into the dynamic interplay of molecular interactions at the interface.

Figure 7.10 display response of oscillatory shear stress amplitude sweeps (for foams) characterized by varying ionic strengths while maintaining a similar gas volume fraction, unveil exciting features within the domain of rheology. Notably, it is observed that G' (storage modulus) and G'' (loss modulus) exhibit a condition of relative constancy at low stress amplitudes, firmly ensconced within the confines of the linear viscoelastic regime. G' values are substantially higher than G'' , and their dynamic interaction establishes that an increase in G' results in a corresponding growth in G'' .

The G' curves unveil a distinctive pattern marked by an apparent decline precursor to their intersection with the G'' curve, denoted by the presence of crosses. Notably, this decline is characterized by an increasingly negative slope as the ionic strength escalates. Simultaneously, the G'' values exhibit intriguing behaviors within the same stress amplitude range. Extending the discussion, for systems devoid of salt and those featuring salt high concentration, the curves exhibit a unique characteristic consisting of a local minimum, succeeded by a subsequent local maximum, just prior to crossing the G' curve. However, as the ionic strength is elevated, the prominence

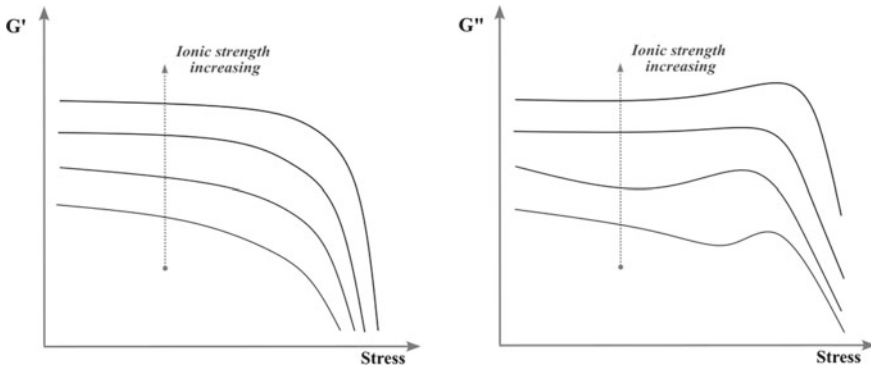


Fig. 7.10 Illustration of shear elasticity moduli of liquid–air interface obtained from oscillatory rheological tests under stress sweep at constant frequency for different ionic strengths

of the minimum in G'' diminishes, and the curves predominantly showcase a well-defined maximum. Moreover, the maximum point tends to relocate to higher stress amplitude values concomitant with the ascending ionic strength.

7.4 Dimensions of Interfacial Elasticity Moduli

Interface elasticity moduli are essential parameters employed for characterizing the elastic response of fluid interfaces. The Young modulus, given by Eq. 7.6, stands as the most frequently employed elasticity modulus, serving as a quantification of the interface resistance to deformation when subjected to a given stress. Young modulus is precisely defined as the stress-to-strain ratio within the linear region of the stress–strain curve.

For three-dimensional materials, it is expressed in units of pressure. Typical values of Young’s modulus for metals generally fall in the range of 45 GPa to 400 GPa. For example, steel has a Young’s modulus of around 200 GPa. Polymers have lower Young’s modulus values compared to metals. They typically range from 1 to 4 GPa. However, some high-performance polymers can have higher values. Ceramic materials can have Young’s modulus values ranging from 100 to 400 GPa, depending on their composition and microstructure. Composite materials can have a wide range of Young’s modulus values, depending on the specific composite design. Biological materials like bone, cartilage, and wood have Young’s modulus values that vary widely. For example, cortical bone has a Young’s modulus of approximately 10–20 GPa. Rubber materials, known for their elasticity, have relatively low Young’s modulus values, often less than 1 GPa. In interfaces, two-dimensional systems, the elasticity modulus is substantially lower than bulk material, and it is given in force per length units. The interfacial Young modulus for the air–water interface can be on the order of 10^{-2} to 10^{-1} N m⁻¹. Interfaces between two immiscible liquids, such as

oil and water, can have interfacial Young modulus values that vary widely, typically ranging from 10^{-2} to 10 N m^{-1} . The Young's modulus at solid–liquid interfaces, which are important in fields like colloid science and materials science, can typically span a wide range, from 10^{-2} to 10^3 N m^{-1} , depending on the properties of the solid and liquid phases. Interfaces in biological systems, such as cell membranes or lipid monolayers, may have interfacial Young's modulus values within the range of 10^{-3} to 10^{-1} N m^{-1} .

The shear modulus, sometimes termed interfacial shear elasticity, gauges the interface capacity to withstand shearing or tangential deformation. The shear modulus is properly delineated as the ratio of shear stress to shear strain and, like Young's modulus, is quantified in pressure units for bulk materials. For liquid–liquid interfaces, interfacial shear elasticity typically falls in the range of tens to hundreds of mN m^{-1} . This behavior is common for interfaces between immiscible liquids like oil and water. For liquid–gas interfaces, the interfacial shear elasticity is usually lower, often in the range of single to low double-digit mN m^{-1} , which is a typical characteristic of interfaces existing between a liquid phase and a gaseous phase, like the interface between air and water. In cases where such interfaces become more intricate due to the presence of surfactants, the interfacial shear elasticity exhibits a broader range of variation, and it's important to note that values outside the typical ranges mentioned can indeed occur in these complex scenarios.

Several crucial parameters must be significantly included in the viscoelastic characterization of interfaces. Among these parameters, the relaxation time stands out as a valuable indicator, indicating the time frame necessary for the interface to return to its initial state after undergoing deformation. The values of the viscoelastic parameters are intricately dependent on a multitude of factors. These factors encompass the composition and temperature of the involved fluids, the presence of surfactants and other supplementary additives, as well as the existence of additional interfaces or boundaries within the system.

Experimental techniques like pendant drop, surface force apparatus, and oscillatory rheology serve as indispensable tools for the empirical determination of interfacial elasticity moduli. The values of interface elasticity moduli can be used to predict the behavior of fluid interfaces under deformation, and it can inform the design and optimization of industrial processes involving complex fluid systems, such as in the production of emulsions, foams, and other multiphase systems. The interface elasticity moduli depend on numerous factors such as the composition and temperature of the fluids involved, the presence of surfactants or other additives. Therefore, there is a wide range of values for these moduli that can be observed in different systems.

7.5 Isothermal Surface Compressibility

Isothermal compressibility is a measure of how much a substance's volume changes in response to changes in pressure, while keeping its temperature constant. The interface isothermal compressibility, as defined by Eq. 6.27, specifically refers to the

compressibility of an interface between two phases, such as a liquid and a gas. Typical values for the interface isothermal compressibility depend on the specific properties of the substances at the interface, as well as the temperature and pressure conditions. However, interface isothermal compressibility values are commonly slight, often in the range of 10^{-6} to 10^{-9} Pa⁻¹. For example, the interface isothermal compressibility of water at room temperature and atmospheric pressure is about 4.6×10^{-7} Pa⁻¹.

In general, monolayers have higher interface isothermal compressibility values than bulk liquids or gases, due to their reduced thickness and increased susceptibility to deformation under pressure. Typical values for the interface isothermal compressibility of monolayers range from 10^{-6} to 10^{-3} Pa⁻¹, depending on the specific properties of the monolayer. For example, the interface isothermal compressibility of a monolayer composed of fatty acids at room temperature and atmospheric pressure is typically in the range of 10^{-5} to 10^{-4} Pa⁻¹. The interface isothermal compressibility for monolayers formed from surfactants depend strongly on molecular and structural factors such as the headgroup size, shape, and charge, as well as the length and flexibility of the hydrophobic tail. Also, the interface isothermal compressibility of a monolayer can be influenced by external factors such as the presence of other molecules or ions at the interface, as well as changes in the temperature or pressure conditions.

References

- Barnes HA. A handbook of elementary rheology. University of Wales; 2000.
- Davies JT. Interfacial phenomena. New York and London: Academic Press; 1961.
- Kabbach CB, Santos RG. Effects of pH and temperature on the phase behavior and properties of asphaltene liquid films. *Energy Fuels*. 2018;32.
- Miller R, Fainerman VB. Interfacial rheology of adsorbed layers. In: *Emulsions: structure stability and interactions*. Elsevier; 2004.
- Neves MAR, Santos RG. Phase behavior of surface films of SARA fractions extracted from heavy oil. *Colloids Surf A Physicochem Eng Aspects*. 2021; 618.
- Rosen M. Surfactants and interfacial phenomena. New York: Wiley; 1989.

Chapter 8

Liquid–Liquid Interfaces



Fluid interfaces, the regions where two different fluids meet, are of paramount importance in various scientific and industrial contexts. These interfaces possess intricate characteristics, including composition, structure, and rheological properties, which can significantly impact various processes. At the molecular level, the interface between two immiscible liquids is characterized by a distinct arrangement of molecules. Molecules at the interface experience different forces and interactions compared to those in the bulk of each liquid phase, exhibiting a surface tension, which measures the energy required to increase the interface area due to the tendency to minimize the contact between the phases. Interfacial tension arises due to the cohesive forces within each liquid phase and the adhesive forces between the two phases. The energy of the interface is thoroughly related to interfacial tension and provides insights into the stability and behavior of the interface. Materials with lower surface energy tend to minimize their contact area with other phases, leading to phenomena like the formation of spherical droplets. Surfactants play a key role at liquid–liquid interfaces, allowing them to reduce interfacial tension and stabilize emulsions. In processes like soap bubble formation and microfluidics, the Marangoni effect occurs when there are gradients in interfacial tension, often induced by changes in temperature or the presence of solutes. The movement of molecules and particles across liquid–liquid interfaces is essential in processes like mass transfer, adsorption, and diffusion. The interfacial properties of liquid–liquid interfaces are fundamental for understanding numerous daily and industrial phenomena.

8.1 The Nature of Fluid Interfaces

The dispersed particles within colloidal systems experience continuous motion that can result collisions between them. The interparticle collisions can cause the rupture of the interfacial film surrounding the colliding particles, become them susceptible to

the surface interaction. In the case of dispersed liquid droplets and gaseous bubbles, such interactions may lead to the coalescence, resulting in the formation of larger dispersed particles due to the decreasing in the overall energy of the system. Hence, the mechanical strength of the interfacial film plays a pivotal role in determining the stability of disperse systems, mainly foams and emulsions.

To achieve maximum mechanical stability, the interfacial film formed by adsorbed surfactants should exhibit a condensate state, featuring robust lateral intermolecular forces, and high film elasticity. It is worth noting that highly purified surfactants scarcely produce interfacial films that are densely packed and consequently they tend to lack mechanical strength. Therefore, effective interfacial agents typically consist of a combination of two or more surfactants rather than relying on a single surfactant molecule. A commonly employed combination includes a water-soluble surfactant and an oil-soluble one. The oil-soluble surfactant is liable to enhance lateral interactions among surface-active molecules within the interfacial film, resulting in condensation and increased mechanical strength (see Chap. 7 for detail on film elasticity).

In emulsions, liquid crystals can also form at the interface. Liquid crystals accumulate around the dispersed particles, creating a high-viscosity region that impedes the coalescence of individual droplets. Furthermore, liquid crystals function as a steric barrier, preventing the dispersed particles from approaching each other closely enough for attractive van der Waals forces to become significant. Notably, in water-in-oil macroemulsions, the interfacial films surrounding the droplets must possess exceptional strength. These films are believed to exhibit characteristics of solid-condensed films, characterized by robust lateral intermolecular forces and well-defined orientation of the film with respect to the interface, which imparts significant rigidity to the film. In water in oil emulsions, where water droplets typically carry little or no charge, the electrical barrier to coalescence is not able to act. Consequently, it is primarily the mechanical strength of the interfacial film that prevents the coalescence of droplets in water in oil macroemulsions. To withstand the continuous impact from neighboring droplets, the interfacial film in water in oil emulsions must possess extraordinary strength. This is evident in the irregular shape of water droplets within W/O emulsions, in stark contrast to the spherical shape exhibited by oil droplets in oil-in-water (O/W) emulsions.

8.2 Thin Liquid Film

During the approach of two colloidal particles suspended within a fluid continuous medium, a flat liquid film is emerged between the particle surfaces (for details see Adamson and Gast 1997; Davies and Rideal 1963). Figure 8.1 illustrates the approaching of two spherical particles with radius R forming a thin film with thickness h . The film formation between two surfaces is governed by a complex interplay

of various forces and interactions, including hydrodynamic effects, buoyancy, Brownian motion, electrostatic forces, van der Waals forces, steric interactions, and others (see Chap. 3 for comprehensive details).

Figure 8.2 illustrates the film formation in foams or emulsions, by means a series of stages depicting the formation and deformation of a thin liquid film between typical bubbles or droplets. The initial stage (stage *a*) involves the gradual approach of surfaces that exhibit slight deformations. Upon reaching a specific separation distance, a significant transformation occurs and the curvature at the center undergoes an inversion, resulting in the formation of a dimple (stage *b*). Subsequently, the dimple gradually diminishes, ultimately yielding an almost planar and parallel film (stage *c*). The film *behavior* is influenced by thermal fluctuations and external disturbances, which can either lead to the rupture or undergo an alteration into a thinner film known as a *Newton Black film* (stage *d*). Finally, the *Newton Black film* expands until it attains its final equilibrium state (going from stage *e* to stage *f*).

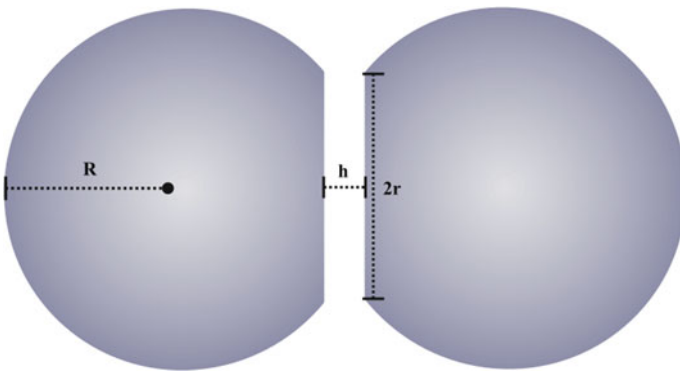


Fig. 8.1 Approaching of two spherical particles forming a thin liquid film with radius r and thickness h

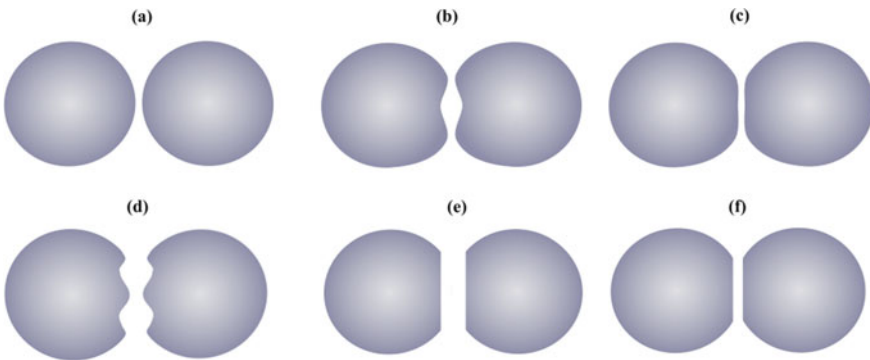


Fig. 8.2 Illustrative of consecutive stages of formation and deformation of a thin liquid film between two fluid particles

As external forces act upon the fluid particles to bringing them closer together, hydrodynamic interactions become prominent, particularly in the frontal region in-between, inducing subtle deformations at the interfaces. In such cases, the well-known *hydrodynamic capillary number*, which is a dimensionless parameter typically applies to non-deformable surfaces, must be modified to account the interfacial separation distance, denoted as h in Fig. 8.1 (for details see Harkins 1952; de Gennes et al. 2004). The modified capillary number (Ca) is described by Eq. 8.1.

$$Ca = \frac{\eta \cdot V \cdot R}{\gamma \cdot h} \quad (8.1)$$

The capillary number is defined as the ratio of viscous to interfacial forces. Here η is the dynamic viscosity of the liquid, V is a characteristic velocity and γ is the interfacial tension between the two fluid. R is the droplet radius. The evolution of the gap between two fluid droplets has been assessed for various characteristic times. In specific scenarios, such as the small air-bubble bursting at an air–water interface, the deformation of the fluid particle surfaces occurs instantly. A critical separation distance (h_i) must be attained, producing a meaningful change in curvature at the contact point between the fluid particles, even droplets or bubbles. The critical distance is defined as the *inversion thickness* and it results in the formation of a concave lens-shaped structure as a dimple, ensuing even in asymmetric films. The determination of the inversion thickness incorporates the van der Waals interaction explicitly, as described by Eq. 8.2

$$h_i = \frac{F \cdot (\gamma_1 + \gamma_2)}{4\pi \cdot \gamma_1 \cdot \gamma_2} \cdot \left(1 - \frac{A_H \cdot R}{12F}\right) \quad (8.2)$$

h_i represents the inversion thickness. F_z is the external force (nonviscous and non-van der Waals in origin) acting on the approaching particles. γ_1 and γ_2 are the interfacial tensions of the phase boundaries of particles 1 and 2, respectively. A_H is the Hamaker constant. In situations where the van der Waals force can be regarded as negligible, Eq. 8.2 simplifies to Eq. 8.3.

$$h_i = \frac{F \cdot (\gamma_1 + \gamma_2)}{4\pi \cdot \gamma_1 \cdot \gamma_2} \quad (8.3)$$

At macroscopic and microscopic scales, substantial differences in the patterns and time scales governing film evolution have been observed in emulsion film formation and thinning (for details see Tadros 2018). Particularly, dimple formation is not found in thin liquid films with small diameters. Instead, a reverse bell-shaped deformation is built, leading to the rapid rupture of the film under the prevailing influence of dominant van der Waals attractions. The thickness at which the reverse bell appears is denoted as h_b , and it can be determined through the Eq. 8.4.

$$h_b = \left(\frac{A_H \cdot R}{12F} \right)^{\frac{1}{2}} \quad (8.4)$$

The formation thickness of the reverse bell is dependent on the radius. For a droplet with tangentially immobile surfaces and radius R is influenced by the buoyancy force, given in Eq. 8.5

$$F = \frac{4}{3} \pi R_d^3 \cdot \Delta\rho \cdot g \quad (8.5)$$

When attractive forces, mainly van der Waals forces, exert a minor influence, the initial response in thinning liquid films is the undulation formation. However, the dimple waves have a short time-life. The fast liquid drainage leads to the undulation diminishing and eventually disappearing. Consequently, the resultant film becomes progressively thinner while maintaining an almost constant radius, denoted as R . When electrostatic repulsion exerts a substantial influence, a thicker primary film is established. The primary film is inherently metastable, according to conventional DLVO theory. A remarkably thin film, sustained by short-range repulsion forces, is referred to as the secondary film (also termed *Newton Black film*). The transition from typical primary films to secondary Newton films is frequently observed in foam films. Figure 8.3 shows a qualitative description of the effect of the attractive forces on the film formation.

The attractive and repulsive energy contributions in the context of DLVO (Derjaguin, Landau, Verwey, and Overbeek) interactions exhibit distinct dependencies on the separation of droplets. Their superposition can give rise to a complex distance-dependent behavior. This phenomenon is elucidated in Chap. 3, where the DLVO interaction is characterized by the interplay of van der Waals attraction and electrostatic repulsion forces. Specifically, the van der Waals energy demonstrates deviation as the inverse of the separation distance h^{-1} at small separations and decays as the inverse sixth power of the separation distance h^{-6} at large distances. Conversely, electrostatic repulsion persists at small distances and decreases exponentially as the separation increases. As a result, the interaction energy is mainly attractive at both small and large separations, primarily due to the dominance of van der Waals forces. However, within the intermediate range, the electrostatic contribution can cause the interaction to become repulsive, as depicted in Fig. 8.3.

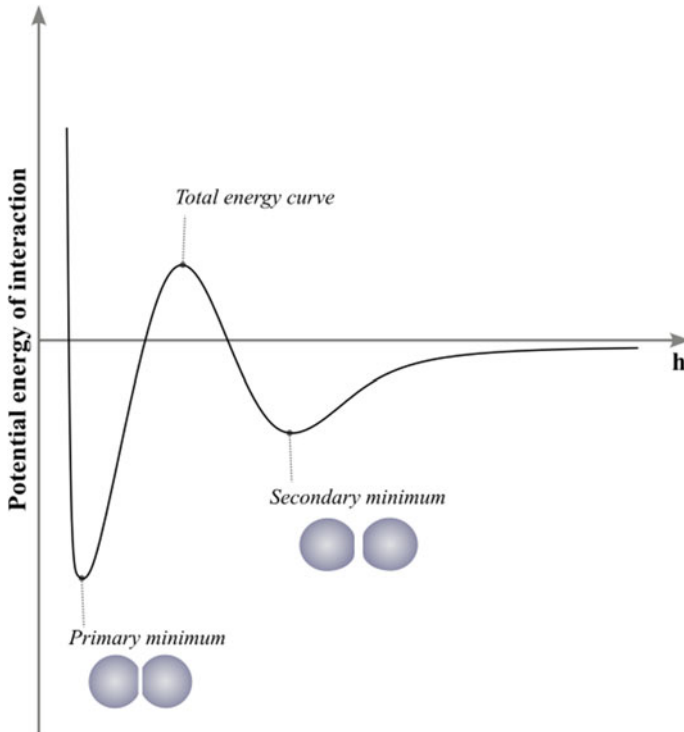


Fig. 8.3 Illustration of the interaction energy as a function of the separation h (liquid film thickness) between two infinite flat surfaces

Notably, Fig. 8.3 suggests the presence of a potent and short-ranged repulsion, even at exceedingly small separations, a feature not originally encompassed in the conventional DLVO theory. The distinctive shape of the total energy curve in Fig. 8.3 implies the possibility of flocculation occurring in either the far-reaching secondary minimum or the closer primary minimum. It's important to highlight the attraction within the secondary minimum is considerably weaker than that within the primary minimum, resulting in weaker flocculation. Accordingly, droplets flocculated in the secondary minimum are more prone to separating than those in the primary minimum. Furthermore, it is conceivable that flocculation in the primary minimum may be preceded by flocculation occurring in the secondary minimum.

The film thinning rate is driven by the capillary pressure, and it depends on the surfactant concentration. The thermal fluctuations or external perturbations lead to the emergence of a secondary film, or film rupture if the secondary film lacks stability. As the derivative of the disjoining pressure assumes a positive value, the amplitude of the thermal fluctuations is increased. The film instability ultimately carries out to either film rupture or the formation of distinct black spots.

8.3 Surface Curvature

The relationship between capillary pressure and interfacial curvature imposes a difference between the chemical potential of components within small particles (phase α) and that in the bulk phase (phase β). This variation serves as the driving mechanism for phenomena such as *nucleation* and *Ostwald ripening*. In the presence of positive interfacial energy, the total energy needed for forming small particles with significant curvature is increased. The Gibbs–Thomson equation, given in Eq. 8.6, is a quantitative expression explaining the impact of capillary or curvature-induced effects on phase transitions within tiny particles and confined systems. More specifically, it elucidates how the size or curvature of a phase interface exerts influence on the equilibrium vapor pressure or melting point of a given material.

$$\left(\mu_i^\beta\right)_R - \left(\mu_i^\beta\right)_{R=\infty} = 2\gamma \cdot \frac{V_i^\alpha}{R} \quad (8.6)$$

In the Gibbs–Thomson equation, μ represents the chemical potential, V_i represents the partial volume. The superscripts indicate the phase, while the subscripts denote the component. When phase β corresponds to an ideal gas model, Eq. 8.6 is altered to Eq. 8.7

$$\frac{P_i^\beta(R)}{P_i^\beta(\infty)} = \exp\left(\frac{2\gamma \cdot V_i^\alpha}{RkT}\right) \quad (8.7)$$

$P_i^\beta(R)$ and $P_i^\beta(\infty)$ represent respectively the equilibrium vapor pressure of component i in a droplet of radius R and in a large liquid phase with the same composition. Equation 8.7 clearly demonstrates that as the size of the droplet decreases, the equilibrium vapor pressure of the droplet increases. For bubble, the opposite trend is seen, then R must be replaced by $-R$ on the right-hand side of Eq. 8.7. Furthermore, Eq. 8.7 suggests that within an aerosol composed of polydisperse droplets, the larger droplets will tend to grow while the smaller ones diminish, potentially disappearing altogether. Nevertheless, when phase α contains a nonvolatile component, the smaller droplets are protected from complete disappearance. Then, Eq. 8.7 must be rewritten as seen in Eq. 8.8.

$$\frac{P_i^\beta(R)}{P_i^\beta(\infty)} = \frac{1 - x(R)}{1 - x(\infty)} \cdot \exp\left(\frac{2\gamma \cdot V_i^\alpha}{RkT}\right) \quad (8.8)$$

Here, x represents the molar fraction of the nonvolatile component within phase α . By setting the ratio on the left-hand side of Eq. 8.8 equal to 1, it is possible to ascertain the required value of $x(R)$ for a liquid droplet with radius R , surrounded by the gas phase β , to achieve equilibrium with a large ($R = \infty$) liquid phase α , having composition represented as $x(\infty)$. Finally, if both phases α and β are liquids, the equilibrium is expressed by Eq. 8.9.

$$\frac{x_i(R)}{x_i(\infty)} = \exp\left(\frac{2\gamma \cdot V_i^\alpha}{RkT}\right) \quad (8.9)$$

where $x_i^\beta(R)$ represents the equilibrium molar fraction of component i within phase β when it coexists with a droplet of radius R . Conversely, $x_i^\beta(\infty)$ represents the value of $x_i^\beta(R)$ when R tend to infinite radius ($R = \infty$), indicating phase β in equilibrium with a larger phase α of identical composition to the droplet. In oil in water emulsions, the x_i^β can correspond to the concentration of oil solubilized within the aqueous phase. If the phase droplets contain a component that is inherently insoluble in phase β , the smaller droplets are protected from complete dissolution.

Strictly, Eq. 8.9 provides valuable insights into the dynamics of dispersed large particles (such as in colloidal suspensions and emulsions) exhibiting a propensity to the size growth at the expense of smaller particles undergoing a size reduction, labelling the *Ostwald ripening phenomenon*. Ostwald ripening is a spontaneous phenomenon characterized by the molecular diffusion-driven transfer of molecular or ions from smaller particles to larger particles, conducted by the chemical potential differences. It is a phenomenon that becomes evident when the substance within emulsion droplets possesses even a minimal degree of solubility within the surrounding continuous phase. Since Ostwald ripening is governed by differences in chemical potential between the substance in smaller droplets and that in larger droplets, then it can be explained by Eq. 8.6. The chemical potential represents the intensive energy, and it is straight related to factors such as solubility and concentration. Smaller particles have a higher chemical potential due to their higher curvature and surface area, causing diffusion toward regions with lower chemical potential, which are found in the larger particles, until equilibrium is reached. A diffusion-driven transfer of the substance ensues, moving it from smaller droplets toward their larger counterparts. Consequently, over time, there is a discernible alteration in the size distribution of the emulsion droplets. Ostwald ripening is a time-dependent process, being relatively slow in the process beginning and becoming more pronounced as time progresses.

Emulsions are typically formed in the presence of surfactants. If surfactant concentration in the continuous media exceed the critical micelle concentration, the swollen micelles can be present. The swollen micelles can assist the transfer of oil between emulsion droplets of varying sizes. Essentially, surfactant micelles can act as intermediary agents in the Ostwald ripening process. Micelles mediating Ostwald ripening have been observed in solutions containing nonionic surfactants (for details see Stokes and Evans 1997). In contrast, the presence of ionic surfactants, with their associated surface charge and resultant double layer repulsion, tends to hinder the interaction between micelles and oil droplets.

Ostwald ripening has practical implications, including the stabilization of colloidal dispersions, the development of nanomaterials, and the aging of emulsions. It can affect the quality and stability of products in industries such as food, cosmetics, and pharmaceuticals (for details see de Meyers 1988). The Ostwald ripening mitigation involve (i) the choose of emulsifier agents that form stable emulsions, once surfactants having strong tendency to create micelles can act as carriers for ripening;

(ii) the ensure of uniform mixing and distribution of droplets, preventing the initial formation of unstable droplets; (iii) the lowering of the temperature to affect the diffusion coefficient and slow down the ripening process; and (iv) the production of tiny size droplets, making the emulsion more stable. In some cases, changing the pH can alter the solubility of components and their interactions. In addition to surfactants, particle stabilizers such as nanoparticles or polymers can be used to hinder ripening by providing a barrier around droplets.

The film elasticity mechanisms relies on two fundamental observations regarding the surface tension of aqueous solutions containing surface-active agents: (i) an elevation in surface tension as the concentration of the surface-active solute decreases, particularly at concentrations below the critical micelle concentration (CMC), and (ii) the time necessary for the surface tension to attain its equilibrium value (it's noteworthy that the initial surface tension at a new surface consistently exceeds the equilibrium value). These fundamentals give rise to two distinct theories explaining concentration and time effects on interfacial surfactant behavior: the *Gibbs effect*, which focus on the change in surface tension in response to alterations in solute concentration, and the *Marangoni effect*, which focuses on the variation in surface tension over time.

The Gibbs and Marangoni effects operate synergistically, offering descriptive frameworks for film elasticity. Both effects share the foundational premise that elasticity stems from localized increments in surface tension as the film extends, mathematically expressed as the positive relationship between $d\gamma$ and dA . When a particular region within the film experiences thinning and stretching, leading to an enlargement of the film area, the local surface tension arises. The surge in surface tension generates a tension gradient, driving the flow of liquid from the surrounding thicker portions toward the thinning region, preventing further thinning of the film. Moreover, the movement of surface material carries underlying material, aiding in the recovery, and thickening of the thinned region via a surface transport mechanism. A distinction between the effects must consider the Marangoni effect attributes the augmentation in surface tension to the instantaneous value of γ , whereas the Gibbs effect expounds it in terms of the equilibrium value of γ .

It is important to note that the Marangoni effect has significance mainly in dilute solutions and within a limited concentration range. Conversely, in highly dilute solutions, the surface tension of the solution approaches that of the pure solvent. Consequently, the restoring force, represented as the difference between the surface tension of a clean surface (in contrast to that of the pure solvent) and the equilibrium surface tension of the solution, becomes excessively weak to withstand typical thermal and mechanical disturbances. By this mechanism, an optimal concentration level exists for achieving maximum foam production in any solution capable of generating transient foams. In such solutions, where the foam-producing effects surpass the foam stabilization effects, this maximum is experimentally well-established in the foam volume-concentration curve.

8.4 The Disjoining Pressure

The surface forces governing the appearance and magnitude of interfacial tension and potential discontinuity can be categorized into two distinct types. The first category encompasses surface forces that act within the interfacial region on molecules, resulting in deviations of relevant intensive properties from their values in the bulk phase. These forces predominantly include dispersion forces, such as van der Waals forces, or originate from the macroscopic electrostatic field generated by electric double layers. Additionally, they may arise from the specific structure of interfacial layers. These forces can give rise to effects that have not been extensively elucidated, such as capillary osmosis, under thermodynamic nonequilibrium conditions.

Conversely, the second category of surface forces consists of long-range forces that emerge when two interfacial regions overlap. The Gibbs capillarity theory considers exclusively scenarios in which interfacial regions do not overlap anywhere within the system. It assumes that within the middle of a thin interlayer in equilibrium with the surrounding phases, a region maintains the intensive properties of the bulk phase. In cases where the interlayer is isolated from the bulk phase, localized overlapping of the two subsurface zones results in deviations from the initially uniform interlayer thickness. The presence of bulk properties within the interlayer can be readily confirmed through comparative experiments, by means of changes in intensive properties along the normal direction to the interlayer surface, provided a sufficiently sensitive technique is employed. Particularly intriguing is the scenario involving the overlapping of two transition zones due to thinning of the interlayer, resulting in a new set of phenomena essential for describing the equilibrium and stability of colloids, foams, thin films, in addition to phenomena like polymolecular adsorption, wetting behavior, and micelle swelling.

Before the overlap, a reduction in interlayer thickness at constant phase volumes and interface areas does not require the expenditure of work to alter the system energy. The energy dissipation occurs only to overcome viscous and other resistive forces. However, when these fields overlap, a change in interlayer thickness can only occur with finite work, which arises from repulsive or attractive forces in the zone where the surfaces overlap. These forces are referred to as surface forces of the second kind. The simplest case involves the thinning of a layer with a uniform thickness h , making the plane-parallel layer model a convenient tool for the experimental investigation of surface forces of the second kind as functions of distance. This analysis led to the introduction of the concept of *disjoining pressure* within a thin interlayer. The disjoining pressure emerges due to an attractive interaction between two surfaces.

Deviations from hydrostatic principles only become remarkable when the interfacial regions within a thin liquid film experience overlapping. In the absence of external forces, the pressure within the layer is equal to the pressure of the bulk phase. Consequently, variations in the interlayer thickness can occur without any effect on the system total energy. Nevertheless, as the thickness of the thin interlayer decreases due to overlapping, the hydrostatic pressure within it deviates from the pressure in

the adjacent bulk phase. The *disjoining pressure* (Π) is defined as the additional pressure within the thermodynamically equilibrium interlayer. It can assume a negative value if surface forces of the second kind act to diminish the interlayer thickness. The measurement of the disjoining pressure requires the application of an external pressure with magnitude enough to maintain the interlayer in a state of mechanical equilibrium. Accordingly, the disjoining pressure $\Pi(h)$ characterizing the interlayer in thermodynamic equilibrium with its surrounding phases equates to the difference between the pressure P_s acting on the interlayer surface and the pressure P_b originating in the bulk phase from which the interlayer extends, such as given in Eq. 8.10.

$$\Pi = P_s - P_b \quad (8.10)$$

For an interlayer situated between two parallel plates, the disjoining pressure (Π) corresponds to the force per unit area (P) that is requisite to maintain the interlayer equilibrium thickness. It is essential that the sign of P aligns with that of Π . The stability in the equilibrium state will occur inherently due to the characteristics of the interlayer, under the condition stated in Eq. 8.11.

$$\frac{d\Pi}{dh} < 0 \quad (8.11)$$

However, if this condition is inverted, as shown in Eq. 8.12, the interlayer becomes inherently unstable.

$$\frac{d\Pi}{dh} > 0 \quad (8.12)$$

Equation 8.12 remains applicable irrespective of the interlayer thickness when two plates are separated by an interlayer filled with gas or vacuum. Under these specific circumstances, the pressure $\Pi(h)$ can be precisely measured at any thickness, provided that the external pressure P experiences a substantially steeper variation with h compared to Π . This condition implies a necessity for the plates to be connected by either a highly stiff elastic or a negative response mechanism serving as a rigid spring.

For a uniform liquid film on the flat surface of an insoluble solid, which is in contact at its perimeter with the bulk phase, such as a liquid interlayer sandwiched between a glass plate and a gas bubble, the pressure deviation described in the disjoining pressure equation can be characterized through the Young–Laplace equation (see Eq. 5.34). This interfacial film is commonly referred to as *wetting film*. The isothermal disjoining pressure, represented by Π as a function of the interlayer thickness (h) at a constant temperature, can be established by altering the bubble diameter or by employing suction to extract liquid from the bulk liquid surrounding the wetting film, for instance.

A particularly exciting case concerns to the assessment of the disjoining pressure within a liquid interlayer between two fluid phases, such as between two gaseous phases. In this case, the film is often termed *free film*, assuming that both interfacial surfaces exhibit ideal smoothness. The calculation of the disjoining pressure in *free films* involves the difference between the pressures within the gaseous phase and the pressure within the bulk liquid from which the film spread out. Under the typical assumption that the surfactants necessary to stabilize a free film exhibit negligible volatility, the pressure P_s must be interpreted as the saturated vapor pressure over a planar surface of the surfactant solution, with a concentration matching that of the solution from which the *free film* originated through thinning. When the film remains isolated from the bulk phase of the solution, as is the case with a free soap bubble, the determination of P_s depends on the measurement of the tension of the *free film*.

8.4.1 Stability of Liquid Thin

The disjoining pressure can be related to the thermodynamic properties of the system, considering the Gibbs energy G of a multiphase system containing a plane-parallel interlayer of thickness h which experiences a reversible equilibrium-state change given through alteration in the interlayer thickness by dh at constant temperature, pressure, and chemical potential. The work realized in the state change to keep the system in equilibrium is equal to the Gibbs energy change (ΔG) during the process. Since the work per area can be denoted as the product of the external forces by the displacement (as Eq. 8.13), the disjoining pressure can be related to the Gibbs energy by Eq. 8.14.

$$W = -\Pi(h) \cdot dh \quad (8.13)$$

$$\Pi(h) = - \left(\frac{\partial G}{\partial h} \right)_{T, P, \mu_i} \quad (8.14)$$

Contrasting with interlayers between solid surfaces, a wetting film possesses the distinctive ability to alter its profile and assume varying thicknesses at discrete locations during changes occurring at constant temperature, pressure, and chemical potentials. Furthermore, the wetting film is able to allow the component exchange with the adjacent gas phase, through processes driven by either evaporation or condensation. Considering a system composed of a solid substrate with an unyielding surface, enveloped by a bulk liquid phase, and featuring a thin, plane-parallel wetting interlayer derived from the bulk phase exposed to a gas phase. Assuming the vapor phase behaves as an ideal gas, the expression governing the disjoining pressure can be articulated as Eq. 8.15

$$\Pi(h) = \frac{RT}{V} \cdot \ln\left(\frac{P}{P_s}\right) \quad (8.15)$$

P_s represents the vapor pressure exerted above a flat surface, while R denotes the universal gas constant, T is the absolute temperature, and V molecular volume. Through the introduction of the excess Gibbs energy per unit area of the film, denoted as $G(h)$, the Eq. 8.16 defines a sufficient condition for the stable equilibrium of interfacial film.

$$\left[\frac{\partial^2 G(h)}{\partial h^2} \right]_{T, P, \mu_i} > 0 \quad (8.16)$$

The thermodynamic stability concerning local fluctuations in film thickness, particularly for films composed of a single nonvolatile component, exhibits a direct correlation between film thickness and the quantity of the nonvolatile component present. This correlation implies that fluctuations in film thickness are intrinsically linked to fluctuations in the amount of the nonvolatile component.

While the DLVO theory provides valuable insights into the stability of colloids and thin liquid films, it cannot comprehensively explain certain observed phenomena. Notably, there are inconsistencies that might thoughtfully be attributed to solvation phenomena occurring at the surfaces of particles. Solvation entails the formation of boundary layers characterized by a distinct molecular structure, distinct from that of the bulk liquid.

The interaction dynamics between lyophilic (oil-attracting) surfaces immersed in polar liquids cannot be fully elucidated by considering only the cumulative influences of dispersion forces and double-layer forces. Additional forces, a kind of third-kind forces, emerge as a consequence of the modification of molecular structure within the boundary layers of solvents. These forces are commonly referred to as *structural forces*, designated as the structural component of disjoining pressure. *Oscillatory structural forces* are specific types of structural forces that exhibit periodic oscillations as a function of distance (or other relevant interaction parameters). The *oscillatory structural forces* arise due to variations in the molecular structure and arrangement within boundary layers, resulting in periodic changes in the intermolecular forces between particles or surfaces. Oscillatory structural forces are comprised in solvation forces.

Structural forces can have a significant impact on the stability, behavior, and phase transitions of colloids, thin films, and emulsions, and their understanding is crucial in the study of interfacial phenomena and complex systems. The oscillatory structural forces are specially exposed in two primary main cases: (i) Thin liquid films between smooth solid surfaces, where oscillatory forces are particularly identified as solvation forces due to their periodic oscillations, with a period typically matching the diameter of solvent molecules, presenting significant contributions to short-range interactions occurring between molecularly smooth solid surfaces; (ii) Liquid films containing colloidal particles, where wield substantial influence over the stability of films found in foams and emulsions containing colloidal particles, including surfactant micelles

and macromolecules. At higher particle concentrations, these colloid structural forces act as stabilizing agents within liquid films and dispersions. In contrast, at lower particle concentrations, these forces transform into the so-called *depletion force*, acting to destabilize various dispersions and inducing coagulation.

Figure 8.4 illustrates the behavior of oscillatory structural forces between surfaces of dispersed particles at different particle concentration.

Theoretical consideration of oscillatory structural forces demands the inclusion of an additional term (named Π_{os}) into the sum of contribution due to van der Waals (Π_{vw}) and double electrical layer (Π_{el}) contributions in the classical DLVO equation. Then, the global equation governing the disjoining pressure can be represented as Eq. 8.17 to account the oscillatory structural forces.

$$\Pi(h) = \Pi_{vw}(h) + \Pi_{el}(h) + \Pi_{os}(h) \quad (8.17)$$

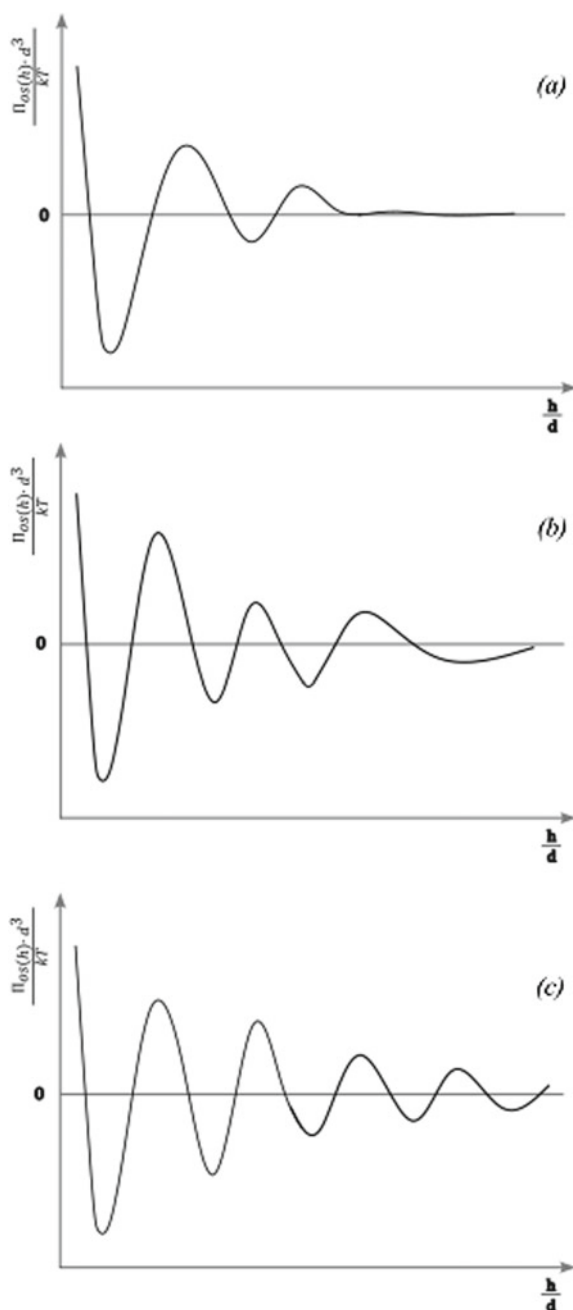
In Eq. 8.17, Π represents the total disjoining pressure, and h represents the film thickness. The classical DLVO theory provides relatively straightforward formulations for the van der Waals disjoining pressure, and the electrostatic disjoining pressure. However, a corresponding and convenient expression for the oscillatory structural disjoining pressure has remained elusive within the current theoretical framework. Attempts to understand and quantify the complexities of oscillatory structural forces in thin liquid films, particularly in the context of molecularly smooth solid surfaces, have underscored the necessity for a robust and easily applicable mathematical model for Π_{os} . While the classical DLVO theory has proven insightful for understanding van der Waals and electrostatic interactions, the formulation of an analogous and practical expression for Π_{os} remains an active area of research. This represents a notable gap in the current theoretical understanding of structural forces in the context of oscillatory phenomena within thin liquid films. Further exploration and development in this area are essential to advance our comprehension of intermolecular interactions in complex systems involving solid–liquid interfaces.

Π_{os} is the component associated with oscillations in film thickness due to structural characteristics within the film. Unlike van der Waals and electrostatic components, the mathematical representation of Π_{os} can be complex and system-specific. It may involve advanced modeling techniques to account for structural fluctuations within the film. In theoretical treatments, Π_{os} incorporate the effects of structural oscillations within the thin liquid film. A useful equation for the oscillatory structural forces is given in Eq. 8.18.

$$\Pi_{os}(h) = P_o \cdot \cos\left(\frac{2\pi h}{d_1}\right) \cdot \exp\left(\frac{d^3}{d_1^2 \cdot d_2} - \frac{h}{d_2}\right) \quad (8.18)$$

Equation 8.18 is only valid for $h > d$. For $h < d$, when the oscillatory structural force equal to the particle osmotic pressure (P_o), and it describes the depletion attraction

Fig. 8.4 Oscillatory structural forces (Π_{os}) contributing to disjoining pressure as a function of the film thickness (h) for different particle volume fraction (φ): $\varphi_a < \varphi_b < \varphi_c$



force. $h < d$ indicates the case when the particles are ejected from the slit into the adjacent bulk phase. The particle osmotic pressure can be assessed by the *Carnahan-Starling equation*, described in Eq. 8.19, where ρ represents the particle number density, k is the Boltzmann constant, and T is temperature.

$$P_o = \rho kT \cdot \frac{1 + \varphi + \varphi^2 - \varphi^3}{(1 - \varphi)^3} \quad (8.19)$$

8.5 Emulsion Stability

Emulsions, colloidal dispersions of two immiscible liquids, play a pivotal role in various industries, ranging from food and cosmetics to pharmaceuticals and petrochemicals. Emulsions can be categorized into three primary types, distinguished by the size of the dispersed particles (see Chap. 4): (i) Macroemulsions are the most common type of emulsion, characterized by opaque appearances and particle size higher than $0.4 \mu\text{m}$, making them visible under an optical microscope; (ii) Microemulsions, in contrast, are transparent dispersions with particles smaller than $0.1 \mu\text{m}$. Their small particle size imparts remarkable optical clarity, making them suitable for specific applications where transparency is a requirement; and (iii) Nanoemulsions (also known as Miniemulsions) have often appearing blue-white, occupy an intermediate position with particle sizes ranging from 0.1 to $0.4 \mu\text{m}$. They offer a balance between the transparency of microemulsions and the versatility of macroemulsions.

Two immiscible pure liquids cannot naturally form a stable emulsion. To an emulsion to be considered stable, a third component known as the emulsifying agent must be present to stabilize the system. Typically, emulsifying agents are surface-active agents, although other substances like finely divided solids can also serve as emulsifying agents. Notably, the most effective emulsifying agents are often mixtures of two or more substances.

Macroemulsions, which constitute a huge portion of practical emulsions, are classified based on the nature of the dispersed phase. In O/W emulsions, a water-immiscible phase, referred to as the oil (O), is dispersed within an aqueous phase (W). Here, the oil phase is the discontinuous (inner) phase, while the aqueous phase acts as the continuous (outer) phase. Conversely, Water-in-Oil (W/O) emulsions consist of water, or an aqueous solution (W) dispersed within a water-immiscible liquid (O). The type of emulsion formed depends primarily on the nature of the emulsifying agent, the emulsion preparation process, and the relative proportions of oil and water present.

Emulsion stability refers primarily to their resistance to the coalescence of dispersed droplets. Numerous factors affect the stability of macroemulsions, with the rate of coalescence being a key quantitative measure (see Myers 1988). Factors influencing coalescence include: (i) The physical properties of the interfacial film,

often containing surfactants, play a crucial role in preventing coalescence; (ii) The presence of electrical or steric barriers on the droplets can inhibit their coalescence; (iii) The viscosity of the continuous phase affects the rate of droplet movement and coalescence; (iv) A narrow size distribution of droplets contributes to stability, as smaller droplets are less likely to coalesce into larger ones; (v) The ratio of oil to water phases influences stability, with certain ratios promoting or hindering coalescence; (vi) Temperature variations can impact the rate of coalescence, with higher temperatures typically accelerating the process.

The relationship between the emulsion stability with the surfactant properties can be outlined by the Bancroft rule, a simple rule which states that in the emulsifying process the surfactant must be soluble in the emulsion continuous phase. The relative solubility of surfactants can be evaluated by means of their hydrophilic–lipophilic balance (HLB). The HLB is a dimensionless numeric scale typically ranging from 0 to 20 (originally from 0 to 40), denoting the surfactant affinity for water or oil phases. Surfactants with higher HLB values (generally higher than 12) are more hydrophilic and consequently more soluble in water, being effective at stabilizing oil-in-water (O/W) emulsions. High HLB surfactants can disperse and solubilize hydrophobic substances in aqueous solutions, making them suitable for applications where water solubility is essential.

On another hand, surfactants with lower HLB values (usually lower than 8) are more lipophilic and have a stronger affinity for oil. They are typically more soluble in organic solvents, leading to dispersing water into oil phases and stabilizing water-in-oil (W/O) emulsions. Surfactants with intermediate HLB (with values ranging usually from 8 to 12) are considered balanced and they can be used in a wide range of applications. The HLB equals to 10 corresponds to an equilibrate solubility between oil and water, indicating a spontaneous curvature of the surface film. Although the surfactant HLB is a reference number, it must be highlighted that HLB points out the preferred emulsion type to be formed, while it does not indicate the surfactant efficiency on the emulsifying process and the stability of the emulsion. Anyway, the emulsification is markedly dependent on several process parameters, since the surfactant affinity is related to the oil and water character, temperature, aqueous phase pH, and other constraints (see Tadros 2018).

The HLB depends on the chemical structure of the surfactant. A series of empirical and theoretical equations has been proposed to determine the HLB from structural parameters. Table 8.1 presents conventional expressions for HLB calculation from the surfactant chemical structure.

Table 8.1 Some expressions to the HLB calculation of nonionic surfactants

Surfactant type	HLB equation	Note
Polyoxyethylene	$\frac{E}{5}$	E: weight percentage of oxyethylene chain
Ester	$\frac{E+P}{5}$	P: weight percentage of polyol chain
Fatty acid ester	$20 \cdot \left(1 - \frac{S}{A}\right)$	S: saponification number

Additionally, the HLB can be obtained from parameters of the chemical groups present in both hydrophilic and hydrophobic portions, using a group contribution tool, such as shown in Eq. 8.20 (for values of chemical group contribution in the surfactant molecule, see Davies and Rideal 1963).

$$\text{HLB} = 7 + \Sigma(\text{hydrophilic group numbers}) - \Sigma(\text{hydrophobic group numbers}) \quad (8.20)$$

Since hydrophilic-lipophilic balance is related to molecular solubility, the HLB meaning has been related to thermodynamic properties, like hydration energy, which can be represented by the solubility parameter or cohesive energy density. Hildebrand solubility parameter is related to the HLB by Eq. 8.21.

$$\text{HLB} = 54 - \frac{243}{\delta - 1.23} \quad (8.21)$$

where δ is the *Hildebrand solubility parameter* (given in $\text{MPa}^{1/2}$). It is reasonable to extend the approach to include the polar, dispersion and hydrogen bond contributions of the three-dimensional solubility parameter in the concept of the *cohesive energy ratio* (R_o) to obtain the HLB expression given in Eq. 8.22.

$$\text{HLB} = \frac{20}{R_o} \cdot \frac{\rho_h}{\rho_l} \cdot \left(\frac{\delta_l}{\delta_h} \right)^2 + 1 \quad (8.22)$$

In Eq. 8.22, ρ_h and ρ_l are the specific gravities respectively of the hydrophilic and hydrophobic portions of the surfactant molecule. δ_l and δ_h are the corresponding solubility parameters of the hydrophilic and hydrophobic portions of the surfactant molecule. R_o is stated by Eq. 8.23 (for details on cohesive energy ratio see Myers 1988; Winsor 1954).

$$R_o = \left(\frac{V_l}{V_h} \right) \cdot \left(\frac{\delta_l}{\delta_h} \right)^2 \quad (8.23)$$

V_l and V_h represent respectively the molar volumes of the hydrophobic and hydrophilic parts of the surfactant molecule.

Since the Critical Micelle Concentration denotes a notable change in the solution bulk due the alteration of the nature of the solubilized species, designating a respective limit of the solubility (see Chap. 2), HLB can be related to CMC according to Eq. 8.24.

$$\text{HLB} = - \left(\frac{C_1}{C_2} - \frac{1}{C_2} \cdot \ln \text{CMC} \right) \quad (8.24)$$

where C_1 and C_2 are characteristic constants. Considering the relationship between CMC and the standard Gibbs energy of micelle formation, given by Eq. 2.9, it is also convenient to write HLB as a function of the ΔG_{mic} , as seen in Eq. 8.25.

$$\text{HLB} = - \left[\frac{C_1}{C_2} - \frac{1}{C_2} \cdot \ln \left(\frac{\Delta G_{\text{mic}}}{RT} \right) \right] \quad (8.25)$$

For surfactant multicomponent systems, a mixture rule can be applied to consider the contribution of each component for the hydrophilic-lyophilic balance of the mixture. A single rule can be written as indicated in Eq. 8.26, where x_i represents the weight fraction of the surfactant i and HLB_i represents the respective HLB of the surfactant i .

$$\text{HLB}_{\text{mix}} = \Sigma(x_i \cdot \text{HLB}_i) \quad (8.26)$$

References

- Adamson AW, Gast AP. Physical chemistry of surfaces. John Wiley & Sons, Inc.; 1997.
- Davies JT, Rideal EK. Interfacial phenomena. Academic Press; 1963.
- de Gennes P, Brochard-Wyart F, Quere D. Capillarity and wetting phenomena: drops, bubbles, pearls, waves. Springer Science Business Media New York; 2004.
- Harkins WD. The physical chemistry of surface films. New York: Reinhold; 1952.
- Myers D. Surfactant science and technology. New York: VCH; 1988.
- Stokes RJ, Evans DF. Fundamentals of interfacial engineering. Wiley-VCH; 1997.
- Tadros TF. Formulation science and technology: basic theory of interfacial phenomena and colloid stability. De Gruyter; 2018.
- Winsor PA. Solvent properties of amphiphilic compounds. The University of California: Butterworths Scientific Publications; 1954.

Chapter 9

Solid–Liquid Interfaces



Solid–liquid interfaces represent critical boundaries where solid materials and liquids interact, encompassing a diverse range of phenomena and applications. These interfaces can experience the adsorption phenomena, where molecules or ions from the liquid phase adhere to the solid surface through physical or chemical interactions. Surface tension acts in systems containing solid–liquid interfaces, influencing capillary action, wetting behavior, and the shape of liquid droplets on solid surfaces. The spreading of liquid on solid surfaces has robust implications in fields like materials science, where controlling wettability is crucial for surface engineering and designing superhydrophobic or superhydrophilic surfaces. Moreover, solid–liquid interfaces play a pivotal role in corrosion processes, particularly when metals encounter corrosive liquids, leading to degradation mechanisms observed in construction, automotive, and aerospace industries. Colloidal systems, consisting of solid particles dispersed in a liquid medium, depend profoundly on the interactions at solid–liquid interfaces for stability and behavior. In electrochemistry, solid–liquid interfaces are central to processes like battery operation and electroplating. Heterogeneous catalysis relies on the activity of solid catalysts at the solid–liquid interface, affecting chemical transformations in various industries. Biological systems, including cell membranes, also feature solid–liquid interfaces that govern essential cellular processes. A wide range of nanotechnology applications lead the solid–liquid properties of nano assemblies of materials for usage in spanning electronics, medicine, and energy. Environmental processes, such as soil–water interactions and groundwater contamination, are intensely influenced by solid–liquid interfaces, with implications for environmental protection and remediation.

9.1 The Solid–liquid Interface

The composition of a solid surface can significantly differ from the bulk material due to surface reconstruction, adsorption of foreign species, or the presence of defects. The surface atoms or molecules may have distinct chemical properties and reactivity compared to their counterparts in the bulk. At the molecular level, the surface atoms or molecules experience unbalanced forces because they have fewer neighboring particles compared to those in the bulk. Consequently, these surfaces have higher energy due to weaker interactions, making them more reactive. This leads to the concept of *surface energy*. The solid surface energy, often referred to as the *surface tension*, is a fundamental property that characterizes the interactions between a solid material surface and surrounding substances, typically liquids or gases. The surface energy arises from the differences in energy between molecules in the bulk of a solid and those at its surface (for details see Davies and Rideal 1963 and Adamson and Gast 1997).

The solid surface energy can be decomposed into two main components: (i) Polar component, which arises from interactions between polar or charged groups on the solid surface and polar molecules in the surrounding medium. For example, in the case of a metal or metal oxide, polar interactions can involve metal cations interacting with polar solvent molecules through electrostatic forces. The polar component contributes significantly to the total surface energy in systems involving polar solids and polar liquids; and (ii) Dispersion component, also denoted to as the dispersive component of the van der Waals forces, arises from temporary fluctuations in electron distribution within atoms or molecules, leading to temporary dipoles. These temporary dipoles induce other similar dipoles in neighboring particles, resulting in attractive van der Waals forces. Even nonpolar solids manifest the dispersive component of surface energy because van der Waals forces are universal. However, for nonpolar solids, the dispersion component typically dominates the surface energy. The determination of solid surface energy is a complex task and often requires the quantifying of the wetting behavior of a liquid on a solid surface.

When a solid surface comes into contact with a polar liquid, a complex interplay of surface phenomena unfolds due to the distinct chemical natures of these substances. Polar liquids, such as water, are characterized by molecules possessing strong dipole moments, which give rise to their inherent polarity. When in contact with a polar solid surface, which can exhibit a similar polarity or possess sites for hydrogen bonding, a strong affinity is established. This leads to favorable attractive behavior, with the liquid spreading on the solid surface. Cohesive forces within polar liquids, including dipole–dipole interactions and hydrogen bonding, work in tandem with the adhesive forces between the liquid and the solid to promote complete spreading. Conversely, when a solid surface interacts with a nonpolar liquid, which is typically characterized by weaker intermolecular forces, a distinctly different set of surface phenomena emerges. Nonpolar liquids, like hydrocarbons and hydrophobic oils, have lower surface tensions due to the absence of intense polar interactions. When they contact a nonpolar solid surface, there is a reduced affinity, resulting in less

favorable attraction. The relatively weaker cohesive forces within the nonpolar liquid and its reduced interaction with the nonpolar solid lead to this diminished spreading tendency.

The presence of solid colloidal particles in a solvent constitutes a dispersed system wherein solid particles, typically ranging in size from 1 nm to 1 μm , are uniformly distributed within a liquid medium. The surface chemistry of solid colloidal particles profoundly influences their behavior. At the molecular level, the particle surfaces are permitted to possess various functional groups, ions, or charges, which can result from chemical reactions or interactions with the surrounding solvent. These surface aspects give rise to electrostatic forces, van der Waals forces, and steric hindrance effects. The magnitude and nature of the forces that arise in dispersed solid particles define the stability and character of the interactions in colloidal systems, such as outlined in Chap. 3. Electromagnetic repulsion or attraction between particles that appear due to their surface charges can prevent or promote aggregation, respectively. Meanwhile, van der Waals forces tend to bring particles closer together, favoring aggregation. The action of attractive forces of van der Waals is often countered by steric hindrance, which inhibits close approach due generally to the presence of adsorbed molecules (especially surfactants or polymers) on the particle surface. Brownian motion, driven by thermal energy, keeps the particles in a state of constant motion, counteracting settling tendencies (for details see Davies and Rideal 1963 and Myers 1988).

9.2 Wetting Behavior on Solid Surface

Wetting characterizes the ability of a liquid phase to uniformly spread across or adhere to a solid surface. The wetting behavior includes the equilibrium between adhesive forces (which enable the interaction of the liquid with the solid substrate), and cohesive forces (which dictate the liquid internal interactions). When adhesive forces predominate, the liquid exhibits a propensity for wetting, resulting in its extensive coverage of the solid surface. Alternatively, in cases where cohesive forces exert dominance, the liquid tends to adopt a spherical shape, resisting to the wetting on the solid and forming discrete droplets. This is genuinely a fascinating force balance. It represents the contrast between internal and external forces.

Wetting occurrences are commonly categorized into binary outcomes: wetting or non-wetting, serving as fundamental descriptors to unveil the intricate dynamics governing the interaction between a liquid and a solid substrate. Wetting extends beyond simple binary distinctions, encompassing situations involving the displacement of one fluid phase by another on a surface, imposing the presence of at least two fluid phases within a three-phase system. Conventional contexts of wetting predominantly revolve around systems wherein air is displaced from a liquid or solid surface by water or an aqueous solution. However, it is important do not disregard situations as the wetting of oil pipelines and fabric fibers, for instances.

The wetting occurrence is influenced by the scale of the surface area to be wetted. In cases where the surface area is relatively limited, as observed in the wetting of non-granular and non-porous solids, often referred to as hard surface wetting, equilibrium conditions can be achieved during the wetting process. In such scenarios, the degree of wetting attained is intricately linked to the underlying energy changes. Conversely, when confronted with substantial surface areas, such as those encountered in wetting porous materials, textile surfaces, or finely divided solids, equilibrium conditions are frequently elusive within the allotted timeframe. As a result, the degree of wetting is predominantly dictated by the kinetics governing the wetting process, rather than relying solely on the principles of thermodynamics (for details see Adamson and Gast 1997 and de Gennes et al. 2004).

For a conscious description of the wetting, three distinct phenomena have been delineated based on the dynamics and characteristics of the interaction between a liquid and a solid substrate: *spreading* wetting, *adhesional* wetting and *immersional* wetting.

Spreading wetting is characterized by the dominance of adhesive forces at the solid–liquid interface. During the spreading, the liquid exhibits a strong affinity for the solid surface, allowing it to uniformly spread and disperse across the substrate. Spreading wetting leads to the formation of a thin continuous liquid film, which is able to cover a significant fraction of the solid surface area.

Spontaneous spreading of a liquid on a solid surface is underlined by a fundamental thermodynamic principle related to the minimization of surface energy. Specifically, it entails that during the spreading process, the overall surface energy of the system must decrease, accordingly to the changes in the interfacial area. When the area of a contacting interface expands, as is the case during spreading, the surface energy at that interface increases. The expansion of the area results from the changes of the interactions between the liquid molecules at the interface, transitioning from cohesive interactions within the liquid to adhesive interactions with the solid substrate. Instead, when the interfacial area diminishes, the surface energy correspondingly decreases, as the liquid molecules have the ability to reestablish stronger cohesive interactions amongst themselves, diminishing the influence of adhesive forces with the solid substrate.

The quantification of the change in surface energy due to spreading is expressed as the ratio between the surface energy and the unitary area (denoted as ΔG_w). ΔG_w represents the total decrease in surface energy per unit area of the system ascribed to the spreading wetting process. Mathematically, it is represented as Eq. 9.1.

$$\Delta G_w = \gamma_{SG} - (\gamma_{SL} + \gamma_{LG}) \quad (9.1)$$

γ_{SG} denoted the surface tension between the solid and gas, γ_{SL} represents the surface tension between the solid and the liquid, and γ_{LG} is the surface tension between the liquid and gas phases. If the value of ΔG_w is positive, it signifies that the system experiences a net decrease in surface energy during the spreading process. In such circumstances, the spreading process is able to proceed spontaneously, driven by the thermodynamic constraints of minimizing surface energy. This foundational concept

elucidates the conditions under which spontaneous spreading of a liquid on a solid substrate occurs.

The ΔG_w is a fundamental parameter for characterizing the force driving the process of spreading, often referred to as the *spreading coefficient* (S_{LS}). It encapsulates the thermodynamic forces at play during the spreading phenomenon. Specifically, it quantifies the difference between the surface tension of the solid–gas interface (γ_{SG}) and the combined surface tensions of the solid–liquid (γ_{SL}) and liquid–air (γ_{LG}) interfaces. Mathematically, the spreading coefficient S_{LS} is equal to ΔG_w . The spreading coefficient is a factor determinant of the spontaneity of the spreading process. When S_{LS} exhibits a positive value, the spreading process is driven by a reduction in surface energy, and therefore occurring spontaneously. Conversely, a negative value of S_{LS} indicates that the spreading process would result in an increase in surface energy, making it non-spontaneous. In essence, the spreading coefficient S_{LS} summarizes the balance between adhesive forces that promote the interaction of the liquid with the solid surface and cohesive forces inside the liquid. Particularly, when one liquid is undergoing spreading over another, the determination of the spreading coefficient counts exclusively on the surface tensions associated with the two pertinent liquids involved. It is entirely possible to computationally obtain the spreading coefficient without the requirement for supplementary experimental data, enabling the prediction spontaneous spreading based on the intrinsic properties of the liquids involved.

For solid a substrate, spreading coefficient results in Eq. 9.2, where Φ is an empirical factor.

$$S_{LS} = 2\gamma_{LG} \cdot \left[\Phi \cdot \left(\frac{\gamma_{SG}}{\gamma_{LG}} \right)^{\frac{1}{2}} - 1 \right] \quad (9.2)$$

Adhesional wetting is also marked by an intricate balance between adhesive and cohesive forces. But in such cases, neither adhesive nor cohesive forces become entirely dominate. As a result, the liquid partially wets the solid surface, leading to an intermediate state between complete spreading and non-wetting. The wetting degree in an adhesional wetting is influenced by the relative strengths of adhesive and cohesive forces. A liquid, initially in contact with a substrate and another immiscible fluid, extends its contact area with the substrate at the expense of the second fluid. On the other hand, adhesional wetting describes the interaction established with a liquid (initially non-contacting the substrate) and subsequently adhesion between them. The adhesional wetting process can be illustrated by means of the representation in Fig. 9.1.

The total change in surface free energy, denoted as $-\Delta G_w$, is described by the opposite of the Eq. 9.1, multiplied by the surface area of the substrate in contact with the liquid. The fundamental driving force is described by Eq. 9.3. This specific quantity is termed *work of adhesion*, denoted as W_{ad} . It signifies the reversible work required to dissociate a unit area of the liquid from the substrate, thereby delineating the energetics underlying the adhesional wetting phenomenon.

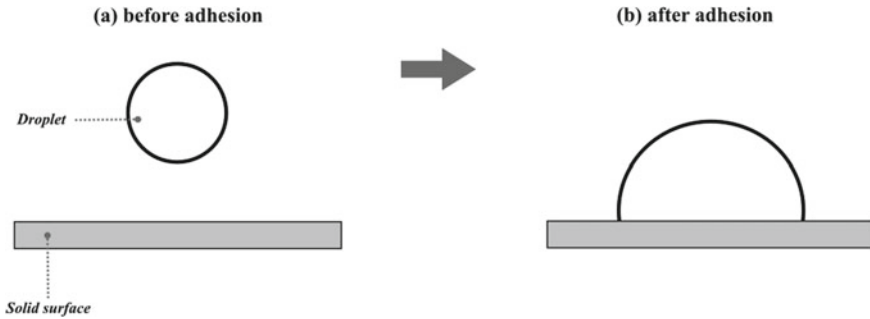


Fig. 9.1 Adhesion wetting due to the deposition of a liquid droplet on solid substrate

$$W_{ad} = \gamma_{SG} + (\gamma_{LG} - \gamma_{SL}) \quad (9.3)$$

Equation 9.3 is the well-known *Dupré equation*. It illustrates the intricate interplay of interfacial tensions in the adhesion process. A reduction in the interfacial tension between the substrate and the wetting liquid intensifies the propensity for adhesion to happen. A decrease in either the surface tension of the liquid or the surface tension of the substrate conversely, diminishes the inclination for adhesion of the liquid on the solid substrate. Adhesion wetting phenomenon elucidates why substances often struggle to adhere to low-energy surfaces, particularly when there are significant disparities between the nature of the substance and the substrate.

It is evident from the Eq. 9.3 that an increase in the surface tension of the wetting liquid consistently augments adhesional wetting. The driving force in adhesional wetting is invariably higher than zero, reaching zero only under non-representative real conditions. The work required for a liquid to self-adhere is referred to as the *work of cohesion*, denoted as W_c in Eq. 9.4. W_c represents the energy needed to create two unitary areas of interface from an initially uniform liquid column, allowing the duplicate of the surface contacting area between liquid and gas phases.

$$W_c = 2 \cdot \gamma_{LG} \quad (9.4)$$

Therefore, if the work of adhesion (W_{ad}) surpasses the work of cohesion (W_c), the spreading coefficient assumes a positive value, and the liquid spontaneously spreads over the substrate to form a thin film. Alternatively, when W_{ad} falls below W_c , the spreading coefficient becomes negative, and the liquid ceases from spreading over the substrate, instead forming droplets or lenses as Fig. 9.1b.

Immersional wetting arises when cohesive forces within the liquid phase are predominant due to the pull-out of a solid particle into a liquid continuous phase (see Fig. 9.2). On immersion wetting conditions, the liquid tends to minimize its contact with the solid surface, leading to a configuration where it forms discrete droplets rather than spreading across the substrate. Immersional wetting is typically

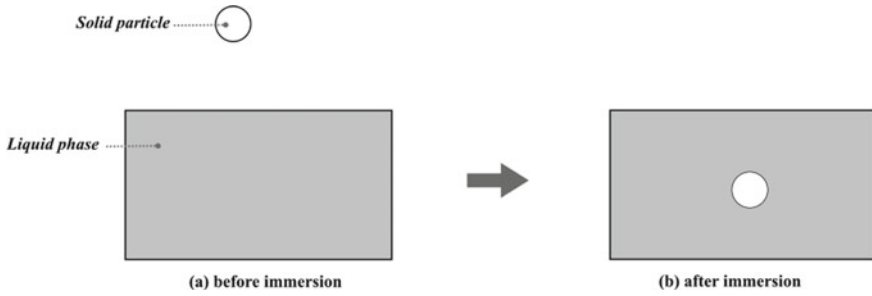


Fig. 9.2 Immersion wetting due to the pull-out of a solid particle into a liquid continuous phase

characterized by spherical shape of distinct droplets due to the dominance of cohesive forces that cause the liquid to resist spreading. The surface energy per unitary area (denoted as ΔG_W) for the immersion wetting is given by Eq. 9.5.

$$W_{ad} = \gamma_{SG} - \gamma_{SL} \tag{9.5}$$

As the immersion process concurrently entails spreading, the spreading coefficient (given by Eq. 9.1) dictates the feasibility of the complete immersion. When the spreading coefficient is higher than zero, it indicates spontaneous and complete immersion. In contrast, when the spreading coefficient is lower than zero, an external work is required for achievement of the complete immersion. In such cases, attaining spontaneous solid immersion demands alterations in the values of any or all of the three surface tension parameters.

9.3 Wettability of Solid Surface

When a droplet of liquid is deposited onto a solid substrate, its behavior can be categorized into two distinct outcomes: droplet formation or film spreading. These behaviors are intrinsically linked to the interplay between the liquid’s properties and the characteristics of the solid surface. Specifically, it hinges upon the concept of wettability, which is a measure of the liquid’s affinity for the solid substrate. Wettability is determined by the surface tension of the liquid and a critical surface tension value, denoted as γ_c , associated with the solid surface. A liquid with surface tension lower than γ_c exhibits a strong affinity for the solid, and it endeavors to maximize its contact with the surface, leading to the formation of a spreading film. On another hand, a liquid with surface tension exceeding γ_c displays weaker affinity and tends to adopt a bead-like configuration.

The degree of spreading is denoted by means of a parameter known as the *contact angle*, labelled as θ . The *Young-Dupré equation*, sometimes referred as simply *Young Equation*, describes the relationship between the contact angle of a liquid droplet on a

solid surface and the liquid surface tension and the solid interfacial energies involved, as illustrated in Eq. 9.6. The Young-Dupré equation essentially illustrates the balance of forces at the solid–liquid–gas interface. When the contact angle is known, and the interfacial tensions are measured or determined, Young’s equation can be used to understand and predict wetting behavior. It assists in elucidation whether a liquid will spread out (low contact angle, $\theta < 90^\circ$) or form a droplet (high contact angle, $\theta > 90^\circ$) on a solid surface.

$$\gamma_{LG} \cdot \cos \theta = \gamma_{SG} - \gamma_{SL} \quad (9.6)$$

The Young-Dupré equation is a fundamental expression that elucidates the interplay of interfacial tensions between the liquid, solid, and gas phases when a droplet is placed on a solid surface. In Eq. 9.6, γ_{LG} represents the interfacial tension between the liquid and gas phases, γ_{SG} signifies the interfacial tension between the solid and vapor phases, γ_{SL} denotes the interfacial tension between the solid and liquid phases, and θ symbolizes the contact angle formed by the droplet on the solid surface. The Young-Dupré equation provides a concise representation of how the surface energies and the contact angle mutually dictate the surface tension of a liquid droplet on a solid substrate. The Eq. 9.6 is a fundamental tool in comprehending intricate phenomena such as wetting and adhesion of liquids on solid surfaces. Its applications extend across diverse fields, including materials science, microfluidics, and surface chemistry, where a deep understanding of interfacial interactions is of paramount importance for technological advancements and scientific inquiries.

The wetting behavior of a liquid droplet when placed upon a solid surface can be comprehensively elucidated through the critical surface tension of the solid substrate, given by the Young equation. Critical surface tension, often denoted as γ_c , refers to the minimum surface tension or surface energy required for a liquid to uniformly wet or spread over a particular solid surface. In other words, it is the surface tension threshold that determines whether a liquid will form a thin film and exhibit wetting behavior on a specific solid substrate. If the surface tension of the liquid is lower than the critical surface tension of the solid, the liquid will have a strong affinity for the solid surface and will readily spread to maximize contact. Conversely, if the surface tension of the liquid is higher than the critical surface tension of the solid, the liquid will tend to bead up and not wet the surface effectively.

However, it is essential to recognize the pivotal role played by temperature, particularly concerning aqueous solutions, where it wields noteworthy influence over surfactant solubility. The manipulation of wetting properties for specific applications demands a nuanced approach. When the objective is to reduce water’s affinity for a hydrophilic surface, the de-wetting or water repellency becomes achievable through the induction of hydrophobic compound adsorption. The adsorption substantially elevates the contact angle, often surpassing the critical threshold of 90° , indicative of de-wetting ($\theta > 90^\circ$). In practical applications, the textile industry, for instance, employs long-chain cationic surfactants to impart water-repellent properties to fabrics (for details on surfactant chemical structures see Chap. 2). These surfactants are characterized by cationic headgroups that adhere to anionic textile

surfaces, exposing their extended hydrocarbon chains to water and thus creating a hydrophobic surface.

Conversely, when the aim is to enhance the wetting behavior of a water droplet on a hydrophobic surface, controlled surfactant adsorption is introduced. This leads to a simultaneous reduction in both surface tension and contact angle, resulting in augmented wetting. Interestingly, the swiftest wetting is often achieved through the utilization of surfactants with limited water solubility. Such surfactants possess relatively modest molar weight or exhibit a structural configuration featuring a branched hydrophobic moiety flanked by a centrally positioned hydrophilic group.

In addition, the extent of solid immersion in a wetting liquid is intricately linked to the contact angle, in a way that a smaller θ corresponds to a greater depth of immersion. When contact angle equals zero, it denotes a complete immersion. Then, the interplay between three-phase surface tension, as given by the young-Dupre equation, defines the precise value of the contact angle. If θ is less than or equal to 0° , the determination of the difference $\gamma_{SG} - \gamma_{SL}$ merely from the contact angle becomes unfeasible. Consequently, an experimentally measurable parameter known as the *heat of immersion* (ΔH_i) assumes significance. The heat of immersion computes the heat change recorded calorimetrically when the substrate experiences immersion in the wetting liquid. The heat of immersion per unit area of the substrate is intricately linked to the surface energy change per unit area attributable to immersional wetting, expressed by the relationship in Eq. 9.7.

$$\Delta G_W = \Delta H_i - T \cdot \Delta S_i \quad (9.7)$$

The equality between heat of immersion and surface energy change is found when the entropy change per unit area linked to immersional wetting, denoted as ΔS_i , is negligible. This signifies that under such conditions, the process is driven by enthalpy.

9.4 Relationship Between Adsorption and Wettability

The process of molecular adsorption onto solid surfaces plays a crucial role in repairing the disparities in surface forces, ultimately leading to a reduction in surface energy. Notably, these energy-related phenomena concerning solid surfaces bear a resemblance to those encountered at liquid interfaces. The wetting behavior of liquids on solid surfaces can be intricately linked to the phenomenon of surface adsorption by combining the Gibbs adsorption equation (as expressed in Eq. 5.28) with the Young-Dupre equation (Eq. 9.3). The coupling of adsorption and wetting principles allows a comprehensive understanding of the interactions and energetics governing wetting phenomena, which finds application in diverse fields such as materials science, surface chemistry, and microfluidics.

The Eq. 5.28 can be written to a solid–liquid interface according to Eq. 9.8.

$$-d\gamma_{SL} = RT \cdot \Gamma_{SL} \cdot d \ln C \quad (9.8)$$

Derivating the Eq. 9.6 to obtain $d\gamma_{SL}$ and inserting into Eq. 9.8, the resulting equation can be written as Eq. 9.9.

$$\frac{d(\gamma_{LG} \cdot \cos \theta)}{d(\gamma_{LG})} = \frac{\Gamma_{SG} - \Gamma_{SL}}{\Gamma_{LG}} \quad (9.9)$$

By Eq. 9.9, the adhesion tension (given by $\gamma_{LG} \cdot \cos \theta$) against the liquid surface tension is an extremely useful tool to analysis the effect of the adsorption on wettability behavior. The gradient (slope) of a plot depicting $\gamma_{LG} \cdot \cos \theta$ against γ_{LG} is a valuable indicator of the surface excess concentrations of surfactants at the interfaces. On solid surfaces characterized by low surface energy, such as it is found in nonpolar surfaces, it has been determined slopes nearly equal to -1 for both solid-aqueous-air systems and solid-aqueous-oil systems. This phenomenon is typically interpreted as a sign that the surface excess Gibbs adsorption (G_{SG}) approaches zero, and the ratio of surface excess Gibbs adsorption at the solid-liquid interface (G_{SL}) to that at the liquid-air interface (G_{LG}) approximates unity. This observation is justifiable by the resembling in efficacy of adsorption at nonpolar liquid-polar liquid interfaces and air-polar liquid interfaces. Consequently, roughly equivalent adsorption is expected at nonpolar solid-polar liquid and air-polar liquid interfaces. On the contrary, for negatively charged polar organic surfaces, a negative slope approximating zero for anionic surfactants has been reported. The interfacial tension at the solid-liquid interface of a negatively charged solid is considerably lower than that of a nonpolar solid against water. Accordingly, limited adsorption of anionic surfactants at the aqueous interface with a negatively charged polar organic solid is reasonable, as such adsorption would place either the hydrophobic group of the surfactant or its negatively charged hydrophilic group in proximity to the negatively charged polar surface. Neither scenario would be expected to diminish the solid-liquid interfacial tension. On the other hand, when the solid phase is nonpolar, the interfacial tension at the solid-aqueous solution interface is high, and adsorption of the surfactant (by means of its nonpolar hydrophobic group oriented toward the nonpolar solid and its hydrophilic group oriented toward the water) would lead to a reduction in solid-liquid surface tension.

In cases involving high-energy surfaces characterized by both positively and negatively charged sites, plots of $\gamma_{LG} \cos \theta$ versus γ_{LG} display substantial positive slopes, particularly at low surfactant concentrations, which corresponds to high γ_{LG} values. This suggests that the surface excess Gibbs adsorption at the solid-liquid interface significantly surpasses that at the liquid-air interface for ionic surfactants. Such phenomenon arises apparently from the direct adsorption of ionic surfactants, facilitated by their hydrophilic heads, onto oppositely charged sites on the solid substrate. For that reason, this type of adsorption of ionic surfactants hinders the wetting and augments the hydrophobicity of the solid surface. This effect serves as the fundamental principle underlying the flotation process applied in the beneficiation of minerals. It is noteworthy that at elevated surfactant concentrations, a reversal in the slope may occur, transitioning to a negative line. The change in slope

is attributed to the heightened adsorption of surfactant molecules at the presently hydrophobic solid-aqueous solution interface.

9.5 Surfactant as Dispersion Agents

The dispersion of solid particles in aqueous and nonaqueous media hinges on a complex interplay of surfactant properties, including wetting, adsorption, charge, and steric effects. The amphiphilic nature of surfactants enables them to create energy barriers preventing particle aggregation in liquid systems by adsorbing onto solid particle surfaces, reducing interfacial tension between solid and liquid phases, and often imparting an electrical charge to the particles. The adsorption process leads to repulsive electrostatic forces between particles carrying the same charge, hindering their close approach. Additionally, some surfactants extend into the liquid phase, supplying steric hindrance to particle interaction. In this context, surfactants are able to act as important dispersing agents. Notably, the polarizable chemical structures in the hydrophobic group of the dispersing agent play a crucial role in allowing the surfactant to interact with charged sites on particle surfaces and subsequently adsorb through its hydrophobic group.

Ionic surfactants are commonly employed to establish electrical barriers to aggregation in situations where the solid to be dispersed is predominantly nonpolar, such as hydrophobic carbon particles, and the dispersing medium is aqueous. Conventional surfactants, featuring a single hydrophilic group and an extended hydrophobic chain, are suitable since the adsorption of these surface-active ions onto the nearly uncharged solid particles imparts a uniform charge of the same polarity to all particles, leading to repulsion between them. The interparticle repulsion establishes an electrical barrier to aggregation. Moreover, adsorbed surfactant ions arrange themselves naturally with their hydrophobic tails oriented toward the nonpolar particle and their hydrophilic heads facing the aqueous phase, thus reducing the interfacial tension between the solid and liquid phases. Notably, longer hydrophobic chains in the surfactant molecules enhance their efficacy as dispersing agents. However, when the solid to be dispersed carries a charge, the introduction of an oppositely charged conventional surfactant typically leads to flocculation. In contrast, for a conventional surfactant with a charge similar to that from the particle, the adsorption of the surfactant ion must enhance the electrical energy barrier to aggregation. This arrangement tends to occur with the ionic hydrophilic head oriented away from the similarly charged particle surface. The resulting repulsion between the adsorbing surfactant ion and the similarly charged particle inhibits adsorption.

Hence, for charged or polar solids in aqueous media, ionic dispersing agents often feature ionic groups distributed at various sites within the surfactant molecule, alongside hydrophobic groups containing polarizable structures like aromatic rings or ether linkages, rather than saturated hydrocarbon chains. The multiple ionic groups serve several purposes: first, they prevent adsorption of the surfactant molecule with the hydrophobic group facing the aqueous phase. Second, they enhance the efficiency

of the surfactant molecule in creating an electrical barrier to aggregation. The greater the number of ionic charges of similar sign per molecule, the stronger the increase in the electrical barrier per adsorbed molecule on similarly charged particles, and the more effective the neutralization of charge leading to the formation of an electrical barrier of the same sign as the surfactant on oppositely charged particles. Third, they enable the extension of the surfactant molecule into the aqueous phase, creating a steric barrier to coalescence, without increasing the system's free energy. The decrease in free energy results from the hydration of the ionic hydrophilic groups and compensates for the free energy increase due to increased contact of the hydrophobic group with the aqueous phase (for details see Davies and Rideal 1963 and Stokes and Evans 1997).

The dispersions tend to flocculate when oppositely charged surfactants are added. However, when surfactants with a single hydrophilic group are used, the flocculated particles can be easily dispersed into a nonpolar solvent. In contrast, surfactants with two hydrophilic groups tend to form a film at the interface between the nonpolar solvent and water, making dispersion into the solvent difficult. This difference arises because the hydrophobic groups of adsorbed surfactant molecules face the aqueous phase in the first case, rendering the flocculated particles lipophilic. In the second case, each hydrophobic group extending into the aqueous phase possesses a terminal hydrophilic group, which prevents the particles from becoming lipophilic.

Ionic dispersing agents for charged or polar solids in aqueous media often incorporate multiple ionic groups and aromatic hydrophobic groups to optimize their performance. Polyelectrolytes derived from ionic monomers can be utilized as highly efficient dispersing agents for solids in aqueous media. The multiple ionic groups of polyelectrolytes are able to impart substantial surface charges to the solid particles on which they adsorb. When individual functional groups in the polymer backbone exhibit low tendencies for adsorption onto the solid particle surface, the number of such groups within the macromolecule must be sufficiently large to ensure strong anchoring to the particle surface. In such cases, copolymers outperform homopolymers, as they are prone to adsorb strongly onto a wider range of substrates. Copolymers whose monomers have different structural characteristics yield products able to adsorb vigorously to a variety of substrates. For nonpolar substrates, copolymerization of short-chain monomers with long-chain monomers is employed to augment the binding energy of the dispersing agent to the particle surface. With an increasing number of hydrophilic groups per molecule of dispersing agent, there is often an increase in solubility in water. However, the binding energy increase must lead to the reduced adsorption onto a specific particle surface, particularly when the interaction between the surfactant and the particle surface is weak. In some instances, the adsorption of the dispersing agent onto the particle surface and its efficacy as a dispersant exhibits a maximum as the number of ionic groups in the surfactant molecule increases. Therefore, achieving optimal dispersion must require selecting dispersing agents with suitable solubility characteristics.

Particles can also be kept effectively dispersed in aqueous media through the use of steric barriers. Both ionic and nonionic surfactants are able to be used as steric stabilizers. Steric barriers to aggregation are established when adsorbed surfactant

molecules extend chains into the aqueous phase, impeding the close approach of two particles. Steric stabilization becomes more pronounced with longer chains extending into the liquid phase. Hence, polymeric surfactants, both ionic and nonionic, are commonly employed as steric stabilizers, as the length of the chain extending into the liquid phase can be conveniently increased by enhancing the degree of polymerization. Surfactants with ionic groups distributed throughout the molecule can also create effective steric barriers, and their effectiveness grows with the distance to which the molecules can extend into the aqueous phase. Therefore, longer compounds are generally more effective, provided that increased solubility in the aqueous phase does not significantly diminish their adsorption onto the particle surface.

Nonionic surfactants, particularly those of the polyoxyethylene (POE) type, are esteemed dispersing agents for many applications. The highly hydrated POE chains extend into the aqueous phase as coils, forming excellent steric barriers to the aggregation process. In addition, the thick layer of hydrated oxyethylene groups, similar in nature to the aqueous phase, reduces the effective Hamaker constant and the resulting van der Waals attraction between particles. Block and graft polymers are also widely utilized as steric stabilizers. Since these molecules contain two blocks separated within the molecule, they can be chemically designed for optimal efficiency and effectiveness. One block is designed to adsorb strongly onto the particle surface while the other block(s) extend into the liquid phase.

In nonaqueous media with low dielectric constants, electrical barriers to aggregation are usually ineffectual, needing the use of steric barriers to disperse solid particles. As the dielectric constant of the dispersing medium increases, electrical barriers become more significant. Steric barriers in nonpolar solvents can emerge either from the energy required to desolvate portions of adsorbed surfactant molecules extending into the medium or from the reduction in system entropy as these adsorbed portions are constrained in their movement or arrangement due to the proximity of two particles. The effective Hamaker constant and the attraction between particles can also be mitigated by the incorporation of molecules that, upon adsorption, extend lyophilic groups from the particle surface that closely resemble the dispersing liquid. In an equivalent manner, the dispersion of ionic solids in nonpolar solvents can be enhanced by the inclusion of long-chain amines.

A proposed mechanism for charging solid particles in nonaqueous media involves acid–base interactions between neutral particles and neutral adsorbed dispersing agents. Charge separation occurs when charged dispersing agents are desorbed and incorporated into bulky reverse micelles in the nonaqueous phase, with the charged sites residing in the micelle interior. Acidic or basic polymers are pointed out as effective dispersing agents for solid particles in nonaqueous media, leveraging this mechanism.

References

- Adamson AW, Gast AP. Physical chemistry of surfaces. John Wiley & Sons, Inc.; 1997.
- Davies JT, Rideal EK. Interfacial phenomena. Academic Press; 1963.
- de Gennes P, Brochard-Wyart F, Quere D. Capillarity and wetting phenomena: drops, bubbles, pearls, waves. Springer Science Business Media New York; 2004.
- Myers D. Surfactant science and technology. New York: VCH; 1988.
- Stokes RJ, Evans DF. Fundamentals of interfacial engineering. Wiley-VCH; 1997.

Chapter 10

Recent Developments and Applications



Surface thermodynamics and surface physical chemistry have undergone remarkable advancements in recent years, spurred by a deepening understanding of the fundamental principles governing interfacial phenomena. These developments have paved the way for novel applications across various scientific and industrial domains, ranging from materials science to biotechnology and beyond. The foundation of surface thermodynamics lies in elucidating the behavior of interfaces between different phases, promoting insights into surface tension, wetting behavior, and adhesion phenomena, among others. Recent advancements in surface thermodynamics have been driven by advancements in experimental techniques and theoretical models. Cutting-edge experimental tools, such as atomic force microscopy (AFM), X-ray photoelectron spectroscopy (XPS), and surface plasmon resonance (SPR), allow for precise measurements of surface properties at the nanoscale. At the same time, theoretical developments, including molecular dynamics simulations and density functional theory calculations, provide valuable insights into the molecular-level mechanisms underlying interfacial phenomena. Especially, significant progress has been noted in the understanding of surface adsorption and its role in governing interfacial behavior, allowing to manipulate surface properties such as surface tension and wetting behavior. Moreover, advances in surface chemistry have led to the development of novel surfactants and dispersants with tailored molecular structures, enabling precise control over surface properties. The implications of surface science advancements are far-reaching, with applications spanning a wide range of industries. In materials science, for example, surface thermodynamics plays a crucial role in the design of functional coatings, adhesives, and biomaterials. Similarly, in biotechnology, surface properties dictate the interactions between cells and biomaterials, influencing processes such as cell adhesion and drug delivery. The recent developments in surface thermodynamics and their implications for interfacial phenomena highlight key advancements and emerging trends that inspire further research in this exciting and evolving field.

10.1 Nanotechnology

In recent years, the field of nanomaterials and nanotechnology has experienced exponential growth, driven by the increasing demand for materials with enhanced properties and functionalities at the nanoscale. At the heart of nanoscience lies the meticulous manipulation of surface properties, enabling the development of advanced materials with tailored characteristics. This deliberate control of surface features has emerged as a cornerstone for the strategic design and engineering of nanomaterials, offering unprecedented opportunities for innovation and technological advancement. By elucidating the underlying principles governing interfacial phenomena, surface thermodynamics provides the framework for designing nanomaterials with exceptional attributes. Through the precise manipulation of surface energy, tension, and interactions, nanomaterials can be engineered with functionalities tailored to specific applications. The impact of engineered nanomaterials extends across a wide spectrum of industries and disciplines, ranging from catalysis and drug delivery to energy storage and electronics. In catalysis, nanomaterials with finely tuned surface properties exhibit unprecedented catalytic efficiencies, revolutionizing processes such as clean energy production and environmental remediation. Similarly, in drug delivery, nanomaterials with precisely controlled surface interactions enable targeted and controlled release of therapeutic agents, offering new avenues for personalized medicine and disease treatment. The unique properties of nanomaterials make them promisor material for energy storage and electronic devices. Nanomaterial-based batteries, supercapacitors, and solar cells demonstrate improved performance and efficiency compared to traditional materials. Similarly, nanoelectronic devices, such as transistors and sensors, benefit from the precise control of surface properties to achieve enhanced functionality and reliability. The convergence of surface thermodynamics and nanotechnology announces a new era of innovation and breakthroughs in materials science and engineering. Despite significant progress, challenges remain in the design, synthesis, and characterization of nanomaterials with tailored surface properties. Addressing these challenges requires multidisciplinary collaboration, innovative research approaches, and advanced experimental techniques.

10.2 Energy Science and Technology

Surface thermodynamics provides a theoretical framework for elucidating the surface properties and interactions that influence the performance of energy storage and conversion devices. By leveraging principles from thermodynamics, kinetics, and materials science, researchers can tailor the surface characteristics of electrode materials and electrolytes to optimize energy storage capacity, cycling stability, and overall efficiency. In lithium-ion batteries, which currently represent the basis of portable electronics and electric vehicles, surface thermodynamics principles

play a crucial role in enhancing battery performance. One notable example is the controlled surface modification of the anode material, such as silicon nanoparticles, using surface thermodynamics principles. Engineering the surface chemistry and morphology of silicon nanoparticles leads to significant improvements in battery energy density and cycle life, addressing key challenges associated with silicon's high theoretical capacity and poor cycling stability. Besides, fuel cells offer a promising pathway towards clean and efficient energy conversion, with applications ranging from stationary power generation to transportation. Surface thermodynamics are involved in optimizing the performance and durability of fuel cell catalyst materials, such as platinum nanoparticles, enhancing the catalytic activity and stability of platinum catalysts and leading to more efficient electrochemical reactions and improved fuel cell performance. The integration of surface thermodynamics principles into the design and optimization of energy storage and conversion technologies represents a critical step towards achieving a sustainable and energy-efficient future. Surface thermodynamics is deeply implicated to the development of innovative solutions to meet the evolving energy requirements of society while minimizing environmental impact and advancing towards a cleaner and more sustainable energy scenario.

10.3 Life Science and Technology

Surface thermodynamics plays a fundamental role in unraveling the intricacies of biological systems, providing indispensable insights into critical processes such as protein adsorption onto solid surfaces. The description of this phenomenon holds extreme implications for biotechnology and the development of medical devices. In the medical implant domain, surface thermodynamics acts as a guiding principle for understanding the complex interactions between implant surfaces and proteins. The investigation of interactions at the molecular level has allowed the development of implant materials that promote biocompatibility and minimize adverse reactions. For instance, the controlled adsorption of blood proteins onto the surface of cardiovascular stents can significantly influence their long-term effectiveness. Also, understanding how proteins adsorb to sensor surfaces is crucial for the development of highly sensitive and specific diagnostic tools. Surface plasmon resonance (SPR) biosensors, for instance, rely on the precise control of protein-surface interactions to detect biomarkers indicative of various diseases, thereby revolutionizing medical diagnostics. Furthermore, drug release rates can be regulated and targeted to specific tissues or cells, enabling the delivery of therapeutic agents with reduced side effects and enhanced efficacy, pointing to a way for personalized medicine. Surface thermodynamics has assisted in fabricating biocompatible scaffolds for tissue regeneration. On this point, materials that facilitate cell adhesion and growth while mitigating immune responses can be designed. This holds promising applications in regenerative medicine, where engineered tissues and organs offer potential solutions to various medical challenges, ranging from organ transplantation to wound healing. In biological science, surface thermodynamics, with interdisciplinary collaboration

and innovative research activities, drives progress in biotechnology, medical development, drug delivery, and tissue engineering, ultimately improving patient outcomes and quality of life.

10.4 Environmental Science and Technology

Surface thermodynamics meets environmental science, particularly concerning the description of contaminant behavior at interfaces involving water, air, and solid surfaces. This description is a critical asset for devising effective remediation strategies and unraveling the intricacies of pollutant transport in natural ecosystems. One notable application of surface thermodynamics in environmental science lies in the study of adsorption phenomena at the water–solid interface. It is feasible to develop innovative approaches to remove pollutants from aqueous systems by means of identifying the forces governing the interaction between contaminants and solid surfaces. This includes the design of novel and efficient adsorbent materials, such as engineered nanoparticles that can selectively adsorb contaminants, offering promising solutions for water purification and environmental remediation. The adsorption of heavy metals onto modified clay minerals in water treatment processes relies on surface thermodynamics principles to optimize removal efficiency. Additionally, surface thermodynamics is a useful tool for interpreting the behavior of contaminants at the water–air interface, particularly relevant in the context of volatile organic compounds (VOCs). The partitioning of VOCs between water and air is governed by surface tension and interfacial energies, involved in assessing the fate and transport of airborne pollutants and their potential impact on both aquatic and terrestrial ecosystems. The environmental domain of surface thermodynamics comprises the study of oil spill remediation, which often involves understanding the adsorption of oil components at the water–air interface. Furthermore, surface thermodynamics contributes to the development of models that accurately predict contaminant behavior in natural systems, assisting in decisions regarding pollutant management and remediation. In groundwater remediation, recognizing the sorption behavior of contaminants on subsurface soils and sediments is crucial for designing effective cleanup strategies. The modeling of adsorption of emerging contaminants, such as pharmaceuticals and personal care products in aquatic environments, provides insights into their environmental impact. Molecular dynamics simulations and density functional theory calculations have become indispensable tools for predicting surface properties and behavior at the atomic and molecular levels.

10.5 Final Remarks

Surface thermodynamics, together with the surface physical chemistry, has signed significant developments in recent years, opening new avenues for its application in diverse scientific and industrial domains. The scientific advancements of the thermodynamics of surfaces stem from a deep understanding of the fundamental principles governing interfacial phenomena and colloidal aspects of complex systems. The application of surface thermodynamics ranges from nanotechnology, where accurate control over surface characteristics is imperative, to the development of innovative approaches for environmental remediation, moving on self-aggregative systems and energetic content assessment. Strategically managing the principles of surface thermodynamics, intricate challenges can be addressed for a future outlined by enhanced energy efficiency, sustainability, and innovation.